

Modelling and Analysis of Anthropomorphic Cable-Driven Robots

Darwin Tat Ming Lau

Submitted in total fulfilment of the requirements for the degree of

Doctor of Philosophy

Department of Mechanical Engineering

THE UNIVERSITY OF MELBOURNE

May 2014

Produced on archival quality paper.

Copyright © 2014 Darwin Tat Ming Lau

All rights reserved. No part of the publication may be reproduced in any form by print, photoprint, microfilm or any other means without written permission from the author.

Abstract

Cable-driven parallel manipulators (*CDPMs*) have been studied in recent years due to their unique characteristics and advantages. In particular, CDPMs have been regarded as bio-inspired mechanisms that are structurally analogous to musculoskeletal systems. In this thesis, the study of anthropomorphic cable-driven robots is investigated. Multilink cable-driven manipulators (*MCDMs*) are a type of CDPM where cables actuate a multi-link rigid body structure in parallel arrangement. The rigid links and cables of MCDMs are analogous to the bones and muscles of musculoskeletal systems, respectively.

The use of MCDMs to study more complex biomechanical structures has been limited due to several reasons. Firstly, musculoskeletal systems are typically open-chain branched structures with complex cable routing and a large number of links. However, there currently exists no generalised model that allows arbitrary cable routing. Secondly, the analysis for MCDMs may require extensions from single link CDPMs to consider the different types of cable routing. Thirdly, the actuation characteristics between muscles and ideal cables are considerably different.

These issues are investigated and addressed in this thesis and the contributions are presented in two parts. The first part deals with the modelling of MCDMs. One major challenge in the modelling of MCDMs is that the number of combinations in possible cable routing increases exponentially with the number of rigid bodies. Introducing the cable-routing matrix (*CRM*), it is shown that all possible cable routing can be encapsulated in a single representation. Using the CRM and a generalised representation for arbitrary joints, generalised kinematic and dynamic models for open-chain branched mechanisms are formulated. The proposed model allow both arbitrary cable routing and arbitrary rigid body structure. The effectiveness and robustness of the model is demon-

strated through two examples, a simple 2 link 4 degree-of-freedom (*DoF*) 6 cable manipulator and a complex human neck inspired 8 link 24 Dof 76 cable system. The more complex example serves to illustrate the potential in using the generalised MCDM model to study musculoskeletal structures.

The second part of this thesis addresses the analysis of anthropomorphic CDPMs for both engineered and biomechanics applications. Using the generalised MCDM model, necessary conditions with respect to the CRM are derived for an MCDM to satisfy wrench-closure. In the design of an MCDM, it is important that the cable routing results in a manipulator that is capable of producing wrench-closure. Finally, the workspace analysis of CDPMs allowing for state dependent force generators is investigated. Examples of state dependent force generators include artificial and physiological muscles. In particular, the static workspace of musculoskeletal systems is studied. The formulation is demonstrated through computationally generating the static workspace of a human shoulder. By validating the workspace against human benchmarks, it is shown that the inclusion of muscles is important to generate a physiologically accurate musculoskeletal workspace.

Through this thesis, the fundamental components required in studying anthropomorphic cable-driven manipulators have been presented. The contributions of the thesis extend the boundaries of the current literature in both the robotics and biomechanics disciplines. In addition to enabling more complex engineered MCDM systems to be studied, the concept of studying biomechanical systems as MCDMs is proposed for the first time. The results of this work highlight the potential of using MCDMs to gain a better understanding of biomechanics.

Declaration

This is to certify that

1. the thesis comprises only my original work towards the PhD,
2. due acknowledgement has been made in the text to all other material used, and
3. the thesis is less than 100,000 words in length, exclusive of tables, maps, bibliographies and appendices.



Darwin Tat Ming Lau, May 2014

This page is intentionally left (almost) blank.

Acknowledgements

The PhD experience has been one journey that words would struggle to describe accurately. If a description was to be made, it would likely to involve words such as: long, brain torment, full of sweat and roadblocks. At the same time, it would be appropriate to describe the journey as enjoyable, exciting, intellectually stimulating and fulfilling. However, if only one word was to be used, I believe it would be most appropriate to use the word unforgettable. At the end of this chapter of life, I would like to sincerely thank all the people who have been in my life and supporting me throughout.

Firstly, I would like to thank my supervisors Dr. Denny Oetomo and Prof. Saman Halgamuge for their support and guidance during my candidature. They have provided me with their valuable time, patience and experience whenever it was needed. In addition to their guidance towards my PhD research, I thank my supervisors for their nurturing to prepare me for the future. I could not be prouder of my academic roots and hope that I can in turn pass on all they have given to me. I would also like to take the opportunity to thank Prof. William Ducker, who gave me the opportunity to get a taste of research during my undergraduate degree. Prof. Ducker inspired and encouraged me to consider research as a life long career and has truly made a difference in my life.

Appreciation also goes to my colleagues and the staff in the Department of Mechanical Engineering for their ongoing support and advice both in and out of my research. I also have to thank my supportive group of friends who have been accompanied me throughout this journey. In particular, I have thoroughly enjoyed the leisure time spent with them when I had to escape from my computer and desk in order to maintain my sanity. Finally, I must acknowledge and thank my family: my father, my mother and my brother who have supported throughout my life and made me the person I am.

To all the people who have made my world.

This page is intentionally left (almost) blank.

Contents

1	Introduction	1
1.1	Motivation	2
1.2	Research questions	4
1.3	Contributions of the Thesis	5
1.4	Structure of the Thesis	6
1.5	Related Publications	7
2	Literature Review of Cable-Driven Parallel Manipulators	9
2.1	History and Development	9
2.2	Practical Applications	13
2.3	Theoretical Problems	19
2.4	Multilink Cable-Driven Manipulators	28
2.5	Conclusion	38
Part I: Modelling of Multilink Cable-Driven Systems		41
3	Introduction to Cable-Driven Parallel Manipulators	45
3.1	Introduction	45
3.2	Kinematic and Dynamic Analyses	47
3.2.1	Inverse Kinematics	48
3.2.2	Direct Kinematics	49
3.2.3	Inverse Dynamics	50
3.2.4	Direct Dynamics	52
3.3	Modelling of Example Manipulators	53
3.3.1	3 DoF Spherical Joint Manipulator	54
3.3.2	6 DoF Spatial Manipulator	59
3.3.3	4 DoF Two Link Manipulator	63
3.4	Conclusion	71
4	Generalised Cable Routing for Multilink Cable-Driven Manipulators	73
4.1	Introduction	73
4.2	Cable-Routing Matrix	78
4.3	Examples of Cable-Routing Matrices	81
4.3.1	Two Link Manipulator	82

4.3.2	8 Link Serial Manipulator	83
4.3.3	11 Link Branched Manipulator	86
4.4	Cable-Routing Matrix Properties	87
4.5	Generalised Cable Segment Vector	89
4.6	Conclusion	93
5	Generalised Multilink Cable-Driven Manipulator Model	95
5.1	Introduction	95
5.2	Generalised Rigid Body Structure	97
5.3	Kinematic Model of Serial Manipulators	100
5.3.1	Direct Kinematics	101
5.3.2	Jacobian Matrix	102
5.4	Equations of Motion for Serial Manipulators	106
5.4.1	Generalised Accelerations	107
5.4.2	Sum of Forces and Moments	110
5.4.3	Generalised Equations of Motion	112
5.5	Extension to Branched Manipulators	116
5.6	Simulation Examples	121
5.6.1	4 DoF Two Link Manipulator	121
5.6.2	24 DoF 8 Link Human Neck Model	124
5.7	Conclusion	129
Part II : Analysis of Anthropomorphic Cable-Driven Manipulators	131	
6	Wrench-Closure Validity Analysis for Multilink Cable-Driven Manipulators	135
6.1	Introduction	135
6.2	Jacobian Matrix Analysis	138
6.3	Necessary Conditions on the Cable-Routing Matrix	142
6.4	Analysis of Example Manipulators	151
6.4.1	Single Link Manipulators	151
6.4.2	Two Link Manipulators	152
6.4.3	Three Link Manipulators	157
6.5	Conclusion	161
7	Muscle Actuation in the Cable Model	163
7.1	Introduction	163
7.2	Hill-type Muscle Model	164
7.3	Active and Passive Muscles	168
7.4	Solution of Muscle Forces	171
7.5	Conclusion	177
8	Musculoskeletal Static Workspace	179
8.1	Introduction	179
8.2	Static Workspace Framework	181
8.2.1	Ideal Force Generator Model	181

8.2.2	State Dependent Force Generator Model	182
8.3	Workspace Generation	183
8.3.1	Ideal Force Generator Static Workspace	184
8.3.2	Musculoskeletal Static Workspace	185
8.4	Static Workspace of the Human Shoulder	187
8.4.1	Shoulder Model	187
8.4.2	Results	192
8.5	Conclusion	201
9	Conclusion and Future Direction	203
9.1	Conclusion	203
9.2	Future Directions	205
A	Wrench-Closure Workspace Generation for Cable-Driven Parallel Manipulators Using a Hybrid Analytical-Numerical Approach	223
A.1	Introduction	224
A.2	Kinematic and Dynamic Model	227
A.3	Wrench-Closure Workspace	229
A.4	Proposed Workspace Determination Approach	231
A.4.1	6-DOF Spatial Manipulator	231
A.4.2	3-DOF Ball Joint Manipulator	234
A.4.3	Workspace Evaluation	237
A.5	Simulation Setup	238
A.5.1	3-DOF Ball Joint Manipulator	239
A.5.2	6-DOF Spatial Manipulator	241
A.6	Results and Discussion	243
A.7	Conclusions	250
B	On the Task Specific Evaluation and Optimisation of Cable-Driven Parallel Manipulators	251
B.1	Introduction	251
B.2	Manipulator Model and Background	253
B.2.1	Inverse Dynamics Problem	254
B.2.2	Wrench-Closure Workspace	255
B.3	Optimisation Problem and Evaluation Methods	255
B.3.1	Cable Force Characteristics	256
B.3.2	Workspace Evaluation	256
B.4	Simulation and Results	257
B.5	Conclusion	260

This page is intentionally left (almost) blank.

List of Figures

1.1	Single link vs multilink CDPMs	2
2.1	Kinematic structure of CDPMs	13
2.2	Analytically and numerically generated workspaces	23
2.3	Cable routing for MCDMs	29
2.4	7 DoF modular MCDM arm	30
2.5	Upper limb exoskeleton MCDM	31
2.6	MCDM with single segment cables	32
2.7	3R planar MCDM with arbitrary cable routing	33
2.8	3 link 5 DoF planar MCDM	34
2.9	3 link 5 DoF planar MCDM cable distribution	35
2.10	Physiological muscle model	36
2.11	Example muscle force curve	37
3.1	Planar CDPM model	48
3.2	Planar CDPM kinematics	48
3.3	Inverse kinematics example	49
3.4	Direct kinematics example	50
3.5	Inverse dynamics example input motion	52
3.6	Inverse dynamics example output cable forces	53
3.7	Direct dynamics example input cable forces	54
3.8	Direct dynamics example output motion	54
3.9	3 DoF spherical joint CDPM model	55
3.10	3 DoF spherical joint CDPM free body diagram	58
3.11	6 DoF spatial CDPM model	59
3.12	4 DoF 2 link CDPM rigid body structure	64
3.13	4 DoF 2 link CDPM cable arrangement	65
3.14	4 DoF 2 link CDPM free body diagram	68
4.1	Class 1 cable routing for 2 link CDPMs	75
4.2	Class 2 cable routing for 2 link CDPMs	75
4.3	p link generalised MCDM rigid body structure	78
4.4	8 link human neck inspired MCDM rigid body structure	83
4.5	8 link human neck inspired MCDM muscle-routing examples	84
4.6	11 link branched MCDM model	86
4.7	p link generalised MCDM coordinate frames	90

4.8	Cable attachment location for MCDMs	90
4.9	8 link human neck inspired MCDM cable segment vector examples	92
5.1	p link generalised MCDM joint and gravity locations	97
5.2	Interaction force and moment for an MCDM joint	99
5.3	Kinematics of Attachment Location for an MCDM link	102
5.4	Free body diagram for an MCDM link	110
5.5	Serial vs branched open-chain structures	117
5.6	2 link 4 DoF example MCDM model	122
5.7	2 link 4 DoF CDPM inverse kinematics cable lengths	123
5.8	2 link 4 DoF CDPM inverse kinematics cable velocities	124
5.9	2 link 4 DoF CDPM inverse dynamics cable forces	125
5.10	8 link 24 DoF 76 cable model	126
5.11	8 link 24 DoF 76 cable MCDM inverse dynamics roll motion cable forces .	127
5.12	8 link 24 DoF 76 cable MCDM inverse dynamics pitch motion cable forces	128
5.13	8 link 24 DoF 76 cable MCDM inverse dynamics yaw motion cable forces .	129
6.1	Example of highest and lowest link number and the CRM	145
6.2	Class 1 routing for the wrench-closure validity analysis of 2 link CDPMs .	153
6.3	Class 2 routing for the wrench-closure validity analysis of 2 link CDPMs .	154
6.4	Example cable arrangements for two link SR MCDM	155
6.5	Valid cable routing showing invalid attachment locations	157
6.6	3 link 3R planar MCDM model	160
6.7	Example cable arrangements for three link 3R MCDM	161
7.1	Modified Hill-type muscle-tendon model	165
7.2	Tendon force curve examples	166
7.3	Muscle force curve examples	168
7.4	Active and passive muscle-tendon force solutions	170
7.5	Active muscle-tendon solution force range	172
7.6	Passive muscle-tendon solution force	173
7.7	Shoulder flexion/extension motion	173
7.8	Length of supraspinatus muscle during flexion/extension motion	175
7.9	Force of supraspinatus muscle during flexion/extension motion	175
7.10	Length of deltoid anterior muscle during flexion/extension motion	176
7.11	Force of deltoid anterior muscle during flexion/extension motion	177
8.1	Shoulder model OpenSim	187
8.2	Shoulder model kinematics	188
8.3	Shoulder motion	190
8.4	Components of the musculoskeletal static workspace analysis	191
8.5	Static workspace of the shoulder	193
8.6	Workspace range of motion error box plot	195
8.7	Static workspace of the shoulder with passive deltoid muscles	198
8.8	Static workspace of the shoulder with passive pectoral muscles	199

A.1	General Model for Cable Manipulator	228
A.2	3-DOF Ball Joint Manipulator Model	239
A.3	6-DOF Ball Joint Manipulator Model	242
A.4	α - β cross-section of the 3-DOF manipulator WCW at $\gamma \approx \frac{\pi}{6}$ rad	244
A.5	3-D Visualisation of the 3-DOF manipulator workspace	245
A.6	α - β cross-section of the 3-DOF manipulator workspace at $\gamma \approx \frac{3\pi}{8}$ rad	245
A.7	α - β cross-section of the 3-DOF manipulator workspace at $\gamma \approx \frac{7\pi}{16}$ rad	246
A.8	α - β cross-section of the 3-DOF manipulator workspace at $\gamma \approx \frac{3\pi}{8}$ rad	246
A.9	α - β cross-section of the 3-DOF manipulator workspace at $\gamma \approx \frac{7\pi}{16}$ rad	247
A.10	x - y cross-section of 6-DOF manipulator WCW for $\alpha = \beta = \gamma = 0^\circ$	249
A.11	x - y cross-section of 6-DOF manipulator WCW for $\alpha = \beta = 0^\circ, \gamma = 5^\circ$	249
B.1	General Model for Cable Manipulator	253
B.2	3-DOF Ball Joint Manipulator	258
B.3	WCW for optimal configurations \mathbf{x}_4^* and \mathbf{x}_1^*	259
B.4	Cable Forces for Trajectory C_3 for optimal configurations \mathbf{x}_4^* and \mathbf{x}_3^*	261

This page is intentionally left (almost) blank.

List of Tables

4.1	Number of MCDM open-chain cable routing combinations	76
5.1	Sample trajectories for 8 link 8S neck model	127
6.1	Analysis of cable routing for 2 link MCDMs	154
6.2	Analysis of cable routing for 3 link MCDMs	159
7.1	Muscle properties for deltoid anterior and supraspinatus muscles	174
8.1	Rotations of the glenohumeral joint	189
8.2	Properties of the shoulder model	189
8.3	Muscle properties of the shoulder	191
8.4	Range of motion limit comparison for the human shoulder	194
8.5	Workspace range of motion errors	195
8.6	Range of motion for the human shoulder with passive muscles	200
A.1	Cable Configuration for 3-DOF Manipulator	239
A.2	Cable Configuration for 6-DOF Manipulator	242
A.3	Computational time and volume ratio for varying $\Delta\alpha = \Delta\beta = \Delta\gamma = \Delta x$.	247
A.4	Computational time and volume ratio for varying $\Delta\alpha$ with $\Delta\beta = \Delta\gamma = \frac{\pi}{20}$ rad	248
B.1	Evaluation Function Descriptions	258
B.2	Comparison of Evaluation Functions	259

This page is intentionally left (almost) blank.

Nomenclature

Acronyms

CDPM	cable-driven parallel manipulator
MCDM	multilink cable-driven manipulator
CRM	cable-routing matrix
DoF	degree-of-freedom
SW	static workspace
WFW	wrench-feasible workspace
WCC	wrench-closure condition
WCW	wrench-closure workspace
ROM	range of motion

Mathematical notations

n	number of degrees-of-freedom (<i>DoFs</i>)
m	number of cables
\mathbf{q}	joint space vector
$\dot{\mathbf{x}}$	body twist vector
\mathbf{l}	vector of cable lengths
\mathbf{f}	vector of cable forces
l_i	length of cable i
f_i	force in cable i
\mathbf{l}_i	cable vector of cable i
$\hat{\mathbf{l}}_i$	unit vector of \mathbf{l}_i
\mathbf{f}_i	cable force vector of cable i
J	Jacobian matrix
M	mass-inertia matrix
\mathbf{C}	centrifugal and Coriolis vector
\mathbf{G}	gravity vector
\mathbf{F}_{ext}	external force vector
$\{F_k\}$	coordinate frame F_k
${}^k \mathbf{r}_{AB}$	position vector from position A to B expressed w.r.t $\{F_k\}$
ω_k	absolute angular velocity of body k
${}^a R_b$	rotational matrix from $\{F_a\}$ to $\{F_b\}$
c_θ	cosine of angle θ
s_θ	sine of angle θ
g	gravity constant 9.81 m/s ²
\mathbf{l}_{ij}	cable segment vector of segment j of cable i
\mathbf{f}_{ij}	cable force vector of segment j of cable i

Chapter 1

Introduction

ANTHROPOMORPHIC cable-driven systems are investigated and studied in this thesis. Cable-driven parallel manipulators (CDPMs) can be regarded as anthropomorphic bio-inspired mechanisms where the rigid bodies and cables are structurally analogous to the bones and muscles of biomechanical systems, respectively. These similarities allow the potential to study biomechanical systems as cable-driven systems.

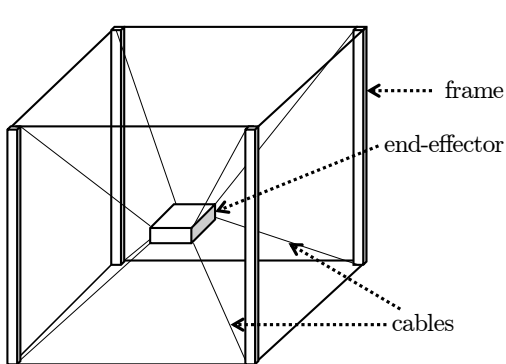
CDPMs are a class of parallel mechanisms [84] where the actuating legs are replaced by cables. Compared to rigid link serial mechanisms, rigid link parallel manipulators benefit from higher payload to weight ratio, increased rigidity, lower end-effector weight and inertia, and greater positional accuracy. The major drawback of rigid link parallel mechanisms is their limited useful workspace compared to the manipulator size. Compared to traditional rigid link serial and parallel mechanisms, CDPMs possess the following desirable characteristics: further reduced end-effector weight and inertia, simplified modelling in dynamics, ability to construct a manipulator with a large reachable workspace, ease of transportation and ease in reconfiguration.

With these advantages, CDPMs have been studied for a wide range of applications. The high payload to weight ratio makes CDPMs appropriate in applications such as high speed manipulation [4, 58, 59], heavy payload suspension [100, 102], motion simulators [75] and haptic devices [33, 57]. To take advantage of the potential in achieving a large reachable workspace, CDPMs have also been used in environment sensing [14, 62, 134], search and rescue [18], building construction [16] and radio telescopes [143]. In medical applications, CDPMs have been studied as rehabilitation devices [79, 104], exoskeletons [2] and bio-inspired mechanisms [76, 93, 141].

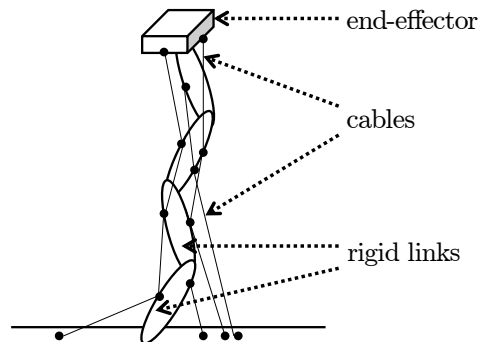
The key feature of cable-driven systems is that cables can only provide unilateral actuation in tension (*positive cable force*) and not compression. As a result, this class of systems is naturally required to be redundantly actuated to generate wrench-closure in all of the degree of freedoms. The constraint and redundancy in actuation creates challenging problems in the analysis of CDPMs, such as the inverse dynamics, control and workspace analysis. Additionally, as the locations in which the cables are attached to the manipulator (*cable attachment locations*) have a significant impact on the manipulator's performance, the modelling and design of this class of systems have also been widely studied.

1.1 Motivation

Traditional CDPMs typically consist of a single end-effector piece that is driven by cables through spools and pulleys located on the stationary frame, as shown in Figure 1.1(a). As a result, the design of the manipulator is typically not compact as the stationary frame must fully encapsulate the desired workspace of the manipulator.



(a) Traditional single link CDPM



(b) Multilink cable-driven manipulator (MCDM)

Figure 1.1: CDPMs can be classified as single link (a) and multilink manipulators (b).

Multilink cable-driven manipulators (MCDMs), as shown in Figure 1.1(b), are anthropomorphically structured hybrid mechanisms where the rigid links form a serial kinematic chain and the cables are arranged in parallel configuration to provide actuation.

MCDMs benefit from the compactness and dexterity of serial mechanisms and the actuation advantages of cable-driven manipulators. The weight and inertia of the manipulator are significantly reduced as the actuating motors can all be located on the stationary frame of the system and the joints of the manipulator are passive. With these advantages, MCDMs are suitable for applications such as high speed manipulation, haptic devices and bio-inspired mechanisms.

Unique difficulties and challenges arise in the modelling and analysis of MCDMs due to the multiple ways in which cables can be routed in the system (*cable routing*). For single link CDPMs, all cables are only confined to route from the stationary frame to the end-effector. In comparison, cables in MCDMs can be attached to any of the links and a single cable can pass through multiple links. As a result, two difficult challenges arise in the study of MCDMs.

Firstly, to determine the system's Jacobian matrix, and hence the equations of motion, each of the possible cable routing combinations would need to be modelled. This is straightforward for single link CDPMs as there is only a single possibility for cables to route. In comparison, this is a challenge in the modelling of MCDMs since the number of combinations of cable routing for MCDMs increase exponentially with the number of links. Secondly, the kinematics and dynamics between the manipulator's links become coupled since a single cable affects the motion of multiple links. The impact of this effect must be considered in the analysis of MCDMs.

In addition to engineered systems, the analysis of MCDMs can also be applied to the study of biomechanical systems. For both MCDMs and musculoskeletal systems, the rigid links form a multilink open chain structure. Furthermore, both cables and muscles are actuation elements that can only produce positive force. Due to the similarities in kinematic structure and actuation dynamics, techniques in modelling and analysis of MCDMs can be applied onto biomechanical systems. For example, the concept of workspace analysis has been well studied in the area of cable robotics and many types of workspace have been defined. The workspace analysis of biomechanical systems provides a physically meaningful computational tool for studying the operational region of musculoskeletal systems. Such a computational tool can assist in medical applications,

such as tendon-transfer surgery, rehabilitation and injury analysis, by providing a greater understanding on the impact of the muscles on the resulting workspace of the system.

Despite the similarities in MCDMs and biomechanical systems, two differences between the systems must be considered in the study of biomechanical systems as MCDMs. Firstly, despite the positive force constraint in both cables and muscles, muscles possess non-linear actuation characteristics where the force that can be produced is dependent on their length and velocity. In comparison, cables for engineered systems have typically been modelled as ideal force generators where any force between a given range can be produced. Furthermore, the joints in skeletal systems differ from the common joints used in robotic systems, such as revolute joints and spherical joints. For example, the shoulder joint is a unilaterally constrained spherical joint with constrained translational motion. These differences should be considered when analysing biomechanical systems using techniques developed for CDPMs.

In summary, MCDMs can be regarded as anthropomorphically structured mechanisms that possesses the advantages of both serial manipulators and CDPMs. The study of this class of manipulators is necessary as there are many new challenges that were not present in the modelling and analysis of single link CDPMs. MCDMs can be applied in engineered systems, such as high speed manipulators, and in the analysis of biomechanical systems, such as the human limb and neck.

1.2 Research questions

The primary objective of this thesis is to develop a general model for multilink cable-driven manipulators (*MCDM*) and thereby perform analysis on the generalised MCDM model for applications in engineered systems and in the study of biomechanics.

The following research questions are considered in this thesis to accomplish the primary research objective:

- *How can MCDMs be modelled such that all of the combinations in cable routing are encapsulated within a single model and representation?*
- *How can the analysis of single link cable-driven manipulators be extended and applied to*

generalised MCDMs?

- *How can analysis techniques developed for robotic CDPM systems be extended and applied on musculoskeletal systems to provide a greater understanding in biomechanics?*

1.3 Contributions of the Thesis

In this thesis, the study on the modelling and analysis of anthropomorphic cable-driven manipulators is presented. In studying the proposed research questions, this thesis makes the following major contributions:

- A generalised branched open-chain MCDM model is proposed by representing arbitrary cable routing for the system within a cable-routing matrix (CRM)
- Analysis on the necessary conditions for wrench-closure of MCDMs is performed using the generalised model and the CRM
- The static workspace analysis for CDPMs is extended to musculoskeletal systems by allowing for more generic cable actuator models, for example, the model of physiological muscles

The contributions of the thesis can be applied in the study of MCDMs for both the fields of robotics and biomechanics.

In the field of robotics, the generalised formulation and analysis of MCDMs would allow this class of systems to be studied in a more convenient and systematic manner. Furthermore, the incorporation of a more general actuator model allows the analysis of a wider range of robotic systems, such as those actuated by pneumatic muscles, as CDPMs.

In biomechanics, the proposed generalised model allows musculoskeletal systems to be studied as MCDMs, due to their similarities in structure and actuation. Hence, a wider range of well established techniques in cable-driven robotics, such as workspace analyses, can be applied to the study of musculoskeletal systems. These computational tools provide additional perspectives on the study of human motion and muscle function, for example, the contribution of particular muscles on specific regions of the workspace. This is particularly beneficial in applications that require simulation of modified muscle properties or muscle attachment locations, such as tendon-transfer surgery, rehabilitation

robotics, and diagnosis of motion impairment.

In summary, this thesis contributes to the fundamental knowledge of cable-driven robotic manipulators, with motivation and application in both engineered robotic and biomechanical systems.

Furthermore, in addition to the contributions to the study of anthropomorphic cable-driven robots described above, analysis on the wrench-closure workspace of cable-driven parallel manipulators have also been performed during the PhD candidature. This work resulted in two publications on the topics of an hybrid analytical-numerical approach for wrench-closure workspace analysis [69]; and the design and optimisation of the wrench-closure workspace of CDPMs [68]. Although these works were completed during the PhD candidature, the studies were performed on traditional CDPMs rather than anthropomorphic CDPMs. As a result, the contributions of the publications [69] and [68] have not been included in the body of the thesis, but have been included as Appendices A and B, respectively.

1.4 Structure of the Thesis

This thesis contains 9 chapters organised into 2 parts to present the contributions towards the three identified research questions. The remainder of the thesis is organised as follows. Chapter 2 reviews the start-of-the-art works that are relevant to the contributions of the thesis.

Part I, containing Chapters 3 to 5, presents the formulation of a generalised model for multilink cable-driven manipulators (*MCDMs*). As an introduction to the modelling of cable-driven parallel mechanisms (*CDPMs*), Chapter 3 formulates the model of several simple CDPMs. Chapter 4 proposes the cable-routing matrix (*CRM*), a representation that encapsulates all combinations of cable routing for MCDMs. Finally, the generalised model that allows for arbitrary kinematic topology and cable routing is formulated in Chapter 5.

Part II, containing Chapters 6 to 8, presents the analysis of anthropomorphically structured CDPMs. Firstly, Chapter 6 performs analysis on the necessary conditions to achieve

wrench-closure validity for MCDMs, expressed with respect to the CRM. Chapters 7 and 8 extend the analysis of CDPMs to the study of musculoskeletal systems. The physiological muscle model and the determination of the range of muscle force for a given manipulator pose is described in Chapter 7. Chapter 8 extends the analysis of static workspace on CDPMs, incorporating muscle physiology into the cable model, such that the static workspace of musculoskeletal systems can be studied. The analysis is demonstrated through the generation of the static workspace for a human shoulder.

Finally, Chapter 9 concludes this thesis and present future directions in this study. In Appendix A, the manuscript for the work published in [69] describes a hybrid analytical-numerical approach to generate the wrench-closure workspace for single link CDPMs. In Appendix B, the manuscript for the work published in [68] describes the evaluation and optimisation of the cable attachment locations for single link CDPMs under task specific objectives.

1.5 Related Publications

During the PhD candidature, the following publications that are related to the study of CDPMs have resulted.

Journal articles

- D. Lau, D. Oetomo, and S. K. Halgamuge, "Inverse Dynamics of Multilink Cable-Driven Manipulators with Consideration of Joint Interaction Forces and Moments", *in review*
- D. Lau, D. Oetomo, and S. K. Halgamuge, "Static Workspace Analysis of Cable-Driven Manipulators with a Physiological Muscle Actuator Model", *accepted, IEEE/ASME Transactions on Mechatronics*
- D. Lau, D. Oetomo, and S. K. Halgamuge, "Generalised Modelling and Analysis of Multilink Cable-Driven Manipulators with Arbitrary Routing Using the Cable-Routing Matrix", *IEEE Transactions on Robotics*, Vol. 29, No. 5, pp. 1102-1113, 2013
- D. Lau, K. Bhalerao, D. Oetomo, and S. K. Halgamuge, "On the Task Specific

Evaluation and Optimisation of Cable-Driven Manipulators”, *Advances in Reconfigurable Mechanisms and Robots I : Part 6*, pp. 707-716, 2012

- D. Lau, D. Oetomo, and S. K. Halgamuge, “Wrench-Closure Workspace Generation for Cable Driven Parallel Manipulators using a Hybrid Analytical-Numerical Approach”, *ASME Journal of Mechanical Design*, Vol. 133, 071004, 2011

Conference publications

- D. Lau, J. Eden, S. K. Halgamuge and D. Oetomo, “Cable Function Analysis for the Musculoskeletal Static Workspace of a Human Shoulder”, *Second International Conference on Cable-Driven Parallel Robots*, Duisburg, German, 2014
- D. Lau, T. Hawke, L. Kempton, D. Oetomo, and S. K. Halgamuge, “Design and Analysis of a 4-DoF Cable-Driven Parallel Mechanism”, *Proceedings Australasian Conference on Robotics and Automation*, Brisbane, Australia, 2010
- D. Lau, D. Oetomo, and S. K. Halgamuge, “Optimisation of the Inverse Dynamics of Parallel-Actuated Cable Driven Manipulator”, *Regional Conference on Mechanical and Aerospace Technology*, Bali, Indonesia, 2010

Chapter 2

Literature Review of Cable-Driven Parallel Manipulators

In this chapter, a study on the state of the arts in cable-driven parallel manipulators (CDPMs) that relate to the modelling and analysis of anthropomorphic cable-driven robots is presented. In Section 2.1, the history and development of traditional CDPMs are reviewed. Section 2.2 reviews the different applications that take advantage of the unique characteristics of CDPMs. Section 2.3 describes the theoretical challenges involved with cable-driven robots. Section 2.4 presents the recent investigations on multilink cable-driven manipulators (MCDMs). From the previous studies in MCDMs, the main limitation identified is the lack of a convenient representation of arbitrary cable routing. The ability to model arbitrarily complex cable routing allows anthropomorphically structured MCDMs to be modelled and analysed. Finally, Section 2.5 summarises the literature review and identifies several key issues that have not yet been resolved.

2.1 History and Development

Historically, many robotic manipulators have been designed to possess the structure and articulation of anthropomorphic systems, such as the human arm. These systems can be regarded as *serial manipulators*, where the rigid bodies are connected in succession by joints in a serial chain structure. The advantages of serial manipulators include their compactness in design, high dexterity and large achievable workspace compared to their size. However, this class of manipulators possess several inherent disadvantages. Firstly, serial robots are generally capable in carrying or manipulating a relatively low effective load. In addition to the load that the system must carry, each link must also carry the weight of the links and actuators of its child links. Secondly, the serial structure means

that each link is subject to large flexure torques and hence decreases in stiffness as the link is further from the base. Finally, the positional accuracy of the end-effector is generally poorer as the error in each link accumulates and amplifies.

Compared with serial robots, parallel manipulators distribute the load over the multiple links forming closed kinematic chains. In this arrangement, the actuated links support the end-effector in a parallel configuration. As a result, parallel manipulators benefit from increased overall stiffness compared with serial mechanisms. The payload to weight ratio is also typically higher as each actuator supports only a fraction of the end-effector load. Furthermore, the accuracy of the end-effector position is higher as errors in the links of the manipulator do not accumulate.

Theoretical problems related to parallel structure mechanisms were reported as early as in the 1800's [20, 22]. On the practical end, functional prototypes of parallel mechanisms were proposed and developed during the early to mid 1900's [45, 109]. In 1928, J. E. Gwinett filed a patent on a spherical mechanism to be used as a platform for a movie theatre [45]. However, this design was never constructed or realised. For a different application, Willard L. G. Pollard Jr. filed a patent in 1934, and was issued in 1942, on a parallel robot used for spray painting [109] that was designed by his father L. V. Pollard.

The first well known and functional prototype of a parallel robot was developed and built by Gough in 1955 to test tyre wear and tear [40, 41]. The development of the aeronautics industry saw increased applications of parallel robots as flight simulators for pilot training. The advantages of decreased manipulator mass and higher accuracy made parallel manipulators attractive for this application compared with serial mechanisms. In 1965, Stewart proposed a mechanism for use in flight simulation [119] named as the Stewart platform. During the same period of time, Cappel proposed a motion simulator device with the same octahedral arrangement as Gough and was patented in 1967 [21].

Since the deployment of the first parallel manipulators as motion simulators, parallel mechanisms have been employed in a wide range of uses. These applications include: motion bases, factory and assembly manipulators, machine-tools, surgical robots, haptic devices and micromanipulators. Due to their significance in practical applications and the richness in the theoretical problems, parallel manipulators have been extensively

studied over the past decades. From these studies, parallel manipulators with a wide range of different structures have been designed and developed. Parallel mechanisms can be classified by the number and type of joints and actuators that support the end-effector. For example, the Gough platform is supported by six legs, where each leg consists of a universal joint (U) at the base, an actuated prismatic joint (P) and a spherical joint (S) that is connected to the end-effector. As a result, the Gough platform can be classified as a 6-UPS structured mechanism.

The primary disadvantage of parallel robots compared with serial manipulators is their limited workspace. The workspace is limited by the geometrical and mechanical limits of the design and its joints. Another challenge in the study of parallel manipulators is that the direct kinematics is usually complex to solve and may result in multiple solutions [51, 70, 96]. In contrast, the inverse kinematics problem is simple and often trivial to solve.

In more recent years, a new class of parallel robots has emerged, where the rigid links are replaced by cables. This class of manipulators have been commonly referred to as cable-driven parallel manipulators (CDPMs), cable-driven parallel robots (CDPRs), or simply cable/wire robots. The idea of CDPMs emerged in the late 1980s and early 1990s from the works of Landsberger [66, 67], Higuchi and Ming [49] and Albus [4].

Landsberger proposed a parallel mechanism in 1985 where its geometry was based on that of a Stewart platform, where the rigid links were replaced with cable links [66]. The motivations and benefits in using the cable legs included the light weight of the cables, the compact manipulator size while permitting a large work region, and the reconfigurability of the system to match different tasks.

In 1988, Higuchi and Ming proposed the concept of a wire crane for use in building construction [49]. The work presented the prototypes and kinematics of a 3 degree-of-freedom (*DoF*) planar manipulator actuated by cables and a 3 DoF spatial manipulator. Compared with a traditional crane, the wire crane robot allows the position of the end-effector to be controlled with high speed and accuracy.

Within the early studies on CDPMs, the most cited cable robot is the NIST RoboCrane [4] developed by Albus and his team at the National Institute of Standard and Technology

(NIST) in 1993. The NIST RoboCrane consists of 6 cables that coil and uncoil to actuate the end-effector crane. It allows manipulation of both the translational and the rotational motions of the crane. The proposed uses of the manipulator included tasks such as cutting, lifting and positioning of load. The primary advantage of the RoboCrane is its high lift-to-weight ratio, where it can lift at least five times its own weight.

CDPMs possess several unique characteristics that have created challenges and drawn interest into the study of this class of manipulators. Firstly, the cable actuators are only able to provide tension cable forces (*positive force constraint*) to the end-effector. In contrast, the legs of traditional rigid link parallel manipulators can provide both tension and compression forces. Due to the positive force constraint, CDPMs require actuation redundancy to produce motion in all the degrees of freedom of the mechanism. The positive force constraint and actuation redundancy creates challenging problems in the analysis of CDPMs. Secondly, the manipulator dynamics are dependent on the type of cables used. For example, if the cables are rigid and lightweight, then the modelling of the dynamics are simplified by assuming that the cable dynamics are negligible. On the other hand, compliance could be introduced into the system by using elastic cables or by adding an elastic element in series with the cable [12, 60, 139]. Finally, CDPMs have been regarded as a bio-inspired mechanism due to the structural similarities between the rigid links and cables of CDPMs to the bones and muscle/tendon complexes of biomechanical systems, respectively.

The structure of CDPMs can be classified with respect to the kinematic structure of the end-effector and the number of cables that can be used to actuate the system. The kinematic structure refers to the number and types of degrees of freedom the end-effector possesses. For example, consider the two different CDPMs shown in Figure 2.1. The manipulator in Figure 2.1(a) is not constrained to the stationary frame and possesses 6 degrees of freedom. Hence, the manipulator can be classified as a 6 DoF spatial manipulator. However, the manipulator in Figure 2.1(b) possesses only 3 degrees of freedom as the end-effector is constrained to the base frame by a spherical joint. Hence, the system can be referred to as a 3 DoF spherical joint CDPM.

In addition to rigid body kinematic structure of the CDPM, the number of cables that

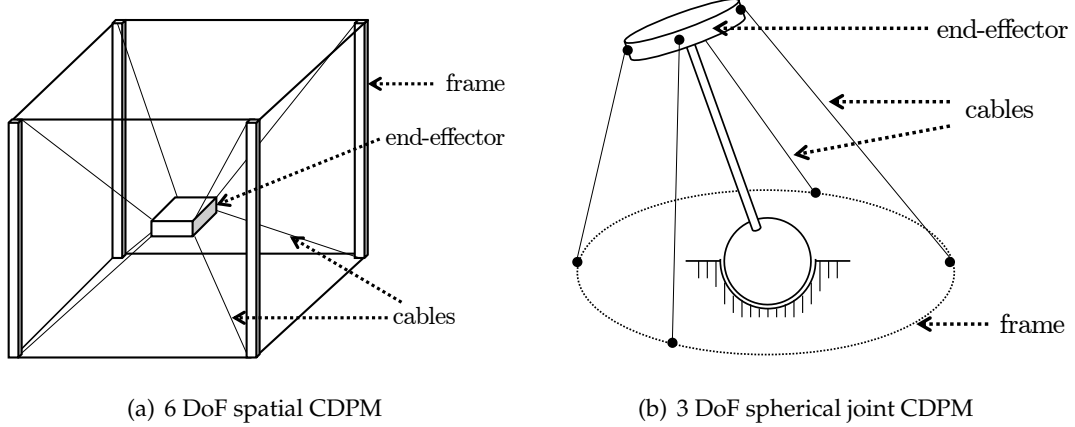


Figure 2.1: The kinematic structure of CDPMs can be classified by the degrees of freedom that the end-effector possesses. Hence, the manipulator shown in (a) can be classified as a 6 DoF spatial CDPM and that in (b) can be referred to as a 3 DoF spherical joint CDPM.

actuate the system is also used in classifying CDPMs. Due to the positive force constraint, an n DoF CDPM requires a minimum of $n + 1$ number of cables to produce wrench-closure in all of the degrees of freedom. Hence, an n DoF CDPM actuated by m cables can be classified as incompletely restrained when $m < n + 1$, completely restrained for $m = n + 1$ and redundantly restrained if $m > n + 1$ [86]. For example, the manipulator shown in Figure 2.1(a) is actuated by 8 cables and hence can be regarded as a 6 DoF 8 cable redundantly restrained spatial CDPM. It will be shown in this chapter that this classification is important in the study of CDPMs.

Due to the unique advantages and characteristics of CDPMs, cable-driven systems have found uses in a wide range of practical applications in the past decades. Additionally, the theoretical problems related to the various aspects of CDPMs have also been well studied. The works in the literature related to the applications and theoretical contributions of CDPMs will be described in Sections 2.2 and 2.3, respectively.

2.2 Practical Applications

From the early studies of CDPMs as robotic cranes, cable-driven robots have been employed in a wide range of different applications to exploit particular advantages that

are unique to CDPMs. In Section 2.2.1, the use of CDPMs as high speed manipulators that take advantage of the high payload to weight ratio is presented. In Section 2.2.2, CDPMs that operate within a large workspace environment are described. Examples of CDPMs used in medical applications are presented in Section 2.2.3. Finally, works related to the design and analysis of CDPMs as anthropomorphic bio-inspired structures are introduced in 2.2.4.

2.2.1 High-Speed Manipulators

The higher payload to weight ratio of CDPMs is contributed to by two factors. Firstly, the actuators used to produce force in the cables can be located on the stationary base, and secondly, the weight of the cables is typically much less than the end-effector weight. These properties make CDPMs attractive for applications that require the manipulator to be light in weight and high in speed [58, 59, 98, 121].

One well-known example of a high-speed CDPM is the FALCON robot [58, 59], developed by Kawamura *et al.*, a 6 DoF completely restrained CDPM. The end-effector is a duralumin rod of 1 m in length and with a mass of 150 g. Each cable is actuated by a 60W DC servomotor driven spool from the base frame. From the experiments, the manipulator under no payload was reported to achieve a peak speed of 13 m/s (46.8 km/h) and a peak acceleration of 421 m/s^2 (43g N).

Another application of high-speed lightweight CDPMs is in motion simulators. Due to the inherent lightweight structure, CDPMs are suitable for use as motion simulators since it is desired to have minimal impact from the dynamics of the actuating cables on the motion of the end-effector load. Examples of CDPM motion simulators include the completely restrained 6 DoF motion base for virtual sensation of acceleration developed by Tadokoro *et al.* [123], the 6 DoF spacecraft dynamics simulator by Ma and Diao [75], the completely restrained 3 DoF r^3 system developed by von Zitzewitz *et al.* for sport simulation, and the incompletely restrained 3 DoF virtual reality hang glider proposed by Karkoub *et al.* [57].

The advantages of CDPMs have also been exploited as wire crane robots. Examples include the 6 DoF cable-driven gantry robot for payload suspension proposed by Zheng

et al. [146] and the under restrained portable wire crane for rescue operations by Merlet and Daney [85]. Similarly, Oh and Agrawal *et al.* suggested the possibility of attaching a cable-driven crane onto the end of another manipulator [100] or a helicopter [102] to take advantage of the lightweight CDPM.

2.2.2 Large Scale Applications

Due to the transportability of cables and their ability to span large distances, cable actuation allows the possibility for CDPMs to have a large reachable workspace. In such applications, it would be difficult or in some cases not possible to use traditional serial and rigid link parallel manipulators to perform the task due to the required size of the manipulator and its workspace. Well known examples include the Skycam [25] and Cablecam [1], used in the recording of sporting events such as basketball and football competitions. In addition to the earlier works applying CDPMs as robotic cranes [25, 49, 117], CDPMs have been employed in a range of other large scale applications.

Bosscher, Williams and Tummino proposed the idea of using CDPMs in rapidly-deployable cable robot search and rescue systems [18]. The base frame consists of several support vehicles located on the perimeter of the site, forming the base frame containing the cable and spool. The 3 translational DoF end-effector was proposed to serve two main tasks: to search for survivors by attaching sensors on the end-effector and to deploy mobile robots at the survivor location to perform the rescue operation.

Similarly, Williams *et al.* proposed the Contour Crafting Cartesian Cable Robot (C^4 robot), a concept for use in building construction [16, 137]. The C^4 robot is a redundantly restrained 3 DoF translational CDPM actuated by 12 cables. In this concept, the stationary frame encapsulates the building to be constructed, and the end-effector is an extrusion system that deposits beads of concrete layer by layer. The C^4 concept allows the potential of robotic building construction to be plausible as it would be unrealistic to construct a serial robot on the order of magnitude of a building.

Another application of large scale CDPMs is to perform field environment measurements. The Five-Hundred Meter Aperture Spherical Radio Telescope (*FAST*) system proposed by Wang *et al.* is a CDPM of 500 m in diameter and carries an end-effector telescope

weighing 30 tonnes [62, 143]. Borgstrom *et al.* proposed the NIMS3D concept [14], a large scale 3 DoF CDPM to perform actuated sensing of the environment.

More recently, the CoGiRo robot developed by Gouttefarde *et al.* is a 6 DoF 8 cable CDPM that performs tasks such as pick-and-place trajectories over a large workspace [26, 64, 65, 97]. The CoGiRo robot has overall dimensions of 15 m (length) \times 11 m (width) \times 6 m (height) and a potential workspace of 677 m³. The cuboid mobile platform with a volume of 1 m³ is able to carry a payload of at least 300 kg over the entire workspace.

The primary challenge involved with large scale CDPMs is the modelling of cable sagging due to the non-negligible cable mass [62, 113]. This effect has significant impact on the dynamics and workspace of such manipulators. Furthermore, the elasticity of the cables due to long cable lengths must also be considered in the modelling and analysis of large scale CDPMs [12].

2.2.3 Medical and Haptic Applications

Cable-driven robots have been studied for medical and haptic applications, such as tele-operation, rehabilitation, exoskeleton and surgical procedures, as the lightweight cables will have a lesser impact on the dynamics of the end-effector. Also, the ease in the reconfiguration of the CDPM cable attachment locations allows flexibility in the operation and workspace of the manipulator. Furthermore, if compliance in the system is desired then elastic cables can be used.

Vilchis *et al.* proposed the use of a planar CDPM as a slave robot with an ultrasound probe for remote echographic examination [131]. Similarly, a range of CDPM haptic devices have been studied by groups such as Gallina *et al.* [36], Williams *et al.* [135], Ferraresi *et al.* [34] and Karkoub *et al.* [57]. The advantage of employing CDPMs as haptic devices is that the effect of the dynamics of the cable actuation is negligible when providing the force feedback to the user.

Another popular application for CDPMs is rehabilitation. Surdilovic *et al.* proposed the STRING-MAN concept [122], where cables are connected from the base frame to the body of the human patient as the end-effector. Rehabilitation is performed as the cables are actuated to assist the patient to perform the required motion exercises. The Multi-

Axis Cartesian-based Arm Rehabilitation Machine (MACARM) developed by Mayhew *et al.* is a redundantly restrained 6 DoF 8 cable CDPM. Gosselin *et al.* studied to use of two 6 DoF CDPM foot platforms as a locomotion interface for the purpose of virtual reality and rehabilitation of the human gait [103, 104].

Taking advantage of the anthropomorphic similarities between cable-driven mechanisms and musculoskeletal systems, Agrawal *et al.* developed the Cable-Driven Arm Exoskeleton (CAREX) rehabilitation exoskeleton robot [2, 3, 78, 79]. The CAREX robot does not restrict the natural degrees of freedom of the human arm as its cables actuate the cuffs that are attached to the shoulder, upper arm and forearm. The CAREX is a lightweight device weighing a mere 1.55 kg and hence is easily wearable. Additionally, the reconfigurability of the cable attachment locations allows optimisation of the manipulator workspace and also targetted treatment to perform specific trajectories. The initial prototype of the device was a 4 DoF 6 cable CDPM to actuate the 3 DoF motion of the shoulder and 1 DoF of the elbow of the human subject [2, 3, 78]. The CAREX robot was further developed to be a 5 DoF 7 cable CDPM [79], adding an additional degree of freedom for the pronation/supination motion of the forearm.

2.2.4 Development of Bio-Inspired Mechanisms

Due to the anthropomorphic similarities with musculoskeletal systems, CDPMs have been studied as bio-inspired mechanisms. For example, both cables and muscles are actuators that are only capable of providing unilateral actuation. Li and Rahn proposed and developed a prototype of a cable-driven continuous backbone [71]. The system is incompletely restrained where each cable is connected through multiple rigid link segments. Tendon-driven fingers and hands can also be regarded as a type of cable actuated bio-inspired manipulators [30, 52, 115].

Yang *et al.* proposed a lightweight and dexterous biologically inspired modular 7 DoF CDPM arm [23, 93, 141, 142]. Inspired by the human arm, the robotic arm consisted of three independent cable-driven modules: the shoulder, the elbow and the wrist, represented by spherical, revolute and spherical joints, respectively. The cables of the manipulator are divided into three sets, where there is one set for each module. Chen *et*

al. proposed a hybrid conventional driven and cable-driven arm [77] where the shoulder joint is directly driven by motors, and the elbow and wrist joints are cable-driven.

Cable-driven manipulators have also been developed as anthropomimetic robots for the study of musculoskeletal systems. The Eccerobot is a robotic musculoskeletal torso with the aim to replicate the inner structures of the human body, such as muscles, tendons, bones and joints [54,139,140]. The first generation Eccerobot, the ECCE-1 [80], featured 44 actuated cables to provide motion for the 45 degrees of freedom torso and upper limbs. The second version ECCE-2 robot introduced a more complex neck and head structure, and ECCE-3 further introduced a more complex spine structure and force sensor for each actuator. The final iteration of the Eccerobot, the ECCE-4, was mounted to a mobile base and consisted of 54 cable actuators as well as detailed human spine and shoulder girdle structures.

At the University of Tokyo JSK Robotics Laboratory, a family of cable-driven musculoskeletal humanoids have been developed by Nakanishi *et al.* The Kenta robot was the first generation robot of this family [88], and possessed a total of 81 degrees of freedom and 96 actuated cables. The robot consisted of several human-inspired subsystems: the head, spine, neck, legs and arm. The second generation robot Kotaro possessed 91 degrees of freedom [89], with a more human-like bone skeletal structure and improved muscle and sensor elements. For example, the Kotaro robot consisted of human-mimetic shoulder bladebones and collarbones. Furthermore, the reinforceable muscle concept was introduced on the Kotaro robot to allow easy reconfiguration of muscle attachment locations. The Kojiro robot further improved on both the aspects of actuator and sensor performances [87]. The Kenzo robot was an upper body humanoid robot that superseded the Kojiro. The design improvements resulted in the Kenzo robot having twice the joint power as Kojiro [95]. The Kenshiro robot, which is the most recent robot in the family, adopted a revised bone and joint structure that is more similar to the human anatomy [8,63].

In the biomechanics research community, the concept of modelling human muscles as segments of cable wires has been employed in the OpenSim software developed by Delp *et al.* [27, 28]. The platform allows the kinematics and dynamics of the motion

for musculoskeletal systems to be computationally simulated. Models for a range of musculoskeletal systems within the human body have been developed, such as the wrist [38], upper extremity [50], lower extremity [29], lumbar spine [24] and the neck [130]. The OpenSim platform allows for the inclusion of physiological muscle models, realistic bone geometry and realistic muscle paths such as muscle wrapping.

Similarly, the notion of modelling human muscles, tendons and ligaments as cable wires was used by Nakamura *et al.* to study the motion and dynamics of musculoskeletal systems [90, 94]. In [94], a simplified full body model of the human consisting of a total of 200 bones, 323 degrees of freedom and 547 wires was presented. Given the highly redundant nature of the system, the inverse dynamics problem was solved as a quadratic programming (*QP*) problem. The proposed objective function was to minimise the difference between the muscle, tendon and ligament forces and the muscle forces derived from biology-based methods, such as electromyography (EMG). Incorporating the Hill type physiological muscle into this model, real time estimation of muscle forces could be performed using a combination of motion capture system measurements, electromyography signals and force plate measurements [90].

2.3 Theoretical Problems

As described in Section 2.2, CDPMs have been used in a wide range of different applications due to their unique advantages. However, the positive cable force constraint has created a set of challenging and interesting problems in the analysis of CDPMs. In this section, three problems that are important in the study of CDPMs will be described. Firstly, the determination of positive cable forces required in the generation and control of motion for a specified trajectory is described in Section 2.3.1. In Section 2.3.2, the concept of workspace analysis for CDPMs is introduced, presenting the various types of workspaces specific to CDPMs. Finally, Section 2.3.3 describes the necessary conditions and methods for determining the wrench-closure workspace for CDPMs.

2.3.1 Resolution of Positive Cable Forces

The resolution of positive cable force required to achieve the desired motion for a CDPM is referred to as the *inverse dynamics* problem. The inverse dynamics problem for CDPMs is unique due to the actuation redundancy and positive cable force constraint of cable-driven mechanisms. The inverse dynamics problem is important to the study of CDPMs as it is required in the motion control of the manipulator to perform the desired trajectory. For an n DoF m cable CDPM, the equations of motion can be expressed in the form of

$$M(\mathbf{q})\ddot{\mathbf{q}} + \mathbf{C}(\mathbf{q}, \dot{\mathbf{q}}) + \mathbf{G}(\mathbf{q}) + \boldsymbol{\Gamma}_{ext} = -J^T(\mathbf{q})\mathbf{f}, \quad (2.1)$$

where $M \in \mathbb{R}^{n \times n}$, $\mathbf{C} \in \mathbb{R}^{n \times 1}$, $\mathbf{G} \in \mathbb{R}^{n \times 1}$ and $\boldsymbol{\Gamma}_{ext} \in \mathbb{R}^{n \times 1}$ represent the mass-inertia matrix, centrifugal and Coriolis force vector, gravity force vector and external wrench vector, respectively. The generalised coordinates $\mathbf{q} \in \mathbb{R}^{n \times 1}$ defines the pose of the manipulator. The forces for the cables can be expressed within cable force vector $\mathbf{f} = [f_1 \ \dots \ f_m]$, where $f_i \geq 0$ represents the force within cable i . The positive cable force constraint can be expressed as $\mathbf{f} \geq 0$. The transpose of the Jacobian matrix $J^T \in \mathbb{R}^{n \times m}$ represents the mapping between the cable forces and the resultant wrench that the cables generate on the end-effector of the system. For completely and redundantly restrained systems, where $m \geq n + 1$, the CDPM is redundantly actuated and J^T contains more columns than rows.

Due to the actuation redundancy, the inverse dynamics problem has been typically treated as an optimisation problem [15, 32, 46, 75, 99, 106, 124, 128]. In addition to satisfying the equations of motion (2.1) constraint, the optimisation problem must also ensure that the resulting cable forces are positive and within the bound $\mathbf{0} \leq \mathbf{f}_{min} \leq \mathbf{f} \leq \mathbf{f}_{max}$, where \mathbf{f}_{min} and \mathbf{f}_{max} are the minimum and maximum allowable cable forces, respectively.

Various techniques have been studied to solve the inverse dynamics optimisation problem. Simple objective functions to minimise are the 1-norm $\|\mathbf{f}\|_1$ and 2-norm $\|\mathbf{f}\|_2$ of the cable forces. Common approaches to solve the 1-norm and 2-norm objective functions are to use linear programming (*LP*) and quadratic programming (*QP*) solvers [15, 99, 106], respectively. However, other analytical approaches have also been studied. Hassan and

Khajepour generated the solution to the minimum 2-norm optimisation problem using Dykstra's projection method [46]. Taghirad *et al.* formulated and solved the convex optimisation problem using the Kurush-Kuhn-Tucker theorem and an analytic-interative approach [124].

The inverse dynamics cable force resolution is required in the implementation of controllers for CDPMs. The control problem is defined as the regulation of cable forces to achieve a desired trajectory $\mathbf{q}_r(t)$. Alp and Agrawal proposed and demonstrated two control schemes derived using the Lyapunov and feedback linearising controller approaches [5]. Using Lyapunov methods, the resulting control law can be expressed using the equations of motion from (2.1) as

$$\mathbf{G}(\mathbf{q}) + \boldsymbol{\Gamma}_{ext} - K_p \mathbf{q}_e - K_d \dot{\mathbf{q}} = -J^T(\mathbf{q})\mathbf{f}, \quad (2.2)$$

where $\mathbf{q}_e = \mathbf{q}_r - \mathbf{q}$ is the error in generalised coordinates, and $K_p, K_d \in \mathbb{R}^n$ are positive definite matrices for the gains. Using the computed-torque feedback linearisation method [5, 61, 137], another possible control law is

$$M(\mathbf{q})(\ddot{\mathbf{q}}_r - K_p \mathbf{q}_e - K_d \dot{\mathbf{q}}_e) + \mathbf{C}(\mathbf{q}, \dot{\mathbf{q}}) + \mathbf{G}(\mathbf{q}) + \boldsymbol{\Gamma}_{ext} = -J^T(\mathbf{q})\mathbf{f}, \quad (2.3)$$

where $K_p \in \mathbb{R}^n$ and $K_d \in \mathbb{R}^n$ are the proportional and derivative controller gains, respectively. Another control scheme was derived by Oh and Agrawal [101] using a sliding surface $\mathbf{s} = \dot{\mathbf{q}} + \Lambda(\mathbf{q} - \mathbf{q}_e)$, resulting in the sliding mode control law

$$M(\mathbf{q})(-\Lambda \dot{\mathbf{q}} - K \cdot \text{sgn}(\mathbf{s})) + \mathbf{C}(\mathbf{q}, \dot{\mathbf{q}}) + \mathbf{G}(\mathbf{q}) + \boldsymbol{\Gamma}_{ext} = -J^T(\mathbf{q})\mathbf{f}, \quad (2.4)$$

where $K, \Lambda \in \mathbb{R}^{n \times n}$ are diagonal matrices of constants.

It can be observed that regardless of the control law, such as (2.2), (2.3) or (2.4), the determination of the cable forces $\mathbf{0} \leq \mathbf{f}_{min} \leq \mathbf{f} \leq \mathbf{f}_{max}$ must be performed. This requires one of the inverse dynamics redundancy resolution schemes reviewed above, where the constraint introduced by the equations of motion is replaced by the control law.

2.3.2 Workspace Analysis

Workspace analysis refers to the generation of the operational region for a manipulator. Different types of workspaces can be generated depending on the desired conditions to define the manipulator as operational. For serial and rigid link parallel manipulators, these conditions are generally dependent on the kinematics of the system, such as mechanical limits on the joints, prevention of self-collision between the elements of the robot and non-singular poses of the manipulator. Dynamic workspaces can also be defined by the system's ability to generate motion or external forces given the actuation limits of the manipulator. Knowledge of the workspace is useful for several purposes, such as trajectory planning [129], and the selection and design of manipulator configurations depending on workspace requirements [104].

The workspace of manipulators are typically generated using two approaches, analytical and numerical techniques. Analytical approaches determine the geometric boundary and hence the workspace region by solving the equations that define the workspace. Numerical methods are typically point-wise evaluation techniques, where the search space is discretised and the workspace condition is evaluated at each point. Figure 2.2 shows two examples of the same workspace generated using analytical and numerical approaches, shown in Figures 2.2(a) and 2.2(b), respectively.

As observed in Figure 2.2(a), analytical methods provide a description of the complete region of the workspace, hence providing insights into its geometry. However, the disadvantage of analytical approaches is that the solution is typically either very complex or there may exist no explicit solution, depending on the type and structure of the manipulator. In comparison, numerical approaches provide only a local measure of the workspace at the evaluated points and hence suffers from the effects of discretisation, as shown in Figure 2.2(b). The accuracy of this approach is dependent on the interval width (*step-size*), where decreased width results in increased accuracy. The drawback of decreasing interval width is that the computational time will be significantly increased. Aside from purely numerical or analytical approaches, other methods such as hybrid analytical-numerical techniques [69] and interval analysis approaches [42, 44] have also been investigated to address some of the drawbacks of traditional approaches.

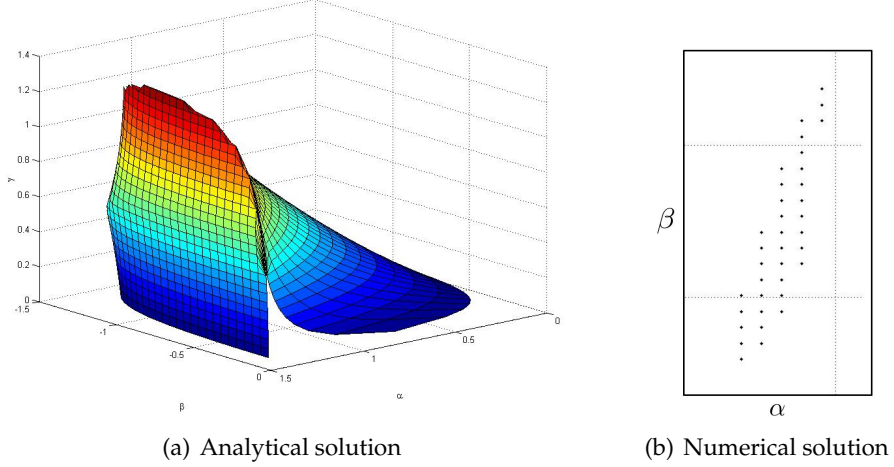


Figure 2.2: Examples of workspace for a 3 DoF manipulator generated using analytical and numerical approaches. (a) the 3D view of the workspace volume determined using the analytical approach. (b) the cross-section view of the discretised workspace generated using a numerical approach with uniform grid size.

In addition to the kinematic conditions such as cable to end-effector interference and cable to cable interference [7, 37, 105, 136], the positive force constraint unique to CDPMs must also be considered in the workspace analysis. The types of dynamic workspaces for CDPMs that have been studied include *static workspace* [73, 110], *wrench-feasible workspace* [17, 19, 42, 44, 107] and *wrench-closure workspace* [9, 31, 43, 47, 69, 73, 92, 107, 108, 120].

The static workspace of CDPMs refers to the set of poses in which the manipulator can achieve static equilibrium, defined as the ability of the manipulator to sustain its own weight under gravity force and no external wrenches. From the equations of motion (2.1), the static workspace SW can be mathematically expressed as

$$SW = \{\mathbf{q} : \mathbf{G}(\mathbf{q}) = -J^T(\mathbf{q})\mathbf{f}, \exists \mathbf{f} \in [\mathbf{0}, \mathbf{f}_{max}]\} . \quad (2.5)$$

The static workspace condition from (2.5) can be regarded as the basic criteria for a CDPM to be regarded as operational, where the cables are able to sustain the manipulator's own weight. However, there is no guarantee that the manipulator is able to produce motion between any two or even adjacent points within the static workspace. As a result, the static workspace can be regarded as an over estimation of the workspace that can be

reached by the CDPM.

In comparison, the *wrench-feasible workspace* (*WFW*) for a CDPM refers to the set of poses for which a specified set of external wrenches, velocities, and accelerations, can be satisfied with a given range of positive cable forces. Mathematically, the wrench-feasible workspace *WFW* can be defined as

$$WFW = \{ \mathbf{q} : \forall \mathbf{w} \in \mathcal{B} \exists \mathbf{f} \in [\mathbf{f}_{min}, \mathbf{f}_{max}], \mathbf{w} = -J^T(\mathbf{q})\mathbf{f} \}, \quad (2.6)$$

where $\mathbf{w} = -[M(\mathbf{q})\ddot{\mathbf{q}} + \mathbf{C}(\mathbf{q}, \dot{\mathbf{q}}) + \mathbf{G}(\mathbf{q}) + \boldsymbol{\Gamma}_{ext}]$ according to (2.1). The set $\mathcal{B} \in \mathbb{R}^n$, where n is the number of degrees of freedom of the system, represents the wrench exertion requirements that the manipulator must be able to generate to be regarded as operational. The complexity in validating the workspace condition (2.6) is highly dependent on the definition of \mathcal{B} .

Bosscher *et al.* derived the analytical solution of the WFW boundaries for both planar CDPMs and incompletely restrained spatial point-mass CDPMs [17]. For a planar CDPM with \mathcal{B} defined as a polyhedral, it was shown that the analytical solution for the lower force boundary was a multivariate second order polynomial equation. Assuming that the upper force limits of the cables were large, the solution to the upper boundary could not be explicitly determined. For a spatial point mass CDPM, assuming that \mathcal{B} is a sphere of known radii, the lower force boundary was found to be a multivariate fifth order polynomial equation with 56 terms and coefficients. Similar to the planar CDPM, the upper boundary was found to be too complex to be analytically described. The disadvantage of the analytical approach is the limitations on the types of \mathcal{B} allowed and the complexity of the solution. Bouchard, Gosselin and Moore proposed a more generic geometry-based method to generate the WFW of redundantly restrained CDPMs [19]. The wrench-feasible condition was verified by checking that the wrench requirements \mathcal{B} is a subset of the wrench that can be generated by the CDPM. The types of wrench requirements allowed by the method were for a point wrench, a convex polytope and an ellipsoid.

To allow a wider range of wrench requirements to be considered, numerical approaches to generate the WFW of CDPMs have also been studied. Gouttefarde, Merlet and Daney

used interval analysis to generate the WFW for any arbitrarily defined set \mathcal{B} [44]. Loloei, Aref and Taghirad determined the WFW for a 6 DoF spatial manipulator using a linear matrix inequalities approach [74]. The primary disadvantages involved with numerical approaches to generate the WFW for CDPMs are their high computational costs and the requirement to define \mathcal{B} .

2.3.3 Wrench-Closure Workspace and Necessary Conditions

The *wrench-closure workspace* (WCW) is a well studied type of workspace analysis for CDPMs. The WCW is defined as the set of poses in which the manipulator can sustain any arbitrary external wrench when no upper bounds are placed on the cable forces. Mathematically, the *wrench-closure condition* (WCC) is satisfied at pose \mathbf{q} if and only if

$$\text{WCC}(\mathbf{q}) \Leftrightarrow \forall \mathbf{w} \in \mathbb{R}^n, \exists \mathbf{f} \geq 0 : \mathbf{w} = J^T(\mathbf{q})\mathbf{f}, \quad (2.7)$$

where $\mathbf{w} = -[M(\mathbf{q})\ddot{\mathbf{q}} + \mathbf{C}(\mathbf{q}, \dot{\mathbf{q}}) + \mathbf{G}(\mathbf{q}) + \Gamma_{ext}]$. From the WCC, the WCW can be expressed as

$$\text{WCW} = \{\mathbf{q} : \forall \mathbf{w} \in \mathbb{R}^n, \exists \mathbf{f} \geq 0 : \mathbf{w} = J^T(\mathbf{q})\mathbf{f}\}. \quad (2.8)$$

If pose \mathbf{q} satisfies (2.7), then the CDPM is capable of producing motion to any adjacent poses. As a result, the WCW can be used in the generation of a trajectory between a start and end pose. By constructing a path that lies within the WCW, the trajectory can be performed by the CDPM while satisfying the positive force constraint. Additionally, the WCW can also be used in the design process of CDPMs. As shown by Lau *et al.* [68], the attachment locations of the cables for CDPMs can have a significant impact on the size and shape of the WCW. In [68], the WCW about a desired pose was optimised by selection of cable attachment locations.

Compared with the wrench-feasible workspace (WFW), the WCW is a more convenient workspace definition. The WCW can be regarded as a more general workspace definition than the WFW as the wrench exertion requirement \mathcal{B} is the entire space \mathbb{R}^n . Since $\mathcal{B} = \mathbb{R}^n$ is unbounded, the allowable range of cable forces is relaxed to have no upper bound ($\mathbf{f} \geq 0$). The WCW is a more convenient workspace definition than the

WFW since no specific requirement on the wrench exertion is required.

The geometrical interpretation of (2.7) is that the WCC is satisfied if the columns of J^T positively span \mathbb{R}^n for full rank J^T . An equivalent definition of the WCC is the existence of some positive cable force vector within the nullspace of J^T [43], where

$$\begin{aligned} \text{rank}(J^T) &= n \\ \exists \mathbf{f} \in \ker(J^T) : \mathbf{f} > 0 . \end{aligned} \quad (2.9)$$

The positive spanning problem for the WCW can be solved by various approaches. Gouttefarde and Gosselin derived the analytical solution for completely and redundantly restrained planar CDPM with 4, 5 or 6 cables [43]. To satisfy the WCC for a four cable planar CDPM, three linearly independent column vectors $\{\mathbf{w}_1, \mathbf{w}_2, \mathbf{w}_3\}$ were selected from J^T to form a convex polyhedral cone $\mathcal{C} = \{-\mathbf{w}_1, -\mathbf{w}_2, -\mathbf{w}_3\}$, and the remaining vector must lie inside \mathcal{C} . The five and six cables cases were also solved using this concept. The resulting WCW boundary was found to be in the form of a set of second degree conic sections of two variables. In a similar manner, Stump and Kumar performed the analytical study of the WCW for both planar and spatial manipulators [120]. It is worth noting that using analytical approaches, the WCW must be derived independently for each type of CDPM structure.

Numerical approaches are more generic and do not assume any particular type of CDPM structure. Pham *et al.* proposed an algorithm that recursively decomposed an n DoF m cable system to a set of $\frac{m!}{[m-(n-1)]!}$ single DoF \mathbb{R}^1 systems [107, 108]. The WCC is then satisfied if all of the subsystems satisfy wrench-closure by consisting of both positive and negative components. Lim *et al.* developed a numerical approach to generate the WCW by checking whether the linearly independent columns of J^T formed a convex hull around the origin [73].

Diao and Ma proposed a numerical approach for completely restrained systems by performing row reduction on the transpose of the Jacobian matrix [31]. Assuming that J^T is of full rank, the $n \times (n + 1)$ transpose of the Jacobian matrix can be expressed in

reduced row echelon form

$$J^T \rightarrow \left[\begin{array}{c|c} I_{n \times n} & \mathbf{v}(\mathbf{q}) \end{array} \right], \quad (2.10)$$

where $I_{n \times n}$ is the $n \times n$ identity matrix and $\mathbf{v}(\mathbf{q}) \in \mathbb{R}^n$ is a function of the pose variables. Applying the row reduction from (2.10) on the WCC in (2.7) resulted in

$$\left[\begin{array}{c|c} I_{n \times n} & \mathbf{v}(\mathbf{q}) \end{array} \right] \mathbf{f} = \mathbf{w}', \mathbf{f} \geq \mathbf{0} \quad (2.11)$$

where \mathbf{w}' is the wrench vector after row reduction. It can be shown that WCC is satisfied if and only if all components of $\mathbf{v}(\mathbf{q})$ from (2.11) are negative. This proof can be found in Appendix A. Using this necessary and sufficient condition on wrench-closure, Lau *et al.* proposed a hybrid analytical-numerical approach to study the WCW for completely restrained CDPMs [69]. For an n DoF system, $n - 1$ of the generalised coordinates were discretised and assumed to be constant for a particular pose. The WCC can then be expressed as a set of univariate inequalities with respect to the remaining variable. It was shown for a 3 DoF spherical joint manipulator and a 6 DoF spatial manipulator that the WCW can be expressed as 6th degree and 3rd degree univariate polynomial equations, respectively. The details and results for this approach have been included in Appendix A. The proposed hybrid approach combines the high accuracy of the analytical approach and the algorithmic versatility of the numerical approach. Additionally, this is achieved with significantly lower computational costs compared to numerical methods.

From the previous studies, it could be observed that the analysis of the WCW is a challenging and important problem for CDPMs. As a result, the ability for a CDPM to achieve wrench-closure is regarded as an important property of the system. For single link CDPMs, a well established necessary condition for wrench-closure is the Caratheodory theorem.

Caratheodory Theorem: If a set $X = \{\mathbf{v}_1, \mathbf{v}_2, \dots, \mathbf{v}_k\}$ positively spans \mathbb{R}^n , then $k \geq n + 1$.

As a result, a minimum of $m = n + 1$ cables is required to actuate an n DoF CDPM.

Mathematically, this necessary condition can be expressed as

$$\exists \mathbf{q} : WCC(\mathbf{q}) \Rightarrow m \geq n + 1. \quad (2.12)$$

It should be noted that (2.12) only represents a necessary but not the sufficient condition for WCC. The sufficient condition for WCC is dependent on the structure of the manipulator and attachment locations of the cables. Although the study of necessary conditions on the number of cables is trivial for a single link CDPM, it will be shown in Section 2.4 that for multilink cable-driven manipulators additional requirements on the distribution of the cable attachments exist.

2.4 Multilink Cable-Driven Manipulators

Since the early developments of CDPMs, the majority of cable-driven robots that have been studied are *single link CDPMs*, where a single rigid body (*end-effector*) is actuated by cables driven from the base frame, as shown in Figure 1.1(a). The design of this type of arrangement is typically not compact as the base frame is required to fully encapsulate the desired manipulator workspace. Additionally, this configuration suffers from cable-to-cable interference [103, 138], particularly as the number of cables increases. Another class of cable actuated manipulators is cable-driven capstan mechanisms, where the joints of the manipulator are driven by cables through capstan pulleys [30, 52, 76, 115]. Advantages of this type of mechanism include its compact design and reduction of weight and inertia as the actuating motors are situated on the base platform.

In recent years, multilink cable-driven manipulators (*MCDMs*) have been studied. As shown in Figure 1.1(b), MCDMs can be regarded as a more general form of capstan mechanisms, where the rigid bodies are actuated by cables in parallel and the cables can be arbitrarily connected through one or more of the manipulator links. This class of mechanisms benefits from the compactness of serial mechanisms, and the actuation and reconfigurability of cable-driven manipulators. Additionally, compared with single link CDPMs, MCDMs can be regarded as being more anthropomorphic in nature, where the rigid bodies and cables are structurally analogous to bones and muscles, respectively.

2.4.1 Modelling of Multilink Cable-Driven Manipulators

As demonstrated in Section 2.3, the analysis of any CDPM requires the kinematic and dynamic models to be established. For MCDMs, the primary challenge in the modelling of this class of systems is the complexity involved in the cable routing. Cable routing refers to the path in which a cable is connected to the links of the manipulator. In the studies of single link CDPMs, there exists only one type of cable routing, where the cable is connected from the motorised spool at the stationary base frame to the end-effector. However, for MCDMs each cable may connect through one or more links of the manipulator. Figure 2.3 shows three examples of the possible types of cable routing for a 2 link MCDM.

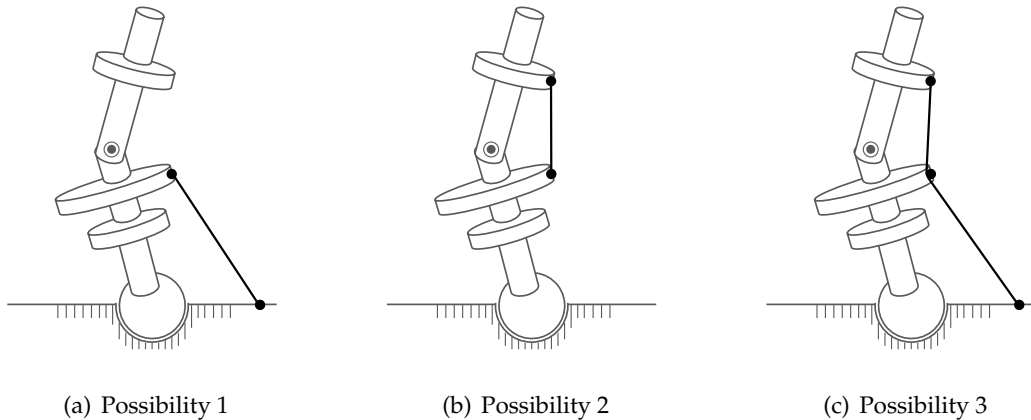


Figure 2.3: Three different types of cable routing for multilink cable-driven manipulators.

Several features can be observed in the cable routing for MCDMs. Firstly, cables are not necessarily attached to the base frame, as shown in Figure 2.3(b). Secondly, a single cable can be attached to multiple links of the manipulator, as shown in Figure 2.3(c). Finally, there exists a number of different combinations of cable routing for MCDMs. *Arbitrary cable routing* refers to the complete set of possible cable routings. Allowing arbitrary cable routing creates two unique challenges in the modelling and analysis of this class of manipulators. Firstly, the links of the manipulator become highly coupled as cables pass through multiple links. Secondly, the number of possible combinations in cable routing that can exist increases exponentially as the number of links increase. The

previous studies in MCDMs have tackled this modelling problem in different ways.

Figure 2.4 shows the 7 DoF cable-driven humanoid arm developed by Yang *et al.* [23, 93, 141, 142]. The design consists of three independent modules with spherical (S), revolute (R) and spherical (S) joints to represent the joints for the shoulder, elbow and wrist, respectively. Since the design uses 14 cables to actuate the rigid body structure, the MCDM can be regarded as a 14 cable SRS MCDM.

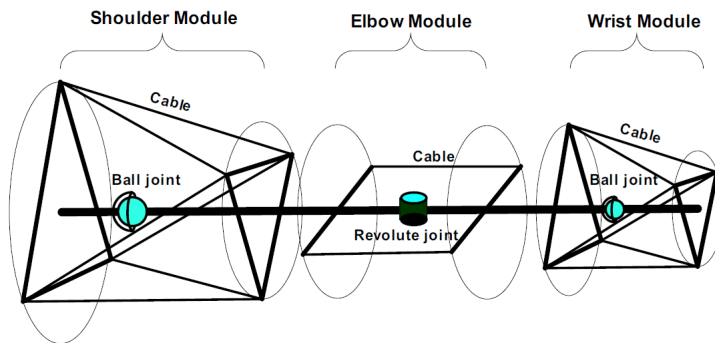


Figure 2.4: 7 DoF modular MCDM arm developed by Yang *et al.* [23, 93, 141, 142].

In this design, each cable provides actuation to only one of the links as each cable is only attached to the immediate link above and below the joint. As a result, no cables provide actuation to multiple links of the manipulator. In this arrangement, the MCDM can be regarded as being equivalent to three independent single link CDPMs connected in series. For example, the cables that actuate the wrist module do not produce any resultant motion on the elbow module as both ends of the cable produce equal and opposite forces on the elbow joint. Under this design, an MCDM with p joints only possesses a total of p types of cable routing. Furthermore, the actuation of the joints in the system are decoupled. As a result, the modelling and analysis for this type of MCDM structure would be identical to that of single link CDPMs.

Another example of an MCDM with a specified set of cables and cable routing is the CAREX exoskeleton developed by Agrawal *et al.* [2, 3, 78, 79]. As shown in Figure 2.5, the exoskeleton is actuated by cables that are spooled from the base frame to actuate the shoulder and elbow joints of the patient to carry out upper limb rehabilitation tasks.

The key feature of this exoskeleton is that the cables actuate cuffs that are attached

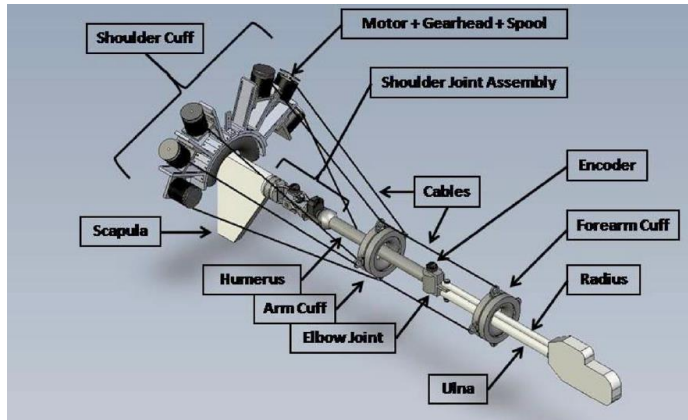


Figure 2.5: Upper limb 2 link exoskeleton developed by Agrawal *et al.* [2,3,78,79].

to the arm of the human subject. As a result, the skeleton of the human forms the rigid links of the MCDM. The CAREX exoskeleton is actuated by a total of 7 cables. To locate all of the motors on the base platform, the CAREX was designed with only two types of cable routing. Four of the cables are connected from the base shoulder cuff to the arm cuff, providing actuation to the shoulder joint. The remaining three cables route from the base to the forearm cuff via the arm cuff. The primary function of the cables attached to forearm is to provide actuation to the elbow joint and the pronation and supination motion of the forearm. However, as the cables also pass through the arm cuff, the actuation of the arm and forearm cuffs become coupled. As a result, the cables that are connected only to the arm cuff must resist and overcome the force induced by the cables when actuating the forearm cuff.

On the theoretical side, Rezazadeh and Behzadipour performed studies on the modelling and analysis of p link MCDMs [111,112]. As shown in Figure 2.6, it was assumed that the cables of the MCDM were connected directly from the base to any one of the links.

In [112], the system dynamics for the p link open-chain manipulator was formulated using the Lagrange approach. Assuming that the cables were connected directly from the base to one of the links, only p different types of cable routing for each cable were identified and modelled. The resulting modelling and analysis of this type of MCDM is simplified as only a subset of the arbitrary cable routing is considered.

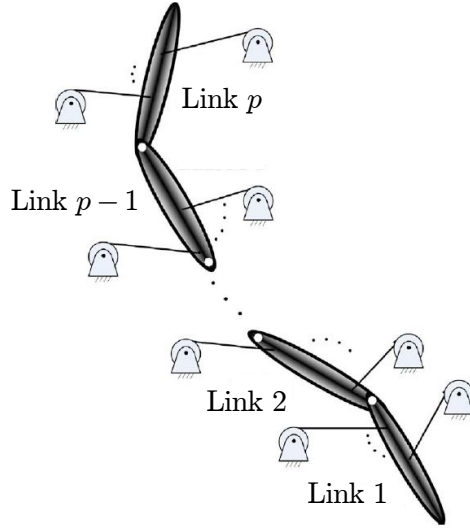


Figure 2.6: p link MCDM with single segment cables studied by Rezazadeh and Behzadipour [111, 112].

More recently, studies of MCDMs that allowed for arbitrary cable routing were performed by Mustafa and Agrawal [91, 92]. The equations of motion for a p link MCDM allowing for arbitrary cable routing was formulated using reciprocal screw theory. The formulation was demonstrated on two example manipulators, a 4 cable 3 link revolute joint (3R) planar manipulator and a 7 cable 3 link spherical-revolute-universal (SRU) spatial manipulator. Figure 2.7 shows the 3R manipulator with 2 different types of cable arrangements demonstrating that arbitrary cable routing can be modelled. The work considered arbitrary cable routing and allowed cables to pass through multiple links. The equations of motion were generated by superimposing the reciprocal screws expressed for each link and each type of cable routing. In this approach, each type of cable routing must be individually modelled when deriving the dynamic model. As a result, the effort and complexity of modelling increases with the number of links in the system.

2.4.2 Analysis of Multilink Cable-Driven Manipulators

Section 2.3 described the various types of analyses that have been studied for single link CDPMs. However, due to the more complex cable routing and coupled actuation, some of these problems and methods must be extended in order to study MCDMs. For ex-

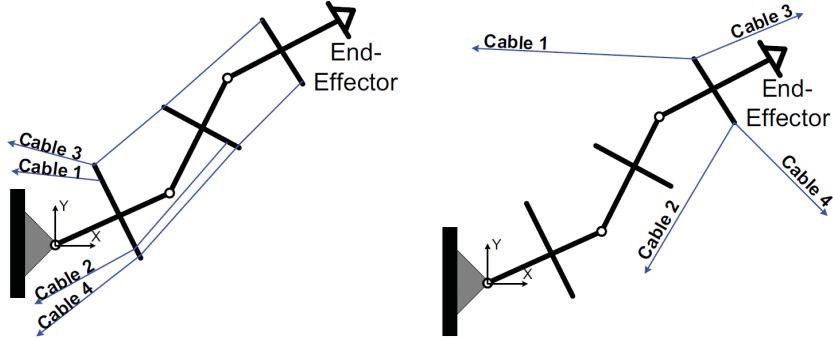


Figure 2.7: 3 link 3R MCDM model with two example arrangements of cable routing demonstrating arbitrary cable routing studied by Mustafa and Agrawal [91, 92].

ample, the study of wrench-closure workspace and the necessary conditions to achieve wrench-closure.

In [112], the analytical solution to the wrench-closure workspace was derived for a 2 link 2 DoF planar manipulator. The workspace was generated for both completely and redundantly restrained cases by analysing the cable actuation null space. This type of approach becomes significantly more complex as the number of links, degrees of freedom and types of cable routing increase. Furthermore, it was shown that different types of cable routing distribution produces significantly different workspace shape and size. Using the generalised modelling approach that allowed for arbitrary cable routing [91], the force closure conditions for MCDMs were derived using reciprocal screw theory in [92].

For single link CDPMs, there exists only a single path in which cables can route to the end-effector. As a result, only the attachment locations of the cables on the base and on the end-effector govern the resulting manipulator workspace. In [91], it was shown that for an m cable n DoF p link MCDM, the minimum number of cables required in satisfying wrench-closure is $m = n + 1$. This condition on the minimum number of cables is identical to that stated for single link CDPMs. However, in addition to the minimum number of cables, it was shown that the distribution of cables (cable routing) must also be considered [92, 111]. It was shown that for particular combinations of cable routing,

the resulting manipulator is incapable of producing wrench-closure for any manipulator pose. As described in Section 2.3.3, the ability to produce wrench-closure is regarded as an important property for CDPMs.

As a result, the necessary conditions on the routing of cables to achieve wrench-closure is a unique and important problem for MCDMs. It was shown in [111] that for a p link system, there exists at most $2^{6p} - 1$ necessary conditions on the distribution of cables that must be satisfied for wrench-closure. To decrease the number of conditions necessary for wrench-closure, it was assumed in [111] that each cable is connected from the base to only *one* of the manipulator links.

The conditions in presented [111] were demonstrated on a planar 3 link manipulator example. As shown in Figure 2.8, link 2 is connected to link 1 through a revolute joint, and similarly link 3 is connected to link 2 via a revolute joint. As a result, the system possesses 5 degrees of freedom with the generalised coordinates $\mathbf{q} = [x \ y \ \theta_1 \ \theta_2 \ \theta_3]^T$, where x and y represent the translational position of link 1, and angles θ_1 , θ_2 and θ_3 represent the orientation of links 1, 2 and 3, respectively.

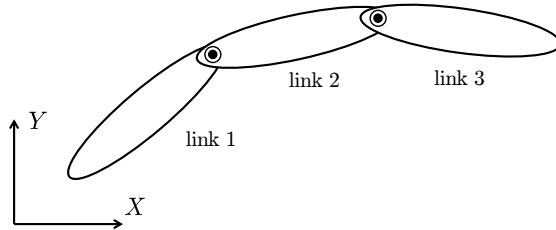


Figure 2.8: 3 link 5 DoF planar MCDM example studied by [111].

Denoting the number of cables attached to link 1, 2 and 3 as m_1 , m_2 and m_3 , respectively, [111] derived a set of necessary conditions required to satisfy the wrench-closure condition. For the entire system, the trivial necessary condition can be expressed as

$$m = m_1 + m_2 + m_3 \geq n + 1 = 6. \quad (2.13)$$

Considering the system as two 2 link subsystems, additional necessary conditions can be

derived as

$$\begin{aligned} m_1 + m_2 &\geq 3 \\ m_2 + m_3 &\geq 3. \end{aligned} \quad (2.14)$$

Finally, the consideration of the three single link subsystems results in the conditions

$$\begin{aligned} m_1 &\geq 2 \\ m_2 &\geq 0 \\ m_3 &\geq 2. \end{aligned} \quad (2.15)$$

The 6 necessary conditions from (2.13), (2.14) and (2.15) on the distribution of cables must be satisfied for wrench-closure to be achieved for the 3 link planar MCDM. Figure 2.9 shows two examples of cable distribution that satisfies the 6 necessary conditions. On the contrary, if any of the conditions from (2.13), (2.14) or (2.15) are not satisfied, then the manipulator is unable to satisfy wrench-closure.

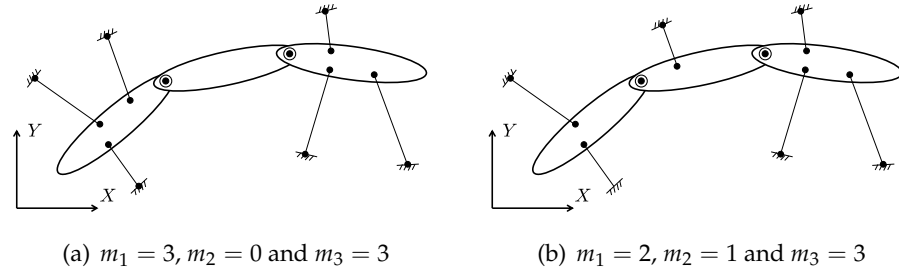


Figure 2.9: Two distributions of cables that generate wrench-closure for the 3 link 5 DoF planar MCDM example studied by [111]. In (a), three cables are attached to both links 1 and 3. In (b), two cables are attached to link 1, one cable is attached to link 2, and finally 3 cables are attached to link 3.

2.4.3 Study of Biomechanical Systems

Since the first cable-driven robot proposed by Landsberger [66], CDPMs have been regarded as bio-inspired manipulators due to their structural and actuation similarities. In past studies, robotic MCDMs that possess a anthropomorphic structure have been devel-

oped by Yang *et al.* [23, 93, 141, 142] and Agrawal *et al.* [2, 3, 78, 79]. However, to the best of the author's knowledge, the use of analysis tool and techniques developed for MCDMs, such as workspace analysis, to study biomechanical systems have not been reported in the literature.

Two primary differences exist between the previously studied MCDMs and biomechanical systems. Firstly, musculoskeletal systems are branched open-chain mechanisms that possess many different types of complex muscle-routing. Hence, the ability to model MCDMs that allows arbitrary cable routing is required in studying biomechanical systems as MCDMs. Furthermore, previous studies have only considered MCDMs with serial open chain kinematic structure. Secondly, the actuation dynamics between cables and muscles are significantly different. Traditionally, the cables for CDPMs have been modelled as massless rigid links that are capable of producing a fixed range of force. This range is also invariant through all manipulator poses. In comparison, the actuation ability of physiological muscles is dependent on the length of the muscle.

One commonly accepted model of the physiological muscle is the *modified Hill-type model* [145], consisting of tendon and muscle elements connected in series, as shown in Figure 2.10. Tendons are passive elements where the tendon force is a function of the tendon strain, while muscles can behave either as passive or active elements depending on their length.

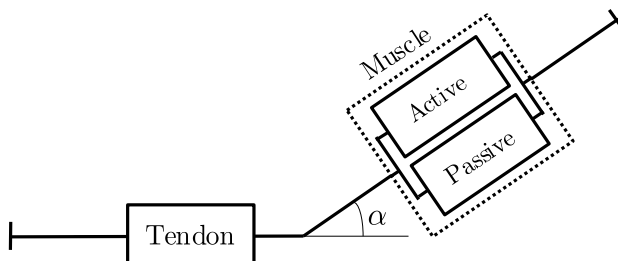


Figure 2.10: The modified Hill-type muscle-tendon model consists of two elements arranged in series: the muscle element and tendon element.

In the Hill-type model, the tendon and muscle force relationships can be modelled by generic relationships. The generic relationships are described with respect to five physiological muscle properties that define the muscle-tendon: peak isometric muscle force,

optimal muscle fibre length, optimal muscle fibre pennation angle and maximum shortening velocity. The force relationships are typically described by splines or analytical expressions that fit experimental data [81, 132]. Figure 2.11 shows the analytical force curve for an example muscle, where it can be observed that the range of force that can be produced by the muscle is dependent on its length.

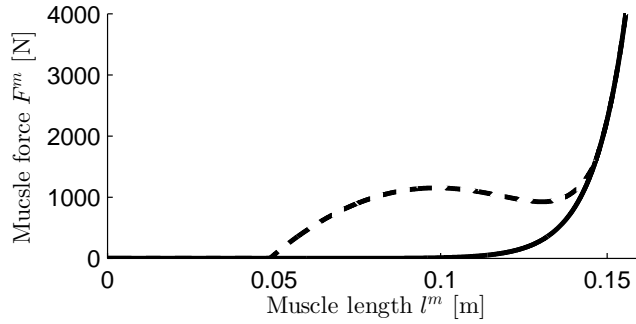


Figure 2.11: The muscle force curve for an example muscle to demonstrate the varying force range with muscle length. The dashed and solid lines represent the maximum and minimum force that the muscle can produce.

Due to the differences between MCDMs and biomechanical systems, techniques developed to analyse cable-driven robots cannot be directly applied onto the analysis of musculoskeletal systems. However, the concept of a wire actuation model to represent muscles have been widely accepted in both the biomechanics [24, 27–29, 38, 50, 130] and robotics [90, 94] communities. These studies have focused on the motion and dynamics of musculoskeletal systems.

Although the kinematic and dynamic analyses are most commonly studied to understand human motion, the range of motion and muscle function identification has also been studied in the biomechanics community. The range of motion refers to the limit in which the musculoskeletal system can physically reach. In biomechanics, the range of motion has been investigated either experimentally or through the simulation of trajectories. Experimental techniques are performed *in vivo* using sensor systems, such as vision systems [48] or motion sensors [13, 55, 83], to record the motion of human subjects performing prescribed or random trajectories. There are two major limitations in this experimental approach. Firstly, the recorded motion only represents a subset of the

true operational region, since poses that are not observed do not imply that they are unreachable by the subject. Secondly, this approach does not allow the effects of changes in muscle properties and their attachment locations on the operational region to be predicted. Existing simulation tools for biomechanics focus on simulating the dynamics for defined trajectories. Despite allowing the possibility to simulate the effects of modified muscle properties and attachment locations, existing simulation tools are unable to perform workspace analysis to determine the operational region with respect to the system poses.

Workspace analysis for such systems addresses the issues involved with existing techniques in studying the range of motion of musculoskeletal systems. Firstly, the complete workspace can be computationally determined with respect to the set of system poses, and is not dependent on a sample set of specific trajectories. Secondly, the computational approach allows for the contributions and effects of different muscles to be simulated and observed.

Musculoskeletal workspace analysis can be beneficial for a range of applications in rehabilitation robotics and biomechatronics. In the treatment of post-stroke rehabilitation, the understanding of muscle contributions to the reachable workspace would eventually allow more targeted rehabilitation treatment of motion impairment. Furthermore, in tendon-transfer surgery, the effects of muscle relocation can be computationally simulated. This surgery is performed to help recover the lost range of motion in a subject, for example due to a shoulder rotator-cuff tear.

2.5 Conclusion

In this review of the literature, the current state-of-the-art studies involved with CDPMs have been described. Replacing the rigid links of parallel manipulators with cables, CDPMs possess the advantages of a high payload to weight ratio, ability for the CDPM to possess a large reachable workspace and the ease in cable attachment reconfiguration. As a result, CDPMs have been studied for a range of unique applications. The positive force constraint of cables and the required actuation redundancy creates chal-

lenging problems in the actuation, control and workspace analysis for CDPMs. Taking advantage of the bio-inspired design, the study of MCDMs has strong potential and applications for both engineered and biomechanical systems. However, several key issues remain unsolved in the study of MCDMs. Firstly, the lack of a generalised model that allows for both arbitrary cable routing and systems with a large number of links limits the study of more complex structured MCDMs. Secondly, branched open-chain mechanisms naturally appear, such as in musculoskeletal systems. Previous studies have only considered serial open-chain MCDMs. Thirdly, the types of analyses performed on MCDMs typically do not consider arbitrary cable routing. Finally, previous studies in CDPMs and MCDMs typically assume the ideal cable model, where cables actuate within a fixed range. As a result, the use of MCDM models and analysis techniques to further understand musculoskeletal systems have been limited. The ability to study biomechanical systems as MCDMs would enrich and complement existing experimental approaches, such as studies in the range of motion and muscle function.

This page is intentionally left (almost) blank.

Part I

Modelling of Multilink Cable-Driven Systems

Introduction to Part I

IN this part, the modelling of the kinematics and dynamics for generalised multilink cable-driven manipulators (MCDMs) will be formulated. The key characteristics of the proposed model is that it allows any number of links and cables, arbitrary joint types and arbitrary cable routing to be modelled within a single formulation. The primary advantage in deriving a model allowing for arbitrary joints and cable routing is that modelling and analysis for any system structure can be performed with respect to the single generalised model. Furthermore, any changes to the kinematic structure or cable routing would not require reformulation of the MCDM model.

To introduce and motivate the challenges involved in the modelling of cable-driven manipulators, Chapter 3 presents the kinematic and dynamic models for three specific manipulator examples: a 3 degree-of-freedom (*DoF*) single link manipulator, a 6 DoF spatial manipulator, and a 4 DoF two link manipulator. The specific examples serve as a background to the modelling and analysis of the proposed generalised model in this thesis. Chapter 4 describes the cable-routing matrix (CRM) that represents the relationship between the attachment of the cables and links of the manipulator. It will be shown that the CRM allows all possible cable routing to be expressed within a single model in Chapter 5. The generalised model allows the analysis of branched open-chain structured MCDMs to be performed on a single model.

To illustrate the simplicity and flexibility of the proposed CRM and the generalised MCDM model, the kinematics and dynamics for two example multilink cable-driven systems are presented: a simple two link 4 DoF 6 cable system and a more complex system 8 link 24 DoF 76 cable manipulator. The 8 link mechanism represents the model of a human neck, and demonstrate that musculoskeletal systems can be modelled as MCDMs. The presented examples serve to illustrate the ability for the proposed formulation to model arbitrarily complex engineered and biomechanical systems. The generalised model forms the foundation for the analysis of MCDMs in the subsequent parts.

This page is intentionally left (almost) blank.

Chapter 3

Introduction to Cable-Driven Parallel Manipulators

This chapter serves as an introduction to cable-driven parallel manipulators (CDPMs). It is intended for readers who have background knowledge in robotic manipulators to understand and appreciate the different challenges involved with CDPMs. Firstly, Section 3.1 introduces some of the notations required in the modelling of CDPMs. Secondly, Section 3.2 describes the different types of problems associated with the kinematic and dynamic analyses of CDPMs. Section 3.3 presents the modelling of several specific example CDPMs to motivate the need for a generalised model, particularly for multilink cable-driven systems. Finally, Section 3.4 summarises and concludes the chapter.

3.1 Introduction

Regarded as a subclass of parallel mechanism, cable-driven parallel mechanisms (CDPMs) are characterised by the use of lightweight cables in place of the rigid legs of traditional parallel manipulators. A unique characteristic of CDPMs is that cables can only provide unilateral action (*positive cable force constraint*), where it can only pull but not push on the end-effector. As a result, CDPMs require actuation redundancy to produce motion in all of the system degrees of freedom, otherwise known as the ability to achieve *wrench-closure*. Therefore, an n degree-of-freedom (*DoF*) system actuated by m cables requires a minimum of $m \geq n + 1$ cables to achieve wrench-closure. Furthermore, a CDPM can be classified as incompletely restrained when $m < n + 1$, completely restrained for $m = n + 1$ and redundantly restrained if $m \geq n + 1$ [86].

In this thesis, the study will focus on completely and redundantly restrained systems. The positive cable force constraint and actuation redundancy of CDPMs result in a range

of unique challenges in the analysis of this class of systems, such as kinematic analysis, dynamic analysis, workspace analysis and control. To perform analysis on the system, the model for the kinematics and dynamics of the system must first be derived.

In the modelling of CDPMs, it is convenient to represent the state of the system through different sets of coordinate spaces. For an n DoF system, the *joint space* $\mathbf{q} \in \mathbb{R}^n$ represents the set of generalised coordinates that uniquely describe the *pose* of the manipulator. The *cable space* contains the cable kinematics (*cable lengths*) and cable dynamics (*cable forces*). For a system actuated by m cables, $\mathbf{l} = [l_1 \ l_2 \ \dots \ l_m]^T$ and $\mathbf{f} = [f_1 \ f_2 \ \dots \ f_m]^T$ denote the vector of cable lengths and vector of cable forces, respectively, where l_i and f_i represent the length and force of cable i , respectively. Due to the positive cable force constraint, the condition $f_i \geq 0 \ \forall i$ must be satisfied. Finally, the *body space* refers to the absolute position of the centre of mass and orientation of the rigid bodies, where $\dot{\mathbf{x}}$ represents the *twist vector*. It should be noted that in existing single link CPDM studies, joint space has been used to refer to set of cable lengths. However, for the study of multi-link cable-driven systems in this thesis with a serial kinematic rigid body structure, joint space has been used to represent the pose of the joints to remain consistent with the studies in serial mechanisms. As a result, the cable space has been introduced to represent the length and forces of the set of cables.

In a similar manner to traditional rigid link parallel mechanisms, the kinematics and forces between the joint and cable spaces can be related by the system Jacobian matrix $J \in \mathbb{R}^{m \times n}$. In the kinematic model, the Jacobian matrix relates the time derivative of cable lengths $\dot{\mathbf{l}}$ and time derivative of the joint space vector $\dot{\mathbf{q}}$, where

$$\dot{\mathbf{l}} = J(\mathbf{q})\dot{\mathbf{q}} . \quad (3.1)$$

The transpose of the Jacobian matrix J^T represents the effect of the cable forces \mathbf{f} onto the joint space force. The equations of motion can be expressed in the general form

$$M(\mathbf{q})\ddot{\mathbf{q}} + \mathbf{C}(\mathbf{q}, \dot{\mathbf{q}}) + \mathbf{G}(\mathbf{q}) + \boldsymbol{\Gamma}_{ext} = -J^T(\mathbf{q})\mathbf{f} , \quad (3.2)$$

where $M \in \mathbb{R}^{n \times n}$, $\mathbf{C} \in \mathbb{R}^n$, $\mathbf{G} \in \mathbb{R}^n$ and $\boldsymbol{\Gamma}_{ext} \in \mathbb{R}^n$ represent the mass-inertia matrix,

centrifugal and Coriolis force vector, gravity force vector and external force vector, respectively.

The relationships from (3.1) and (3.2) represent the kinematic and dynamic models for the system. For completely and redundantly restrained CDPMs, a key characteristic of the Jacobian matrix J is that it is a non-square matrix where the number of rows is greater than the number of columns.

3.2 Kinematic and Dynamic Analyses

In this section, the problems involved in the analysis of the kinematics and dynamics of CDPMs are classified and described. For both the kinematic and dynamic analyses, the problem can be classified into inverse analysis and direct analysis. The direct problem refers to the determination of the joint space vector given the knowledge of the cable space. Conversely, the inverse problem refers to the solving of the cable space when provided with the joint space vector. The cable space refers to either the cable length vector \mathbf{l} or cable force vector \mathbf{f} depending on whether kinematic or dynamic analysis is performed, respectively.

To illustrate the different kinematic and dynamic problems of CDPMs, a 3 DoF planar CDPM actuated by 4 cables shown in Figure 3.1, will be used as an example. The pose of the manipulator can be described by the generalised coordinates $\mathbf{q} = [x \ y \ \theta]^T$, where x and y represent the position of the centre of mass and θ represents the orientation of the manipulator.

The kinematics of the cable space can be described by the cable length vector $\mathbf{l} = [l_1 \ l_2 \ l_3 \ l_4]^T$, where l_1, l_2, l_3 and l_4 represent the lengths of cable 1, 2, 3 and 4, respectively. For every cable, one end is attached onto the base frame and the other end is attached onto the end-effector. Coordinates on the base and the end-effector frames can be expressed with respect to the inertial coordinate frame $\{F_O\}$ and non-inertial coordinate frame $\{F_E\}$, respectively. As shown in Figure 3.2, the origins of $\{F_O\}$ and $\{F_E\}$ can be denoted by locations O and o , respectively. The position of o can be described with respect to $\{F_O\}$ by the position vector ${}^O\mathbf{r}_{Oo} = [x \ y]^T$. The notation ${}^k\mathbf{r}$ denotes that

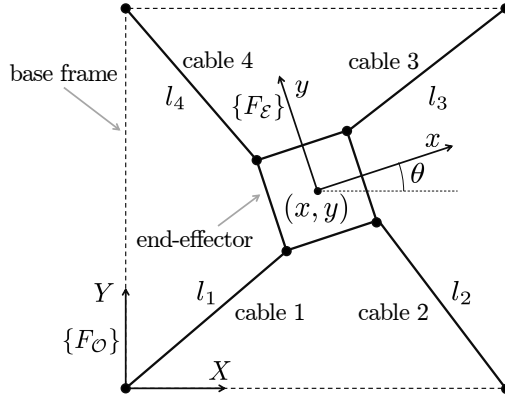


Figure 3.1: Planar CDPM model showing the generalised coordinates and cable lengths.

the vector \mathbf{r} is expressed with respect to frame $\{F_k\}$. The attachment location of cable i at the base and the end-effector can be denoted by A_i and B_i , respectively. Hence, the vectors ${}^O\mathbf{r}_{OA_i}$ and ${}^E\mathbf{r}_{OB_i}$ are fixed vectors in $\{F_O\}$ and $\{F_E\}$, respectively, and define the attachment locations of cable i .

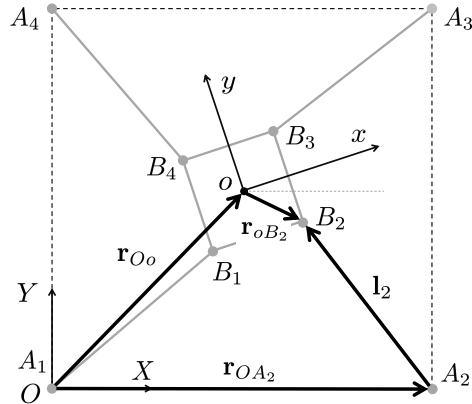


Figure 3.2: The relationship between cable vector and the attachment locations for cable 2 of the planar CDPM.

3.2.1 Inverse Kinematics

The inverse kinematics problem refers to the determination of the cable lengths \mathbf{l} given the pose of the system \mathbf{q} . As with rigid link parallel manipulators, inverse kinematics for CDPMs is trivial and there exists a unique solution that can be analytically expressed [84].

In determining the cable lengths, it is necessary to first define the cable vector \mathbf{l}_i for cable i . In Figure 3.2, the cable vector \mathbf{l}_2 for cable 2 can be related to the attachment location at the base \mathbf{r}_{OA_2} , the attachment location at the end-effector \mathbf{r}_{oB_2} and the manipulator position \mathbf{r}_{Oo} , where $\mathbf{l}_2 = -\mathbf{r}_{OA_2} + \mathbf{r}_{Oo} + \mathbf{r}_{oB_2}$. In general, the cable vector for cable i expressed in $\{F_O\}$ can be defined as

$${}^O\mathbf{l}_i(\mathbf{q}) = {}^O\mathbf{r}_{Oo}(\mathbf{q}) - {}^O\mathbf{r}_{OA_i} + {}^O_R(\mathbf{q}) {}^E\mathbf{r}_{oB_i}, \quad (3.3)$$

where O_R represents the rotation matrix from $\{F_O\}$ to $\{F_E\}$. The length of cable i can be determined from (3.3), where $l_i = \|\mathbf{l}_i\|$. As a result, the solution to the inverse kinematics problem is a set of explicit non-linear equations that can be expressed with respect to the joint space vector \mathbf{q} , where $\mathbf{l} = [\|l_1(\mathbf{q})\| \ \|l_2(\mathbf{q})\| \ \|l_3(\mathbf{q})\| \ \|l_4(\mathbf{q})\|]^T$.

Figure 3.3 shows an example scenario of inverse kinematic analysis performed on the planar CDPM example. At the system pose $\mathbf{q} = [0.5 \ 0.5 \ \frac{\pi}{6}]^T$, all cables are of the same length and the inverse kinematic solution is $\mathbf{l} = [0.56 \ 0.56 \ 0.56 \ 0.56]^T$.

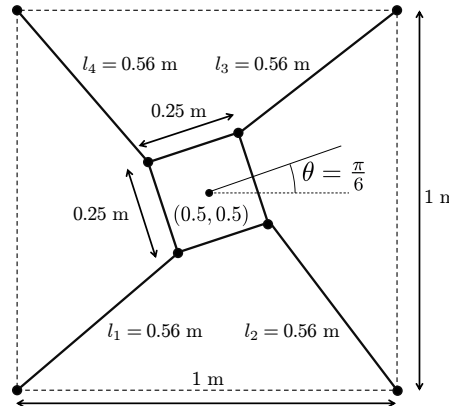


Figure 3.3: The solution to the inverse kinematics is $\mathbf{l} = [0.56 \ 0.56 \ 0.56 \ 0.56]^T$, at system pose $\mathbf{q} = [0.5 \ 0.5 \ \frac{\pi}{6}]^T$ for the planar CDPM.

3.2.2 Direct Kinematics

The direct kinematics problem refers to the determination of the manipulator pose \mathbf{q} given the cable lengths \mathbf{l} , and can be regarded as the dual problem of the inverse kinematics analysis. As a type of parallel mechanism, the direct kinematics of CDPMs is a

challenging problem where a closed form solution may not exist. Furthermore, a known set of cable lengths can result in multiple solutions for \mathbf{q} [51, 70, 96].

The direct kinematics can be determined through solving the set of m non-linear equations from (3.3) for every cable. For redundantly actuated CDPMs, one simple approach is to select a subset of n equations to solve for the manipulator pose \mathbf{q} as with rigid link parallel mechanisms [84]. However, the direct kinematic analysis is typically required in determining the manipulator's pose from obtained sensor readings of the cable lengths.

Figure 3.4 shows the direct kinematic analysis performed on the planar CDPM example from Section 3.2.1. For the cable lengths $\mathbf{l} = [0.56 \ 0.56 \ 0.56 \ 0.56]^T$, one obvious solution for the manipulator pose is $\mathbf{q} = [0.5 \ 0.5 \ \frac{\pi}{6}]^T$ from the inverse kinematics example, as shown in Figure 3.4(a). However, the cable length vector $\mathbf{l} = [0.56 \ 0.56 \ 0.56 \ 0.56]^T$ results in multiple direct kinematic solutions. Another valid solution is $\mathbf{q} = [0.5 \ 0.5 \ -\frac{\pi}{6}]^T$, as shown in Figure 3.4(b).

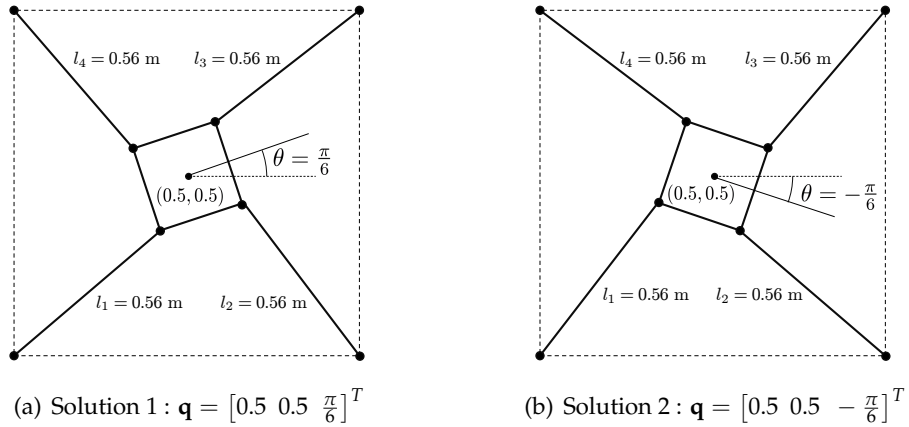


Figure 3.4: The solutions to the direct kinematics problem for cable lengths $\mathbf{l} = [0.56 \ 0.56 \ 0.56 \ 0.56]^T$. There exists two real solutions in this scenario, the first solution $\mathbf{q} = [0.5 \ 0.5 \ \frac{\pi}{6}]^T$ is shown in (a) and the second solution $\mathbf{q} = [0.5 \ 0.5 \ -\frac{\pi}{6}]^T$ is shown in (b).

3.2.3 Inverse Dynamics

The inverse dynamics problem for CDPMs refers to the resolution of a set of positive cable forces \mathbf{f} to achieve a desired joint space motion described by \mathbf{q}_r , $\dot{\mathbf{q}}_r$ and $\ddot{\mathbf{q}}_r$. The

resulting cable forces must satisfy the equations of motion from (3.2) as well as other constraints of the system. For CDPMs, the positive cable force and bounds in cable actuation forces must also be considered as constraints in the inverse dynamics problem.

For completely and redundantly restrained systems, there exists a greater number of actuators than the number of degrees of freedom ($m \geq n + 1$). Hence, there may exist an infinite number of cable force solutions to the inverse dynamics problem. As such, the resolution of positive cable forces can be formulated as an optimisation problem in order to resolve the redundancy. The simplest of these can be expressed in the form

$$\begin{aligned} \mathbf{f}^* &= \arg \min_{\mathbf{f}} Q(\mathbf{f}) \\ \text{s.t.} \quad & M(\mathbf{q}_r)\ddot{\mathbf{q}}_r + \mathbf{C}(\mathbf{q}_r, \dot{\mathbf{q}}_r) + \mathbf{G}(\mathbf{q}_r) + \boldsymbol{\Gamma}_{ext} = -J^T(\mathbf{q}_r)\mathbf{f} \\ & \mathbf{0} \leq \mathbf{f}_{min} \leq \mathbf{f} \leq \mathbf{f}_{max}, \end{aligned} \quad (3.4)$$

where \mathbf{f}^* represents the optimum cable forces solution subject to all system constraints and the objective function $Q(\mathbf{f})$. The vectors $\mathbf{f}_{min}, \mathbf{f}_{max} \in \mathbb{R}^m$ represent the minimum and maximum bounds on the cable forces, respectively.

The selection of $Q(\mathbf{f})$ allows different characteristics in the cable forces to be achieved for the desired motion. One of the common objective functions is to minimise the actuation forces exerted by the cables, and can be expressed as the sum of cable forces. Furthermore, since both constraints in (3.4) are linear, the objective function determines the class of the optimisation problem to be solved. For example, if $Q(\mathbf{f})$ is a linear or quadratic function, then the inverse dynamic analysis (3.4) becomes a linear programming or quadratic programming problem, respectively.

To illustrate the inverse dynamics problem, consider the translational motion of the planar CDPM shown in Figure 3.5(a) with the corresponding trajectory in direction X as shown in Figure 3.5(b). The trajectory was generated through interpolating between the initial pose $\mathbf{q} = [0.3 \ 0.5 \ 0]^T$ and the final pose $\mathbf{q} = [0.7 \ 0.5 \ 0]^T$.

The set of cable forces $\mathbf{f}(t)$ required to produce the described trajectory motion can be determined by solving the inverse dynamics problem (3.4) at each instance in time. No additional external forces were applied onto the system during the trajectory. The

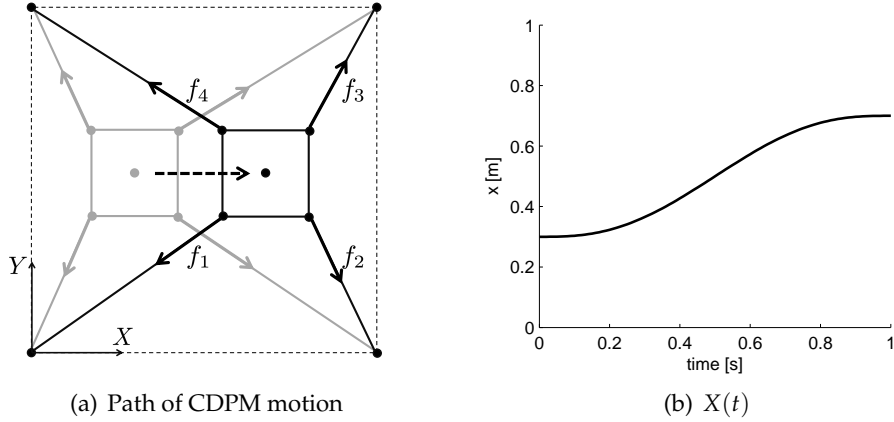


Figure 3.5: The input trajectory for the inverse dynamics example can be described by the motion in X shown in (b), resulting in the path as depicted by (a).

minimum and maximum cable forces for all cables were set as 0.1 N and 1000 N, respectively, and hence $\mathbf{f}_{min} = [0.1 \ 0.1 \ 0.1 \ 0.1]^T$ and $\mathbf{f}_{max} = [1000 \ 1000 \ 1000 \ 1000]^T$. Figure 3.6 shows the resultant cable forces resolved from the objective function $Q(\mathbf{f}) = f_1^2 + f_2^2 + f_3^2 + f_4^2 = \mathbf{f}^T \mathbf{f}$, where the sum of cable forces squared is minimised.

3.2.4 Direct Dynamics

The direct dynamics problem can be regarded as the dual to the inverse dynamic analysis problem, where the motion of the manipulator $\mathbf{q}(t)$ is solved for a given profile of the cable forces $\mathbf{f}(t)$. The solution to the direct dynamics problem can be determined by solving the second order differential equations from the equations of motion in (3.2) or alternatively as $\dot{\mathbf{y}} = \mathbf{g}(t, \mathbf{y})$, where $\mathbf{y} = [\mathbf{q}^T \ \dot{\mathbf{q}}^T]^T$, and

$$\dot{\mathbf{y}} = \mathbf{g}(t, \mathbf{y}) = \begin{bmatrix} \dot{\mathbf{q}} \\ M^{-1}(\mathbf{q}) (-J^T(\mathbf{q})\mathbf{f} - \mathbf{C}(\mathbf{q}, \dot{\mathbf{q}}) - \mathbf{G}(\mathbf{q}) - \boldsymbol{\Gamma}_{ext}) \end{bmatrix}. \quad (3.5)$$

Due to the non-linear nature of the equations of motion, the ordinary differential equation from (3.5) is typically solved using numerical techniques.

To demonstrate direct dynamic analysis, the motion for the planar CDPM example is generated for the input cable force profiles shown in Figure 3.7. The force in cables 2 and

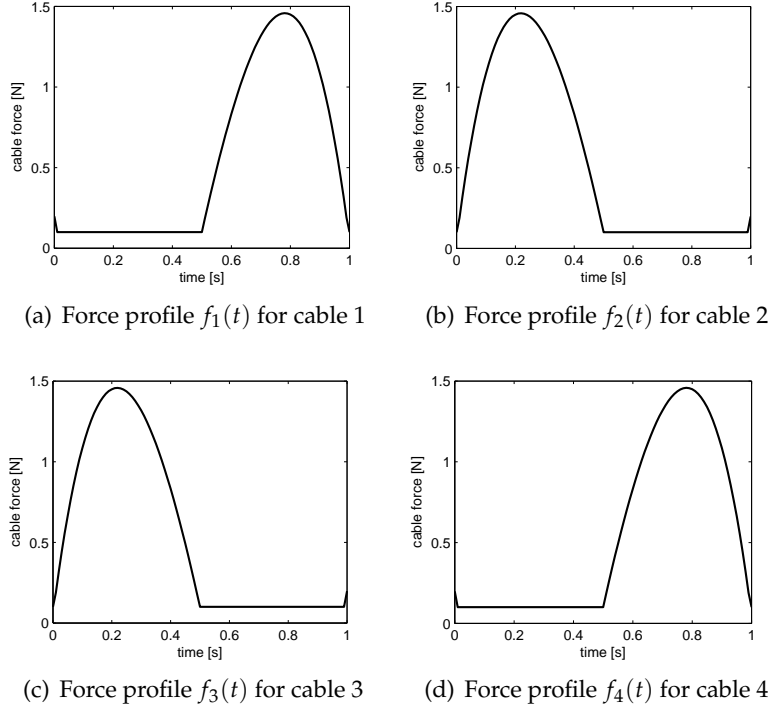


Figure 3.6: The resultant force profile obtained by performing inverse dynamic analysis on the motion described by Figure 3.5 for each of the cables.

3 are prescribed as a constant force of 1 N, while cables 1 and 4 provides no actuation forces onto the system. Aside from the cable forces, no other external forces are applied onto the system.

The resultant motion is generated for initial conditions $\mathbf{q} = [0.3 \ 0.5 \ 0]^T$ and $\dot{\mathbf{q}} = [0 \ 0 \ 0]^T$, and is shown in Figure 3.8. As only cables 2 and 3 provide actuation, it is expected that pure translational motion in X direction results, as depicted in Figure 3.8(a). The resulting trajectory for the motion in the X direction is shown in Figure 3.8(b).

3.3 Modelling of Example Manipulators

As demonstrated in Section 3.2, the analysis of CDPMs requires the model of the manipulator. The kinematics and dynamics of a CDPM system can be described by the relationships from (3.1), (3.2) and (3.3). In this section, the model of several example manipulators will be presented. Firstly, the model of a 3 DoF single link manipulator that is

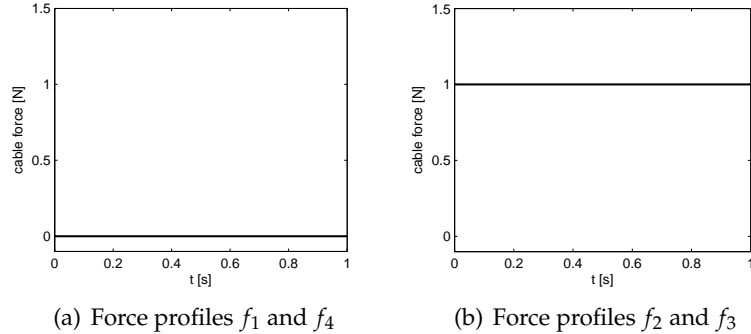


Figure 3.7: The cable forces for the input of the direct dynamics example. Cables 1 and 4 exert 0 N of force, while cables 2 and 3 exert a constant force of 1 N.

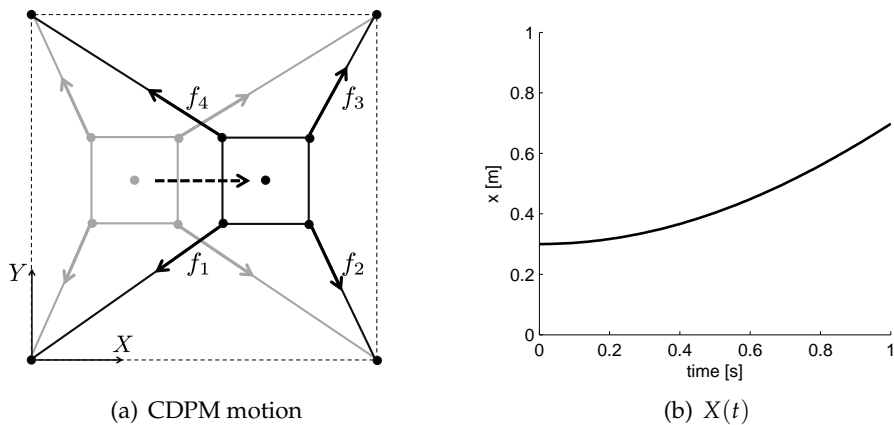


Figure 3.8: The resultant motion from direct dynamic analysis under the cable forces described in Figure 3.7. The resulting path is shown in (a) and the trajectory in the X direction is plotted in (b).

constrained by a spherical joint is presented, followed by the commonly studied 6 DoF spatial manipulator. Finally, the model for a 4 DoF two link manipulator is formulated, illustrating the increased complexity involved with the modelling of both the kinematic structure and the cable routing for multilink systems.

3.3.1 3 DoF Spherical Joint Manipulator

The kinematic model and equations of motion for the 3 DoF manipulator shown in Figure 3.9 is derived in this section. The manipulator possesses three rotational degrees of freedom, where the end-effector is constrained to the base frame at O through a spherical

joint.

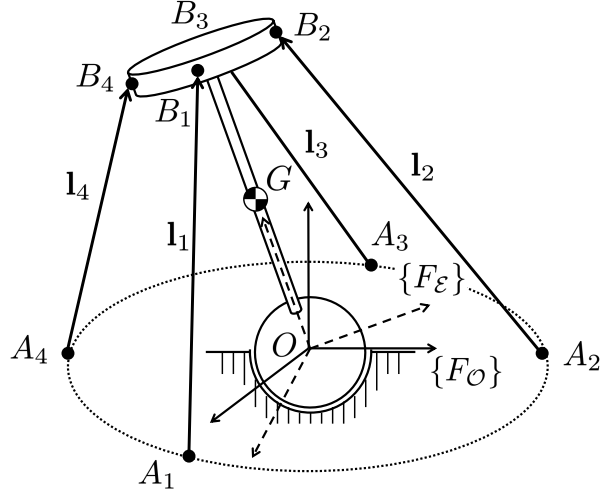


Figure 3.9: The model for a 3 DoF spherical joint CDPM showing the coordinate frames and cable vectors. The cable attachments for cable i at the base and the end-effector are denoted by A_i and B_i , respectively.

The end-effector pose can be described by $\mathbf{q} = [\alpha \ \beta \ \gamma]^T$, where α , β and γ represent the xyz -Euler angles of the spherical joint, respectively. Positions on the base frame can be expressed with respect to the inertial coordinate frame $\{F_O\}$. Positions on the end-effector manipulator can be expressed with respect to the non-inertial coordinate frame $\{F_E\}$, where $\{F_E\}$ is rigidly attached onto the manipulator. The rotational matrix ${}^O_R E$ transforms a vector expressed in frame $\{F_E\}$ to $\{F_O\}$, where

$${}^O_R E(\mathbf{q}) = \begin{bmatrix} c_\beta c_\gamma & -c_\beta s_\gamma & s_\beta \\ c_\alpha s_\gamma + s_\alpha s_\beta c_\gamma & c_\alpha c_\gamma - s_\alpha s_\beta s_\gamma & -s_\alpha c_\beta \\ s_\alpha s_\gamma - c_\alpha s_\beta c_\gamma & s_\alpha c_\gamma + c_\alpha s_\beta s_\gamma & c_\alpha c_\beta \end{bmatrix}. \quad (3.6)$$

The 3 DoF system is actuated by 4 cables and hence is classified as a completely restrained system. The attachment locations for cable i at the base and the end-effector can be denoted by A_i and B_i , respectively. Hence, the vectors ${}^O \mathbf{r}_{OA_i}$ and ${}^E \mathbf{r}_{OB_i}$ are fixed in $\{F_O\}$ and $\{F_E\}$, respectively. From Figure 3.9, the cable vector \mathbf{l}_i for cable i with respect

to $\{F_{\mathcal{E}}\}$ can be expressed as

$$\varepsilon \mathbf{l}_i = -\mathcal{O}^{\mathcal{O}} R \mathbf{r}_{OA_i} + \varepsilon \mathbf{r}_{OB_i}. \quad (3.7)$$

From (3.6) and (3.7), the length l_i of cable i can be expressed explicitly with respect to \mathbf{q} as $l_i = \|\mathbf{l}_i\|$. This relationship allows the inverse kinematics of the manipulator to be solved.

The Jacobian matrix from (3.1) can be determined by taking the time derivative of l_i for each cable. The time derivative of the length of cable i can be expressed as $\dot{l}_i = \hat{\mathbf{l}}_i \cdot \mathbf{l}_i$, where $\hat{\mathbf{l}}_i$ represents the unit vector of \mathbf{l}_i . Since \mathbf{r}_{OA_i} is fixed to the inertial frame, then $\dot{\mathbf{r}}_{OA_i} = \mathbf{0}$. The time derivative of vector \mathbf{r}_{OB_i} in $\{F_{\mathcal{E}}\}$ can be expressed as $\dot{\mathbf{r}}_{OB_i} = \boldsymbol{\omega}_{\mathcal{E}} \times \mathbf{r}_{OB_i}$, where $\boldsymbol{\omega}_{\mathcal{E}}$ is the absolute angular velocity of the end-effector. Hence, taking the time derivative from (3.7) results in the relationship

$$\dot{l}_i = (\mathbf{r}_{OB_i} \times \hat{\mathbf{l}}_i) \cdot \boldsymbol{\omega}_{\mathcal{E}}. \quad (3.8)$$

The absolute angular velocity of the end-effector can be expressed in the form

$$\begin{aligned} \boldsymbol{\omega}_{\mathcal{E}} &= S \dot{\mathbf{q}} \\ &= \begin{bmatrix} c_{\beta}c_{\gamma} & s_{\gamma} & 0 \\ -c_{\beta}s_{\gamma} & c_{\gamma} & 0 \\ s_{\beta} & 0 & 1 \end{bmatrix} \begin{bmatrix} \dot{\alpha} \\ \dot{\beta} \\ \dot{\gamma} \end{bmatrix}. \end{aligned} \quad (3.9)$$

It should be noted that the matrix S is dependent on the choice of the generalised coordinates \mathbf{q} and may result in singularities. For example, S is singular in some configurations as Euler angles have been used in this case for the purpose of illustration. This could be avoided by the selection of other generalised coordinate representations such as twist or quaternion.

The Jacobian matrix $J \in \mathbb{R}^{4 \times 3}$ can be determined by combining (3.8) and (3.9) for the

set of cables and expressing in the form $\dot{\mathbf{i}} = J\dot{\mathbf{q}}$

$$\begin{bmatrix} \dot{l}_1 \\ \dot{l}_2 \\ \dot{l}_3 \\ \dot{l}_4 \end{bmatrix} = \begin{bmatrix} (\mathbf{r}_{OB_1} \times \hat{\mathbf{l}}_1)^T \\ (\mathbf{r}_{OB_2} \times \hat{\mathbf{l}}_2)^T \\ (\mathbf{r}_{OB_3} \times \hat{\mathbf{l}}_3)^T \\ (\mathbf{r}_{OB_4} \times \hat{\mathbf{l}}_4)^T \end{bmatrix} \begin{bmatrix} c_\beta c_\gamma & s_\gamma & 0 \\ -c_\beta s_\gamma & c_\gamma & 0 \\ s_\beta & 0 & 1 \end{bmatrix} \begin{bmatrix} \dot{\alpha} \\ \dot{\beta} \\ \dot{\gamma} \end{bmatrix}. \quad (3.10)$$

The dynamics for the manipulator can be modelled by deriving the equations of motion for the system and expressing in the form (3.2). The equations of motion for the spherical joint manipulator can be determined by taking the sum of moments about the inertial point of rotation O and hence expressed as

$$I_O \ddot{\omega}_{\mathcal{E}} + \omega_{\mathcal{E}} \times (I_O \omega_{\mathcal{E}}) = \sum \mathbf{M}, \quad (3.11)$$

where I_O represents the moment of inertia of the manipulator about O . The free body diagram in Figure 3.10 shows the forces and moments acting on the system. Hence, the sum of moments $\sum \mathbf{M}$ about O from (3.11) is comprised of the moment due to the gravity force $m\mathbf{g}$, where m represents the manipulator mass and ${}^O\mathbf{g} = [0 \ 0 \ -g]^T$, interaction moment \mathbf{M}_O at the joint O and the moment produced by the cable force vectors \mathbf{f}_i for $i = 1, \dots, 4$.

Hence, (3.11) can be expressed in $\{F_{\mathcal{E}}\}$ as

$$I_O \ddot{\omega}_{\mathcal{E}} + \omega_{\mathcal{E}} \times (I_O \omega_{\mathcal{E}}) = \mathbf{r}_{OG} \times ({}^O\mathbf{R} m\mathbf{g}) + \mathbf{M}_O + \sum_{i=1}^4 \mathbf{r}_{OB_i} \times \mathbf{f}_i, \quad (3.12)$$

where \mathbf{r}_{OG} is the position vector from O to the manipulator's centre of mass G . The cable force vector of cable i can be defined as

$$\mathbf{f}_i = -\hat{\mathbf{l}}_i f_i. \quad (3.13)$$

From (3.12), the equations of motion can be determined by projecting the interaction moments at O onto the degrees of freedom of the system. For a spherical joint defined by

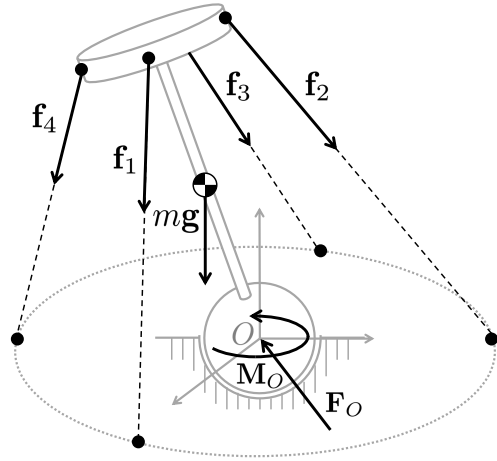


Figure 3.10: The free body diagram for the 3 DoF spherical joint CDPM, showing the cable forces \mathbf{f}_1 , \mathbf{f}_2 , \mathbf{f}_3 and \mathbf{f}_4 , the gravity force $m\mathbf{g}$, interaction force \mathbf{F}_O and interaction moment \mathbf{M}_O at O .

xyz-Euler angles, the projection results in the relationship

$$\begin{bmatrix} c_\beta c_\gamma & -c_\beta s_\gamma & s_\beta \\ s_\gamma & c_\gamma & 0 \\ 0 & 0 & 1 \end{bmatrix} \mathbf{M}_O = \mathbf{0}. \quad (3.14)$$

It should be noted that the projection matrix from (3.14) is the transpose of S from (3.9), where $S^T \mathbf{M}_O = \mathbf{0}$. From (3.12) and (3.14), the equations of motion can be determined and expressed in the form (3.2), where the mass-inertia matrix M , the centrifugal and Coriolis vector \mathbf{C} and the gravity vector \mathbf{G} can be expressed as

$$\begin{aligned} M(\mathbf{q}) &= S^T \begin{bmatrix} I_{O_x} c_\beta c_\gamma & I_{O_x} s_\gamma & 0 \\ -I_{O_y} c_\beta s_\gamma & I_{O_y} c_\gamma & 0 \\ I_{O_z} s_\beta & 0 & I_{O_z} \end{bmatrix}, \\ \mathbf{C}(\mathbf{q}, \dot{\mathbf{q}}) &= S^T \begin{bmatrix} I_{O_x} (-\dot{\alpha} \dot{\beta} s_\beta c_\gamma - \dot{\alpha} \dot{\gamma} c_\beta s_\gamma + \dot{\beta} \dot{\gamma} c_\gamma) \\ I_{O_y} (\dot{\alpha} \dot{\beta} s_\beta s_\gamma - \dot{\alpha} \dot{\gamma} c_\beta c_\gamma - \dot{\beta} \dot{\gamma} s_\gamma) \\ I_{O_z} \dot{\alpha} \dot{\beta} c_\beta \end{bmatrix} + S^T (\boldsymbol{\omega}_{\mathcal{E}} \times (I_O \boldsymbol{\omega}_{\mathcal{E}})), \\ \mathbf{G}(\mathbf{q}) &= -S^T (\mathbf{r}_{OG} \times (\overset{\mathcal{E}}{\mathcal{O}} R m\mathbf{g})). \end{aligned}$$

Under no external forces on the manipulator, the external force vector is $\Gamma_{ext} = \mathbf{0}$. Finally, using the definition of \mathbf{f}_i from (3.13) and applying the projection (3.14) onto (3.12) allows the transpose of the Jacobian matrix J^T from (3.2) to be expressed as

$$J^T = \begin{bmatrix} c_\beta c_\gamma & -c_\beta s_\gamma & s_\beta \\ s_\gamma & c_\gamma & 0 \\ 0 & 0 & 1 \end{bmatrix} \begin{bmatrix} \mathbf{r}_{OB_1} \times \hat{\mathbf{l}}_1 & \mathbf{r}_{OB_2} \times \hat{\mathbf{l}}_2 & \mathbf{r}_{OB_3} \times \hat{\mathbf{l}}_3 & \mathbf{r}_{OB_4} \times \hat{\mathbf{l}}_4 \end{bmatrix}. \quad (3.15)$$

From (3.15), it can be observed that J^T represents the mapping between the cable forces and the manipulator motion. Furthermore, it is shown in this example that the Jacobian matrix within (3.10) and (3.15) is consistent between the kinematics and dynamics of the manipulator, respectively.

3.3.2 6 DoF Spatial Manipulator

The 6 DoF spatial manipulator, as shown in Figure 3.11, is one of the most commonly investigated CDPMs with a wide range of applications, such as high speed manipulation, environment sensing and rehabilitation.

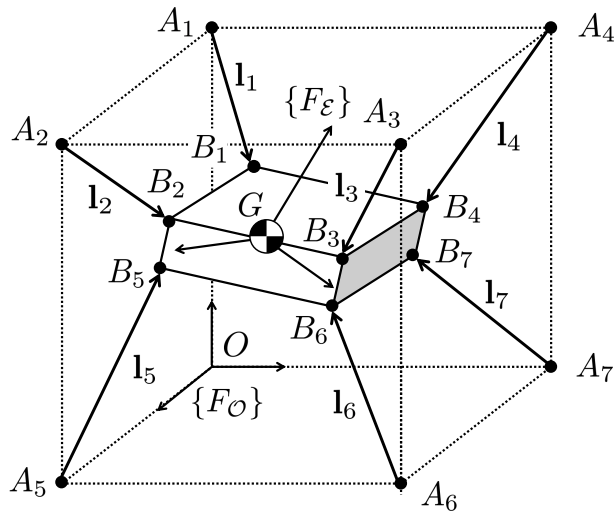


Figure 3.11: The model for a 6 DoF spatial CDPM showing the coordinate frames and cable vectors. The cable attachments for cable i at the base and the end-effector are denoted by A_i and B_i , respectively.

The end-effector pose of the manipulator can be described by $\mathbf{q} = [x \ y \ z \ \alpha \ \beta \ \gamma]^T$. The translation of the manipulator's centre of mass is described by ${}^O\mathbf{r}_{OG} = [x \ y \ z]^T$. The orientation of the manipulator can be described by α, β and γ , representing xyz-Euler angles, respectively. Positions on the base frame can be described as fixed with respect to the inertial coordinate frame $\{F_O\}$. Positions on the end-effector are fixed with respect to the non-inertial coordinate frame $\{F_E\}$, where $\{F_E\}$ is rigidly attached onto the manipulator with its origin fixed to the centre of mass of the end-effector G . The rotational matrix ${}^O_R E$ converts a vector expressed in $\{F_E\}$ to $\{F_O\}$, where

$${}^O_R E(\mathbf{q}) = \begin{bmatrix} c_\beta c_\gamma & -c_\beta s_\gamma & s_\beta \\ c_\alpha s_\gamma + s_\alpha s_\beta c_\gamma & c_\alpha c_\gamma - s_\alpha s_\beta s_\gamma & -s_\alpha c_\beta \\ s_\alpha s_\gamma - c_\alpha s_\beta c_\gamma & s_\alpha c_\gamma + c_\alpha s_\beta s_\gamma & c_\alpha c_\beta \end{bmatrix}. \quad (3.16)$$

The 6 DoF system is actuated by 7 cables and hence is classified as a completely restrained system. The attachment locations for cable i at the base and the end-effector can be denoted by A_i and B_i , respectively. Hence, the vectors ${}^O\mathbf{r}_{OA_i}$ and ${}^E\mathbf{r}_{GB_i}$ are fixed in $\{F_O\}$ and $\{F_E\}$, respectively. From Figure 3.11, the cable vector \mathbf{l}_i for cable i with respect to $\{F_E\}$ can be expressed as

$${}^E\mathbf{l}_i = -{}^O_R E {}^O\mathbf{r}_{OA_i} + {}^E\mathbf{r}_{OG} + {}^E\mathbf{r}_{GB_i}. \quad (3.17)$$

From (3.16) and (3.17), the length l_i of cable i can be expressed explicitly with respect to \mathbf{q} , where $l_i = \|\mathbf{l}_i\|$. This allows the manipulator inverse kinematics to be solved.

The Jacobian matrix from (3.1) can be determined by taking the time derivative of l_i for each cable. The time derivative of the length of cable i can be expressed as $\dot{l}_i = \hat{\mathbf{l}}_i \cdot \dot{\mathbf{l}}_i$, where $\hat{\mathbf{l}}_i$ represents the unit vector of \mathbf{l}_i . Since \mathbf{r}_{OA_i} is fixed to the inertial frame, then $\dot{\mathbf{r}}_{OA_i} = \mathbf{0}$. The time derivative of vector \mathbf{r}_{GB_i} in $\{F_E\}$ can be expressed as $\dot{\mathbf{r}}_{GB_i} = \boldsymbol{\omega}_E \times \mathbf{r}_{GB_i}$, where $\boldsymbol{\omega}_E$ is the absolute angular velocity of the end-effector. Hence, taking the time derivative from (3.17) results in the relationship

$$\dot{l}_i = \hat{\mathbf{l}}_i \cdot \dot{\mathbf{r}}_{OG} + (\mathbf{r}_{GB_i} \times \hat{\mathbf{l}}_i) \cdot \boldsymbol{\omega}_E. \quad (3.18)$$

Expressing (3.18) for the entire set of cables allows the time derivative of the cable length vector to be expressed in the form $\dot{\mathbf{l}} = V\dot{\mathbf{x}}$

$$\begin{bmatrix} l_1 \\ l_2 \\ \vdots \\ l_7 \end{bmatrix} = \begin{bmatrix} \hat{\mathbf{l}}_1^T & (\mathbf{r}_{GB_1} \times \hat{\mathbf{l}}_1)^T \\ \hat{\mathbf{l}}_2^T & (\mathbf{r}_{GB_2} \times \hat{\mathbf{l}}_2)^T \\ \vdots & \vdots \\ \hat{\mathbf{l}}_7^T & (\mathbf{r}_{GB_7} \times \hat{\mathbf{l}}_7)^T \end{bmatrix} \begin{bmatrix} \dot{\mathbf{r}}_{OG} \\ \boldsymbol{\omega}_{\mathcal{E}} \end{bmatrix}, \quad (3.19)$$

where $\dot{\mathbf{x}} = [\varepsilon \dot{\mathbf{r}}_{OG}^T \ \varepsilon \boldsymbol{\omega}_{\mathcal{E}}^T]^T$ can be described as the *twist vector* containing the absolute velocity of the centre of mass and the absolute angular velocity of the end-effector, respectively. Furthermore, the body twist vector $\dot{\mathbf{x}}$ can be related to the joint space velocity vector $\dot{\mathbf{q}}$ linearly in the form $\dot{\mathbf{x}} = S\dot{\mathbf{q}}$, where

$$\dot{\mathbf{x}} = \begin{bmatrix} c_\beta c_\gamma & c_\alpha s_\gamma + s_\alpha s_\beta c_\gamma & s_\alpha s_\gamma - c_\alpha s_\beta c_\gamma & 0 & 0 & 0 \\ -c_\beta s_\gamma & c_\alpha c_\gamma - s_\alpha s_\beta s_\gamma & s_\alpha c_\gamma + c_\alpha s_\beta s_\gamma & 0 & 0 & 0 \\ s_\beta & -s_\alpha c_\beta & c_\alpha c_\beta & 0 & 0 & 0 \\ 0 & 0 & 0 & c_\beta c_\gamma & s_\gamma & 0 \\ 0 & 0 & 0 & -c_\beta s_\gamma & c_\gamma & 0 \\ 0 & 0 & 0 & s_\beta & 0 & 1 \end{bmatrix} \begin{bmatrix} \dot{x} \\ \dot{y} \\ \dot{z} \\ \dot{\alpha} \\ \dot{\beta} \\ \dot{\gamma} \end{bmatrix}. \quad (3.20)$$

From (3.19) and (3.20), the Jacobian matrix $J \in \mathbb{R}^{7 \times 6}$ can be expressed as $J = VS$.

The dynamics for the manipulator can be modelled by deriving the equations of motion for the system and expressing in the form (3.2). The equations of motion for the spatial manipulator can be determined by taking the sum of forces and the sum of moments about the centre of mass G in $\{F_{\mathcal{E}}\}$

$$\begin{aligned} m\ddot{\mathbf{r}}_{OG} &= \sum \mathbf{F}, \\ I_G \dot{\boldsymbol{\omega}}_{\mathcal{E}} + \boldsymbol{\omega}_{\mathcal{E}} \times (I_G \boldsymbol{\omega}_{\mathcal{E}}) &= \sum \mathbf{M}, \end{aligned} \quad (3.21)$$

where m and I_G represent the mass and moment of inertia of the manipulator about the centre of mass G . Similar to the 3 DoF manipulator presented in Section 3.3.1, the forces

and moments acting on the system include the gravity force $m\mathbf{g}$, the platform interaction force \mathbf{F}_G and platform interaction moment \mathbf{M}_G at G , and the cable force vectors \mathbf{f}_i for $i = 1, \dots, 7$. The cable force vector of cable i can be expressed as $\mathbf{f}_i = -\hat{\mathbf{l}}_i f_i$. Hence, (3.21) can be expressed as

$$\begin{aligned} m\ddot{\mathbf{r}}_{OG} &= \dot{\mathcal{E}}_O R m\mathbf{g} + \mathbf{F}_G - \sum_{i=1}^7 \hat{\mathbf{l}}_i f_i \\ I_G \dot{\boldsymbol{\omega}}_{\mathcal{E}} + \boldsymbol{\omega}_{\mathcal{E}} \times (I_G \boldsymbol{\omega}_{\mathcal{E}}) &= \mathbf{M}_G - \sum_{i=1}^7 \mathbf{r}_{GB_i} \times \hat{\mathbf{l}}_i f_i. \end{aligned} \quad (3.22)$$

From (3.22), the equations of motion can be determined by projecting the interaction force and moment at the centre of mass onto the degrees of freedom of the system. For a spatial manipulator, this can be achieved through the projection S^T , the transpose of S obtained in (3.20), where

$$S^T \begin{bmatrix} \mathbf{F}_G \\ \mathbf{M}_G \end{bmatrix} = \mathbf{0}. \quad (3.23)$$

From (3.22) and the projection (3.23), the equations of motion can be determined and expressed in the form (3.2), where

$$\begin{aligned} M(\mathbf{q}) &= S^T \begin{bmatrix} mc_\beta c_\gamma & m(c_\alpha s_\gamma + s_\alpha s_\beta c_\gamma) & m(s_\alpha s_\gamma - c_\alpha s_\beta c_\gamma) & 0 & 0 & 0 \\ -mc_\beta s_\gamma & m(c_\alpha c_\gamma - s_\alpha s_\beta s_\gamma) & m(s_\alpha c_\gamma + c_\alpha s_\beta s_\gamma) & 0 & 0 & 0 \\ ms_\beta & -ms_\alpha c_\beta & mc_\alpha c_\beta & 0 & 0 & 0 \\ 0 & 0 & 0 & I_{G_x} c_\beta c_\gamma & I_{G_x} s_\gamma & 0 \\ 0 & 0 & 0 & -I_{G_y} c_\beta s_\gamma & I_{G_y} c_\gamma & 0 \\ 0 & 0 & 0 & I_{G_z} s_\beta & 0 & I_{G_z} \end{bmatrix}, \\ \mathbf{C}(\mathbf{q}, \dot{\mathbf{q}}) &= S^T \begin{bmatrix} 0 \\ 0 \\ 0 \\ I_{O_x}(-\dot{\alpha}\dot{\beta}s_\beta c_\gamma - \dot{\alpha}\dot{\gamma}c_\beta s_\gamma + \dot{\beta}\dot{\gamma}c_\gamma) \\ I_{O_y}(\dot{\alpha}\dot{\beta}s_\beta s_\gamma - \dot{\alpha}\dot{\gamma}c_\beta c_\gamma - \dot{\beta}\dot{\gamma}s_\gamma) \\ I_{O_z}\dot{\alpha}\dot{\beta}c_\beta \end{bmatrix} + S^T \begin{bmatrix} \mathbf{0} \\ \boldsymbol{\omega}_{\mathcal{E}} \times (I_O \boldsymbol{\omega}_{\mathcal{E}}) \end{bmatrix}, \end{aligned}$$

$$\mathbf{G}(\mathbf{q}) = \begin{bmatrix} -\mathcal{E}_O R mg \\ \mathbf{0} \end{bmatrix}.$$

Under no external forces on the manipulator, the external force vector is $\Gamma_{ext} = \mathbf{0}$. Finally, using the definition of \mathbf{f}_i from (3.13) and the projection (3.23) on (3.22) allows J^T to be expressed as

$$J^T = S^T \begin{bmatrix} \hat{\mathbf{l}}_1 & \hat{\mathbf{l}}_2 & \dots & \hat{\mathbf{l}}_7 \\ \mathbf{r}_{GB_1} \times \hat{\mathbf{l}}_1 & \mathbf{r}_{GB_2} \times \hat{\mathbf{l}}_2 & \dots & \mathbf{r}_{GB_7} \times \hat{\mathbf{l}}_7 \end{bmatrix}. \quad (3.24)$$

As expected, it can be observed from (3.24) that $J^T = S^T V^T$ relates the cable forces to the manipulator motion and is the transpose of the Jacobian matrix $J = VS$ obtained from the kinematic relationships (3.19) and (3.20).

3.3.3 4 DoF Two Link Manipulator

In the previous examples shown in Sections 3.3.1 and 3.3.2, both manipulators can be classified as single link CDPMs. In this section, the model for a two link mechanism possessing 4 DoF is presented. As shown in Figure 3.12, link 1 of the manipulator is constrained to the base at O through a spherical joint, and link 2 is connected to link 1 at P_1 through a revolute joint. The purpose of this example is to illustrate and motivate the challenges involved in the modelling of multilink cable-driven manipulators. In particular, the increased complexity in modelling the different possible cable routing arrangements is demonstrated.

The pose of the manipulator can be described by $\mathbf{q} = [\mathbf{q}_1^T \ \mathbf{q}_2^T]^T$, where the generalised coordinates for link 1 and link 2 can be denoted by \mathbf{q}_1 and \mathbf{q}_2 , respectively. For link 1, $\mathbf{q}_1 = [\alpha \ \beta \ \gamma]^T$ represents the xyz -Euler angles of the spherical joint, respectively. Similarly, $\mathbf{q}_2 = [\theta]$ represents the rotation in the x -axis of link 2 relative to link 1.

For the two link manipulator, three coordinate frames, $\{F_0\}$, $\{F_1\}$ and $\{F_2\}$, can be used to describe positions for the system. Positions on the base frame can be described with respect to the inertial coordinate frame $\{F_0\}$. Positions on link 1 and link 2 can be described with respect to the non-inertial coordinate frames $\{F_1\}$ and $\{F_2\}$, respectively. The non-inertial coordinate frames $\{F_1\}$ and $\{F_2\}$ are rigidly attached onto link 1 and

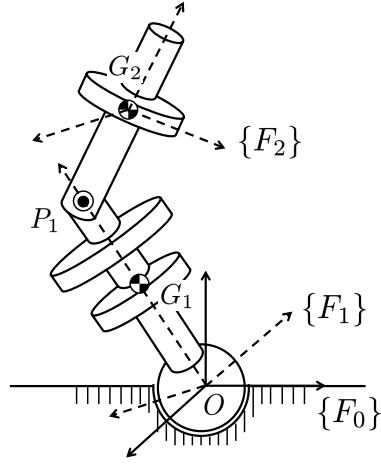


Figure 3.12: The rigid body structure for a 4 DoF 2 link CDPM showing the coordinate frames, centre of mass locations and joint locations.

link 2 of the manipulator, respectively, with origins fixed to O and G_2 , respectively. The rotational matrices ${}_1^0R$ and ${}_2^1R$ are defined as

$$\begin{aligned} {}_1^0R(\mathbf{q}) &= \begin{bmatrix} c_\beta c_\gamma & -c_\beta s_\gamma & s_\beta \\ c_\alpha s_\gamma + s_\alpha s_\beta c_\gamma & c_\alpha c_\gamma - s_\alpha s_\beta s_\gamma & -s_\alpha c_\beta \\ s_\alpha s_\gamma - c_\alpha s_\beta c_\gamma & s_\alpha c_\gamma + c_\alpha s_\beta s_\gamma & c_\alpha c_\beta \end{bmatrix}, \\ {}_2^1R(\mathbf{q}) &= \begin{bmatrix} 1 & 0 & 0 \\ 0 & c_\theta & -s_\theta \\ 0 & s_\theta & c_\theta \end{bmatrix}. \end{aligned} \quad (3.25)$$

Figure 3.13 shows the arrangement of the 6 cables that actuate the system. Since the system possesses two links, multiple ways in which cables can route through the system (*cable routing*) exist. In this example, as shown in Figure 3.13, two different ways of cable routing are presented:

1. Cables 1 to 4 are directly connected from the base to link 1. The attachment locations at the base and link 1 are denoted by A_i and B_i , respectively, for $i = 1, \dots, 4$.
2. Cables 5 and 6 are connected from the base at A_i to link 2 at C_i , while passing through link 1 at location B_i for $i = 5, 6$.

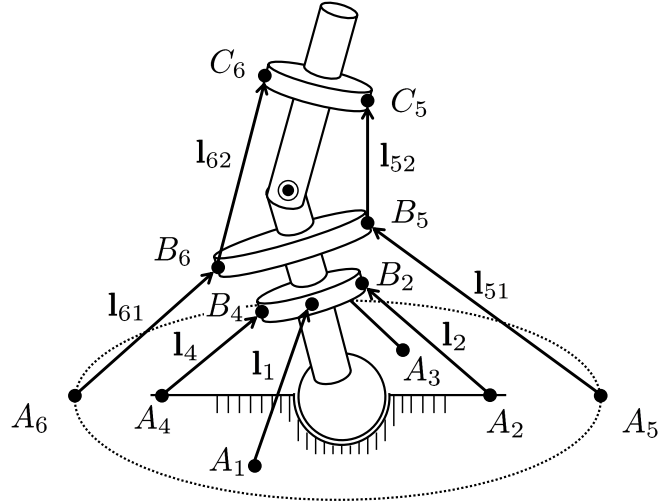


Figure 3.13: The cable arrangement of the 4 DoF 2 link CDPM showing the cable vectors. The cable attachments for cable i at the base, link 1 and link 2 are denoted by A_i , B_i and C_i , respectively.

Cable routing for cables 1 to 4

From Figure 3.13, the cable vector \mathbf{l}_i for $i = 1, \dots, 4$ with respect to $\{F_1\}$ can be expressed as

$${}^1\mathbf{l}_i = - {}^1R {}^0\mathbf{r}_{OA_i} + {}^1\mathbf{r}_{OB_i} \quad \forall i = 1, \dots, 4. \quad (3.26)$$

The length of cables 1 to 4 can be determined with respect to \mathbf{q} from (3.26), where $l_i = \|\mathbf{l}_i\| \quad \forall i = 1, \dots, 4$. The time derivative of the length of cable i can be expressed as $\dot{l}_i = \hat{\mathbf{l}}_i \cdot \dot{\mathbf{l}}_i$. Hence, taking the time derivative from (3.26) results in

$$\dot{l}_i = (\mathbf{r}_{OB_i} \times \hat{\mathbf{l}}_i) \cdot \boldsymbol{\omega}_1 \quad \forall i = 1, \dots, 4. \quad (3.27)$$

Cable routing for cables 5 and 6

For cables $i = 5, 6$, the kinematics of the cables can be modelled as two individual segments. The cable vector for segment 1, denoted by \mathbf{l}_{i1} , can be expressed with respect to $\{F_1\}$ as

$${}^1\mathbf{l}_{i1} = - {}^1R {}^0\mathbf{r}_{OA_i} + {}^1\mathbf{r}_{OB_i} \quad \forall i = 5, 6. \quad (3.28)$$

Similarly, the cable vector for segment 2, denoted by \mathbf{l}_{i2} can be expressed with respect to $\{F_2\}$ as

$${}^2\mathbf{l}_{i2} = - {}^1R {}^1\mathbf{r}_{OB_i} + {}^2\mathbf{r}_{OG_2} + {}^2\mathbf{r}_{G_2C_i} \quad \forall i = 5, 6. \quad (3.29)$$

The cable length can be determined by summing the lengths of each segment from (3.28) and (3.29), where $l_i = \|\mathbf{l}_{i1}\| + \|\mathbf{l}_{i2}\| \quad \forall i = 5, 6$. These relationships allow the inverse kinematics of the manipulator to be determined.

For cables 5 and 6, the time derivative of the length of cable i must consider the change in length of both segments and can be expressed as $\dot{l}_i = \hat{\mathbf{l}}_{i1} \cdot \dot{\mathbf{l}}_{i1} + \hat{\mathbf{l}}_{i2} \cdot \dot{\mathbf{l}}_{i2}$. Hence from (3.28) and (3.29), \dot{l}_i can be expressed as

$$\dot{l}_i = (\mathbf{r}_{OB_i} \times (\hat{\mathbf{l}}_{i1} - \hat{\mathbf{l}}_{i2})) \cdot \boldsymbol{\omega}_1 + \hat{\mathbf{l}}_{i2} \cdot \mathbf{r}_{OG_2} + (\mathbf{r}_{G_2C_i} \times \hat{\mathbf{l}}_{i2}) \cdot \boldsymbol{\omega}_2 \quad \forall i = 5, 6. \quad (3.30)$$

Jacobian Matrix

Expressing (3.27) and (3.30) for the set of cables allows the time derivative of the cable length vector to be expressed in the form $\dot{\mathbf{l}} = V\dot{\mathbf{x}}$

$$\begin{bmatrix} \dot{l}_1 \\ \vdots \\ \dot{l}_4 \\ \dot{l}_5 \\ \dot{l}_6 \end{bmatrix} = \begin{bmatrix} (\mathbf{r}_{OB_1} \times \hat{\mathbf{l}}_1)^T & \mathbf{0}^T & \mathbf{0}^T \\ \vdots & \vdots & \vdots \\ (\mathbf{r}_{OB_4} \times \hat{\mathbf{l}}_4)^T & \mathbf{0}^T & \mathbf{0}^T \\ (\mathbf{r}_{OB_5} \times (\hat{\mathbf{l}}_{51} - \hat{\mathbf{l}}_{52}))^T & \hat{\mathbf{l}}_{52}^T & (\mathbf{r}_{G_2C_5} \times \hat{\mathbf{l}}_{52})^T \\ (\mathbf{r}_{OB_6} \times (\hat{\mathbf{l}}_{61} - \hat{\mathbf{l}}_{62}))^T & \hat{\mathbf{l}}_{62}^T & (\mathbf{r}_{G_2C_6} \times \hat{\mathbf{l}}_{62})^T \end{bmatrix} \begin{bmatrix} {}^1\boldsymbol{\omega}_1 \\ {}^2\dot{\mathbf{r}}_{OG_2} \\ {}^2\boldsymbol{\omega}_2 \end{bmatrix}, \quad (3.31)$$

where $\dot{\mathbf{x}} = [{}^1\boldsymbol{\omega}_1 \ {}^2\dot{\mathbf{r}}_{OG_2} \ {}^2\boldsymbol{\omega}_2]^T$ is the twist vector that contains the angular velocity of link 1, the absolute velocity of G_2 and the absolute angular velocity of link 2.

Considering the kinematics of each link, the absolute velocities of each rigid link can be related to the generalised coordinate velocities. Firstly, the absolute angular velocity

ω_1 of link 1 can be related to $\dot{\mathbf{q}}_1$ in the form $\omega_1 = S_1 \dot{\mathbf{q}}_1$, where

$${}^1\boldsymbol{\omega}_1 = \begin{bmatrix} c_\beta c_\gamma & c_\alpha s_\gamma + s_\alpha s_\beta c_\gamma & s_\alpha s_\gamma - c_\alpha s_\beta c_\gamma \\ -c_\beta s_\gamma & c_\alpha c_\gamma - s_\alpha s_\beta s_\gamma & s_\alpha c_\gamma + c_\alpha s_\beta s_\gamma \\ s_\beta & -s_\alpha c_\beta & c_\alpha c_\beta \end{bmatrix} \begin{bmatrix} \dot{\alpha} \\ \dot{\beta} \\ \dot{\gamma} \end{bmatrix}. \quad (3.32)$$

Similarly, the relative angular velocity of link 2 relative to link 1 can be expressed as $\omega_{2,1} = S_2 \dot{\mathbf{q}}_2$, where

$${}^2\boldsymbol{\omega}_{2,1} = \begin{bmatrix} 1 \\ 0 \\ 0 \end{bmatrix} \dot{\theta}. \quad (3.33)$$

From (3.32) and (3.33), ω_2 can be determined by ${}^2\boldsymbol{\omega}_2 = {}_1^2R {}^1\boldsymbol{\omega}_1 + {}^2\boldsymbol{\omega}_{2,1}$. Similarly, the absolute velocity of G_2 can be expressed as $\dot{\mathbf{r}}_{OG_2} = {}_1^2R({}^1\boldsymbol{\omega}_1 \times {}^1\mathbf{r}_{OP_1}) + {}^2\boldsymbol{\omega}_2 \times {}^2\mathbf{r}_{P_1G_2}$. As a result, the body twist vector $\dot{\mathbf{x}}$ can be related to the joint space velocity vector $\dot{\mathbf{q}}$ in the form $\dot{\mathbf{x}} = W\dot{\mathbf{q}}$, where

$$\begin{bmatrix} {}^1\boldsymbol{\omega}_1 \\ {}^2\dot{\mathbf{r}}_{OG_2} \\ {}^2\boldsymbol{\omega}_2 \end{bmatrix} = \begin{bmatrix} S_1 & 0_{3 \times 1} \\ -{}_1^2R [{}^1\mathbf{r}_{OG_2}]^\times S_1 & -[{}^2\mathbf{r}_{P_1G_2}]^\times S_2 \\ {}_1^2R S_1 & S_2 \end{bmatrix} \begin{bmatrix} \dot{\mathbf{q}}_1 \\ \dot{\mathbf{q}}_2 \end{bmatrix}. \quad (3.34)$$

Hence, from (3.31) and (3.34), the Jacobian matrix $J \in \mathbb{R}^{6 \times 4}$ can be expressed as $J = VW$.

Equations of Motion

The dynamics for the manipulator can be modelled by deriving the equations of motion for the system and expressing in the form (3.2). The equations of motion for the 4 DoF 2 link manipulator can be determined by taking the sum of moments for link 1 about point O , the sum of forces for link 2 and the sum of moments for link 2 about point G_2 . Firstly, the sum of moments for link 1 about point O can be expressed as

$$I_{1O}\ddot{\omega}_1 + \boldsymbol{\omega}_1 \times (I_{1O}\boldsymbol{\omega}_1) = \sum \mathbf{M}_1, \quad (3.35)$$

where I_{1O} represents the moment of inertia of link 1 about O . Subsequently, the sum of forces for link 2 can be expressed as

$$m_2 \ddot{\mathbf{r}}_{OG_2} = \sum \mathbf{F}_2 , \quad (3.36)$$

where m_2 is the mass of link 2. Finally, the sum of moments for link 2 about G_2 can be expressed as

$$I_{2G_2} \dot{\omega}_2 + \omega_2 \times (I_{2G_2} \omega_2) = \sum \mathbf{M}_2 , \quad (3.37)$$

where I_{2G_2} represents the moment of inertia of link 2 about G_2 .

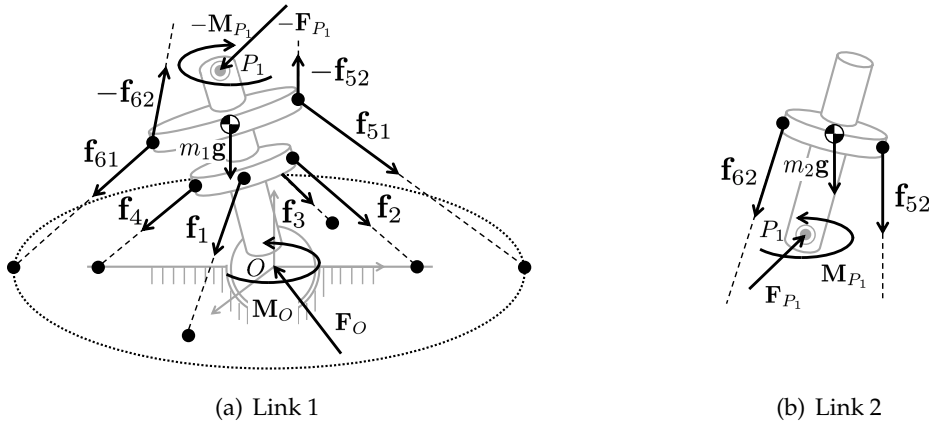


Figure 3.14: The free body diagram for the 4 DoF 2 link CDPM for each of the links. Note the interaction forces and moments at joint locations O and P_1 .

Figure 3.14 shows the forces and moments acting on the individual bodies of the two link manipulator. As shown in Figure 3.14(b), the sum of forces and moments acting on link 2 is comprised of

- gravity force $m_2\mathbf{g}$, where m_2 is the mass of link 2
- joint interaction force \mathbf{F}_{P_1} and joint interaction moment \mathbf{M}_{P_1} at P_1
- cable forces \mathbf{f}_{52} and \mathbf{f}_{62} from segment 2 of cables 5 and 6, respectively.

Hence, the sum of forces of link 2 and the sum of moments of link 2 about G_2 can be expressed as

$$\sum \mathbf{F}_2 = m_2 \frac{d}{dt} \mathbf{r}_{OG_2} + \mathbf{F}_{P_1} - \sum_{i=5}^6 \hat{\mathbf{l}}_{i2} \mathbf{f}_i$$

$$\sum \mathbf{M}_2 = -\mathbf{r}_{P_1G_2} \times \mathbf{F}_{P_1} + \mathbf{M}_{P_1} - \sum_{i=5}^6 \mathbf{r}_{G_2C_i} \times \hat{\mathbf{l}}_{i2} f_i . \quad (3.38)$$

The forces and moments acting on link 1, as shown in Figure 3.14(a), is comprised of

- gravity force $m_1\mathbf{g}$, where m_1 is the mass of link 1
- reaction joint interaction force $-\mathbf{F}_{P_1}$ and moment $-\mathbf{M}_{P_1}$ at P_1
- joint interaction force \mathbf{F}_O and joint interaction moment \mathbf{M}_O at O
- cable forces $-\mathbf{f}_{52}$ and $-\mathbf{f}_{62}$ from segment 2 of cables 5 and 6, respectively
- cable forces \mathbf{f}_{51} and \mathbf{f}_{61} from segment 1 of cables 5 and 6, respectively
- cable forces $\mathbf{f}_1, \mathbf{f}_2, \mathbf{f}_3$ and \mathbf{f}_4 , from cables 1, 2, 3 and 4, respectively

$$\begin{aligned} \sum \mathbf{M}_1 = & \mathbf{r}_{OG} \times (\frac{1}{0}R m_1\mathbf{g}) + \mathbf{M}_O - \mathbf{r}_{OP_1} \times (\frac{1}{2}R \mathbf{F}_{P_1}) - \frac{1}{2}R \mathbf{M}_{P_1} \\ & - \sum_{i=1}^4 \mathbf{r}_{OB_i} \times \hat{\mathbf{l}}_i f_i - \sum_{i=5}^6 \mathbf{r}_{OB_i} \times (\hat{\mathbf{l}}_{i1} - \hat{\mathbf{l}}_{i2}) f_i \end{aligned} \quad (3.39)$$

From Figures 3.13 and 3.14, it can be observed that the cable force vectors relate to the cable vectors through

$$\begin{aligned} \mathbf{f}_i &= -\hat{\mathbf{l}}_i f_i \quad \forall i = 1, \dots, 4, \\ \mathbf{f}_{i1} &= -\hat{\mathbf{l}}_{i1} f_i \quad \forall i = 5, 6, \\ \mathbf{f}_{i2} &= -\hat{\mathbf{l}}_{i2} f_i \quad \forall i = 5, 6. \end{aligned} \quad (3.40)$$

Incorporating (3.38), (3.39) and (3.40) into the Newton's second law equations (3.35), (3.36) and (3.37) results in

$$\begin{aligned} I_{1O}\dot{\omega}_1 + \boldsymbol{\omega}_1 \times (I_{1O}\boldsymbol{\omega}_1) &= \mathbf{r}_{OG} \times (\frac{1}{0}R m_1\mathbf{g}) + \mathbf{M}_O - \mathbf{r}_{OP_1} \times (\frac{1}{2}R \mathbf{F}_{P_1}) - \frac{1}{2}R \mathbf{M}_{P_1} \\ & - \sum_{i=1}^4 \mathbf{r}_{OB_i} \times \hat{\mathbf{l}}_i f_i - \sum_{i=5}^6 \mathbf{r}_{OB_i} \times (\hat{\mathbf{l}}_{i1} - \hat{\mathbf{l}}_{i2}) f_i, \\ m_2\ddot{\mathbf{r}}_{OG_2} &= m_2 \frac{2}{0}R \mathbf{g} + \mathbf{F}_{P_1} - \sum_{i=5}^6 \hat{\mathbf{l}}_{i2} f_i, \\ I_{2G_2}\dot{\omega}_2 + \boldsymbol{\omega}_2 \times (I_{2G_2}\boldsymbol{\omega}_2) &= -\mathbf{r}_{P_1G_2} \times \mathbf{F}_{P_1} + \mathbf{M}_{P_1} - \sum_{i=5}^6 \mathbf{r}_{G_2C_i} \times \hat{\mathbf{l}}_{i2} f_i. \end{aligned} \quad (3.41)$$

From (3.41), the interaction forces $\begin{bmatrix} \mathbf{M}_O^T & \mathbf{M}_{P_1}^T \end{bmatrix}^T$ can be expressed as

$$\begin{bmatrix} {}^1\mathbf{M}_O \\ {}^2\mathbf{M}_{P_1} \end{bmatrix} = \begin{bmatrix} I_{3 \times 3} & [\mathbf{r}_{OG_2}]^\times \frac{1}{2}\mathbf{R} & \frac{1}{2}\mathbf{R} \\ 0_{3 \times 3} & [\mathbf{r}_{P_1G_2}]^\times & I_{3 \times 3} \end{bmatrix} (\mathbf{w} + V^T \mathbf{f}), \quad (3.42)$$

where

$$\mathbf{w} = \begin{bmatrix} I_{1O}\dot{\omega}_1 + \boldsymbol{\omega}_1 \times (I_{1O}\boldsymbol{\omega}_1) - \mathbf{r}_{OG} \times (\frac{1}{0}\mathbf{R} m_1 \mathbf{g}) \\ m_2 \ddot{\mathbf{r}}_{OG_2} - m_2 \frac{2}{0}\mathbf{R} \mathbf{g} \\ I_{2G_2}\dot{\omega}_2 + \boldsymbol{\omega}_2 \times (I_{2G_2}\boldsymbol{\omega}_2) \end{bmatrix}.$$

Finally, the equations of motion for the system can be determined by projecting the interaction moments from (3.42) onto the degrees of freedom of the manipulator, where

$$\begin{bmatrix} S_1^T & 0_{3 \times 3} \\ 0_{1 \times 3} & S_2^T \end{bmatrix} \begin{bmatrix} {}^1\mathbf{M}_O \\ {}^2\mathbf{M}_{P_1} \end{bmatrix} = \mathbf{0}. \quad (3.43)$$

Applying the projection from (3.43) onto (3.42) results in the equations of motion of the form

$$W^T \mathbf{w} = -W^T V^T \mathbf{f}, \quad (3.44)$$

where W^T is the transpose of the matrix W from (3.34). The terms M , \mathbf{C} and \mathbf{G} from (3.2) can be determined from $W^T \mathbf{w}$. It is assumed that no external forces and moments act on the system and hence $\boldsymbol{\Gamma}_{ext} = \mathbf{0}$. As with previous examples, it can be observed from (3.44) that $J^T = W^T V^T$ relates the cable forces to the manipulator motion and is the transpose of the Jacobian matrix $J = VW$ obtained from the kinematic relationships (3.31) and (3.34).

From the simple two link example, it can be observed that the modelling of multilink mechanisms differs from that of single link systems in several ways. Firstly, the complexity in the modelling of cable kinematics and dynamics is increased as there exists multiple types of cable routing arrangement for multilink systems. The kinematic and dynamic relationships from (3.31) and (3.42), respectively, must be modelled for each cable routing. From the examples presented in Sections 3.3.1 and 3.3.2, single link CDPMs only possess one type of cable routing, that is, from the base to the end-effector. However, it can be observed that for the two link mechanism multiple types of cable routing exist. In

in this example, two types of cable routing were presented, but it should be noted that other types also exist.

Furthermore, the effect of cable forces on the motion of the manipulator links becomes highly coupled and is dependent on the type of cable routing. This coupling effect can be explained by two characteristics in the cable routing of multilink CDPMs. First, a single cable may be connected to multiple links, resulting in multiple sections for each cable. For example, cables 5 and 6 are connected to both links 1 and 2 of the manipulator and possess two sections of cable. As a result, the cable force in cables 5 and 6 directly affects the motion of both links, increasing the complexity of the manipulator dynamics. Second, the interaction forces and moments in the joints of multilink mechanisms propagate the effect of the cable forces through the kinematic structure. Hence, the resultant motion from the cable actuation becomes furthered coupled. From the simple two link manipulator presented, it can be observed that the described complexities and effects become more significant as the number of links increase.

3.4 Conclusion

In this chapter, the modelling of the kinematics and dynamics for CDPMs were introduced. The unique characteristics of cable-driven systems are the required actuation redundancy and positive cable force constraint. The different types of kinematic and dynamic analyses for CDPMs were presented. It was shown that the direct kinematics and inverse dynamics problems for CDPMs possess unique challenges compared to that of traditional serial and parallel mechanisms. However, in order to solve the unique challenges, it is important to first derive the kinematic and dynamic models. To demonstrate the procedure in modelling CDPMs, the model for three different example manipulators were formulated. From these examples, it was observed that the Jacobian matrix is required to be derived for each individual system depending on the manipulator structure. For single link CDPMs, this can be considered as trivial due to the simplicity in manipulator structure and the single type of cable routing. However, for multilink CDPMs, the cable routing and kinematic structure presents challenges in individually formulating the

system model. As a result, this motivates the need for a generalised model for multilink cable-driven parallel manipulators.

Chapter 4

Generalised Cable Routing for Multilink Cable-Driven Manipulators

In this chapter, a generalised representation for the cable routing of multilink cable-driven manipulators (MCDMs) is presented. Introducing the cable-routing matrix (CRM), it is shown that arbitrary cable routing can be encapsulated within a single representation. The proposed CRM resolves a major challenge in the modelling of complex MCDMs that possess a large number of links, where the kinematics and dynamics for each of the possible combinations in cable routing must be individually modelled otherwise. Section 4.1 motivates the need for a generalised cable routing model for MCDMs, particularly for complex bio-inspired and engineered MCDMs. To represent the cable routing, the definition of the CRM is presented in Section 4.2. The examples presented in Section 4.3 illustrate how the CRM can be used to represent the cable routing of arbitrarily complex MCDM systems. To ensure that the CRM represents valid cable routing, properties that can be regarded as necessary and sufficient conditions for a valid CRM are defined in Section 4.4. Section 4.5 demonstrates the effectiveness in how the CRM can be used to establish a generalised definition for the vectors of the cable segments. Finally, Section 4.6 concludes the chapter by summarising the contributions.

4.1 Introduction

In the modelling of multilink cable-driven manipulators (MCDMs), one of the primary challenges is that the kinematics and dynamics for each *type of cable routing* (Definition 4.1) must be individually considered. As demonstrated from the example in Section 3.3.3, the cable routing of MCDMs may consist of multiple *cable segments*, where the definition for a cable segment in the context of MCDMs is described in Definition 4.2.

Definition 4.1. *Type of cable routing* refers to the path that a cable routes through the links of

an MCDM.

Definition 4.2. *Cable segment* refers to the single section of cable between two cable attachment points (refer to Definition 4.3).

Definition 4.3. *Cable attachment point* refers to the point where a cable is connected to or passes through a link.

To ensure that the cable routing is physically realisable, Property 4.1 must be satisfied for the cables within the system. Defining the number of segments for cable i as s_i , the maximum number of segments for any cable within the MCDM system can be denoted by $s = \max_i s_i$.

Property 4.1. *Each cable must have a finite number of cable segments, where s_i is the number of segments for cable i .*

To illustrate the complexity in modelling the cable routing for MCDMs, the number of types of *open-chain cable routing* (Definition 4.4) for MCDMs of varying number of links is presented. Equivalently, open-chain cable routing means that each cable can only be attached to each link at most once. Hence for a p link MCDM that allows for open-chain cable routing, the maximum number of cable segments for any cable is $s = p$.

Definition 4.4. *Open-chain cable routing* refers to cables that do not form closed loops on the links of the manipulator.

Consider the types of open-chain cable routing for the 2 link manipulator example presented in Section 3.3.3, where each consists of a maximum of two segments. From Definition 4.5, the types of cable routing can be categorised either as class 1 or class 2 cable routing.

Definition 4.5. *The class of cable routing is the number of segments that the cable possesses.*

As shown in Figure 4.1, the 2 link manipulator possesses three types of class 1 cable routing. Assuming that the system is actuated by ideal cables that produce equal and opposite cable forces on both links it is attached to, the actuating motor can be situated on either attachment locations. Class 1 cable routing consists of only one segment and

hence two cable attachment points. Figures 4.1(a) and 4.1(b) show examples in which the cable is attached from the base to the manipulator. However, it is also possible for a cable to connect from link 1 to link 2, as shown in Figure 4.1(c).

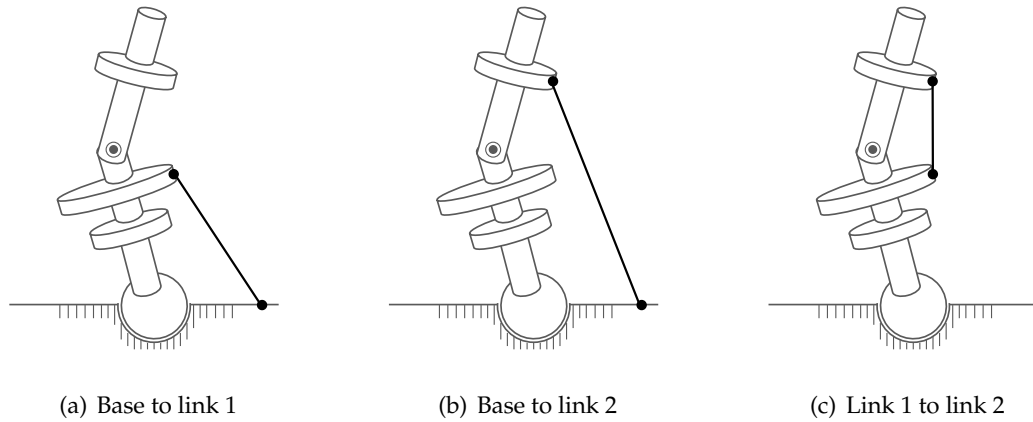


Figure 4.1: The types of class 1 cable routing for a 2 link CDPM.

For two link mechanisms, it is also possible to route the cables such that they consist of two segments. As shown in Figure 4.2, there exists three types of class 2 cable routings that connect the base, link 1 and link 2 of the manipulator.

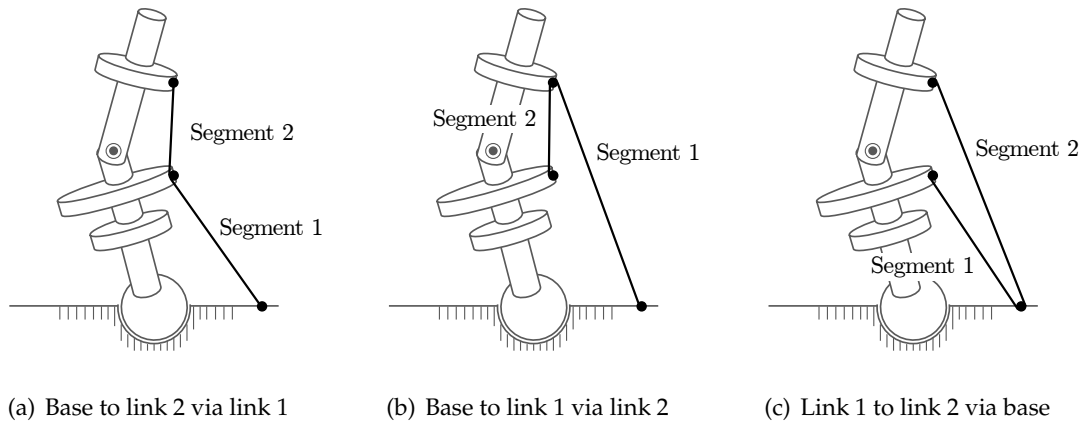


Figure 4.2: The types of class 2 cable routing for a 2 link CDPM.

For class 2 cable routings, each cable possesses three cable attachment points. In addition to the two ends of the cable, the cable also possesses a pass-through attachment point. For example, the cable routings shown in Figures 4.2(a), 4.2(b) and 4.2(c) bypass

Links (p)	Number of types of cable routing for class c (N_{pc})								Total (N_p)
	1	2	3	4	5	...	11		
1	1	-	-	-	-	...	-	1	
2	3	3	-	-	-	...	-	6	
3	6	12	12	-	-	...	-	30	
4	10	30	60	60	-	...	-	160	
5	15	60	180	360	360	...	-	975	
8	36	252	1512	7560	30240	...	-	$\approx 49 \times 10^4$	
11	66	660	5940	47520	332640	...	$\approx 24 \times 10^7$	$\approx 65 \times 10^7$	

Table 4.1: The number of open-chain cable routing combinations for MCDMs of varying number of links showing the exponential growth in the number of combinations as the number of links increase.

through link 1, link 2 and the base, respectively.

For the two link manipulator, there exists a total of 6 types of open-chain cable routing (Definition 4.4) that can be categorised into two classes (Definition 4.5). For a p link MCDM, class c open-chain cable routings can be generated by selecting c links from the p links and the base of the manipulator. Hence, if the location of the actuating motor is disregarded, the number of types of class c open-chain cable routing N_{pc} for a p link MCDM can be determined as

$$N_{pc} = \frac{^{p+1}P_{c+1}}{2} = \frac{(p+1)!}{2(p-c)!}, \quad (4.1)$$

where aP_b refers to the number of b -permutations of a . From (4.1), the total number of types of open-chain cable routing for a p link MCDM can be computed as

$$N_p = \sum_{c=1}^p \frac{^{p+1}P_{c+1}}{2}. \quad (4.2)$$

As a result, it is apparent from (4.2) that the number of types of open-chain cable routing N_p increases exponentially with the number of links of the manipulator. Table 4.1 shows the number of types of cable routing for manipulators with varying number of links, as determined from (4.1) and (4.2).

From Table 4.1, it can be observed that single link and two link manipulators possess

a total of 1 type and 6 types of open-chain cable routing, respectively, and is consistent with the example shown in Figures 4.1 and 4.2. Furthermore, since the number of types of cable routing increases exponentially as the number of links increase, it is impractical to individually model every type of cable routing even for a system with a relatively small number of links. For example, for 5 link and 11 link manipulators, there exists a total of approximately 10^3 and 10^8 number of open-chain cable routing types, respectively. It should also be noted that for a p link manipulator, the majority of the types of open-chain cable routing (Definition 4.4) is due to the higher classes of cable routing, such as class p and class $p - 1$.

Furthermore, the types of open-chain cable routing only represent a subset of the total types of arbitrary cable routing. Compared with open-chain cable routing, the number of types of arbitrary cable routing increases even more as the number of segments or the number of links increase. As reviewed in Section 2.4, previous studies in MCDMs have avoided the need to model a large number of cable routing types in several ways. In the humanoid arm design proposed in [141], the types of cable routing were limited by only connecting the cable to the links directly below and above the joint to be actuated. Similarly, the studies from [111, 112] assume that each cable is connected from the base to only one of the manipulator links. As a result, the above studies consider only the subset of p of the class 1 cable routings. More recently, the modelling and analysis of MCDMs to allow arbitrary cable routing have been studied [91, 92]. However, as each class and type of cable routing must be individually modelled, the proposed techniques are practical only for MCDMs with a low number of links, such as those with two or three links.

As a result, the previous approaches would be unsuitable in the study of more complex MCDMs that possess a large number of links, while also allowing for arbitrary cable routing. Both of these characteristics are common in bio-inspired and some engineered MCDMs, as described in Section 2.1. For example, the human neck and human upper limb can be modelled as an 8 link serial chained MCDM and a 17 link branched MCDM, respectively. Furthermore, both of these systems possess many different classes and types of cable routing. Hence, the ability to model arbitrarily complex MCDMs would allow a much wider range of biological and engineered systems to be studied.

4.2 Cable-Routing Matrix

In this section, the *cable-routing matrix* (CRM) that represents the generalised cable routing for MCDMs is defined. The proposed representation allows *arbitrary cable routing* for MCDMs with *any number of links* to be represented within a single representation. The primary advantage of the proposed approach is that all types of cable routing can be modelled and analysed through the single form, eliminating the need to formulate each type of cable routing individually. In defining the CRM, the generalised cable routing for single segment (class 1) cables is first presented in Section 4.2.1, and is then extended to allow for cables with multiple segments in Section 4.2.2.

To formulate the arbitrary cable routing for an MCDM with any number of links, consider the p link manipulator model shown in Figure 4.3. The system can be modelled as possessing a total of $p + 1$ links, where link 0 refers to the inertial base and links 1 to p are the corresponding links of the manipulator.

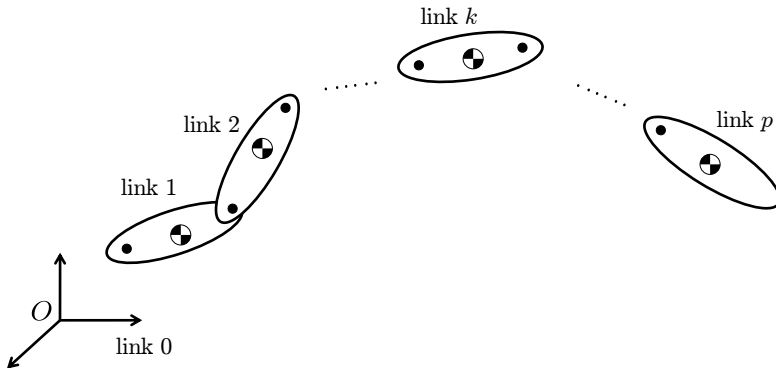


Figure 4.3: The rigid body structure for a serial p link MCDM, where link 0 refers to the inertial base and links 1 to p are the corresponding links of the manipulator.

4.2.1 Single Segment Cable Routing

The cable routing for any single segment cable can be described by the two links in which the cable attaches from and to, defined as the *beginning attachment link* (Definition 4.6) and *ending attachment link* (Definition 4.7), respectively. Furthermore, the cable does not attach onto the remaining links of the manipulator.

Definition 4.6. *The beginning attachment of a cable refers to the location of the actuating motor of the cable.*

Definition 4.7. *The ending attachment of a cable refers to the location of the unactuated end of the cable.*

Hence, the relationship between any cable and link can be expressed by $c \in \mathcal{C}$, where the set \mathcal{C} is defined as

$$\mathcal{C} = \{-1, 0, 1\}. \quad (4.3)$$

The value $c = -1$ signifies that the link is the beginning attachment link for the cable. If $c = 1$, then the link is the ending attachment link. Finally, $c = 0$ denotes that the cable is not attached onto the link. As a result, it is possible to express the cable routing for a single segment cable by the vector

$$\mathbf{c} = \begin{bmatrix} c_1 & c_2 & \dots & c_{p+1} \end{bmatrix}, \quad (4.4)$$

where the element $c_{k+1} \in \mathcal{C}$, $k = 0, 1, \dots, p$ represents the routing relationship between the cable and link k of the manipulator. Physically, c_{k+1} has the following interpretation:

- $c_{k+1} = -1$ denotes that the cable's beginning attachment is on link k
- $c_{k+1} = 1$ denotes that the cable's ending attachment is on link k
- $c_{k+1} = 0$ denotes that the cable does not attach onto link k

For example, consider the class 1 cable routings for the two link manipulator shown in Figure 4.1. The cable routing in Figure 4.1(a), where the cable begins from the base (link 0) and ends at link 1, can be expressed by the vector $\mathbf{c} = [-1 \ 1 \ 0]$. Similarly, the vector $\mathbf{c} = [-1 \ 0 \ 1]$ represents the cable routing in Figure 4.1(b), where the cable begins from the base (link 0) and ends at link 2. Finally, the cable routing from Figure 4.1(c) can be expressed as $\mathbf{c} = [0 \ -1 \ 1]$.

The generalised form of cable routing of a single segment cable from (4.4) allows all class 1 cable routings to be described within a single representation. As a result, if the system kinematics and dynamics are modelled with respect to the elements c_1, c_2 to c_{p+1} from (4.4) for every cable, then all possible class 1 cable routings can be inherently considered.

4.2.2 Multi-Segment Cable Routing

In this section, the single segment cable routing representation presented in (4.4) is extended to allow arbitrary cable routings for a p link MCDM actuated by m cables to be represented. In the proposed cable-routing matrix (CRM) representation, the cables are characterised by two important properties. Firstly, no assumptions are made on the types of cable routing allowed for the system. Secondly, each cable may possess multiple segments, where s_i is defined as the number of segments for cable i and $s = \max_i s_i$ is the maximum number of segments for any cable within the MCDM.

Definition 4.8. *The Cable-Routing Matrix (CRM), denoted by*

$$C \in \mathcal{C}^{m \times s \times (p+1)}, \quad (4.5)$$

is a three-dimensional matrix that constructed of terms C defined in (4.3) that describes the cable routing information for the entire set of m cables for an MCDM system.

The CRM can be described as $C = \{C_1, C_2, \dots, C_m\}$, where $C_i \in \mathcal{C}^{s \times (p+1)}$ represents the cable routing of cable i . The matrix C_i can be expressed as

$$C_i = \begin{bmatrix} c_{i11} & c_{i12} & \dots & c_{i1(p+1)} \\ \vdots & & & \vdots \\ c_{is1} & c_{is2} & \dots & c_{is(p+1)} \end{bmatrix}, \quad (4.6)$$

where the element $c_{ij(k+1)}$ describes the cable routing relationship between segment j of cable i and link k . Each row of C_i represents the cable routing for a particular segment of cable i , as described by (4.4), where row j of C_i represents the cable routing of segment j of cable i . In a similar manner to Section 4.2.1, the CRM element $c_{ij(k+1)}$ has the following physical interpretation:

- $c_{ij(k+1)} = -1$ denotes that segment j of cable i begins from link k
- $c_{ij(k+1)} = 1$ denotes that segment j of cable i ends at link k
- $c_{ij(k+1)} = 0$ denotes that segment j of cable i is not connected to link k

For link k , if $c_{ij(k+1)} = -1$ or $c_{ij(k+1)} = 1$, then link k is the beginning or ending

attachment link for segment j of cable i , respectively. Constructing the CRM such that the segments are consecutive, the beginning attachment for the first segment can be referred to as the beginning attachment of the cable as defined in Definition 4.6. Similarly, the ending attachment of the final segment of a cable can be considered as ending attachment of the cable as defined in Definition 4.7. For cables with multiple segments, the remaining attachment locations can be referred to as *pass-through attachments* (Definition 4.9).

Definition 4.9. *Pass-through attachment* of a cable refers to the connection point between two consecutive segments of a cable.

The CRM can be regarded as the cable routing description for generalised MCDMs, where all possible cable routings are encapsulated within the single matrix C . Modelling the kinematics and dynamics of the system with respect to the CRM results in a generalised model that does not require the cable routing to be known prior to constructing the model. Furthermore, any analysis performed on the generalised model, such as inverse dynamics, control, workspace analysis and cable attachment location optimisation, can be performed with respect to the CRM and inherently considers all possible cable routings. As such, the primary advantage of using the CRM is that the modelling and analysis of MCDMs is only performed once on the generalised model, and any reconfiguration of the cable routing only requires modification to the elements of the CRM. Finally, it is worth noting that the definition of the CRM in (4.6) results in a sparse matrix representation where a majority of the CRM terms are zero elements. However, it will be shown in Section 4.5 and subsequently Chapter 5 that the zero elements are an integral part in the generalised model of MCDMs.

4.3 Examples of Cable-Routing Matrices

To illustrate the simplicity in describing arbitrarily complex cable routing through the CRM, the routing of cables for various MCDMs will be presented. In Section 4.3.1, the CRM that describes the cable routing for the two link manipulator from Section 4.1 is presented. In Section 4.3.2, the ability of the CRM to model the complex cable routing of biomechanically inspired systems will be shown through the 8 link MCDM that is

inspired by the human neck. Finally, Section 4.3.3 shows that the proposed CRM is not only able to represent the cable routing of serial chain MCDMs, but also that of branched structured MCDMs. Without loss of generality, it will be assumed in all examples in this section that the maximum number of segments is equivalent to the number of links of the MCDM. This assumption is only applied to ensure that the presented CRMs have finite dimensions and does not impact on the ability of the CRM to achieve arbitrary cable routing.

4.3.1 Two Link Manipulator

Consider the set of cable routings for the two link manipulator presented in Figures 4.1 and 4.2. For the class 1 cable routings, the matrices C_1 , C_2 and C_3 describe the cable routing from Figures 4.1(a), 4.1(b) and 4.1(c), respectively, where

$$C_1 = \begin{bmatrix} -1 & 1 & 0 \\ 0 & 0 & 0 \end{bmatrix}, C_2 = \begin{bmatrix} -1 & 0 & 1 \\ 0 & 0 & 0 \end{bmatrix}, C_3 = \begin{bmatrix} 0 & -1 & 1 \\ 0 & 0 & 0 \end{bmatrix}.$$

The description of the first segment (row 1) of C_1 , C_2 and C_3 is consistent with that presented in Section 4.2.1. As the cable only consists of a single segment, all elements of the second segment (row 2) are set to be zero.

For the class 2 cables shown in Figure 4.2, the matrices C_4 , C_5 and C_6 describe the cable routing from Figures 4.2(a), 4.2(b) and 4.2(c), respectively, where

$$C_4 = \begin{bmatrix} -1 & 1 & 0 \\ 0 & -1 & 1 \end{bmatrix}, C_5 = \begin{bmatrix} -1 & 0 & 1 \\ 0 & 1 & -1 \end{bmatrix}, C_6 = \begin{bmatrix} 1 & -1 & 0 \\ -1 & 0 & 1 \end{bmatrix}.$$

For the cables shown in Figure 4.2(a), the first segment begins from the base and ends at link 1, denoted by $c_{411} = -1$ and $c_{412} = 1$, respectively. As segment 1 of the cable does not attach onto link 2, the value of the CRM element is $c_{413} = 0$. Consequently, the second segment begins on link 1, ends at link 2 and is unattached to the base (link 0), denoted by $c_{422} = -1$, $c_{423} = 1$ and $c_{421} = 0$, respectively. Similarly, C_5 describes the cable routing in Figure 4.2(b). Segment 1 begins from link 0 ($c_{511} = -1$), ends on link 2 ($c_{513} = 1$) and

hence does not attach onto link 1 ($c_{512} = 0$). Segment 2 begins from link 2 ($c_{523} = -1$), ends on link 1 ($c_{522} = 1$) and is not attached onto link 0 ($c_{521} = 0$). Finally, the cable routing from Figure 4.2(c) can be described by the matrix C_6 .

From the two link manipulator example, it can be observed that the matrix C_i from (4.6) is able to describe all the possible types for a single cable. Hence, the CRM (Definition 4.8) for a p link m cable system, $C \in \mathcal{C}^{m \times s \times (p+1)}$ from (4.5), can describe the entire set of cable routings for an MCDM with both arbitrary number of links and cables.

4.3.2 8 Link Serial Manipulator

To demonstrate the use of the proposed CRM for more complex MCDMs, such as the routing of muscles within biomechanical systems, consider the model of the human neck shown in Figure 4.4. The human neck can be modelled as an MCDM, where the bones and muscles are structurally analogous to the rigid links and cables, respectively. The human neck can be modelled as a serial mechanism consisting of 8 rigid bodies: the 7 *cervical vertebrae* bones (C7 - C1 bones) and the skull. Furthermore, 14 muscle groups, modelled as 76 muscles, have been identified as the contributors of the motion in the neck [130].

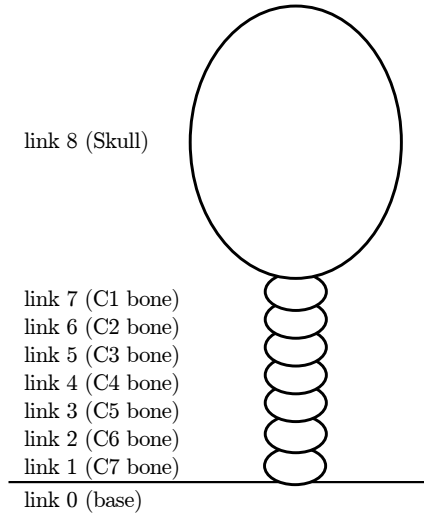


Figure 4.4: The rigid body structure for an 8 link MCDM inspired by the human neck, consisting of the inertial base (link 0), 7 *cervical vertebrae* bones (links 1 to 7) and the skull (link 8).

The 76 muscles can be divided into two sets of 38 symmetrically arranged muscles, regarded as the left and right neck muscles. The muscle-routing and attachment locations for each of the muscles were obtained from the Vasavada musculoskeletal neck model [130] for a 50th percentile male. From the model, it can be observed that the entire set of muscle-routings can be represented within a CRM (Definition 4.8) $C \in \mathcal{C}^{76 \times 8 \times 9}$, where the routing for each muscle can be described by the matrix $C_i \in \mathcal{C}^{8 \times 9} i = 1, \dots, 76$. Two muscles, as shown in Figure 4.5, have been selected as examples to illustrate the use of the CRM to describe the human neck muscles.

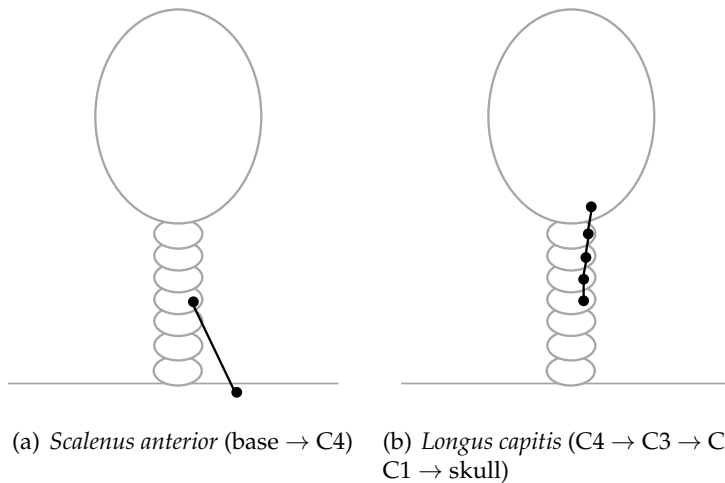


Figure 4.5: Example muscle-routings for the human neck, the *scalenus anterior* (a) is a single segment muscle and the *longus capitis* (b) is a muscle that is connected to multiple bones.

Firstly, the *scalenus anterior* muscle is a single segment muscle that begins from the base and ends at the C4 bone. The routing matrix for the *scalenus anterior* muscle C_{scal_ant} can be expressed as

$$C_{scal_ant} = \begin{bmatrix} -1 & 0 & 0 & 0 & 1 & 0 & 0 & 0 & 0 \\ 0 & 0 & 0 & 0 & 0 & 0 & 0 & 0 & 0 \\ \vdots & & & & & & & & \vdots \\ 0 & 0 & 0 & 0 & 0 & 0 & 0 & 0 & 0 \end{bmatrix}.$$

Assigning $i = 1$ for the *scalenus anterior* muscle, the CRM elements $c_{111} = -1$ and $c_{115} = 1$

denote that the starting and ending attachment links for the first segment of C_{scal_ant} are the base and link 4 (C4 bone), respectively. Subsequently, as the *scalenus anterior* muscle consists of a single segment, the CRM terms for the remaining segments are all zero and hence $c_{1jk} = 0 \forall j \geq 2 \forall k$.

The *longus capititis* muscle, assigned as cable $i = 2$, is a multi-segment muscle that is responsible for flexing the head and neck laterally. The muscle begins from the C4 bone and ends at the skull, passing through the C3, C2 and C1 bones. As a result, the muscle can be modelled as a 4 segment cable. The first segment begins from the C4 bone and ends at the bone C3, represented by the terms $c_{215} = -1$ and $c_{216} = 1$, respectively. The second segment begins from the C3 bone and ends at bone C2, represented by the terms $c_{226} = -1$ and $c_{227} = 1$, respectively. Similarly, segment 3 routes from the bone C2 ($c_{237} = -1$) to the bone C1 ($c_{238} = 1$). The final segment begins from bone C1 ($c_{248} = -1$) and ends at the skull ($c_{249} = 1$). As the muscle consists of 4 segments, the CRM terms of the remaining segments are zero and hence $c_{2jk} = 0 \forall j \geq 5, \forall k$. The corresponding matrix for the *longus capititis* muscle can be expressed as

$$C_{longus.capitis} = \begin{bmatrix} 0 & 0 & 0 & 0 & -1 & 1 & 0 & 0 & 0 \\ 0 & 0 & 0 & 0 & 0 & -1 & 1 & 0 & 0 \\ 0 & 0 & 0 & 0 & 0 & 0 & -1 & 1 & 0 \\ 0 & 0 & 0 & 0 & 0 & 0 & 0 & -1 & 1 \\ 0 & 0 & 0 & 0 & 0 & 0 & 0 & 0 & 0 \\ 0 & 0 & 0 & 0 & 0 & 0 & 0 & 0 & 0 \\ 0 & 0 & 0 & 0 & 0 & 0 & 0 & 0 & 0 \\ 0 & 0 & 0 & 0 & 0 & 0 & 0 & 0 & 0 \end{bmatrix}.$$

Similarly, the remaining 74 muscles can be represented by the matrices C_i for $i = 3$ to $i = 76$ from (4.6) and hence form the CRM (Definition 4.8) for the neck-inspired MCDM system. Furthermore, in addition to the types of cable routing required to model the musculoskeletal neck system, the complete set of arbitrary cable routing for any 8 link system can be described by the CRM. The example presented in this section demonstrates the flexibility of the CRM, where all types of cable routing for MCDMs with an arbitrary

number of links can be encapsulated within a single CRM.

4.3.3 11 Link Branched Manipulator

Previous examples on the CRM presented in Sections 4.3.1 and 4.3.2 considered the cable routing for multilink serial mechanisms. In this example, it is shown that the CRM can also be applied in the modelling of cable routing for branched mechanisms. Branched mechanisms can be commonly observed in musculoskeletal systems, such as the human hand and the lower extremity.

Consider the 11 link branched mechanism model shown in Figure 4.6, where link 1 is connected to the base through a spherical joint and the remaining joints are revolute joints. The CRM for the branched system can be constructed identically to that of serial mechanisms. If the system possesses m cables, the CRM (Definition 4.8) can be represented as $C \in \mathcal{C}^{m \times 11 \times 12}$. The cable routing for cable i can consequently be represented by the matrix $C_i \in \mathcal{C}^{11 \times 12}$ in the form (4.6).

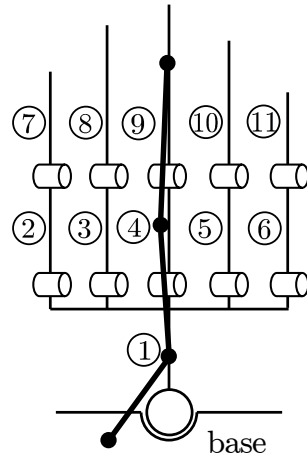


Figure 4.6: The rigid body structure for an 11 link MCDM inspired by a human hand.

Consider the example 3 segment cable, denoted by cable number i , shown in Figure 4.6. The cable begins from the base, passes through links 1 and 4, and ends at link 9. Hence, segment 1 can be represented by terms $c_{i11} = -1$ and $c_{i12} = 1$, segment 2 can be denoted by $c_{i22} = -1$ and $c_{i25} = 1$, and segment 3 by $c_{i35} = -1$ and $c_{i3(10)} = 1$. The remaining terms of the matrix are zero elements and the routing of the cable is represented

by

$$C_i = \begin{bmatrix} -1 & 1 & 0 & 0 & 0 & 0 & 0 & 0 & 0 & 0 & 0 & 0 \\ 0 & -1 & 0 & 0 & 1 & 0 & 0 & 0 & 0 & 0 & 0 & 0 \\ 0 & 0 & 0 & 0 & -1 & 0 & 0 & 0 & 0 & 1 & 0 & 0 \\ 0 & 0 & 0 & 0 & 0 & 0 & 0 & 0 & 0 & 0 & 0 & 0 \\ \vdots & & & & & & & & & & \vdots & \\ 0 & 0 & 0 & 0 & 0 & 0 & 0 & 0 & 0 & 0 & 0 & 0 \end{bmatrix}.$$

4.4 Cable-Routing Matrix Properties

To ensure that the cable routing of a system is feasible and physically meaningful, a set of properties for the CRM that represent the necessary and sufficient conditions for valid cable routing are defined in this section. Properties on the CRM can be used to verify the validity of the CRMs and in constructing feasible cable routing. Construction of feasible CRMs is important in automating the design process of MCDMs.

Properties 4.2 and 4.3 ensure that every cable segment $j \leq s_i$ is feasible, where each segment has exactly one beginning and one ending attachment. Additionally, Property 4.4 ensures that the remaining segments $j > s_i$ are not attached onto any links.

Property 4.2. $\sum_{k=1}^{p+1} c_{ijk} = 0 \forall i \in \{1, \dots, m\} \forall j \in \{1, \dots, s\}$. Every cable segment must have an equal number of beginning and ending attachments.

Property 4.3. $\sum_{k=1}^{p+1} |c_{ijk}| = 2 \forall i \in \{1, \dots, m\} \forall j \in \{1, \dots, s_i\}$. Each segment from 1 to s_i must be attached to two different links, where $1 \leq s_i \leq s$ is the total number of segments for cable i .

Property 4.4. $c_{ijk} = 0 \forall i \in \{1, \dots, m\} \forall j \in \{s_i + 1, \dots, s\} \forall k \in \{1, \dots, p+1\}$. Following from Property 4.3, the remaining segments $j > s_i$ must not have any attachment points to any links.

Property 4.5 ensures that for cables with multiple segments, the ending attachment of a segment and the beginning attachment of the next segment (pass-through attachments in Definition 4.9) are connected at the same link.

Property 4.5. $\forall i \in \{1, \dots, m\} \forall j \in \{1, \dots, s_i - 1\} \exists k \in \{1, \dots, p + 1\} : c_{ijk} - c_{i(j+1)k} = 2$. Combining with Properties 4.2 and 4.3, consecutive segments are connected such that the ending attachment of segment j and beginning attachment of segment $j + 1$ are attached onto the same link. Furthermore, to ensure that segments connect at the same point, that is, the attachment locations must satisfy $A_{ijk} = A_{i(j+1)k} \forall j = \{1, \dots, s_i - 1\}$.

As a result of Property 4.5, the CRM is structured such that row 1 and row s_i of C_i represent the first and last segments of cable i . Hence, if cable i begins on link a , then $c_{i1(a+1)} = -1$ and location A_{i1a} can be regarded as the beginning attachment point for cable i (Definition 4.6). Similarly, if cable i ends on link b , then $c_{is_i(b+1)} = 1$, and location A_{is_ib} can be regarded as the ending attachment point for cable i (Definition 4.7). From the above properties, each cable must have only one beginning and one ending attachment point. For cables with multiple segments $s_i > 1$, the connection locations between consecutive segments can be regarded as pass-through attachment points (Definition 4.9).

Properties 4.2 to 4.5 represent a minimum set of properties for any MCDM such that the cables and their segments defined by the CRM are valid and consistent with that presented in Section 4.2.2. Additional properties can be defined to impose constraints on how the cables attach or pass through the links of the manipulator. For example, Properties 4.6 and 4.7 can be defined to ensure that all cables have open-chain cable routing (Definition 4.4), such that each cable is only attached to each body at most once.

Property 4.6. $\sum_{k=1}^{p+1} \left| \sum_j c_{ijk} \right| = 2 \forall i$. The beginning attachment point and ending attachment point of every cable are located at different links. If the beginning or ending attachment point of cable i is located at link $k - 1$, then $\sum_j c_{ijk} = -1$ or $\sum_j c_{ijk} = 1$, respectively. Otherwise, if cable i does not attach onto or pass through link $k - 1$, then $\sum_j c_{ijk} = 0$. If the beginning and ending attachments of cable i are on the same link, then $\sum_k \left| \sum_j c_{ijk} \right| = 0$ and the cable forms a closed loop.

Property 4.7. $\sum_j |c_{ijk}| \leq 2 \forall i \forall k$. Following from Property 4.6, cable i is connected to link $k - 1$ at most once. Cable i is either not connected to link $k - 1$ ($\sum_j |c_{ijk}| = 0$), begins or ends on link $k - 1$ ($\sum_j |c_{ijk}| = 1$), or passes through link $k - 1$ ($\sum_j |c_{ijk}| = 2$).

In a similar manner to the presented properties, additional properties can be con-

structed depending on the specific requirements for the cable routing on the manipulator.

4.5 Generalised Cable Segment Vector

In this section, the generalised representation of the cable segment vector for MCDMs is presented. As shown in Chapter 3, the cable segment vector is essential in the modelling of the system kinematics and dynamics for CDPMs. For single link systems, the cable vector from (3.3) for each cable requires knowledge of the cable attachment locations. Furthermore, it was shown in Section 3.3.3 that the definition of the cable vectors for MCDMs is also dependent on the type of cable routing. As a result, the challenge in modelling the cable segment vectors naturally increases with the number of links. To resolve this, the proposed generalised cable segment vector is formulated with respect to the CRM, where arbitrary cable routing can be described by a single representation.

In formulating the generalised cable segment vector, Section 4.5.1 first defines the description of the cable attachment locations required in the generalised cable segment vector representation. Using this definition and the CRM proposed in Section 4.5.2, the generalised cable segment vector is formulated.

4.5.1 Generalised Cable Attachments

For single link CDPMs, each cable only possesses two attachment locations, one at the base and the other on the end-effector. However, for MCDMs the number of attachment locations for a cable varies depending on the number of segments. In defining the cable attachment locations, consider the coordinate frames for the p link MCDM shown in Figure 4.7.

The coordinate frames of the system consists of the inertial frame $\{F_0\}$ and p non-inertial frames, where $\{F_k\} \forall k \in \{1, \dots, p\}$ is rigidly attached onto link k . The origin of the inertial frame is defined as O or o_0 , and the origin $o_k \forall k \in \{1, \dots, p\}$ is located at the centre of mass G_k of link k . Hence, positions of the cable attachment locations on link k can be described relative to o_k and is fixed with respect to the coordinate frame $\{F_k\}$.

The attachment locations for the cables within an MCDM can be defined by the set

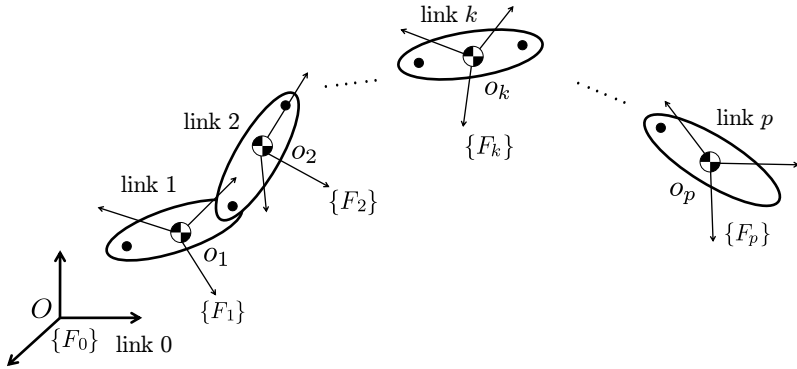


Figure 4.7: The coordinate frames for a p link MCDM. Frame $\{F_0\}$ is the inertial frame with origin O and frame $\{F_k\}$ is a non-inertial frame attached to body k with origin o_k .

of attachment locations for each segment of each cable. Figure 4.8 shows the attachment of a cable onto link k of the MCDM. The attachment location for segment j of cable i on link k can be uniquely defined as $A_{ijk} \forall i \in \{1, \dots, m\} \forall j \in \{1, \dots, s_i\} \forall k \in \{0, \dots, p\}$. Since the attachment point A_{ijk} is located on link k , it can be described by the vector ${}^k\mathbf{r}_{o_k A_{ijk}}$ relative to the centre of mass of link k and is fixed to frame $\{F_k\}$. To ensure that consecutive segments are connected at the same pass-through attachment location, then $A_{ijk} = A_{i(j+1)k} \forall j \in \{1, \dots, s_i - 1\}$ if segment j of cable i is attached onto link k (Property 4.5).

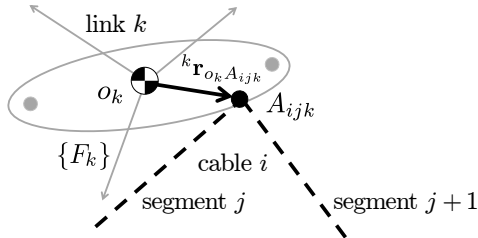


Figure 4.8: The attachment location of segment j of cable i on body k can be denoted as A_{ijk} and defined by the vector $\mathbf{r}_{o_k A_{ijk}}$.

It will be demonstrated in Section 4.5.2 that if a cable segment does not attach onto a particular link, the assignment of the attachment location does not affect the system model. For example, if segment j of cable i does not attach onto link k , then its attachment location A_{ijk} can be arbitrarily assigned since $c_{ij(k+1)} = 0$. Hence, $c_{ij(k+1)}\mathbf{r}_{o_k A_{ijk}} = \mathbf{0}$ will be satisfied regardless of the value of $\mathbf{r}_{o_k A_{ijk}}$. The value $c_{ij(k+1)}\mathbf{r}_{o_k A_{ijk}} = \mathbf{0}$ if segment j of cable

i is not attached onto link k is required in the definition of the generalised cable segment vector and will be shown in Section 4.5.2. Furthermore, if cable i has less than s segments, that is, $s_i < s$, the attachment locations $A_{ijk} \forall j \in \{s_i + 1, \dots, s\} \forall k$ can also be arbitrarily assigned.

4.5.2 Modelling With the Cable-Routing Matrix

For MCDMs, the cable segment vector refers to the cable vector of a segment for a cable, where \mathbf{l}_{ij} denotes the cable segment vector for segment j of cable i . The convention adopted for direction of the cable segment vector is that it begins from the beginning attachment location and ends at the ending attachment location of the segment. Hence, if segment j of cable i begins from link a and ends at link b , the cable segment vector can be expressed as

$$\mathbf{l}_{ij} = -\mathbf{r}_{OA_{ija}} + \mathbf{r}_{OA_{ijb}} . \quad (4.7)$$

Denoting the number of segments for cable i as s_i , the remaining segments $j > s_i$ are defined as zero vectors $\mathbf{l}_{ij} = \mathbf{0} \forall j > s_i$.

To illustrate the physical meaning of the cable segment vector for MCDMs, Figure 4.9 shows the cable segment vectors for the two example muscles within the neck that were introduced in Section 4.3.2. The *scalenus anterior* muscle shown in Figure 4.9(a), denoted as cable 1, consists for a single segment defined as $\mathbf{l}_{11} = -\mathbf{r}_{OA_{110}} + \mathbf{r}_{OA_{114}}$. The remaining cable segment vectors are therefore $\mathbf{l}_{1j} = \mathbf{0} \forall j > 1$. The cable segment vectors for a multi-segment muscle, *longus capitis*, are shown in Figure 4.9(b). Cable 2 consists of 4 segments and are defined as $\mathbf{l}_{21} = -\mathbf{r}_{OA_{214}} + \mathbf{r}_{OA_{215}}$, $\mathbf{l}_{22} = -\mathbf{r}_{OA_{225}} + \mathbf{r}_{OA_{226}}$, $\mathbf{l}_{23} = -\mathbf{r}_{OA_{236}} + \mathbf{r}_{OA_{237}}$ and $\mathbf{l}_{24} = -\mathbf{r}_{OA_{247}} + \mathbf{r}_{OA_{248}}$. Similarly, the remaining segments are defined as $\mathbf{l}_{2j} = \mathbf{0} \forall j > 4$.

From the definition of the CRM presented in Section 4.2.2, $c_{ij(a+1)} = -1$ and $c_{ij(b+1)} = 1$ represent that segment j of cable i begins on link a and ends at link b , respectively. For the remaining links that segment j of cable i is not attached to, the corresponding CRM values are $c_{ij(k+1)} = 0$. Hence, the definition of the cable segment vector from (4.7) can be

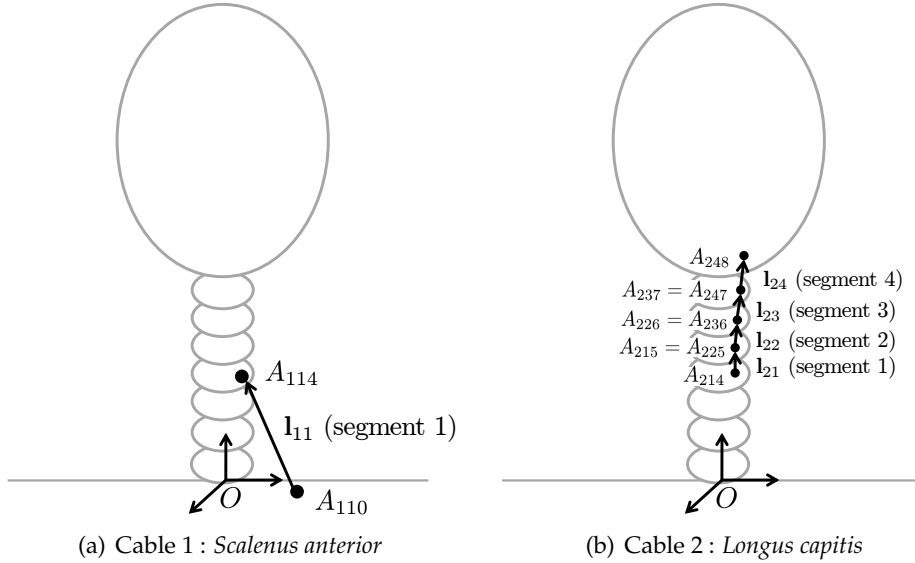


Figure 4.9: Cable segment vectors shown for example muscles for the human neck, the *scalenus anterior* (a) and the *longus capitis* (b), to illustrate the convention for the cable segment vector and the cable attachment locations.

expressed with respect to the CRM as

$$\mathbf{l}_{ij} = \sum_{k=0}^p \left[c_{ij(k+1)} \mathbf{r}_{OA_{ijk}} \right] . \quad (4.8)$$

Since $c_{ij(k+1)} = 0 \forall i \forall k$ for cable segments $j > s_i$ (Property 4.4), the cable segment vector from (4.8) also naturally satisfies the requirement that $\mathbf{l}_{ij} = \mathbf{0} \forall j > s_i$.

From the cable-routing matrices for the *scalenus anterior* muscle $i = 1$ and the *longus capitis* muscle $i = 2$ defined in Section 4.3.2, it is apparent that the generalised definition from (4.8) results in a consistent definition of the cable segment vectors shown in Figure 4.9. The cable segment vector from (4.8) can be regarded as a generalised definition that does not pre-assume any particular cable routing for the MCDM system. As a result, (4.8) allows the cable segment vectors for any p link m cable system to be determined given knowledge of the CRM and cable attachment locations.

4.6 Conclusion

In this chapter, the CRM was proposed to allow the cable routing for MCDMs to be encapsulated within a single representation. From the CRM definition and presented examples, it was shown that the CRM is able to describe the cable routing of MCDMs without making any assumptions on the allowable types of cable routing and the kinematic structure of the system. As a result, the CRM is able to resolve a major challenge in modelling arbitrary cable routing for complex MCDMs possessing an arbitrary number of links. Furthermore, properties on the CRM were presented to allow verification and generation of CRMs with valid cable routing. Finally, the generalised definition of the cable segment vector is formulated with respect to the CRM, allowing the segment vector for all cable segments to be represented within a single definition. Using the CRM and the generalised cable segment vector, the generalised kinematic and dynamic models for MCDMs will be formulated in Chapter 5.

This page is intentionally left (almost) blank.

Chapter 5

Generalised Multilink Cable-Driven Manipulator Model

In this chapter, a generalised model for the kinematics and dynamics of multilink cable-driven manipulators (MCDMs) is formulated. The proposed model considers MCDMs with arbitrary kinematic and joint structure. The model inherently allows for arbitrary cable routing as the Jacobian matrix of the overall system is formulated with respect to the cable-routing matrix (CRM). The generalised kinematic relationship and equations of motion provide increased flexibility in the study of complex MCDMs by eliminating the need to reconstruct the model for different types of manipulator structure and cable routing. Section 5.1 motivates the need of a generalised MCDM model. Section 5.2 introduces the generalised kinematic structure and joint models required in the MCDM model. Section 5.3 presents the formulation of the kinematics and Jacobian matrix for generalised serial MCDMs. The generalised equations of motion are derived in Section 5.4. Section 5.5 extends the model to manipulators with a branched rigid body structure. To illustrate the effectiveness and robustness of the proposed model, Section 5.6 shows the simulation of the kinematics and dynamics for two example manipulators: a 2 link 4 degree-of-freedom (DoF) manipulator actuated by 6 cables and a more complex 8 link 24 DoF human neck manipulator actuated by 76 cables. Section 5.7 concludes the chapter by summarising the contributions.

5.1 Introduction

The kinematic and dynamic models of multilink cable-driven manipulators (MCDMs) refer to the relationships between the cable lengths and cable forces, respectively, with the motion of the manipulator. These models are required in the analysis of cable-driven parallel manipulators (CDPMs), such as manipulator control, optimisation of cable routing and attachment locations, and workspace analysis.

As reviewed in Section 2.4, previous studies in the modelling of MCDMs derive the kinematics and dynamics for each specific rigid body structure and cable routing configuration. The inconvenience of this approach was demonstrated in Chapter 3, where the kinematic and dynamic models must be derived for each manipulator individually, as shown in the three manipulator examples from Section 3.3. Additionally, it was shown in Section 3.3.3 that the modelling of multilink systems is further complicated by the increased types of cable routing and the interaction forces between links. The need to model each type of manipulator limits the study and application of more complex MCDMs with a large number of links and cables.

The complications resulting from increased types of cable routing for MCDMs were addressed in Chapter 4 by the introduction of the CRM. In Section 4.5, it was demonstrated that a generalised cable segment vector can be derived using the cable-routing matrix (CRM). As a result, it was shown that all possible cable routings are inherently considered within a single representation. Using the generalised cable segment vector and the CRM to formulate a generalised MCDM model allows arbitrary cable routing to be achieved.

In a similar manner to the CRM description, generalised representations for the rigid bodies and joint models are used to formulate the proposed MCDM model. As a result, the model does not make assumption on the type of joints, kinematic structure or the number of links. The specific manipulator structure can then be defined when performing analysis on the generalised system, similar to the substitution of the CRM elements in Chapter 4 to describe the cable cable routing.

As a result, the proposed generalised MCDM model allows for both arbitrary cable routing and kinematic structure within a single representation. The proposed method provides additional flexibility in the modelling of existing real-world MCDMs, such as those from [91, 92, 111, 112]. Furthermore, the ability to derive the kinematics and dynamics of MCDMs without assuming their kinematic structure and types of cable routing is beneficial in the modelling and analysis of more complex MCDM systems. For example, biomechanical systems, such as the human limbs, neck and spine, are mechanisms that can be modelled as MCDMs. Furthermore, biomechanical systems typically possess a

large number of rigid bodies with complex routing of muscles.

From the generalised model, it will be shown that analysis on the system only needs to be performed once with respect to the single formulation. Any changes to the kinematic structure and cable routing only requires modification to the joint definitions and the CRM, respectively, as opposed to reformulation of the entire system model. As a result, the proposed formulation increases the flexibility and convenience in the study of complex MCDMs.

5.2 Generalised Rigid Body Structure

In constructing the generalised MCDM model, an abstraction is required to describe the kinematic structure for the system. Section 5.2.1 introduces the notation and description of the kinematic structure of the rigid bodies for multilink manipulators. Section 5.2.2 presents the abstracted joint representation to describe any type of joint.

5.2.1 Rigid Body Structure

In this section, the description of the kinematic rigid body structure for a p link manipulator is presented. For a p link mechanism, such as the one shown in Figure 5.1, $p + 1$ coordinate frames could be introduced.

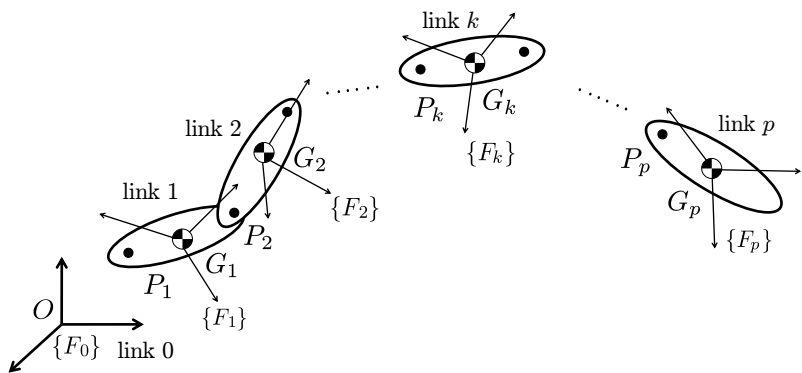


Figure 5.1: The rigid body structure of the generalised p link MCDM. The centre of mass and joint location of link k are denoted by points G_k and P_k , respectively.

Frame $\{F_0\}$ represents the inertial coordinate system with origin O . The non-inertial

coordinate frame $\{F_k\}$ $\forall k \in \{1, \dots, p\}$ is fixed to body k and has origin o_k that is located at the centre of mass G_k of link k . The connections between the links of the manipulator are represented by the joints of the system. The location of the joint that connects links $k - 1$ and k is denoted by point P_k . The joint location for the base frame P_0 is defined to be at the origin location O .

For an n degree-of-freedom (*DoF*) system, the pose of the manipulator can be described uniquely by the *joint space* coordinates, or generalised coordinates, $\mathbf{q} \in \mathbb{R}^n$. The generalised coordinates for a multilink manipulator is comprised of the generalised coordinates for each joint and hence $\mathbf{q} = [\mathbf{q}_1^T \ \mathbf{q}_2^T \ \dots \ \mathbf{q}_p^T]^T$, where $\mathbf{q}_k \in \mathbb{R}^{n_k}$ represents the generalised coordinates for link k and n_k is the number of degrees of freedom for link k relative to link $k - 1$. The *body space* coordinates $\mathbf{x} = [\mathbf{x}_1^T \ \dots \ \mathbf{x}_p^T]^T$ describes the position and orientation of the links of the manipulator, where $\mathbf{x}_k \in \mathbb{R}^6$ is the body space displacement of link k . The twist vector for link k can be expressed as $\dot{\mathbf{x}}_k = [{}^k\dot{\mathbf{r}}_{OG_k}^T \ {}^k\omega_k^T]^T$, where $\dot{\mathbf{r}}_{OG_k}$ and ω_k represent absolute velocity of G_k and absolute angular velocity of link k , respectively. The notation ${}^k\mathbf{r}$ denotes that the vector \mathbf{r} is expressed with respect to $\{F_k\}$.

5.2.2 Joint Model

The joints of the manipulator represent the type of connection and hence describe the degrees of freedom of the system. For link k , the position and orientation of link k relative to link $k - 1$ can be described by the relative body space vector $\mathbf{x}_{k,k-1}$. This relative displacement vector can be expressed as a function of the generalised coordinates \mathbf{q}_k , where

$$\mathbf{x}_{k,k-1} = \mathbf{s}_k(\mathbf{q}_k). \quad (5.1)$$

Denoting the number of degrees of freedom of joint k as n_k , then $\mathbf{q}_k \in \mathbb{R}^{n_k}$ and n_k is an integer where $1 \leq n_k \leq 6$. The relative velocity vector is comprised of the relative translational velocity ${}^{k-1}\mathbf{r}'_{P_{k-1}P_k}$ and relative angular velocity ${}^k\omega_{k,k-1}$ of link k relative to link $k - 1$. The relative velocity vector $\mathbf{x}'_{k,k-1}$ can be derived from (5.1) and expressed in the linear form

$$\mathbf{x}'_{k,k-1} = \begin{bmatrix} {}^{k-1}\mathbf{r}'_{P_{k-1}P_k} \\ {}^k\omega_{k,k-1} \end{bmatrix} = S_k \dot{\mathbf{q}}_k, \quad (5.2)$$

where $S_k = \nabla \mathbf{s}_k$ is the gradient of \mathbf{s}_k .

In the study of kinematics, the matrix S_k relates the velocities in the generalised coordinates to the relative linear and angular velocities of the joint. Furthermore, S_k consists of translational S_{kt} and rotational S_{rt} components, where (5.2) can be expressed as

$$\begin{aligned} {}^{k-1}\mathbf{r}'_{P_{k-1}P_k} &= S_{kt}\dot{\mathbf{q}}_k \\ {}^k\boldsymbol{\omega}_{k,k-1} &= S_{kr}\dot{\mathbf{q}}_k. \end{aligned} \quad (5.3)$$

The matrix S_k is also significant in the study of dynamics, where the transpose matrix S_k^T represents the projection of the joint interaction force and moment at P_k onto the generalised coordinates of joint k . The joint interaction force \mathbf{F}_{P_k} and moment \mathbf{M}_{P_k} for link k refer to the interaction between links k and $k - 1$ at P_k , as shown in Figure 5.2.

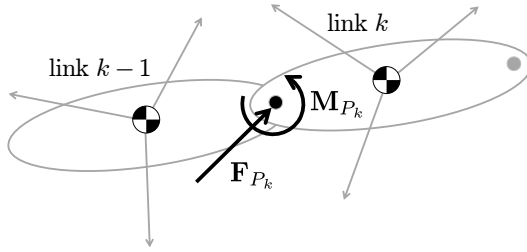


Figure 5.2: The interaction force \mathbf{F}_{P_k} and moment \mathbf{M}_{P_k} between links k and $k - 1$ at joint location P_k .

The degrees of freedom of link k can be described as the directions of generalised coordinates, and can be represented by the constraint

$$S_k^T \begin{bmatrix} {}^{k-1}\mathbf{F}_{P_k} \\ {}^k\mathbf{M}_{P_k} \end{bmatrix} = \begin{bmatrix} S_{kt}^T & S_{kr}^T \end{bmatrix} \begin{bmatrix} {}^{k-1}\mathbf{F}_{P_k} \\ {}^k\mathbf{M}_{P_k} \end{bmatrix} = 0_{n_k \times 1}. \quad (5.4)$$

The relationships from (5.3) and (5.4) can be regarded as the generalised kinematic and dynamic relationships, respectively, for a joint. Using the generic joint representation, the manipulator can be modelled without any assumptions on the actual type of joints. The definition of S_k is dependent on the specific joint type. For example, consider a revolute joint that rotates about the x axis by angle θ . The generalised coordinates for the joint can be expressed as $\mathbf{q}_k = [\theta]$ and the relative velocity vector can be determined

by $\mathbf{x}'_{k,k-1} = S_{rev,x}\dot{\mathbf{q}}_k$, where

$$S_{rev,x} = \begin{bmatrix} 0 & 0 & 0 & 1 & 0 & 0 \end{bmatrix}^T.$$

Similarly, a spherical joint can be defined by the generalised coordinates $\mathbf{q}_k = [\alpha \ \beta \ \gamma]^T$, where α , β and γ represent the xyz -Euler angles of the joint, respectively. The matrix $S_{spherical}$ relates $\mathbf{x}_{k,k-1}$ to $\dot{\mathbf{q}}_k$ in the form $\mathbf{x}'_{k,k-1} = S_{spherical}\dot{\mathbf{q}}_k$, where

$$S_{spherical} = \begin{bmatrix} 0 & 0 & 0 & c_\beta c_\gamma & -c_\beta s_\gamma & s_\beta \\ 0 & 0 & 0 & s_\gamma & c_\gamma & 0 \\ 0 & 0 & 0 & 0 & 0 & 1 \end{bmatrix}^T.$$

Finally, the S_k matrix for a 6 DoF spatial body can be expressed as

$$S_{spatial} = \begin{bmatrix} 1 & 0 & 0 & 0 & 0 & 0 \\ 0 & 1 & 0 & 0 & 0 & 0 \\ 0 & 0 & 1 & 0 & 0 & 0 \\ 0 & 0 & 0 & c_\beta c_\gamma & -c_\beta s_\gamma & s_\beta \\ 0 & 0 & 0 & s_\gamma & c_\gamma & 0 \\ 0 & 0 & 0 & 0 & 0 & 1 \end{bmatrix}^T,$$

and $\mathbf{x}'_{k,k-1} = S_{spatial}\dot{\mathbf{q}}_k$, where $\dot{\mathbf{q}}_k = [\dot{x} \ \dot{y} \ \dot{z} \ \dot{\alpha} \ \dot{\beta} \ \dot{\gamma}]^T$. The translational degrees of freedom of the spatial manipulator are defined by x , y and z , and the orientation is defined by the xyz -Euler angles α , β and γ , respectively.

In a similar manner to the presented examples of revolute, spherical and spatial joints, any arbitrary joint can be defined in the following manner given knowledge of the joint motion expressed in the form (5.1).

5.3 Kinematic Model of Serial Manipulators

In this section, the generalised kinematic relationship between the cable and joint spaces for serial MCDMs will be derived. The formulation uses the CRM introduced in Chapter

4 and the generalised structure presented in Section 5.2 to achieve arbitrary cable routing for any MCDM structure. The generalised kinematic relationship allows kinematic analysis, such as those described in Sections 3.2.1 and 3.2.2, to be performed on the generalised MCDM. Furthermore, this kinematic model is fundamental in the formulation of the equations of motion for the generalised MCDM. Firstly, Section 5.3.1 derives the direct kinematic relationship to determine the cable lengths given the generalised coordinates of the system. From this direct relationship, the Jacobian matrix that relate the cable and joint space derivatives will be formulated in Section 5.3.2.

5.3.1 Direct Kinematics

The direct kinematics, as introduced in Section 3.2.2, refer to the relationship between the cable length vector \mathbf{l} and the generalised coordinates \mathbf{q} . It will be shown that for an n DoF m cable MCDM system the direct kinematics can be expressed in the form

$$\mathbf{l} = \mathbf{j}(\mathbf{q}), \quad \mathbf{l} \in \mathbb{R}^m \quad \mathbf{q} \in \mathbb{R}^n, \quad (5.5)$$

where \mathbf{j} is an m dimensional vector function.

The generalised cable segment vector (4.8) introduced in Section 4.5 represents the vector between the two attachment locations of a cable segment. As shown in Figure 5.3, the attachment location that segment j of cable i attaches onto link k can be expressed as

$$\mathbf{r}_{OA_{ijk}}(\mathbf{q}) = \mathbf{r}_{Oo_k}(\mathbf{q}) + \mathbf{r}_{o_k A_{ijk}}, \quad (5.6)$$

where $\mathbf{r}_{o_k A_{ijk}}$ is a fixed vector within $\{F_k\}$.

The length of cable i can be determined by summing the length of each segment for cable i . From the definition of \mathbf{l}_{ij} in (4.8) and the attachment location in (5.6), the length of cable i can be expressed with respect to the CRM and generalised coordinates as

$$l_i = \sum_{j=1}^{s_i} \|\mathbf{l}_{ij}\| = \sum_{j=1}^s \left\| \sum_{k=0}^p [c_{ij(k+1)} \mathbf{r}_{OA_{ijk}}] \right\|. \quad (5.7)$$

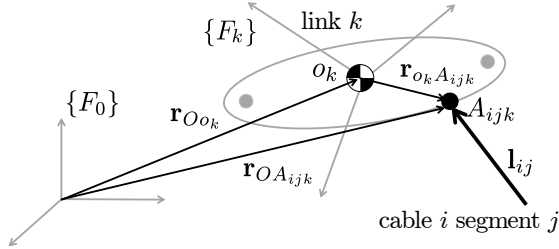


Figure 5.3: Attachment location for link k of an MCDM showing the kinematics of the link.

From (5.7), the relationship from (5.5) can be expressed in the form $\mathbf{j} = [j_1(\mathbf{q}) \ \dots \ j_m(\mathbf{q})]^T$, where (5.7) represents $l_i = j_i(\mathbf{q})$. As described in Section 4.2.2, the maximum number of segments s allows for the possibility in the number of segments exceeding the number of links p .

5.3.2 Jacobian Matrix

In the modelling of kinematics for MCDMs, the Jacobian matrix $J \in \mathbb{R}^{m \times n}$ from (3.1) represents the relationship between the derivatives of the *cable space* and *joint space* $\dot{\mathbf{i}} = \nabla \mathbf{j} \cdot \dot{\mathbf{q}} = J \dot{\mathbf{q}}$. The Jacobian matrix can be derived in two parts, where the relationship between the derivatives of the *cable space* and the *body space* $\dot{\mathbf{i}} = V \dot{\mathbf{x}}$ is first formulated, followed by the relationship between the derivatives of the *body space* and the *joint space* $\dot{\mathbf{x}} = W \dot{\mathbf{q}}$.

Cable Jacobian Matrix

The time derivative of the length of segment j of cable i can be expressed as

$$\dot{l}_{ij} = \hat{\mathbf{i}}_{ij} \cdot \dot{\mathbf{i}}_{ij} . \quad (5.8)$$

The time derivative of the length of cable i can be determined by the summing all of the derivatives of its segment lengths (5.8). Substituting (5.8) and time derivative of (4.8) into

the time derivative of (5.7) allows \dot{l}_i to be expressed with respect to the CRM, where

$$\begin{aligned}\dot{l}_i &= \sum_{j=1}^s \dot{l}_{ij} \\ &= \sum_{j=1}^s \sum_{k=0}^p \left[c_{ij(k+1)} {}^k \hat{\mathbf{l}}_{ij} \cdot {}^k \dot{\mathbf{r}}_{OA_{ijk}} \right].\end{aligned}\quad (5.9)$$

Since ${}^0 \dot{\mathbf{r}}_{OA_{ij0}} = \mathbf{0}$ $\forall i \forall j$ as ${}^0 \mathbf{r}_{OA_{ij0}}$ is fixed in $\{F_0\}$, and ${}^k \dot{\mathbf{r}}_{OA_{ijk}} = {}^k \dot{\mathbf{r}}_{OG_k} + {}^k \boldsymbol{\omega}_k \times {}^k \mathbf{r}_{G_k A_{ijk}}$ $\forall k \in \{1, \dots, p\}$, then (5.9) can be expressed in the form

$$\begin{aligned}\dot{l}_i &= \sum_{k=1}^p \sum_{j=1}^s \left[c_{ij(k+1)} {}^k \hat{\mathbf{l}}_{ij} \cdot \left({}^k \dot{\mathbf{r}}_{OG_k} + {}^k \boldsymbol{\omega}_k \times {}^k \mathbf{r}_{G_k A_{ijk}} \right) \right] \\ &= \sum_{k=1}^p [V_{i\mathbf{x}_k} \dot{\mathbf{r}}_{OG_k} + V_{i\theta_k} \boldsymbol{\omega}_k],\end{aligned}\quad (5.10)$$

where

$$\begin{aligned}V_{i\mathbf{x}_k} &= \left(\sum_{j=1}^s \left[c_{ij(k+1)} {}^k \hat{\mathbf{l}}_{ij} \right] \right)^T \\ V_{i\theta_k} &= \left(\sum_{j=1}^s \left[c_{ij(k+1)} {}^k \mathbf{r}_{G_k A_{ijk}} \times {}^k \hat{\mathbf{l}}_{ij} \right] \right)^T.\end{aligned}\quad (5.11)$$

The terms $V_{i\mathbf{x}_k}$ and $V_{i\theta_k}$ represent the relationship between the velocities $\dot{\mathbf{r}}_{OG_k}$ and $\boldsymbol{\omega}_k$ of link k , respectively, and the time derivative of the length of cable i . From (5.10), the relationship between $\dot{\mathbf{i}}$ and $\dot{\mathbf{x}}$ can be expressed in the form $\dot{\mathbf{i}} = V\dot{\mathbf{x}}$, where

$$V = \begin{bmatrix} V_{1\mathbf{x}_1} & V_{1\theta_1} & \dots & V_{1\mathbf{x}_p} & V_{1\theta_p} \\ \vdots & & & & \vdots \\ V_{m\mathbf{x}_1} & V_{m\theta_1} & \dots & V_{m\mathbf{x}_p} & V_{m\theta_p} \end{bmatrix} \in \mathbb{R}^{m \times 6p}. \quad (5.12)$$

Body Jacobian Matrix

The relationship between the body space derivative $\dot{\mathbf{x}}$ and joint space derivative $\dot{\mathbf{q}}$ can be determined by expressing the absolute linear and angular velocities of each body with respect to its relative velocities. The absolute angular velocity of body k for $k = 1, \dots, p$

in $\{F_k\}$ can be expressed as

$$\begin{aligned} {}^k \boldsymbol{\omega}_k &= {}^1 R {}^1 \boldsymbol{\omega}_{1,0} + {}^2 R {}^2 \boldsymbol{\omega}_{2,1} + \cdots + {}^k R {}^k \boldsymbol{\omega}_{k,k-1} \\ &= \sum_{a=1}^k {}^a R {}^a \boldsymbol{\omega}_{a,a-1}. \end{aligned} \quad (5.13)$$

Similarly, the absolute velocity of the centre of mass of link k in $\{F_k\}$ can be expressed as

$${}^k \dot{\mathbf{r}}_{OG_k} = \sum_{a=1}^k \left[{}^k \dot{\mathbf{r}}_{P_{a-1} P_a} \right] + {}^k \dot{\mathbf{r}}_{P_k G_k}, \quad (5.14)$$

where P_a is the joint location between links a and $a - 1$ as shown in Figure 5.1. The velocity term ${}^{a-1} \dot{\mathbf{r}}_{P_{a-1} P_a}$ from (5.14) can be expressed as

$${}^{a-1} \dot{\mathbf{r}}_{P_{a-1} P_a} = {}^{a-1} \mathbf{r}'_{P_{a-1} P_a} + {}^{a-1} \boldsymbol{\omega}_{a-1} \times {}^{a-1} \mathbf{r}_{P_{a-1} P_a}. \quad (5.15)$$

Substituting (5.15) and (5.13) into (5.14) allows the absolute velocity of G_k to be expressed with respect to the relative velocities as

$$\begin{aligned} {}^k \dot{\mathbf{r}}_{OG_k} &= \sum_{a=1}^k \left[{}^k_{a-1} R {}^{a-1} \mathbf{r}'_{P_{a-1} P_a} \right] - \sum_{a=1}^k \left[{}^k_{a-1} R \left({}^{a-1} \mathbf{r}_{P_{a-1} P_a} \times {}^{a-1} \boldsymbol{\omega}_{a-1} \right) \right] - {}^k \mathbf{r}_{P_k G_k} \times {}^k \boldsymbol{\omega}_k \\ &= \sum_{a=1}^k \left[{}^k_{a-1} R {}^{a-1} \mathbf{r}'_{P_{a-1} P_a} \right] - \sum_{a=1}^k \sum_{b=1}^{a-1} \left[{}^k \mathbf{r}_{P_{a-1} P_a} \times {}^k \boldsymbol{\omega}_{b,b-1} \right] - \sum_{b=1}^k \left[{}^k \mathbf{r}_{P_k G_k} \times {}^k \boldsymbol{\omega}_{b,b-1} \right] \\ &= \sum_{a=1}^k \left[{}^k_{a-1} R {}^{a-1} \mathbf{r}'_{P_{a-1} P_a} \right] - \sum_{b=1}^k \left[\left(\sum_{a=b+1}^k \left[{}^k \mathbf{r}_{P_{a-1} P_a} \right] + {}^k \mathbf{r}_{P_k G_k} \right) \times {}^k \boldsymbol{\omega}_{b,b-1} \right] \\ &= \sum_{a=1}^k \left[{}^k_{a-1} R {}^{a-1} \mathbf{r}'_{P_{a-1} P_a} \right] - \sum_{a=1}^k \left[{}^k_a R [{}^a \mathbf{r}_{P_a G_k}]^\times {}^a \boldsymbol{\omega}_{a,a-1} \right]. \end{aligned} \quad (5.16)$$

From (5.13), (5.16) and the generalised joint representation (5.2) presented in Section 5.2.2, the absolute linear and angular velocities for link k can be expressed in matrix form as

$$\begin{bmatrix} {}^k \dot{\mathbf{r}}_{OG_k} \\ {}^k \boldsymbol{\omega}_k \end{bmatrix} = \sum_{a=1}^k \begin{bmatrix} \begin{bmatrix} {}^k_{a-1} R & - {}^k_a R [{}^a \mathbf{r}_{P_a G_k}]^\times \\ 0_{3 \times 3} & {}^k_a R \end{bmatrix} S_a \dot{\mathbf{q}}_a \end{bmatrix}, \quad (5.17)$$

where S_a is the transformation matrix as defined in (5.2). From (5.17), the twist vector $\dot{\mathbf{x}}$ can be expressed in the form $\dot{\mathbf{x}} = PS\dot{\mathbf{q}}$

$$\begin{bmatrix} {}^1\dot{\mathbf{r}}_{OG_1} \\ {}^1\omega_1 \\ {}^2\dot{\mathbf{r}}_{OG_2} \\ {}^2\omega_2 \\ \vdots \\ {}^p\dot{\mathbf{r}}_{OG_p} \\ {}^p\omega_p \end{bmatrix} = \begin{bmatrix} P_{11} & 0_{6 \times 6} & \dots & 0_{6 \times 6} \\ P_{21} & P_{22} & \dots & 0_{6 \times 6} \\ \vdots & & & \vdots \\ P_{p1} & P_{p2} & \dots & P_{pp} \end{bmatrix} \begin{bmatrix} S_1 & 0_{6 \times n_2} & \dots & 0_{6 \times n_p} \\ 0_{6 \times n_1} & S_2 & \dots & 0_{6 \times n_p} \\ \vdots & & & \vdots \\ 0_{6 \times n_1} & 0_{6 \times n_2} & \dots & S_p \end{bmatrix} \begin{bmatrix} \dot{\mathbf{q}}_1 \\ \dot{\mathbf{q}}_2 \\ \dot{\mathbf{q}}_3 \\ \vdots \\ \dot{\mathbf{q}}_p \end{bmatrix}, \quad (5.18)$$

where

$$P_{ka} = \begin{bmatrix} {}^k_{a-1}R & -{}^k_aR [{}^a\mathbf{r}_{P_a G_k}]^\times \\ 0_{3 \times 3} & {}^k_aR \end{bmatrix}. \quad (5.19)$$

The matrix P represents the relationship between the absolute and relative velocities of the MCDM links. Alternatively, the relationship (5.18) can be expressed in the form $\dot{\mathbf{x}} = W\dot{\mathbf{q}}$ where $W = PS$. In matrix form, W can be expressed as

$$W = \begin{bmatrix} W_{1\mathbf{x}_1} & 0_{3 \times n_2} & 0_{3 \times n_3} & \dots & 0_{3 \times n_p} \\ W_{1\theta_1} & 0_{3 \times n_2} & 0_{3 \times n_3} & \dots & 0_{3 \times n_p} \\ W_{1\mathbf{x}_2} & W_{2\mathbf{x}_2} & 0_{3 \times n_3} & \dots & 0_{3 \times n_p} \\ W_{1\theta_2} & W_{2\theta_2} & 0_{3 \times n_3} & \dots & 0_{3 \times n_p} \\ \vdots & & & & \vdots \\ W_{1\mathbf{x}_p} & W_{2\mathbf{x}_p} & W_{3\mathbf{x}_p} & \dots & W_{p\mathbf{x}_p} \\ W_{1\theta_p} & W_{2\theta_p} & W_{3\theta_p} & \dots & W_{p\theta_p} \end{bmatrix}, \quad (5.20)$$

where

$$\begin{aligned} W_{a\mathbf{x}_k} &= \left[{}^k_{a-1}R \quad -{}^k_aR [{}^a\mathbf{r}_{P_a G_k}]^\times \right] S_a \\ W_{a\theta_k} &= \left[0_{3 \times 3} \quad {}^k_aR \right] S_a. \end{aligned} \quad (5.21)$$

The terms W_{ax_k} and $W_{a\theta_k}$ represent the contribution to the absolute velocity of G_k and the absolute angular velocity of link k , respectively, from the joint space velocity $\dot{\mathbf{q}}_a$.

Generalised Jacobian Matrix

Combining the relationships (5.12) and (5.20), the Jacobian matrix can be determined as $J = VW$ since $\dot{\mathbf{l}} = V\dot{\mathbf{x}} = VW\dot{\mathbf{q}}$. As a result, the Jacobian matrix can be expressed in the form

$$J = \begin{bmatrix} J_{1\mathbf{q}_1} & J_{1\mathbf{q}_2} & \dots & J_{1\mathbf{q}_p} \\ \vdots & & & \vdots \\ J_{m\mathbf{q}_1} & J_{m\mathbf{q}_2} & \dots & J_{m\mathbf{q}_p} \end{bmatrix} \in \mathbb{R}^{m \times n}, \quad (5.22)$$

where the term $J_{i\mathbf{q}_a}$ represents the relationship between the joint space velocity of link a and the derivative of the length of cable i and can be expressed with respect to (5.11) and (5.21) as

$$J_{i\mathbf{q}_a} = \sum_{k=a}^p [V_{ix_k} W_{ax_k} + V_{i\theta_k} W_{a\theta_k}]. \quad (5.23)$$

In addition to its importance in the kinematic model, it will be shown in Section 5.4 that the transpose of the Jacobian matrix relates the cable force vector and the motion of the rigid bodies within the equations of motion of MCDMs.

5.4 Equations of Motion for Serial Manipulators

The generalised equations of motion represent the relationship between the cable forces and the motion of the MCDM. The equations of motion allow analysis on the system dynamics, such as inverse dynamics and direct dynamics presented in Sections 3.2.3 and 3.2.4, respectively, to be performed. As with the generalised system kinematic model presented in Section 5.3, the generalised equations of motion represent the system dynamics of arbitrarily structured MCDMs within a single model. This model allows the analysis for serial MCDMs to be performed with ease as remodelling of the system only requires the redefinition of the type of joints and the CRM.

The equations of motion for generalised MCDMs are derived using the Newton-Euler

approach. The Newton's second law of motion relationship for body k can be expressed in $\{F_k\}$ as

$$m_k \ddot{\mathbf{r}}_{OG_k} = \sum \mathbf{F}_k, \quad (5.24)$$

$$I_{kG_k} \dot{\boldsymbol{\omega}}_k + \boldsymbol{\omega}_k \times (I_{kG_k} \boldsymbol{\omega}_k) = \sum \mathbf{M}_{G_k}, \quad (5.25)$$

where (5.24) and (5.25) are the sum of forces and sum of moments equations, respectively. The terms $\ddot{\mathbf{r}}_{OG_k}$ and $\dot{\boldsymbol{\omega}}_k$ represent the absolute acceleration of G_k and the absolute angular acceleration of link k , respectively. In (5.25), the moments are summed about the centre of mass of the link G_k . The mass of link k and moment of inertia of link k about G_k are m_k and I_{kG_k} , respectively. The terms $\sum \mathbf{F}_k$ and $\sum \mathbf{M}_{G_k}$ represent the sum of forces acting on link k and the sum of moments about G_k .

The equations of motion for the generalised MCDM system will be presented in three parts. Firstly, Section 5.4.1 formulates the generalised expressions of the acceleration $\ddot{\mathbf{x}}$ for the rigid bodies of the MCDM. Secondly, Section 5.4.2 describes the sum of forces $\sum \mathbf{F}_k$ and sum of moments $\sum \mathbf{M}_{G_k}$ that act on each link of the manipulator. Finally, the generalised equations of motion are derived in Section 5.4.3. The equations of motion are represented in the generalised form (3.2), where the mass-inertia matrix M , centrifugal and Coriolis force vector \mathbf{C} , gravity force vector \mathbf{G} and the transpose of the Jacobian matrix J^T are expressed with respect to the generalised coordinates and the CRM. It will also be shown that the Jacobian matrix is consistent with that derived from the system kinematics in Section 5.3.

5.4.1 Generalised Accelerations

In the Newton's second law equations from (5.24) and (5.25), the acceleration terms $\ddot{\mathbf{r}}_{OG_k}$ and $\dot{\boldsymbol{\omega}}_k$ are required. The absolute accelerations can be determined through the relative accelerations, in the same manner as the determination of velocities in Section 5.3.2.

Firstly, the relative angular acceleration $\dot{\boldsymbol{\omega}}_{k,k-1}$ of link k relative to link $k - 1$ in $\{F_k\}$

can be determined by taking the time derivative of (5.3), where

$${}^k\dot{\omega}_{k,k-1} = {}^k\omega'_{k,k-1} + {}^k\omega_k \times {}^k\omega_{k,k-1}. \quad (5.26)$$

From (5.26), the absolute angular acceleration of link k can be expressed with respect to $\{F_k\}$ as

$${}^k\ddot{\omega}_k = \sum_{a=1}^k {}_a^k R \left({}^a\omega'_{a,a-1} + {}^a\omega_a \times {}^a\omega_{a,a-1} \right). \quad (5.27)$$

In a similar manner to determining the absolute angular acceleration, the absolute acceleration $\ddot{\mathbf{r}}_{OG_k}$ requires the relative accelerations $\ddot{\mathbf{r}}_{P_{a-1}P_a}$ and $\ddot{\mathbf{r}}_{P_kG_k}$, where

$$\ddot{\mathbf{r}}_{OG_k} = \sum_{a=1}^k [\ddot{\mathbf{r}}_{P_{a-1}P_a}] + \ddot{\mathbf{r}}_{P_kG_k}. \quad (5.28)$$

Taking the time derivative of (5.15) results in

$$\begin{aligned} {}^{a-1}\ddot{\mathbf{r}}_{P_{a-1}P_a} &= {}^{a-1}\mathbf{r}''_{P_{a-1}P_a} + {}^{a-1}\dot{\omega}_{a-1} \times {}^{a-1}\mathbf{r}_{P_{a-1}P_a} + 2{}^{a-1}\omega_{a-1} \times {}^{a-1}\mathbf{r}'_{P_{a-1}P_a} \\ &\quad + {}^{a-1}\omega_{a-1} \times ({}^{a-1}\omega_{a-1} \times {}^{a-1}\mathbf{r}_{P_{a-1}P_a}). \end{aligned} \quad (5.29)$$

The acceleration from P_k to G_k can be expressed in $\{F_k\}$ as

$${}^k\ddot{\mathbf{r}}_{P_kG_k} = {}^k\dot{\omega}_k \times {}^k\mathbf{r}_{P_kG_k} + {}^k\omega_k \times ({}^k\omega_k \times {}^k\mathbf{r}_{P_kG_k}). \quad (5.30)$$

Substituting (5.27), (5.29) and (5.30) into (5.28) allows the absolute acceleration of G_k to be expressed in $\{F_k\}$ as

$$\begin{aligned} \ddot{\mathbf{r}}_{OG_k} &= \sum_{a=1}^k \left[{}_{a-1}^k R \left({}^{a-1}\mathbf{r}''_{P_{a-1}P_a} + {}^{a-1}\dot{\omega}_{a-1} \times {}^{a-1}\mathbf{r}_{P_{a-1}P_a} + 2{}^{a-1}\omega_{a-1} \times {}^{a-1}\mathbf{r}'_{P_{a-1}P_a} \right) \right] \\ &\quad + \sum_{a=1}^k \left[{}_{a-1}^k R \left({}^{a-1}\omega_{a-1} \times ({}^{a-1}\omega_{a-1} \times {}^{a-1}\mathbf{r}_{P_{a-1}P_a}) \right) \right] \\ &\quad + {}^k\dot{\omega}_k \times {}^k\mathbf{r}_{P_kG_k} + {}^k\omega_k \times ({}^k\omega_k \times {}^k\mathbf{r}_{P_kG_k}). \end{aligned} \quad (5.31)$$

From (5.27) and (5.31), $\ddot{\mathbf{x}}_k$ can be expressed in matrix form

$$\begin{bmatrix} {}^k\ddot{\mathbf{r}}_{OG_k} \\ {}^k\dot{\boldsymbol{\omega}}_k \end{bmatrix} = \sum_{a=1}^k \left[P_{ak} \mathbf{x}_{k,k-1}'' + P_{ak} \begin{bmatrix} 2 [{}^{a-1}\boldsymbol{\omega}_{a-1}]^\times & 0_{3 \times 3} \\ 0_{3 \times 3} & [{}^a\boldsymbol{\omega}_a]^\times \end{bmatrix} \mathbf{x}'_{k,k-1} \right] \\ + \sum_{a=1}^k \begin{bmatrix} {}^k\boldsymbol{\omega}_{a-1} \times ({}^k\boldsymbol{\omega}_{a-1} \times {}^k\mathbf{r}_{P_{a-1}P_a}) \\ 0_{3 \times 1} \end{bmatrix} + \begin{bmatrix} {}^k\boldsymbol{\omega}_k \times ({}^k\boldsymbol{\omega}_k \times {}^k\mathbf{r}_{P_kG_k}) \\ 0_{3 \times 1} \end{bmatrix}, \quad (5.32)$$

where P_{ak} is introduced in (5.19). Taking the derivative of (5.2) allows the relative acceleration $\mathbf{x}_{k,k-1}''$ of link k relative to link $k-1$ to be expressed as

$$\mathbf{x}_{k,k-1}'' = \begin{bmatrix} {}^{k-1}\mathbf{r}_{P_{k-1}P_k}'' \\ {}^k\boldsymbol{\omega}'_{k,k-1} \end{bmatrix} = S_k \ddot{\mathbf{q}}_k + \dot{S}_k \dot{\mathbf{q}}_k. \quad (5.33)$$

Substituting (5.2) and (5.33) into (5.32) results in the expression of $\ddot{\mathbf{x}}_k$ with respect to the generalised joint model introduced in Section 5.2.2

$$\begin{bmatrix} {}^k\ddot{\mathbf{r}}_{OG_k} \\ {}^k\dot{\boldsymbol{\omega}}_k \end{bmatrix} = \sum_{a=1}^k \left[P_{ak} (S_a \ddot{\mathbf{q}}_a + \dot{S}_a \dot{\mathbf{q}}_a) + P_{ak} X_a S_a \dot{\mathbf{q}}_a \right] + \mathbf{b}_k, \quad (5.34)$$

where

$$X_a = \begin{bmatrix} 2 [{}^{a-1}\boldsymbol{\omega}_{a-1}]^\times & 0_{3 \times 3} \\ 0_{3 \times 3} & [{}^a\boldsymbol{\omega}_a]^\times \end{bmatrix},$$

and

$$\mathbf{b}_k = \sum_{a=1}^k \begin{bmatrix} {}^k\boldsymbol{\omega}_{a-1} \times ({}^k\boldsymbol{\omega}_{a-1} \times {}^k\mathbf{r}_{P_{a-1}P_a}) \\ 0_{3 \times 1} \end{bmatrix} + \begin{bmatrix} {}^k\boldsymbol{\omega}_k \times ({}^k\boldsymbol{\omega}_k \times {}^k\mathbf{r}_{P_kG_k}) \\ 0_{3 \times 1} \end{bmatrix}.$$

Combining (5.34) for each link allows the acceleration of the system $\ddot{\mathbf{x}}$ to be expressed as a function of the generalised coordinates

$$\ddot{\mathbf{x}} = W \ddot{\mathbf{q}} + P \dot{S} \dot{\mathbf{q}} + P X S \dot{\mathbf{q}} + \mathbf{b}(\mathbf{q}, \dot{\mathbf{q}}), \quad (5.35)$$

where $X = \text{diag}(X_1, X_2, \dots, X_p)$ and $\mathbf{b} = [\mathbf{b}_1^T \ \mathbf{b}_2^T \ \dots \ \mathbf{b}_p^T]^T$. The matrices W , P and S are those from (5.18) and (5.20).

The expression for the system acceleration from (5.35) can be regarded as a gener-

alised formulation that accommodates an arbitrary number of links and types of joints. The generalised accelerations will be used in the formulation of the Netwon's second law relationships in (5.24) and (5.25).

5.4.2 Sum of Forces and Moments

In this section, the expressions for the sum of forces and moments acting on the MCDM system are derived. Consider the free body diagram for link k shown in Figure 5.4, where the forces and moments that act on the link are shown.

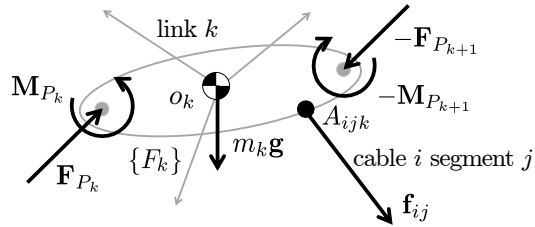


Figure 5.4: Free body diagram for link k of an MCDM showing the forces and moments acting on the link.

The forces and moments that act on body k are comprised of: interaction forces and moments between connected links, gravity force, external forces and moments, and forces due to cables acting on the link. Hence, the sum of forces $\sum \mathbf{F}_k$ that act on link k from (5.24) can be expressed in $\{F_k\}$ as

$$\sum \mathbf{F}_k = m_k \mathbf{g} + \mathbf{F}_{P_k} - \mathbf{F}_{P_{k+1}} + \mathbf{F}_{T_k} + \mathbf{F}_{E_k}, \quad (5.36)$$

where \mathbf{F}_{P_k} , \mathbf{F}_{T_k} and \mathbf{F}_{E_k} represent the interaction force between links k and $k-1$, the sum of cable forces acting on link k and any other external forces acting on link k , respectively. The interaction force $-\mathbf{F}_{P_{k+1}}$ is the opposite reaction interaction force between links k and $k+1$. Similarly, the sum of moments $\sum \mathbf{M}_{G_k}$ that act on link k about G_k from (5.25) can be expressed in $\{F_k\}$ as

$$\sum \mathbf{M}_{G_k} = \mathbf{r}_{G_k P_k} \times \mathbf{F}_{P_k} - \mathbf{r}_{G_k P_{k+1}} \times \mathbf{F}_{P_{k+1}} + \mathbf{M}_{P_k} - \mathbf{M}_{P_{k+1}} + \mathbf{M}_{T_k} + \mathbf{M}_{E_k}, \quad (5.37)$$

where \mathbf{M}_{T_k} and \mathbf{M}_{E_k} represent the moments due to the cable forces acting on link k and any other moments due to external forces/moments on link k .

The cables forces \mathbf{F}_{T_k} and moments \mathbf{M}_{T_k} that act on link k are dependent on the whether a cable is connected to link k . The forces and moments that cable i produces on link k can be expressed as

$$\begin{aligned}\mathbf{F}_{T_{ik}} &= \sum_{j=1}^s c_{ij(k+1)} \mathbf{f}_{ij}, \\ \mathbf{M}_{T_{ik}} &= \sum_{j=1}^s c_{ij(k+1)} \mathbf{r}_{G_k A_{ijk}} \times \mathbf{f}_{ij}\end{aligned}\quad (5.38)$$

where \mathbf{f}_{ij} is the cable force vector of segment j of cable i and can be defined with respect to the cable segment vector as

$$\mathbf{f}_{ij} = -\hat{\mathbf{l}}_{ij} f_i. \quad (5.39)$$

The CRM element $c_{ij(k+1)}$ in (5.38) represents the relationship between \mathbf{f}_{ij} and link k . From the definition of the CRM introduced in Chapter 4, $c_{ij(k+1)} = 0$ indicates that segment j of cable i is not attached onto link k . Correspondingly, in the context of (5.38), if $c_{ij(k+1)} = 0$ then segment j of cable i does not produce any resultant force or moment onto link k . On the other hand, if $c_{ij(k+1)} = -1$ or $c_{ij(k+1)} = 1$, then segment j of cable i is attached to link k and hence \mathbf{f}_{ij} should contribute to the forces and moments that cable i induces on link k . Furthermore, following the convention for the direction of \mathbf{l}_{ij} , where the cable vector is defined from the beginning attachment to the ending attachment, the CRM element $c_{ij(k+1)} = -1$ or $c_{ij(k+1)} = 1$ ensures that the cable force produced on any link will always be acting in tension and not compression.

Using the definition from (5.39) in (5.38) allows the forces and moments that cable i produces on link k to be expressed with respect to the terms introduced in (5.11) as

$$\begin{aligned}\mathbf{F}_{T_{ik}} &= -V_{i\mathbf{x}_k}^T f_i, \\ \mathbf{M}_{T_{ik}} &= -V_{i\theta_k}^T f_i.\end{aligned}\quad (5.40)$$

The terms $V_{i\mathbf{x}_k}^T$ and $V_{i\theta_k}^T$ represent the relationship between the force of cable i onto the

force and moment on link k , respectively. From (5.40), the forces and moments that act on link k induced by the entire set of cables can be expressed as

$$\begin{aligned}\mathbf{F}_{T_k} &= - \sum_{i=1}^m V_{i\mathbf{x}_k}^T f_i, \\ \mathbf{M}_{T_k} &= - \sum_{i=1}^m V_{i\theta_k}^T f_i.\end{aligned}\quad (5.41)$$

From (5.41), the cable forces and moments acting on the entire system can be represented in matrix form $\Gamma_T = -V^T \mathbf{f}$

$$\begin{bmatrix} \mathbf{F}_{T_1} \\ \mathbf{M}_{T_1} \\ \vdots \\ \mathbf{F}_{T_p} \\ \mathbf{M}_{T_p} \end{bmatrix} = - \begin{bmatrix} V_{1\mathbf{x}_1}^T & V_{2\mathbf{x}_1}^T & \dots & V_{m\mathbf{x}_1}^T \\ V_{1\theta_1}^T & V_{2\theta_1}^T & \dots & V_{m\theta_1}^T \\ \vdots & \vdots & & \vdots \\ V_{1\mathbf{x}_p}^T & V_{2\mathbf{x}_p}^T & \dots & V_{m\mathbf{x}_p}^T \\ V_{1\theta_p}^T & V_{2\theta_p}^T & \dots & V_{m\theta_p}^T \end{bmatrix} \begin{bmatrix} f_1 \\ f_2 \\ \vdots \\ f_m \end{bmatrix}, \quad (5.42)$$

where the matrix V^T is the transpose of kinematic matrix relationship (5.12). In the kinematics formulation, V represents the relationship between the derivative of the cable lengths and the twist vector. Analogously, in (5.42) the transpose matrix V^T represents the relationship between the cable forces and the body forces. The relationship from (5.42) is defined with respect to the CRM and can be regarded as a generalised relationship that inherently allows for arbitrary cable routing.

5.4.3 Generalised Equations of Motion

In this section, the equations of motion for generalised MCDMs are formulated through the generalised accelerations presented in Section 5.4.1 and the sum of forces and moments derived in Section 5.4.2. The equations of motion are determined by projecting the interaction forces and moments of every joint of the MCDM onto the generalised coordinates of the system. Using the projection S_a^T introduced in (5.4) from Section 5.2.2 for link

a , the projection for the entire system can be expressed in the form $S^T \Gamma_P = \mathbf{0}$

$$\begin{bmatrix} S_1^T & 0_{n_1 \times 6} & \dots & 0_{n_1 \times 6} \\ 0_{n_2 \times 6} & S_2^T & \dots & 0_{n_2 \times 6} \\ \vdots & & & \vdots \\ 0_{n_p \times 6} & 0_{n_p \times 6} & \dots & S_p^T \end{bmatrix} \begin{bmatrix} {}^0\mathbf{F}_{P_1} \\ {}^1\mathbf{M}_{P_1} \\ \vdots \\ {}^{p-1}\mathbf{F}_{P_p} \\ {}^p\mathbf{M}_{P_p} \end{bmatrix} = \begin{bmatrix} 0_{n_1 \times 1} \\ 0_{n_2 \times 1} \\ \vdots \\ 0_{n_p \times 1} \end{bmatrix}, \quad (5.43)$$

where Γ_P represents the vector of interaction forces and moments at all of the joints within the system.

From (5.24), (5.25), (5.36) and (5.37), the interaction force and moment acting at joint P_a can be expressed in $\{F_a\}$ as

$$\begin{aligned} \mathbf{F}_{P_a} &= \mathbf{F}_{B_a} + \mathbf{F}_{P_{a+1}}, \\ \mathbf{M}_{P_a} &= \mathbf{M}_{B_a} - \mathbf{r}_{G_a P_a} \times \mathbf{F}_{P_a} + \mathbf{r}_{G_a P_{a+1}} \times \mathbf{F}_{P_{a+1}} + \mathbf{M}_{P_{a+1}}, \end{aligned} \quad (5.44)$$

where the terms \mathbf{F}_{B_a} and \mathbf{M}_{B_a} can be expressed in $\{F_a\}$ as

$$\begin{aligned} \mathbf{F}_{B_a} &= m_a \ddot{\mathbf{r}}_{OG_a} - m_a \mathbf{g} - \mathbf{F}_{E_a} - \mathbf{F}_{T_a}, \\ \mathbf{M}_{B_a} &= I_{aG_a} \dot{\boldsymbol{\omega}}_a + \boldsymbol{\omega}_a \times (I_{aG_a} \boldsymbol{\omega}_a) - \mathbf{M}_{E_a} - \mathbf{M}_{T_a}. \end{aligned} \quad (5.45)$$

Using the relationships from (5.44), the interaction forces and moments acting on each joint can be expressed with respect to only the terms from (5.45) by propagating (5.44) from the outermost link p to any arbitrary link $a \in \{1, 2, \dots, p\}$ in the system. The boundary conditions for the propagation of forces and moments are $\mathbf{F}_{P_{p+1}} = \mathbf{M}_{P_{p+1}} = \mathbf{0}$. Beginning from link p , the joint interaction can be expressed as

$$\begin{aligned} \mathbf{F}_{P_p} &= \mathbf{F}_{B_p}, \\ \mathbf{M}_{P_p} &= \mathbf{M}_{B_p} + \mathbf{r}_{P_p G_p} \times \mathbf{F}_{B_p}. \end{aligned} \quad (5.46)$$

Similarly, the interaction force and moment at joint $p - 1$ can be determined by substitut-

ing (5.46) into (5.44)

$$\begin{aligned}\mathbf{F}_{P_{p-1}} &= \mathbf{F}_{B_{p-1}} + {}_p^{p-1}R \mathbf{F}_{B_p}, \\ \mathbf{M}_{P_{p-1}} &= \mathbf{r}_{P_{p-1}G_{p-1}} \times \mathbf{F}_{B_{p-1}} + \mathbf{M}_{B_{p-1}} + \mathbf{r}_{P_{p-1}G_p} \times \left({}_p^{p-1}R \mathbf{F}_{B_p} \right) + {}_p^{p-1}R \mathbf{M}_{P_p}.\end{aligned}\quad (5.47)$$

From (5.46) and (5.47), the interaction force and moment of joint a can be expressed in frames $\{F_{a-1}\}$ and $\{F_a\}$, respectively, as

$$\begin{bmatrix} {}^{a-1}\mathbf{F}_{P_a} \\ {}^a\mathbf{M}_{P_a} \end{bmatrix} = \sum_{k=a}^p \left[\begin{bmatrix} {}_k^{a-1}R & 0_{3 \times 3} \\ [{}^a\mathbf{r}_{P_a G_k}]^\times & {}_k^a R \end{bmatrix} \begin{bmatrix} {}^k\mathbf{F}_{B_k} \\ {}^k\mathbf{M}_{B_k} \end{bmatrix} \right]. \quad (5.48)$$

Observing that the matrix term in (5.48) is the transpose of P_{ak} derived in (5.19), the joint interaction forces and moments for the MCDM system can be expressed in the following matrix form $\boldsymbol{\Gamma}_P = P^T \boldsymbol{\Gamma}_B$

$$\begin{bmatrix} {}^0\mathbf{F}_{P_1} \\ {}^1\mathbf{M}_{P_1} \\ \vdots \\ {}^{p-1}\mathbf{F}_{P_p} \\ {}^p\mathbf{M}_{P_p} \end{bmatrix} = \begin{bmatrix} P_{11}^T & P_{21}^T & \dots & P_{(p-1)1}^T & P_{p1}^T \\ 0_{6 \times 6} & P_{22}^T & \dots & P_{(p-1)2}^T & P_{p2}^T \\ \vdots & & & \vdots & \\ 0_{6 \times 6} & 0_{6 \times 6} & \dots & 0_{6 \times 6} & P_{pp}^T \end{bmatrix} \begin{bmatrix} {}^1\mathbf{F}_{B_1} \\ {}^1\mathbf{M}_{B_1} \\ \vdots \\ {}^p\mathbf{F}_{B_p} \\ {}^p\mathbf{M}_{B_p} \end{bmatrix}, \quad (5.49)$$

where $\boldsymbol{\Gamma}_B$ is the vector that contains terms (5.45) for every link of the system. The matrix P^T propagates the forces and accelerations on the links to the joint forces and moments.

Finally, the equations of motion can be determined by eliminating $\boldsymbol{\Gamma}_P$ from (5.49) by projecting the joint interaction forces and moments onto the degrees of freedom of the system through (5.43) and (5.49) since $S^T \boldsymbol{\Gamma}_P = \mathbf{0}$, and hence

$$S^T P^T \boldsymbol{\Gamma}_B = W^T \boldsymbol{\Gamma}_B = \mathbf{0}. \quad (5.50)$$

From the projection (5.50), the relationship (5.45) for the MCDM system can be expressed compactly as

$$W^T \boldsymbol{\Gamma}_A + W^T \boldsymbol{\Gamma}_G + W^T \boldsymbol{\Gamma}_E = W^T \boldsymbol{\Gamma}_T, \quad (5.51)$$

where

$$\boldsymbol{\Gamma}_A = \begin{bmatrix} m_1 \ddot{\mathbf{r}}_{OG_1} \\ I_{1G_1} \dot{\boldsymbol{\omega}}_1 + \boldsymbol{\omega}_1 \times (I_{1G_1} \boldsymbol{\omega}_1) \\ \vdots \\ m_p \ddot{\mathbf{r}}_{OG_p} \\ I_{pG_p} \dot{\boldsymbol{\omega}}_p + \boldsymbol{\omega}_p \times (I_{pG_p} \boldsymbol{\omega}_p) \end{bmatrix}, \quad \boldsymbol{\Gamma}_G = \begin{bmatrix} -m_1 \mathbf{g} \\ 0_{3 \times 1} \\ \vdots \\ -m_p \mathbf{g} \\ 0_{3 \times 1} \end{bmatrix}, \quad \boldsymbol{\Gamma}_E = \begin{bmatrix} -\mathbf{F}_{E_1} \\ -\mathbf{M}_{E_1} \\ \vdots \\ -\mathbf{F}_{E_p} \\ -\mathbf{M}_{E_p} \end{bmatrix}. \quad (5.52)$$

The velocity and acceleration terms of the manipulator motion from (5.52) can be expressed in the form

$$\boldsymbol{\Gamma}_A = \begin{bmatrix} m_1 I_{3 \times 3} & 0_{3 \times 3} & \dots & 0_{3 \times 3} & 0_{3 \times 3} \\ 0_{3 \times 3} & I_{1G_1} & \dots & 0_{3 \times 3} & 0_{3 \times 3} \\ \vdots & & & \vdots & \\ 0_{3 \times 3} & 0_{3 \times 3} & \dots & m_p I_{3 \times 3} & 0_{3 \times 3} \\ 0_{3 \times 3} & 0_{3 \times 3} & \dots & 0_{3 \times 3} & I_{pG_p} \end{bmatrix} \begin{bmatrix} \ddot{\mathbf{r}}_{OG_1} \\ \dot{\boldsymbol{\omega}}_1 \\ \vdots \\ \ddot{\mathbf{r}}_{OG_p} \\ \dot{\boldsymbol{\omega}}_p \end{bmatrix} + \begin{bmatrix} 0_{3 \times 1} \\ \dot{\boldsymbol{\omega}}_1 \times (I_{1G_1} \dot{\boldsymbol{\omega}}_1) \\ \vdots \\ 0_{3 \times 1} \\ \dot{\boldsymbol{\omega}}_p \times (I_{pG_p} \dot{\boldsymbol{\omega}}_p) \end{bmatrix}, \quad (5.53)$$

where $I_{3 \times 3}$ is a 3×3 identity matrix. The matrix M_B represents the mass-inertia matrix that contains the mass and moments of inertia for the manipulator. Using the generalised accelerations from (5.35), the expression from (5.53) can be expressed as

$$\boldsymbol{\Gamma}_A = M_B W \ddot{\mathbf{q}} + M_B P \dot{S} \dot{\mathbf{q}} + M_B P X S \dot{\mathbf{q}} + \mathbf{c}, \quad (5.54)$$

where $\mathbf{c} = [\mathbf{c}_1^T \ \mathbf{c}_2^T \ \dots \ \mathbf{c}_p^T]^T$ and

$$\mathbf{c}_k = m_k \sum_{a=1}^k \begin{bmatrix} {}^k \boldsymbol{\omega}_{a-1} \times ({}^k \boldsymbol{\omega}_{a-1} \times {}^k \mathbf{r}_{P_{a-1} P_a}) \\ 0_{3 \times 1} \end{bmatrix} + \begin{bmatrix} m_k {}^k \boldsymbol{\omega}_k \times ({}^k \boldsymbol{\omega}_k \times {}^k \mathbf{r}_{P_k G_k}) \\ \boldsymbol{\omega}_k \times (I_{kG_k} \boldsymbol{\omega}_k) \end{bmatrix}.$$

Substituting (5.54) into (5.51) allows the equation of motion to be represented in the form

$$M(\mathbf{q}) \ddot{\mathbf{q}} + \mathbf{C}(\mathbf{q}, \dot{\mathbf{q}}) + \mathbf{G}(\mathbf{q}) + \boldsymbol{\Gamma}_{ext} = -J^T(\mathbf{q}) \mathbf{f},$$

as stated in (3.2). The terms M , \mathbf{C} , \mathbf{G} and $\boldsymbol{\Gamma}_{ext}$ from the equations of motion can be ex-

pressed as

$$\begin{aligned}
 M &= W^T M_B W, \\
 \mathbf{C} &= W^T M_B P (\dot{S} + XS) \dot{\mathbf{q}} + W^T \mathbf{c}, \\
 \mathbf{G} &= W^T \boldsymbol{\Gamma}_G, \\
 \boldsymbol{\Gamma}_{ext} &= W^T \boldsymbol{\Gamma}_E.
 \end{aligned} \tag{5.55}$$

The terms from (5.55) can be regarded as the generalised equations of motion to allow arbitrary joint type in the matrix S and arbitrary number of links in the matrix P from (5.18). From (5.42) and (5.51), the relationship between the cable force and the motion of the system can be described by $W^T V^T = J^T$, the transpose of the Jacobian matrix (5.22) derived in Section 5.3.

The transpose of the Jacobian matrix J^T derived allows for not only arbitrary joint type, but also arbitrary cable routing. This is achieved since the matrix V^T from (5.42) is formulated with respect to the CRM. Analogous to the kinematic relationship $J_{i\mathbf{q}_a}$ from (5.23) in Section 5.3.2, the term $J_{i\mathbf{q}_a}^T$ represents the effect of the force of cable i on the motion of the generalised coordinates \mathbf{q}_a of the manipulator.

The formulated equations of motion in (5.55) represent the dynamic model for generalised MCDMs. The kinematic model presented in Section 5.3 and the dynamic model in this section are the fundamental models required in the study and analysis of serial MCDMs.

5.5 Extension to Branched Manipulators

The generalised formulations proposed in Sections 5.3 and 5.4 assume that the rigid links of the MCDM system form a serial chain. In this section, the generalised formulation is extended to model MCDMs with an open-chain branched rigid link structure. Figure 5.5 shows examples of both serial and branched kinematic structures. The key characteristic of serial structures, as shown in Figure 5.5(a), is that each link is connected to one or at most two adjacent links without forming any closed chains. In comparison, the links

of the branched structure in Figure 5.5(b) can be connected to one, two or more links without forming any closed chains. Branched structures can be regarded as analogous to tree structures.

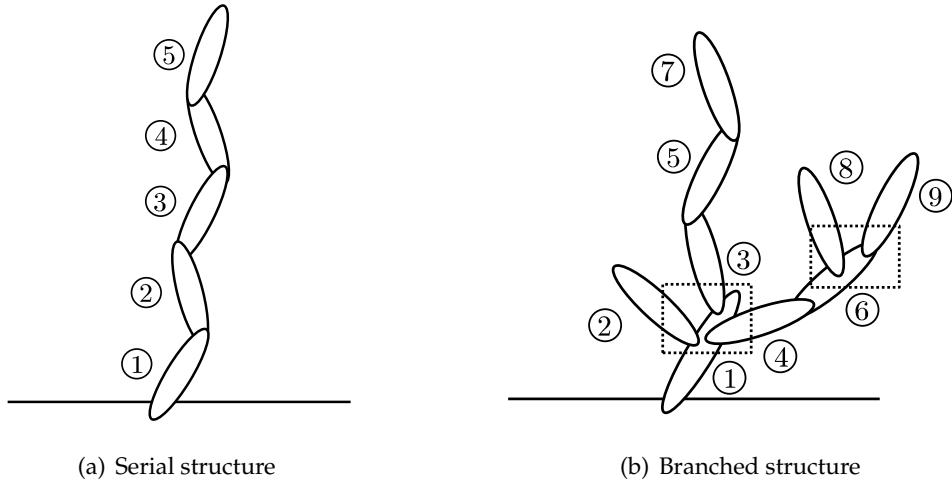


Figure 5.5: Open-chain structures can be classified as serial structured (a) and branched structured (b). The link numbers are shown beside each link in the figures. The dashed boxes in (b) indicates the locations of the branches.

Rigid body structure

For open-chain structures, two links that are interconnected form a parent and child relationship. The terms *parent* and *child* are described in Definitions 5.1 and 5.2, respectively.

Definition 5.1. *The parent link in a kinematic chain refers to a connected link that is closer to the base frame.*

Definition 5.2. *The child link in a kinematic chain refers to a connected link that is further from the base frame than its connected link.*

From the definitions of parent and child links, it can be observed from Figure 5.5 that each link has exactly one parent link. For serial mechanisms, each parent link has at most one child link. However, for branched mechanisms each parent link is allowed to have more than one child link.

As a result, the structure for all serial mechanisms are the same and can be modelled as a consecutive chain that begins from the base frame extending to the outermost link. From the convention introduced in Section 5.2.1, the links of a p link serial mechanism are numbered consecutively from 1 to p , where link 1 is connected to the base and link p is the outermost link. In comparison, the structure of branched mechanisms differ depending on how the links are interconnected. The links of the branched mechanisms can be numbered arbitrarily but must satisfy Property 5.1.

Property 5.1. *Links are numbered such that a parent link have a smaller link number than its children.*

The structure of a branched mechanism can be described by an *adjacency matrix* that represents a directed mathematical graph. For a p link branched MCDM, the adjacency matrix is a $(p + 1) \times (p + 1)$ matrix that contains the connections between the base frame and the p links. The matrix B can be represented in the form

$$B = \begin{bmatrix} 0 & b_{01} & b_{02} & \dots & b_{0p} \\ 0 & 0 & b_{12} & \dots & b_{1p} \\ \vdots & & & & \vdots \\ 0 & 0 & 0 & \dots & b_{(p-1)p} \\ 0 & 0 & 0 & \dots & 0 \end{bmatrix}, \quad (5.56)$$

where $b_{ij} = 1$ denotes that link i is the parent of link j , and $b_{ij} = 0$ otherwise. Since the structure of the system must satisfy Property 5.1 and links cannot be connected to itself, $b_{ij} = 0 \forall j \leq i$ and hence B is an upper triangular matrix. To ensure that the structure does not form closed loops, each link must only have one parent and B from (5.56) must satisfy Property 5.2.

Property 5.2. $\sum_{i=0}^p b_{ij} = 1 \forall j$. For every link j , there is only one parent (link i) such that $b_{ij} = 1$ and the relationship with the remainder links is $b_{ik} = 0 \forall k \neq i$.

To illustrate how (5.56) defines the structure of the mechanism, B_1 and B_2 describe the

structure of the manipulators in Figures 5.5(a) and 5.5(b), respectively, where

$$B_1 = \begin{bmatrix} 0 & \mathbf{1} & 0 & 0 & 0 & 0 \\ 0 & 0 & \mathbf{1} & 0 & 0 & 0 \\ 0 & 0 & 0 & \mathbf{1} & 0 & 0 \\ 0 & 0 & 0 & 0 & \mathbf{1} & 0 \\ 0 & 0 & 0 & 0 & 0 & \mathbf{1} \\ 0 & 0 & 0 & 0 & 0 & 0 \end{bmatrix}, \quad B_2 = \begin{bmatrix} 0 & \mathbf{1} & 0 & 0 & 0 & 0 & 0 & 0 & 0 & 0 \\ 0 & 0 & \mathbf{1} & \mathbf{1} & \mathbf{1} & 0 & 0 & 0 & 0 & 0 \\ 0 & 0 & 0 & 0 & 0 & 0 & 0 & 0 & 0 & 0 \\ 0 & 0 & 0 & 0 & 0 & 0 & \mathbf{1} & 0 & 0 & 0 \\ 0 & 0 & 0 & 0 & 0 & 0 & 0 & \mathbf{1} & 0 & 0 \\ 0 & 0 & 0 & 0 & 0 & 0 & 0 & 0 & \mathbf{1} & 0 \\ 0 & 0 & 0 & 0 & 0 & 0 & 0 & 0 & 0 & \mathbf{1} \\ 0 & 0 & 0 & 0 & 0 & 0 & 0 & 0 & 0 & 0 \\ 0 & 0 & 0 & 0 & 0 & 0 & 0 & 0 & 0 & 0 \\ 0 & 0 & 0 & 0 & 0 & 0 & 0 & 0 & 0 & 0 \end{bmatrix}.$$

The matrix B can be regarded as the footprint for the rigid link structure of branched mechanisms providing the connection relationships between links. From (5.56), a dependency matrix can be expressed that describes the dependency in motion between the links. The dependency matrix D is an upper triangle $p \times p$ matrix that can be expressed as

$$D = \begin{bmatrix} d_{11} & d_{12} & d_{13} & \dots & d_{1p} \\ 0 & d_{22} & d_{23} & \dots & d_{2p} \\ 0 & 0 & d_{33} & \dots & d_{3p} \\ \vdots & & & & \vdots \\ 0 & 0 & 0 & \dots & d_{pp} \end{bmatrix}, \quad (5.57)$$

where $d_{ak} = 1$ denotes that the motion of link k is dependent on the generalised coordinates \mathbf{q}_a . The elements within the matrix (5.57) are useful in the determination of the absolute velocities and accelerations for the links within branched MCDMs, and also the propagation of joint interaction forces and moments. The matrix from (5.57) can be generated by tracing through the parent links for each of link within the system.

Manipulator Model

Section 5.5 introduced the generalised representation for the structure of branched mechanisms. In this section, the generalised representation will be used to extend the generalised model from Sections 5.3 and 5.4 to branched MCDMs. It was shown in Section 4.3.3 that the CRM is inherently able to describe the cable routing for branched MCDMs.

There are two key differences in the modelling of serial and branched MCDMs. Firstly, in Sections 5.3, the absolute velocity and acceleration of link k are determined from the generalised coordinates \mathbf{q}_1 to \mathbf{q}_k . However, for branched MCDMs, the dependency matrix from (5.57) must be considered in the formulation. Secondly, in Sections 5.4, the joint interaction forces and moments of link k are determined by propagating the forces and moments from link p down to link k . However, for branched MCDMs, not all links $a > k$ are connected to link k . As a result, it is required to include the dependency matrix terms into the kinematic relationship P from (5.18).

It can be observed in Sections 5.3.2 and 5.4.2 that the expressions V and V^T represent the relationship between the cable and body space velocities and forces, respectively, where the expression for V remains the same for both serial and branched MCDMs. Following the same method to formulate the absolute velocities for link k in Section 5.3.2, the absolute velocity of G_k and absolute angular velocity of link k from (5.17) can be expressed as

$$\begin{bmatrix} {}^k\dot{\mathbf{r}}_{OG_k} \\ {}^k\boldsymbol{\omega}_k \end{bmatrix} = \sum_{a=1}^k d_{ak} \begin{bmatrix} {}^k_{a_p}R & -{}^k_aR [{}^a\mathbf{r}_{P_a}G_k]^{\times} \\ 0_{3 \times 3} & {}^k_aR \end{bmatrix} S_a \dot{\mathbf{q}}_a . \quad (5.58)$$

From (5.58), the P matrix for branched MCDMs can be expressed as

$$P = \begin{bmatrix} d_{11}P_{11} & 0_{6 \times 6} & \dots & 0_{6 \times 6} \\ d_{12}P_{21} & d_{22}P_{22} & \dots & 0_{6 \times 6} \\ \vdots & & & \vdots \\ d_{1p}P_{p1} & d_{2p}P_{p2} & \dots & d_{pp}P_{pp} \end{bmatrix} . \quad (5.59)$$

The extended relationship (5.59) impacts on the relationship $W = PS$ from (5.20) and $J = VW$ from (5.22). Similarly, it can be shown that the branched structure affects the

propagation of forces and moments in (5.49) such that the P^T is equivalent to that introduced in (5.59). Using (5.59) in the equations of motion from (5.55) results in a generalised dynamic model that allows for branched MCDMs of any structure and joint types.

5.6 Simulation Examples

To illustrate the effectiveness and robustness of modelling MCDMs using the generalised model presented in Section 5.5, the inverse kinematics and inverse dynamics are simulated for two example MCDMs: a 2 link 4 DoF manipulator actuated by 6 cables and a more complex 8 link 24 DoF manipulator actuated by 76 cables with a range of different types of cable routing. The inverse dynamics is performed using the approach described in Section 3.2.3 with an objective function of $Q(\mathbf{f}) = f_1^2 + f_2^2 + \dots + f_m^2 = \mathbf{f}^T \mathbf{f}$.

5.6.1 4 DoF Two Link Manipulator

A 2 link spatial manipulator with 4 degrees of freedom is shown in Figure 5.6. Link 1 is constrained to the origin of the inertial frame through a spherical (S) joint, and links 2 and 1 are constrained by a revolute (R) joint. The generalised coordinates for the system can be expressed by $\mathbf{q} = [\alpha \ \beta \ \gamma \ \theta]^T$, where α , β and γ represent the xyz -Euler angles of the spherical joint and θ represents the relative angle of the revolute joint.

The system is actuated by 6 cables, where cables 1 to 4 are connected from the base to link 1, as shown in Figure 4.1(a), and cables 5 and 6 are connected from the base to link 2, passing via link 1, as shown in Figure 4.2(a). From the example in Section 4.3.1, the CRMs for cables 1 to 4 can be described by C_1 and cables 5 and 6 can be described by C_4 , where

$$C_1 = \begin{bmatrix} -1 & 1 & 0 \\ 0 & 0 & 0 \end{bmatrix}, \quad C_4 = \begin{bmatrix} -1 & 1 & 0 \\ 0 & -1 & 1 \end{bmatrix}.$$

For this manipulator, the attachment locations of the cables $\mathbf{r}_{o_k A_{ijk}}$ are symmetrically arranged, such that when the manipulator is in its zero upright position, cables 1 and 3 are located in the XZ -plane, and the remainder cables are located in the YZ -plane.

A simple trajectory was selected to demonstrate the inverse kinematics and inverse

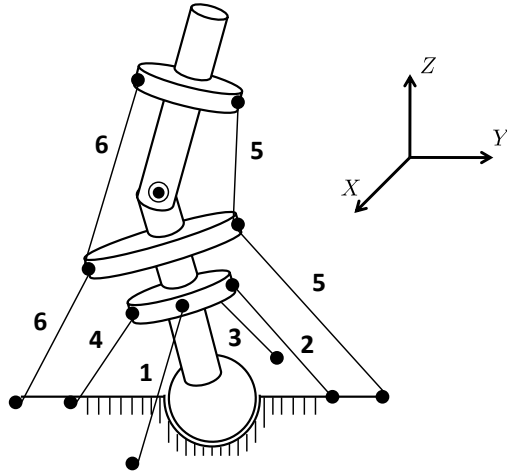


Figure 5.6: 2 link Spherical-Revolute (SR) model actuated by 6 cables.

dynamics for the 2 link system. The desired trajectory $\mathbf{q}_r(t)$ was constructed by interpolating from the initial pose $\mathbf{q}_s = \left[\begin{array}{cccc} \frac{\pi}{10} & 0 & 0 & -\frac{\pi}{6} \end{array} \right]^T$ to the final pose $\mathbf{q}_e = \left[\begin{array}{cccc} -\frac{\pi}{10} & 0 & 0 & \frac{\pi}{6} \end{array} \right]^T$. Additionally, the initial and final velocities and accelerations for the desired trajectory were set to zero $\dot{\mathbf{q}}_s = \dot{\mathbf{q}}_e = \ddot{\mathbf{q}}_s = \ddot{\mathbf{q}}_e = \mathbf{0}$. Figure 5.6 shows the manipulator in its initial pose \mathbf{q}_s . For the interpolated trajectory, the motion of the manipulator is entirely in the YZ -plane.

The length of the cables $\mathbf{l}(t)$ for the entire trajectory was determined by solving (5.7) for each of the cables at each instance in time. Figure 5.7 shows the length of each cable, the solution to the inverse kinematic analysis for trajectory $\mathbf{q}_r(t)$.

Figure 5.7 shows that the generalised cable segment vector formulated using the CRM produced the expected cable lengths. It can be observed that cables 1 (Figure 5.7(a)) and 3 (Figure 5.7(c)) remain constant in length since the motion is purely in the YZ -plane. As the motion begins from $\alpha = \frac{\pi}{10}$ to $\alpha = -\frac{\pi}{10}$, the length of cable 2 (Figure 5.7(b)) decreased from $l_2 = 0.17$ m to $l_2 = 0.11$ m. Since the motion is symmetrical about the XZ -plane, cable 4 (Figure 5.7(d)) mirrors $l_2(t)$ about $t = 0.5$ s and correspondingly increased in length from $l_4 = 0.11$ m to $l_4 = 0.17$ m. In a similar manner to cables 2 and 4, the cable lengths $l_5(t)$ and $l_6(t)$ are symmetrical, where cable 5 decreases from $l_5 = 0.34$ m to $l_5 = 0.32$ m and cable 6 increases from $l_6 = 0.32$ m to $l_6 = 0.34$ m, as shown in Figures

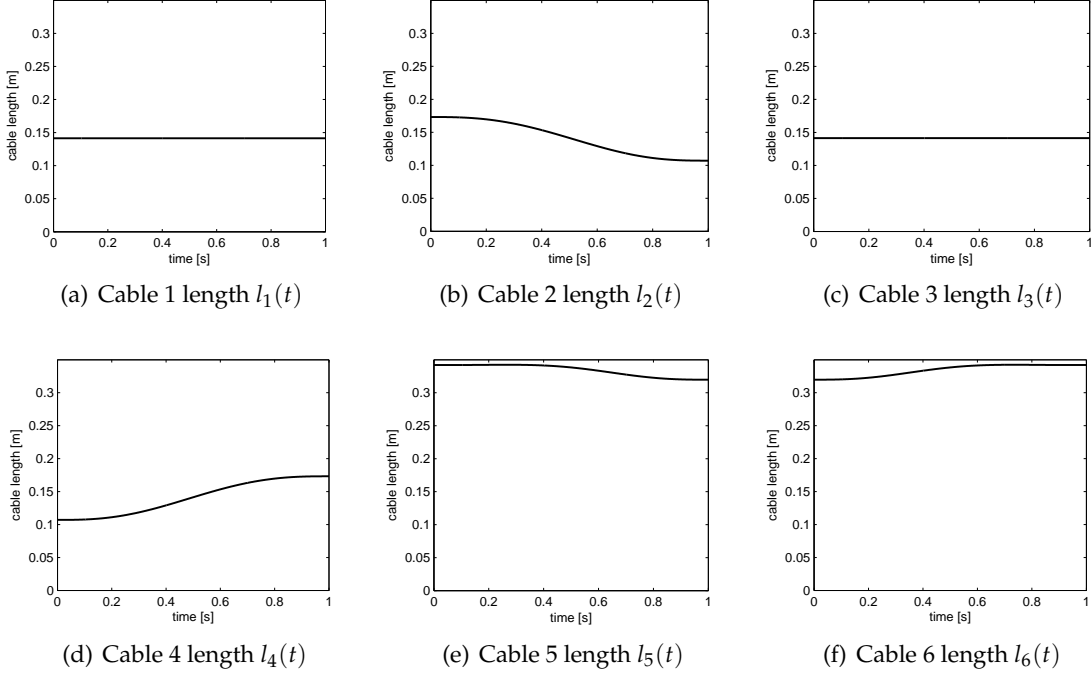


Figure 5.7: The cable lengths from the inverse kinematic analysis on the 2 link 4 DoF manipulator for trajectory $\mathbf{q}_r(t)$. The length $l_i(t)$ for cables 1 to 6 are shown in (a)-(f).

5.8(e) and 5.8(f), respectively.

To demonstrate the formulated generalised Jacobian matrix terms from (5.23) on the 2 link system, the derivatives of cable lengths \dot{l} were determined through the relationship $\dot{l} = J\dot{\mathbf{q}}$ in (5.22). Figure 5.8 shows the derivatives of cable lengths \dot{l} over the entire trajectory $\mathbf{q}_r(t)$.

Comparing Figure 5.8 to Figure 5.7, it can be observed that the profiles in Figure 5.8 correspond to the derivatives of the cable lengths in Figure 5.7. In Figures 5.8(a) and 5.8(c), the derivatives of the cable lengths are zero $\dot{l}_1(t) = \dot{l}_3(t) = 0$ and correspond to the constant lengths of cables 1 and 3 for the trajectory. Similarly, the lengths of cables 2 and 5 decreased in length, indicated by $\dot{l}_2(t) \leq 0$ and $\dot{l}_5(t) \leq 0$, respectively, and the lengths of cable 4 and 6 increased over the trajectory. These observations are consistent with the description of the cable lengths from Figure 5.7.

To demonstrate the dynamic model formulated in Section 5.4, the inverse dynamics was also performed on the trajectory $\mathbf{q}_r(t)$. Figure 5.9 shows the determined cable forces

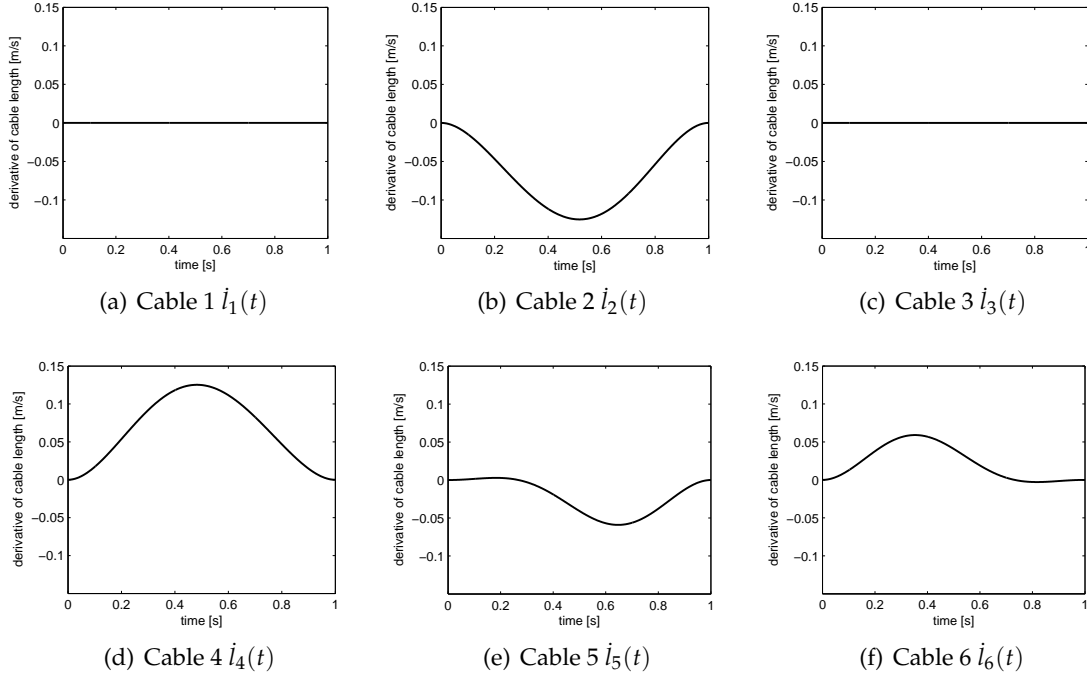


Figure 5.8: The derivative of cable lengths on the 2 link 4 DoF manipulator for trajectory $\mathbf{q}_r(t)$. The derivative $\dot{l}_i(t)$ for cables 1 to 6 are shown in (a)-(f).

required to produce the desired trajectory $\mathbf{q}_r(t)$. The minimum and maximum bounds on cable forces were set to 0.001 N and 1000 N, respectively.

Since motion $\mathbf{q}_r(t)$ is purely in the YZ-plane, it is expected that cables 1 and 3 both exert the minimum tension value, as shown in Figures 5.9(a) and 5.9(c), respectively. For the motion during $t \leq 0.5$ s, cables 2 and 6 are required to actuate the motion of links 1 and 2, respectively. Since cable 6 is connected to both links 1 and 2, cable 2 is required to produce a higher cable force to counteract the undesired direction of motion caused by cable 6, as shown in Figure 5.9(b). Since the motion is symmetrical about the XZ-plane, cables 4 and 5 behave similarly for the motion during $t \geq 0.5$ s.

5.6.2 24 DoF 8 Link Human Neck Model

To show the versatility and scalability of the generalised CRM formulation, a more complex 8 link example is presented. The kinematic structure is modelled to represent the human neck or cervical vertebrae, consisting of 7 cervical bones and the skull. As shown

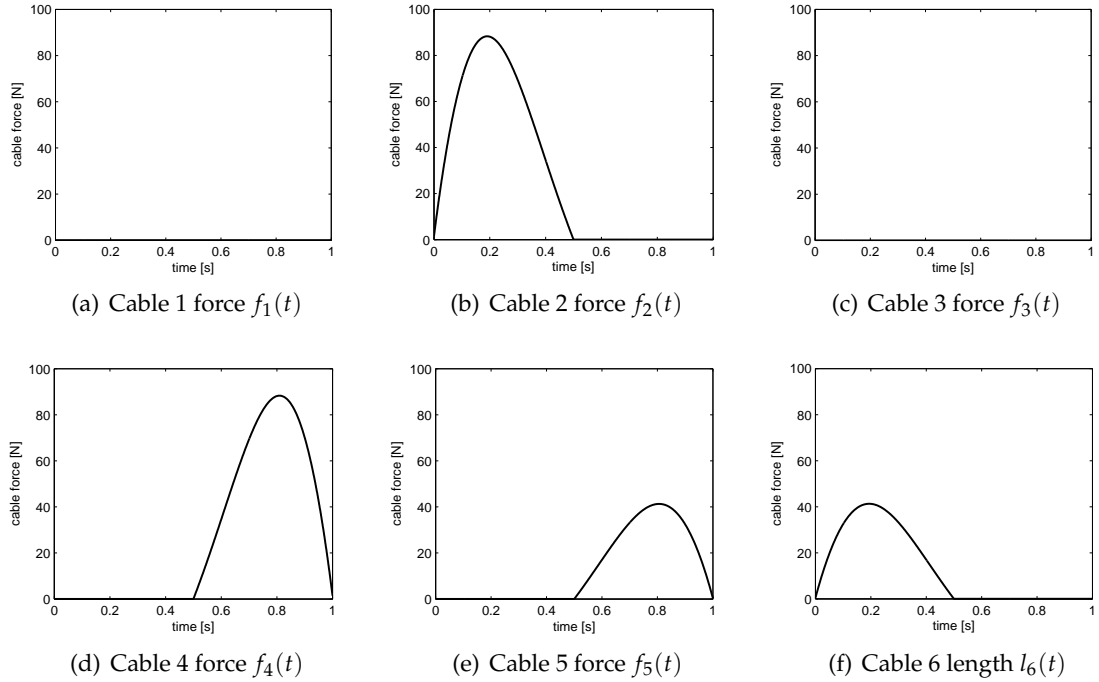
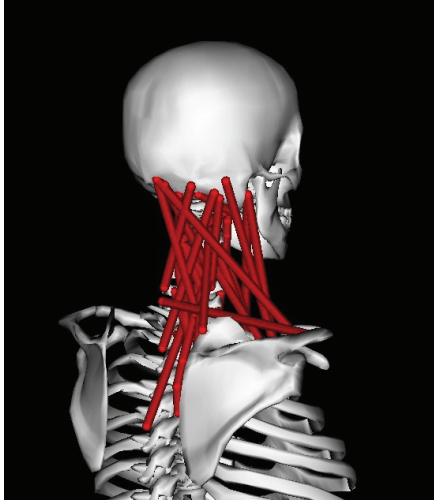


Figure 5.9: Cables force for the 2 link manipulator performing $\mathbf{q}_r(t)$. The cable force $f_i(t)$ for cables 1 to 6 are shown in (a)-(f).

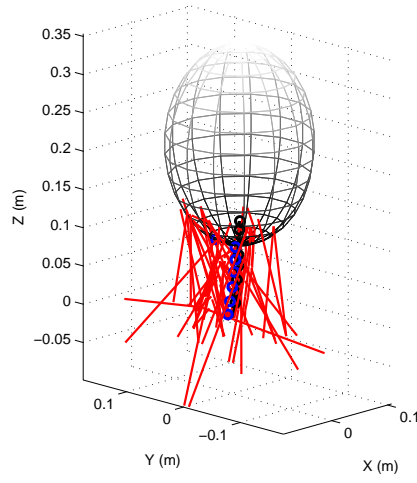
in Figure 4.4, links 1 to 7 represent bones C7 to C1, respectively, and link 8 represents the skull. The base of the system represents the shoulder and remainder of the spine and can be denoted as link 0. The C7 bone is connected to the base and C1 bone is connected to the skull. As each joint possesses 3 degrees of freedom, the total number of degrees of freedom for the system is $n = 24$. The joints between the bones of the system have been modelled as spherical (S) joints to represent the cervical vertebrae joints.

The system consists of $m = 76$ cables, where the cable routing and attachment locations were obtained from a biomechanics model of the neck [130]. The muscles are symmetrically arranged such that 38 cables represent the left neck muscles and 38 cables are the right neck muscles. Figure 5.10(a) shows the OpenSim model from [130] and Figure 5.10(b) shows the MCDM model constructed from the generalised CRM model.

The 8 link example demonstrates the simplicity in which arbitrary cable routing can be achieved for complex systems. The neck model consists of many different types of cable routing, from simple cable routings consisting of a single segment to complex rout-



(a) OpenSims neck model



(b) 8 link 8S 76 cable model

Figure 5.10: 8 link 8 Spherical (S) model actuated by 76 cables representing the human neck. The model from OpenSim neck model is shown in (a) and the corresponding MCDM model is shown in (b).

ings with multiple pass-through attachment points. It was shown in Section 4.3.2 that the muscle-routings for all of the neck muscles can be described by the CRM.

The generalised coordinates for the system can be represented by 8 sets of Euler angles, where $\mathbf{q}_k = [\alpha_k \ \beta_k \ \gamma_k]^T$ are the xyz -Euler angles for joint k . Three simple trajectories were selected for the inverse dynamics simulation: roll motion $\mathbf{q}_{roll}(t)$, pitch motion $\mathbf{q}_{pitch}(t)$ and yaw motion $\mathbf{q}_{yaw}(t)$, corresponding to pure rotations in the X , Y and Z axes, respectively. The roll, pitch and yaw trajectories were generated by interpolating between initial and final generalised coordinates, as shown in Table 5.1, using a quintic polynomial function of time assuming zero initial and final velocities and accelerations. The total time for each trajectory was set to be 1 s.

The resulting force profiles for the roll, pitch and yaw motion trajectories are shown in Figures 5.11, 5.12 and 5.13, respectively. Note that in this example muscles have been assumed to be *ideal force generator elements* that can produce force from zero to a maximum value as modelled in [144]. For the roll trajectory $\mathbf{q}_{roll}(t)$, motion is purely in the YZ -plane and is symmetrical about the XZ -plane. Physically, this is analogous to the tilting of the head from left to right. For this motion, it is expected that the left and right cables should

	Trajectory	Initial pose	Final pose
Roll Motion	$\mathbf{q}_1(t) - \mathbf{q}_7(t)$	$(-\frac{\pi}{45}, 0, 0)$	$(\frac{\pi}{45}, 0, 0)$
	$\mathbf{q}_8(t)$	$(-\frac{\pi}{30}, 0, 0)$	$(\frac{\pi}{30}, 0, 0)$
Pitch Motion	$\mathbf{q}_1(t) - \mathbf{q}_7(t)$	$(0, -\frac{\pi}{45}, 0)$	$(0, \frac{\pi}{45}, 0)$
	$\mathbf{q}_8(t)$	$(0, -\frac{\pi}{30}, 0)$	$(0, \frac{\pi}{30}, 0)$
Yaw Motion	$\mathbf{q}_1(t) - \mathbf{q}_7(t)$	$(0, 0, -\frac{\pi}{45})$	$(0, 0, \frac{\pi}{45})$
	$\mathbf{q}_8(t)$	$(0, 0, -\frac{\pi}{30})$	$(0, 0, \frac{\pi}{30})$

Table 5.1: The beginning and ending generalised coordinates used to generate the sample trajectories for the 8 link MCDM. The roll, pitch and yaw motions correspond to the left/right tilting motion, front/back tilt motion and left/right panning motion of the neck, respectively.

be symmetrical about time $t = 0.5$ s. Figures 5.11(a) and 5.11(b) show the set of left and right cables, respectively, and symmetry about $t = 0.5$ s can be observed. For this trajectory, the maximum cable force observed is approximately 23 N.

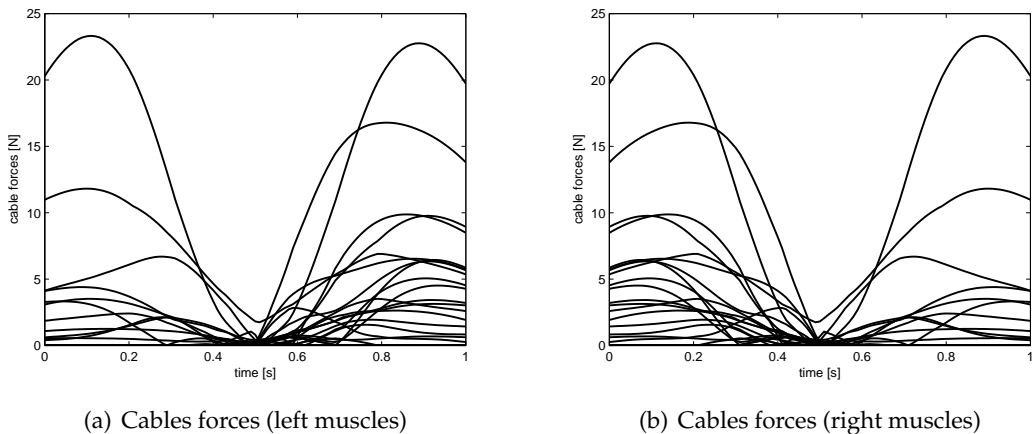


Figure 5.11: Cables force for the 8 link 8S manipulator performing roll trajectory $\mathbf{q}_{roll}(t)$. The left neck muscles and the right neck muscles are shown in (a) and (b), respectively.

In comparison, $\mathbf{q}_{pitch}(t)$ motion is analogous to the tilting of the head from back to front. Since motion is in the XZ-plane, Figures 5.12(a) and 5.12(b) show that the corresponding left and right cables exert the same force for the entire trajectory. Furthermore, it can be observed that the first part of the motion $t < 0.5$ s requires a considerably larger amount of cable force, with a maximum of approximately 230 N, than the second half

of the trajectory, with a maximum force of less than 10 N. This observation suggests that the cable attachment locations are arranged such that the neck is able to operate in the positive XZ-plane with much lower forces. Similar to single link cable-driven systems, the performance and cable force characteristics heavily depend on the location of cable attachment locations. However, for MCDMs the performance is highly dependent on both cable routing and attachment locations.

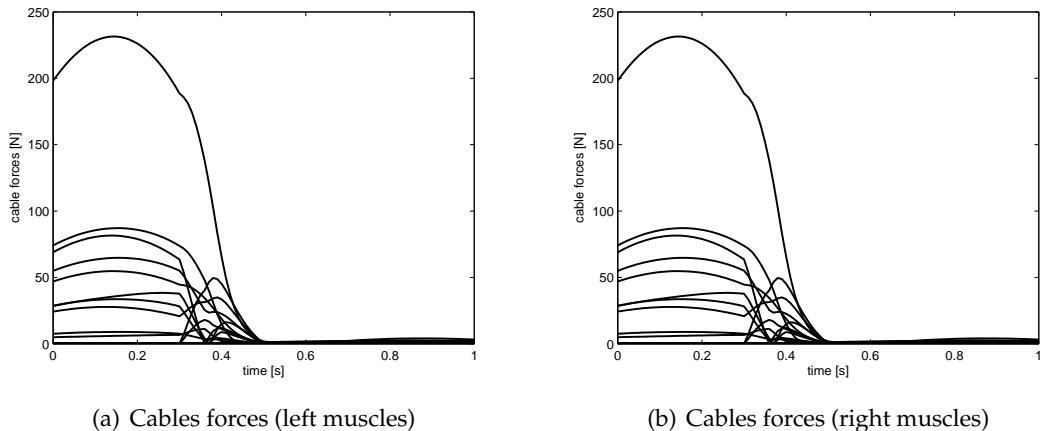


Figure 5.12: Cables force for the 8 link 8S manipulator performing pitch trajectory $\mathbf{q}_{pitch}(t)$. The left neck muscles and the right neck muscles are shown in (a) and (b), respectively.

The effect of cable arrangement on manipulator's performance is further illustrated through the yaw motion $\mathbf{q}_{yaw}(t)$. The cable forces for the yaw trajectory for the left and right cables are shown in Figure 5.13. The yaw motion is analogous to the panning motion of the head from right to left. Similarly to the roll motion, it is expected that the set of left and right cable forces are symmetrical about time $t = 0.5$ s, as observed in Figures 5.13(a) and 5.13(b). In comparison to the roll and pitch trajectories, it is apparent that the yaw motion requires the least cable force to perform, with a maximum cable force of approximately 2 N.

The 8 link model example demonstrates that the generalised model based on the CRM is able to describe the cable routing for complex systems, such as the routing of muscle within biomechanical systems. After formulating the generalised Jacobian matrix, analysis such as inverse dynamics, workspace analysis and cable configuration optimi-

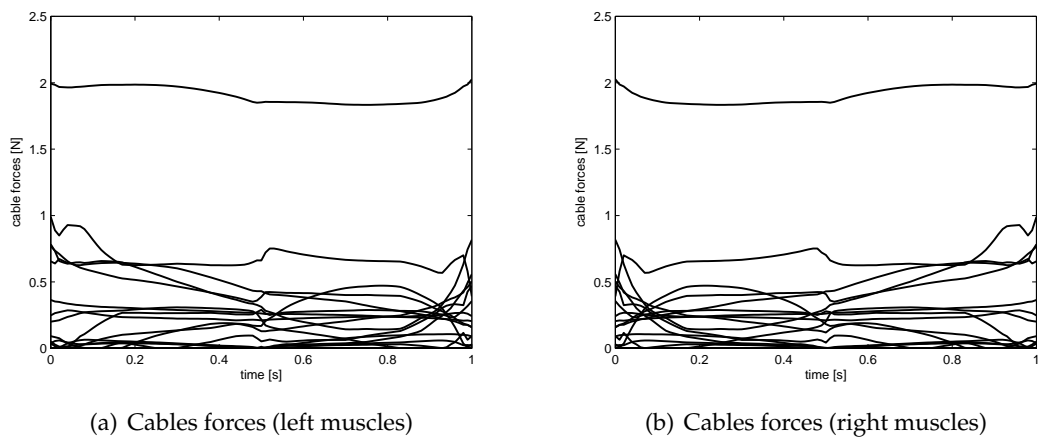


Figure 5.13: Cables force for the 8 link 8S manipulator performing yaw trajectory $\mathbf{q}_{yaw}(t)$. The left neck muscles and the right neck muscles are shown in (a) and (b), respectively.

sation can be performed on the generalised system. Since the Jacobian matrix formulation is independent of the number of links, type of joints and cable routing, analysis can be formulated and performed for the generalised system.

5.7 Conclusion

In this chapter, the generalised kinematic and dynamic models for MCDMs were formulated. The key characteristics of the generalised model are that it allows for arbitrary joint and branch kinematic structure, and arbitrary cable routing to be represented within a single formulation. The kinematic and dynamic models were formulated with respect to the branch structure matrix, generalised joint representations and the CRM introduced in Chapter 4. The Jacobian matrix was derived with respect to the CRM through the formulation of the system kinematics and equations of motion, and was shown to be consistent between both models. To demonstrate the versatility and advantages of the generalised system formulation, the kinematic and dynamic analyses were performed on two example MCDMs: a simple 2 link 4 DoF 6 cable system and a more complex 8 link 24 DoF 76 cable system. From the MCDM examples, it was observed that the generalised model allows complex anthropomorphically structured cable-driven manipulators to be studied. The kinematic and dynamic models for MCDMs allow further analysis, such as

workspace analysis, to be performed. Furthermore, the proposed generalised model allows analysis to be performed with respect to the single model, and changes to the rigid link structure or cable routing only require the abstracted representations, such as the joint model and the CRM, to be redefined.

Part II

Analysis of Anthropomorphic Cable-Driven Manipulators

Introduction to Part II

CABLE-DRIVEN parallel manipulators (CDPMs) can be regarded as anthropomorphic mechanisms due to their structural similarities with musculoskeletal systems, where the cables and rigid links are analogous to the muscles and bones, respectively. Parts I addressed aspects related to the modelling of multilink cable-driven manipulators (MCDMs).

As single link CDPMs are a specific case of MCDMs, analysis techniques for single link CDPMs may need to be extended for MCDMs. Chapter 6 investigates the necessary conditions required on the cable routing arrangement for wrench-closure to be achieved for MCDMs. By extending the necessary conditions from single link cable-driven manipulators to MCDMs, it is shown that the cable routing must also be considered for MCDMs. Furthermore, the analysis is performed with respect to the cable-routing matrix (CRM) and hence the generalised model. This allows for the ability to verify whether an MCDM is able to satisfy wrench-closure using the CRM.

In most previous studies of CDPMs, cables have been assumed to be *ideal force generators*, where their ability to produce force is fixed regardless of system state. However, one of the key characteristics of anthropomorphic musculoskeletal systems is that muscles behave as *state dependent force generators*, where their ability to actuate is dependent on their length and velocity. Due to the differences in actuation dynamics, workspace analysis has not been previously conducted for musculoskeletal systems. Chapter 7 introduces the Hill-type muscle model used for the analysis in this part. It is shown that if the system and hence the muscles are in static equilibrium, it is possible to determine whether a muscle is passive or active from the length of the muscle-tendon complex. Furthermore, the range of forces that can be produced by the muscle can also be determined.

Using the model of state dependent force generator, musculoskeletal static workspace analysis is formulated and performed in Chapter 8. The proposed formulation allows the static workspace for a musculoskeletal system to be computed. To demonstrate the formulation, the static workspace is generated for a human shoulder and compared to human benchmarks for the range of motion. From the results, it is demonstrated that the inclusion of physiological muscle characteristics is critical for producing a workspace

that is accurate compared to that of a human. The workspace analysis of musculoskeletal systems as CDPMs demonstrates that established analysis techniques for CDPMs can be extended to the study of musculoskeletal systems. As a result, the study of biomechanical systems can be enriched by the new computational tools, such as workspace analysis.

Chapter 6

Wrench-Closure Validity Analysis for Multilink Cable-Driven Manipulators

In this chapter, the necessary conditions on the cable routing to achieve wrench-closure for multilink cable-driven manipulators (MCDMs) are investigated. The wrench-closure condition (WCC) refers to the ability for the manipulator to sustain any external wrench, or produce any velocity and acceleration, by a set of positive cable forces. A manipulator is defined as wrench-closure valid if the WCC can be achieved in at least one pose, and can be regarded as a requirement in designing MCDMs. Using the generalised MCDM model formulated in Chapter 5, the necessary conditions for wrench-closure validity are described with respect to the cable-routing matrix (CRM) introduced in Chapter 4. As a result, it is shown that the routing of cables, independent of the exact attachment locations, are important in the design of MCDMs. Section 6.1 introduces the definition of wrench-closure and its significance in cable-driven parallel manipulators (CDPMs). In Section 6.2, necessary conditions on wrench-closure with respect to the elements of the Jacobian matrix are presented. The analysis is extended to conditions on the cable routing in Section 6.3, and it is shown that the necessary conditions can be expressed with respect to the CRM. Section 6.4 illustrates the proposed necessary conditions on several MCDM examples of different numbers of links. Finally, Section 6.5 concludes the chapter by summarising the contributions.

6.1 Introduction

The ability for a manipulator to achieve a particular workspace criterion, such as wrench-closure condition (WCC), is an important property that describes the feasibility of the motion of cable-driven parallel manipulators (CDPMs) and the attachment of the cables. At a particular manipulator pose, the WCC is defined as the ability for the CDPM to sustain any external wrench, or produce any velocity and acceleration, by a set of positive

cable forces. Mathematically, the WCC for an n degree-of-freedom (*DoF*) CDPM system at pose \mathbf{q} can be defined as

$$\forall \mathbf{w} \in \mathbb{R}^n, \exists \mathbf{f} > \mathbf{0} : \mathbf{w} = J^T(\mathbf{q})\mathbf{f}, \quad (6.1)$$

where $\mathbf{w} = -[M(\mathbf{q})\ddot{\mathbf{q}} + \mathbf{C}(\mathbf{q}, \dot{\mathbf{q}}) + \mathbf{G}(\mathbf{q}) + \boldsymbol{\Gamma}_{ext}]$ from (3.2). The geometrical interpretation of (6.1) is that the WCC is satisfied if the column vectors of J^T positively span \mathbb{R}^n , given that J^T is of full rank.

The wrench-closure workspace (WCW) represents the set of poses where the manipulator satisfies the WCC from (6.1) and can be defined as

$$WCW = \left\{ \mathbf{q} : \forall \mathbf{w} \in \mathbb{R}^n, \exists \mathbf{f} > \mathbf{0} : \mathbf{w} = J^T(\mathbf{q})\mathbf{f} \right\}. \quad (6.2)$$

Hence, the WCW represents the poses in which the manipulator is able to generate motion in any direction in the generalised coordinates space. As a result, the WCW has a wide range of uses in the design and analysis of CDPMs. For example, consider the generation of trajectories to be performed under the positive force constraint. Generating a continuous trajectory within the WCW ensures that the entire trajectory can be executed by positive cable forces. Furthermore, the volume of the WCW can give an indication on the versatility in the arrangement of the cable attachments to generate motion in different manipulator poses [68].

The WCW can be regarded as an important property of a CDPM and has been well studied due to its significance [31, 43, 47, 69, 73, 92, 108]. Typically, the WCW can be generated through either analytical or numerical approaches. By solving (6.2) analytically, the WCW region can be defined by a set of inequalities using the analytical expressions of the workspace boundaries. Analytical approaches provide a more accurate description of the workspace and insights into its geometry. The limitation of analytical approaches is that the workspace boundary must be solved individually for each type of CDPM. Furthermore, the form and complexity of the solution is dependent on the type of CDPM, and in some cases there may not exist a closed form solution. On the other hand, numerical methods are point-wise evaluation techniques where the condition in (6.1) is checked

for each point in the discretised search space. The advantage of this type of approach is its algorithmic simplicity, since the method can be generically applied to any type of CDPM. However, this approach provides only a local measure of the workspace at the evaluated points and hence suffers from the effects of discretisation. The computational time of numerical approaches increases significantly when the size of the search space is increased, for example, by decreasing the discretisation step-size or when the number of the manipulator degrees of freedom increases.

As a result, the WCW analysis for MCDMs is difficult due to the increased number of potential degrees of freedom. The ability for an MCDM to achieve wrench-closure is important in the design of CDPMs. However, it would be impractical to generate the WCW for every potential cable routing and attachment location during the design process of the manipulator. By defining a CDPM as being *wrench-closure valid* if the WCC can be achieved in at least some pose, then wrench-closure validity can be used as a basic requirement in designing MCDMs.

Necessary conditions on wrench-closure validity can be regarded as basic criteria in designing MCDMs that can achieve wrench-closure in at least one pose. Any cable arrangement that do not satisfy the necessary conditions will result in an empty WCW and can be regarded as having a very restricted range of motion. The validation of wrench-closure validity does not require the WCW to be generated, and hence is beneficial in rejecting invalid cable arrangements in a computationally efficient manner. Furthermore, the necessary conditions that are expressed independently of the exact cable attachment locations can form design requirements. For example, for a single body n DoF manipulator actuated by m cables, it was shown that a minimum of $m = n + 1$ cables is required to achieve wrench-closure validity [86, 133]. Verification of the sufficient conditions for the WCC would require knowledge of cable attachment locations and is dependent on the manipulator pose. The verification of both necessary and sufficient conditions for the wrench-closure of CDPMs is equivalent to validating WCC.

For MCDMs, in addition to requiring a minimum of $m = n + 1$ cables [91], it was shown that the distributions of cables (cable routing) must also be considered [111]. However, the analysis in [111] only considered single segment cable routings that began from

the base and ended at one of the manipulator links. For MCDMs allowing for arbitrary cable routing, the wrench-closure validity analysis is complicated by the large number of different cable routing types and the coupled cable actuation on the manipulator links. Using the cable-routing matrix (CRM) introduced in Chapter 4, necessary conditions on wrench-closure validity that are expressed with respect to the CRM therefore inherently considers arbitrary cable routing.

Necessary conditions on wrench-closure validity of MCDMs are extremely beneficial in determining suitable cable routing for this class of systems. Cable routings that do not satisfy the necessary conditions would result in a manipulator that cannot achieve wrench-closure, and can be rejected as a valid design and from further analysis. Hence the necessary conditions can be used as a preliminary check on the whether the cable routing is suitable for CDPMs.

6.2 Jacobian Matrix Analysis

In a similar manner as WCW analysis, wrench-closure validity analysis can be performed by studying the transpose of the Jacobian matrix J^T from (6.1). For single link CDPMs to achieve wrench-closure, $J^T \in \mathbb{R}^{n \times m}$ must be of full rank and contain more columns than rows due to the positive cable force constraint. Hence, one necessary condition for the wrench-closure validity of single link CDPMs is that a minimum of $m \geq n + 1$ cables is required to positively span \mathbb{R}^n . Hence, the wrench-closure validity for single link CDPMs can be mathematically expressed as

$$\exists \mathbf{q} : WCC(\mathbf{q}) \Rightarrow m \geq n + 1, \quad (6.3)$$

where $WCC(\mathbf{q})$ denotes that the WCC from (6.1) is satisfied in pose \mathbf{q} .

MCDMs differ from single link CDPM systems in that it is possible for cables to provide actuation forces to only a subset of the manipulator's links. Consider the situation that a cable does not contribute to the motion of a particular link. As introduced in Section 5.4, the vector term $J_{i\mathbf{q}_a}^T(\mathbf{q})$ from (5.23) within the matrix J^T represents the effect of the force of cable i onto the motion of link a in pose \mathbf{q} . Property 6.1 describes the physical

interpretation of zero elements in J^T .

Property 6.1. *If the force of cable i does not contribute to the generalised force of link a at pose \mathbf{q} then $J_{i\mathbf{q}_a}^T(\mathbf{q}) = \mathbf{0}$. Hence, if $J_{i\mathbf{q}_a}^T(\mathbf{q}) \neq \mathbf{0}$ then force in cable i contributes to the motion of link a at pose \mathbf{q} .*

Alternatively, a cable can be regarded as unusable in the actuation of a particular link if the cable is required in generating motion for another link.

Necessary conditions for the wrench-closure validity can be derived by considering and analysing a p link MCDM system as p individual subsystems. Wrench-closure validity is satisfied if and only if every link of the manipulator satisfies wrench-closure validity. Theorem 6.1 presents a trivial necessary condition on the minimum number of cables required for MCDMs to achieve wrench-closure validity, by extending the condition in (6.3) for single link CDPMs.

Theorem 6.1. *Each link of an MCDM requires a minimum number of $n_a + 1$ cables that can be used to actuate the link, where n_a denotes the number of degrees of freedom of link a relative to link $a - 1$. Hence, the wrench-closure validity for an MCDM system can be expressed as*

$$\exists \mathbf{q} : \text{WCC}(\mathbf{q}) \Rightarrow m_a(\mathbf{q}) \geq n_a + 1 \quad \forall a \in \{1, \dots, p\}, \quad (6.4)$$

where $m_a(\mathbf{q})$ refers to the number of cables that can be used to actuate link a in pose \mathbf{q} .

Proof. The definition of WCC from (6.1) for MCDMs requires that any wrench can be produced by every link simultaneously. Hence, if any of the links are unable to independently generate an arbitrary wrench, the WCC for the entire system cannot be satisfied at pose \mathbf{q} . Extending from the single link condition from (6.3), if any link has less than $n_a + 1$ cables that can actuate link a , then the manipulator cannot satisfy WCC

$$\exists \mathbf{q} \exists a : m_a(\mathbf{q}) < n_a + 1 \Rightarrow \neg \text{WCC}(\mathbf{q}). \quad (6.5)$$

The negation of (6.5) completes the proof for the minimum number of required cables to achieve the wrench-closure validity of MCDMs. \square

By the fact that the minimum number of cables required for a single link n DoF system is $n + 1$ [31, 69, 108], then if the system is actuated by $m \geq n + 1$ cables, the resulting redundancy is $m - n$. Property 6.2 extends this concept to each link for a multilink manipulator.

Property 6.2. *Given that the system satisfies the WCC from Theorem 6.1, the maximum redundancy for link a is $m_a - n_a$, where m_a is the number of cables that can be used to actuate link a .*

The number of cables that can actuate link a can be determined by analysing the generalised J^T from (5.22). From Theorem 6.1, necessary conditions on J^T for MCDMs to achieve wrench-closure validity can be expressed. At pose \mathbf{q} , the number of cables actuating link a can be expressed as

$$m_a(\mathbf{q}) = A_a(\mathbf{q}) + B_a(\mathbf{q}), \quad (6.6)$$

where:

1. $A_a(\mathbf{q})$ refers to the number of cables that produce a wrench on link a , but not on links $b > a$ at pose \mathbf{q} (Lemma 6.1).
2. $B_a(\mathbf{q})$ refers to the number of cables that produce a wrench on link a and on some link(s) $b > a$, but are not required in actuating links $b > a$ at pose \mathbf{q} (Lemma 6.2).

Physically, A_a represents the number of cables that produce motion on link a but not the ones above, and B_a represents the number of cables that produce force on link a and above, and can be used to actuate link a . Lemmas 6.1 and 6.2 present the mathematical definitions for A_a and B_a , respectively.

Lemma 6.1. $A_a(\mathbf{q}) = \sum_i \alpha_{ia}(\mathbf{q})$ represents the number of cables that produce a wrench on link a at pose \mathbf{q} , but not on links $b > a$, where

$$\alpha_{ia}(\mathbf{q}) = \begin{cases} 1 & , \quad J_{i\mathbf{q}_a}^T(\mathbf{q}) \neq \mathbf{0}, J_{i\mathbf{q}_b}^T(\mathbf{q}) = \mathbf{0} \forall b > a \\ 0 & , \quad \text{otherwise} \end{cases} . \quad (6.7)$$

Proof. The condition $\alpha_{ia}(\mathbf{q}) = 1$ from (6.7) can be directly obtained from Property 6.1. \square

Property 6.3. *Without loss of generality, it can be shown that $J_{i\mathbf{q}_a}^T(\mathbf{q}) \neq \mathbf{0}$ and $J_{i\mathbf{q}_b}^T(\mathbf{q}) \neq \mathbf{0}$, then $J_{i\mathbf{q}_c}^T(\mathbf{q}) \neq \mathbf{0}$ where $a < c < b$. That is, if cable i produces a resultant wrench on both joints a and b , then a resultant wrench is also produced on the joints of the links in between. The validity of this property will be shown in Property 6.4.*

Lemma 6.2. $B_a(\mathbf{q}) = \min \{\sum_i \beta_{ia}(\mathbf{q}), m_{a+1}(\mathbf{q}) - n_{a+1}\}$ represents the number of cables that produce a resultant wrench on link a and on some link(s) $b > a$, but are not required in actuating links $b > a$, where

$$\beta_{ia}(\mathbf{q}) = \begin{cases} 1 & , \quad J_{i\mathbf{q}_a}^T(\mathbf{q}) \neq \mathbf{0}, J_{i\mathbf{q}_{a+1}}^T(\mathbf{q}) \neq \mathbf{0} \\ 0 & , \quad \text{otherwise} \end{cases}, \quad (6.8)$$

with the boundary conditions $n_{p+1} = m_{p+1} = 0$ and $\beta_{ip}(\mathbf{q}) = 0 \forall \mathbf{q}$ can be arbitrarily assigned since $J_{i\mathbf{q}_{p+1}}^T(\mathbf{q})$ does not exist.

Proof. At the outermost link, $B_p(\mathbf{q}) = 0$ due to the fact that there exists no link $b > p$. For the remaining links $a < p$, $\sum_i \beta_{ia}(\mathbf{q})$ from (6.8) represents the number of cables that produce a resultant wrench on both links a and $a + 1$ in pose \mathbf{q} (Property 6.1).

The number of cables $B_a(\mathbf{q})$ must also consider the fact that some cables may be required to actuate link $a + 1$. From Property 6.2, the maximum number of redundant cables that can be inherited from link $a + 1$ is $m_{a+1}(\mathbf{q}) - n_{a+1}$. From Property 6.3, since cable forces produce wrench over consecutive joints, $m_{a+1}(\mathbf{q}) - n_{a+1}$ not only represents the number of redundant cables from link $a + 1$, but also from links $b \geq a + 1$. Considering maximum number of redundant cables from links $b \geq a + 1$, the number of cables $B_a(\mathbf{q})$ can be expressed as $\sum_i \beta_{ia}(\mathbf{q})$ and cannot exceed $m_{a+1}(\mathbf{q}) - n_{a+1}$, resulting in $B_a(\mathbf{q}) = \min \{\sum_i \beta_{ia}(\mathbf{q}), m_{a+1}(\mathbf{q}) - n_{a+1}\}$. \square

From Lemma 6.1, Lemma 6.2 and (6.6), the condition (6.4) from Theorem 6.1 can be expressed as

$$\exists \mathbf{q} : \text{WCC}(\mathbf{q}) \Rightarrow A_a(\mathbf{q}) + B_a(\mathbf{q}) \geq n_a + 1 \quad \forall a. \quad (6.9)$$

The necessary condition (6.9) for the WCC at a particular pose can be evaluated from the

terms of the J^T matrix. It should be noted that the necessary condition is dependent on both the manipulator pose and cable attachment locations, and requires the determination of J^T at \mathbf{q} .

Although the necessary conditions do not describe the exact WCW of cable-driven manipulators, they can be highly useful in the initial design process for the arrangement of cables for MCDMs. For example, these conditions allow the cable routing of MCDMs that are unable to satisfy the WCC in any pose (wrench-closure invalid) to be identified and rejected. By expressing the necessary conditions with respect to the cable routing that are independent of the exact attachment locations, the cable routings that satisfy wrench-closure validity can be first identified prior to designing the attachment locations.

6.3 Necessary Conditions on the Cable-Routing Matrix

Formulating the necessary conditions with respect to the CRM, the conditions can be expressed independent of the exact attachment locations. It was shown in Section 6.2 that necessary conditions can be formulated with respect to whether the vector terms $J_{i\mathbf{q}_a}^T(\mathbf{q})$ within the Jacobian matrix are zero or non-zero. Section 6.3.1 presents the relationship between the CRM terms and the Jacobian matrix terms. Using this relationship, the necessary conditions for wrench-closure validity with respect the CRM are derived in Section 6.3.2.

6.3.1 Relationship With the Jacobian Matrix

In the generalised MCDM model formulated in Chapter 5, it was shown that the Jacobian matrix is expressed with respect to the CRM. From this relationship, it can be shown for MCDMs that whether the Jacobian matrix terms $J_{i\mathbf{q}_a}(\mathbf{q})$ are zero or non-zero is also dependent on the cable routing. Theorem 6.2 presents the necessary condition for the Jacobian matrix terms to be zero vectors.

Theorem 6.2. $\sum_{k=a}^p c_{ij(k+1)} = 0 \forall j \Leftrightarrow J_{i\mathbf{q}_a}^T(\mathbf{q}) = \mathbf{0} \forall \mathbf{q}$. *Cable i has no effect on the motion of link a for all manipulator poses and cable attachment locations if and only if all segments of cable i begin and end on, or are not attached to, links a or above.*

Proof. From (5.11), the relationship between $V_{i\mathbf{x}_k}^T$ and $V_{i\theta_k}^T$ can be expressed as $V_{i\theta_k}^T = \mathbf{r}_{G_k A_{ijk}} \times V_{i\mathbf{x}_k}^T$. Substituting the definition of $V_{i\mathbf{x}_k}^T$ from (5.11), $W_{a\mathbf{x}_k}^T$ and $W_{a\theta_k}^T$ from (5.21), into (5.23) results in

$$\begin{aligned} J_{i\mathbf{q}_a}^T(\mathbf{q}) &= \sum_{k=a}^p \left[W_{a\mathbf{x}_k}^T V_{i\mathbf{x}_k}^T + W_{a\theta_k}^T \left[\mathbf{r}_{G_k A_{ijk}} \right]^\times V_{i\mathbf{x}_k}^T \right] \\ &= \sum_{k=a}^p \left[S_a^T \left[\begin{array}{c} {}_k^a R \\ \left[\mathbf{r}_{P_a A_{ijk}} \right]^\times {}_k^a R \end{array} \right] V_{i\mathbf{x}_k}^T \right] \\ &= S_a^T \sum_{k=a}^p \sum_{j=1}^s \left[\left[\begin{array}{c} I_{3 \times 3} \\ \left[\mathbf{r}_{P_a A_{ijk}} \right]^\times \end{array} \right] c_{ij(k+1)} \hat{\mathbf{l}}_{ij} \right], \end{aligned} \quad (6.10)$$

where p and s represent the number of links of the system and the maximum number of segments for a cable, respectively. Substituting the definition of the cable segment vector from (4.8) into (6.10) results in

$$J_{i\mathbf{q}_a}^T(\mathbf{q}) = S_a^T \sum_{j=1}^s \sum_{k=a}^p \sum_{b=0}^p \left[\left[\begin{array}{c} I_{3 \times 3} \\ \left[\mathbf{r}_{P_a A_{ijk}} \right]^\times \end{array} \right] \frac{c_{ij(k+1)} c_{ij(b+1)} \mathbf{r}_{OA_{ijb}}(\mathbf{q})}{l_{ij}} \right]. \quad (6.11)$$

From (6.11), the statement $J_{i\mathbf{q}_a}^T(\mathbf{q}) = \mathbf{0}$ for any pose \mathbf{q} is true if

$$J_{ia_j}^T(\mathbf{q}) = \mathbf{0} \quad \forall j \quad \forall \mathbf{q} \Leftrightarrow J_{i\mathbf{q}_a}^T(\mathbf{q}) = \mathbf{0} \quad \forall \mathbf{q}, \quad (6.12)$$

where

$$J_{ia_j}^T(\mathbf{q}) = \sum_{k=a}^p \sum_{b=0}^p \left[\left[\begin{array}{c} I_{3 \times 3} \\ \left[\mathbf{r}_{P_a A_{ijk}} \right]^\times \end{array} \right] c_{ij(k+1)} c_{ij(b+1)} \mathbf{r}_{OA_{ijb}}(\mathbf{q}) \right]. \quad (6.13)$$

The conditions for $J_{ia_j}^T(\mathbf{q}) = \mathbf{0} \quad \forall j \quad \forall \mathbf{q}$ in (6.12) can be expressed with respect to the CRM terms for the cable segments $j \leq s_i$ and $j > s_i$, and are described in Conditions 6.1 and 6.2, respectively. The number of segments for cable i is denoted by s_i .

Condition 6.1. For cable segments $j > s_i$, $J_{ia_j}^T(\mathbf{q}) = \mathbf{0} \quad \forall \mathbf{q}$, $\forall j > s_i$ is true by Property 4.4 since $c_{ijk} = 0 \quad \forall j > s_i$.

Condition 6.2. For segments $j \leq s_i$, $J_{ia_j}^T(\mathbf{q}) = \mathbf{0} \quad \forall \mathbf{q}$ is true if and only if the beginning and

ending attachments for segment j are both below or both on and above link a .

For segments $j \leq s_i$, Properties 4.2 and 4.3 state that each segment must have exactly one beginning attachment and one ending attachment. Assuming that segment j of cable i begins on link x and ends on link y , then $c_{ij(x+1)} = -1$, $c_{ij(y+1)} = 1$ and $c_{ij(k+1)} = 0 \forall k \neq x, y$. Consider the following scenarios for links x and y :

- $x, y < a$: both beginning and ending attachments are below link a , hence $c_{ij(k+1)} = 0 \forall k \geq a$, resulting in $J_{ia_j}^T(\mathbf{q}) = \mathbf{0} \forall \mathbf{q}$.
- $x, y \geq a$: both beginning and ending attachments are on link a or above, substituting $c_{ij(x+1)} = -1$ and $c_{ij(y+1)} = 1$ into (6.13), then $J_{ia_j}^T = \mathbf{0} \forall \mathbf{q}$ is always true.
- $x < a, y \geq a$ or $x \geq a, y < a$: one of the attachments is below link a and the other is on or above link a , it can be observed that there would always exist some \mathbf{q} such that $J_{ia_j}^T(\mathbf{q}) \neq \mathbf{0}$ in general. For example, if $x < a, y \geq a$ then

$$J_{ia_j}^T(\mathbf{q}) = \begin{bmatrix} I_{3 \times 3} \\ \left[\mathbf{r}_{P_a A_{ijy}} \right]^\times \end{bmatrix} (\mathbf{r}_{OA_{ijy}}(\mathbf{q}) - \mathbf{r}_{OA_{ijx}}(\mathbf{q})).$$

It can be observed that Conditions 6.1 and 6.2 are satisfied for $\sum_{k=a}^p c_{ij(k+1)} = 0$, and hence

$$\sum_{k=a}^p c_{ij(k+1)} = 0 \Leftrightarrow J_{ia_j}^T(\mathbf{q}) = \mathbf{0} \forall \mathbf{q}. \quad (6.14)$$

Combining (6.14) and (6.12) results in $\sum_{k=a}^p c_{ij(k+1)} = 0 \forall j \Leftrightarrow J_{ia}^T(\mathbf{q}) = \mathbf{0} \forall \mathbf{q}$ to complete the proof. \square

The physical interpretation of $\sum_{k=a}^p c_{ij(k+1)} = 0 \forall j$ is that all segments of cable i are either not attached to, or both begin and end on link a and above. When a cable begins and ends above link a , the equal and opposite forces on both ends of the cable produce a zero resultant wrench on link a . On the other hand, if $\exists j : \sum_{k=a}^p c_{ij(k+1)} \neq 0$, then there is some segment of cable i where one of its end is attached to link a or above and the other end is attached to a link below link a . In such a scenario, then cable i has the potential to produce a resultant wrench on the motion of link a .

Since from Property 4.5 consecutive segments of a cable must be connected, the condi-

tion $\exists j : \sum_{k=a}^p c_{ij(k+1)} \neq 0$ applies to all links between links k_l and k_u , where k_l and k_u refer to the lowest and highest link number that the cable is attached to, respectively. Property 6.4 describes the set of links in which Theorem 6.2 holds for any particular cable.

Property 6.4. Denoting the lowest and highest link number that cable i is attached to as k_l and k_u , respectively, then $\exists j : \sum_{k=a}^p c_{ij(k+1)} \neq 0$ holds for links $k_l < a \leq k_u$ and $\sum_{k=a}^p c_{ij(k+1)} = 0 \forall j$ for links $a \leq k_l$ and $a > k_u$.

Figure 6.1 shows a 5 link MCDM with an example cable to demonstrate Property 6.4.

The CRM for cable i can be described as

$$C_i = \begin{bmatrix} 0 & -1 & 0 & 1 & 0 & 0 \\ 0 & 0 & 0 & -1 & 1 & 0 \\ 0 & 0 & 0 & 0 & 0 & 0 \\ \vdots & & & & & \vdots \\ 0 & 0 & 0 & 0 & 0 & 0 \end{bmatrix}.$$

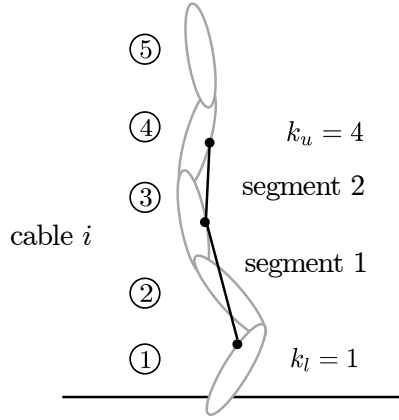


Figure 6.1: 5 link MCDM example to demonstrate Property 6.4. The cable routing for cable i can be described as link 1 → link 3 → link 4. The lowest and highest link numbers for cable i are $k_l = 1$ and $k_u = 4$, respectively.

From Figure 6.1, it can be observed that the lowest link number for cable i is $k_l = 1$ and the highest link number is $k_u = 4$. For link 1, the value $\sum_{k=1}^5 c_{ij(k+1)} = 0 \forall j$ for all segments represent that link $a = 1$ is either $a \leq k_l$ or $a > k_u$. However, for link 2 it can be observed that $\sum_{k=2}^5 c_{ij(k+1)} = 1, j = 1$ since link $a = 2$ satisfies $k_l < a \leq k_u$. Furthermore, it

can be observed that segment 1 of cable i has the potential to produce a resultant wrench on link 2. Similarly, for link $a = 3$, $\sum_{k=3}^5 c_{ij(k+1)} = 1, j = 1$ satisfies $k_l < a \leq k_u$. For link $a = 4$, $\sum_{k=4}^5 c_{ij(k+1)} = 1, j = 2$ satisfies $k_l < a \leq k_u$, and suggests that segment 2 of cable i has the potential to produce a resultant wrench on link 4. Finally, link $a = 5$ satisfies both $a > k_u$ and $\sum_{k=5}^5 c_{ij(k+1)} = 0 \forall j$. The presented example shows that from Property 6.4, the lowest and highest links that a particular cable is attached to can be determined from $\sum_{k=a}^p c_{ij(k+1)}$ for each of the links and cable segments.

6.3.2 Cable-Routing Matrix Terms

From the relationship between the CRM and Jacobian matrix terms introduced in Section 6.3.1, necessary conditions on the CRM to achieve wrench-closure validity can be derived in a similar manner to the analysis performed in Section 6.2. From Property 6.4 and Theorem 6.2, Definitions 6.1 and 6.2 present analogous terms to those introduced in Lemmas 6.1 and 6.2, respectively, but are expressed with respect to the CRM.

Definition 6.1. $\sum_i \alpha_{ia}^*$ represents the number of cables that are attached to link a and link a is the highest link number to which cable i is attached to, where

$$\alpha_{ia}^* = \begin{cases} 1 & , \quad \exists j : \sum_{k=a}^p c_{ij(k+1)} \neq 0, \sum_{k=a+1}^p c_{ij(k+1)} = 0 \forall j \\ 0 & , \quad \text{otherwise} \end{cases} . \quad (6.15)$$

From Property 6.4, $\exists j : \sum_{k=a}^p c_{ij(k+1)} \neq 0$ and $\sum_{k=a+1}^p c_{ij(k+1)} = 0 \forall j$ imply that $a = k_u$ for cable number i .

Definition 6.2. $\sum_i \beta_{ia}^*$ represents the number of cables where some segments are connected to links both above and below link a , where

$$\beta_{ia}^* = \begin{cases} 1 & , \quad \exists j : \sum_{k=a}^p c_{ij(k+1)} \neq 0, \exists j : \sum_{k=a+1}^p c_{ij(k+1)} \neq 0 \\ 0 & , \quad \text{otherwise} \end{cases} , \quad (6.16)$$

with the boundary condition $\beta_{ip}^* = 0$ since at $a = p$, $c_{ij(p+2)}$ does not exist.

Definitions 6.1 and 6.2 allow necessary conditions on wrench-closure validity to be expressed in a similar manner to (6.9). The resulting conditions are described with respect to the CRM and are independent of manipulator pose and attachment locations. It is important to note that these criteria represent only the necessary, but not sufficient, conditions on the wrench-closure validity of MCDMs. Verifying the sufficient conditions for the WCC require the knowledge of cable attachment locations and is dependent on the manipulator pose.

In the same manner as Section 6.2, the number of cables m_a^* that have the potential to actuate joint a consists of:

- Cables that are connected to link a , where link a is the highest numbered link to which the cable is attached to.
- Cables that are connected to links both above and below link a .

Lemma 6.3 introduces the number of cables m_a^* that have the potential to actuate link a based from the CRM.

Lemma 6.3.

$$m_a^* = \sum_i \alpha_{ia}^* + \min \left\{ \sum_i \beta_{ia}^*, m_{a+1}^* - n_{a+1} \right\}, \quad (6.17)$$

with the boundary conditions $m_{p+1}^* = n_{p+1} = 0$.

Proof. The negation of Theorem 6.2 suggests that cable i has an effect on joint a if and only if the condition $\exists j : \sum_{k=a}^p c_{ij(k+1)} \neq 0$ is true, where

$$\exists \mathbf{q} : J_{i\mathbf{q}_a}^T(\mathbf{q}) \neq \mathbf{0} \Leftrightarrow \exists j : \sum_{k=a}^p c_{ij(k+1)} \neq 0. \quad (6.18)$$

Hence Definitions 6.1 and 6.2 not only provide knowledge on how cables are attached to link a , but also whether the cables have the potential to actuate link a .

Firstly, since $\sum_i \alpha_{ia}^*$ cables are attached to link a but not to the links above a , all of these cables can be potentially used to actuate joint a . However, from the number of cables $\sum_i \beta_{ia}^*$ that are attached to both links a and $a + 1$, it is possible that only a subset of the cables can be used to actuate joint a as they may be required to actuate joint $a + 1$ or above. From Property 6.2, the maximum number of redundant cables from link $a + 1$ is hence

$m_{a+1}^* - n_{a+1}$. In a similar manner to Lemma 6.2, the number of redundant cables that can actuate link a is hence $\min \{\sum_i \beta_{ia}^*, m_{a+1}^* - n_{a+1}\}$. From Property 6.4, since $\beta_{ia}^* = 1$ applies to links k_l to $k_u - 1$, m_a^* represents the number of redundant cables from links $b > a$. \square

Theorem 6.3 represents the relationship between m_a introduced in Section 6.2 and m_a^* from (6.17). The theorem states that the number of cables that have the potential to actuate link a as observed from the cable routing must be greater than the number of cables that actually produces a resultant wrench on link a . Using Theorem 6.3, the necessary conditions on WCC in some pose \mathbf{q} from (6.9) can then be extended to the necessary conditions on wrench-closure validity expressed with respect to the CRM. The following properties and lemmas that relate the terms α_{ia} and β_{ia} to α_{ia}^* and β_{ia}^* will be required in proving Theorem 6.3.

Property 6.5. *From the definitions of α_{ia} and β_{ia} presented in Lemmas 6.1 and 6.2, respectively, it is not possible for $\alpha_{ia}(\mathbf{q}) = 1$ and $\beta_{ia}(\mathbf{q}) = 1$ simultaneously. Mathematically, this can be expressed as*

$$\alpha_{ia}(\mathbf{q}) = 1 \Rightarrow \beta_{ia}(\mathbf{q}) = 0 \text{ and } \beta_{ia}(\mathbf{q}) = 1 \Rightarrow \alpha_{ia}(\mathbf{q}) = 0. \quad (6.19)$$

Similarly, from Definitions 6.1 and 6.2, it is not possible for $\alpha_{ia}^* = 1$ and $\beta_{ia}^* = 1$ simultaneously. Hence, this can be expressed as

$$\alpha_{ia}^* = 1 \Rightarrow \beta_{ia}^* = 0 \text{ and } \beta_{ia}^* = 1 \Rightarrow \alpha_{ia}^* = 0. \quad (6.20)$$

However, note that it is possible for both $\alpha_{ia}(\mathbf{q}) = 0$ and $\beta_{ia}(\mathbf{q}) = 0$ simultaneously. Similarly, it is possible for $\alpha_{ia}^* = 0$ and $\beta_{ia}^* = 0$ simultaneously.

Lemma 6.4. $\exists \mathbf{q} : \alpha_{ia}(\mathbf{q}) + \beta_{ia}(\mathbf{q}) = 1 \Leftrightarrow \alpha_{ia}^* + \beta_{ia}^* = 1$. If there exists some pose such that cable i produces a wrench on link a then it implies that there is some segment of cable i where one end is attached onto link a and above, and the other end is attached to some link below link a .

Proof. Properties 6.3 and 6.4 state that resultant wrenches are produced on consecutive links. Furthermore, since it is not possible for $\alpha_{ia}(\mathbf{q}) = 1$ and $\beta_{ia}(\mathbf{q}) = 1$ simultaneously

(Property 6.5), then by the definitions of α_{ia} and β_{ia} in (6.7) and (6.8), respectively,

$$\alpha_{ia}(\mathbf{q}) + \beta_{ia}(\mathbf{q}) = 1 \Leftrightarrow J_{i\mathbf{q}_a}^T(\mathbf{q}) \neq \mathbf{0}. \quad (6.21)$$

Similarly, by using the definitions of α_{ia}^* and β_{ia}^* in (6.15) and (6.16), respectively,

$$\alpha_{ia}^* + \beta_{ia}^* = 1 \Leftrightarrow \exists j : \sum_{k=a}^p c_{ij(k+1)} \neq 0. \quad (6.22)$$

Combining the relationships (6.21) and (6.22) with the implication in (6.18) completes the proof. \square

Property 6.6. $\alpha_{ia}(\mathbf{q}) = 1 \Rightarrow \alpha_{ib}(\mathbf{q}) = 0 \forall b > a$. By the definition of $\alpha_{ia}(\mathbf{q})$ from (6.7), if $\alpha_{ia}(\mathbf{q}) = 1$ then $J_{i\mathbf{q}_b}^T = \mathbf{0} \forall b > a$ and hence $\alpha_{ib}(\mathbf{q}) = 0$.

Property 6.7. $\alpha_{ia}(\mathbf{q}) = 1 \Rightarrow \beta_{ib}(\mathbf{q}) = 0 \forall b > a$. By the definition of $\alpha_{ia}(\mathbf{q})$ from (6.7), if $\alpha_{ia}(\mathbf{q}) = 1$ then $J_{i\mathbf{q}_b}^T = \mathbf{0} \forall b > a$ and hence $\beta_{ib}(\mathbf{q}) = 0$.

Lemma 6.5. $\exists \mathbf{q} : \alpha_{ia}(\mathbf{q}) = 1 \Rightarrow \exists k_u \geq a : \alpha_{ik_u}^* = 1, \beta_{ib}^* = 1, a \leq b < k_u$. If $\exists \mathbf{q} : \alpha_{ia}(\mathbf{q}) = 1$ then it implies that cable i is attached to some link(s) below link a and also to link a or above. Note that link k_u denotes the highest link number that cable i is attached to.

Proof. By definition $\alpha_{ia}(\mathbf{q})$ from (6.7), if $\exists \mathbf{q} : \alpha_{ia}(\mathbf{q}) = 1$ then it implies that $\exists \mathbf{q} : J_{i\mathbf{q}_a}^T(\mathbf{q}) \neq \mathbf{0}$. Hence by (6.18) and (6.22), the implication can be expressed as $\exists \mathbf{q} : \alpha_{ia}(\mathbf{q}) = 1 \Rightarrow \alpha_{ia}^* + \beta_{ia}^* = 1$. By Property 6.4, $\beta_{ib}^* = 1$ holds for links for consecutive links from $a \leq b < k_u$ and $\alpha_{ik_u}^* = 1$, where k_u is the highest link number that cable i is attached to. \square

Theorem 6.3.

$$\exists \mathbf{q} \forall a : m_a(\mathbf{q}) = L_a \Rightarrow m_a^* \geq L_a \quad (6.23)$$

If in any pose the number of cables m_a from (6.6) that can be used to actuate link a is L_a , that is, $m_a = L_a$, then it implies that the number of cables m_a^* from (6.17) determined based on the cable routing and the CRM must be greater than or equal to L_a .

Proof. For link a , m_a from (6.6) and m_a^* from (6.17) can be expressed as

$$\begin{aligned} m_a(\mathbf{q}) &= \min \left\{ \sum_i [\alpha_{ia}(\mathbf{q}) + \beta_{ia}(\mathbf{q})], \sum_i [\alpha_{ia}(\mathbf{q})] + m_{a+1}(\mathbf{q}) - n_{a+1} \right\} \\ m_a^* &= \min \left\{ \sum_i [\alpha_{ia}^* + \beta_{ia}^*], \sum_i [\alpha_{ia}^*] + m_{a+1}^* - n_{a+1} \right\}. \end{aligned} \quad (6.24)$$

From (6.24), it can be observed that the implication (6.23) is satisfied if both of the following statements are true

$$\exists \mathbf{q} \forall a : \sum_i [\alpha_{ia}(\mathbf{q}) + \beta_{ia}(\mathbf{q})] = X \Rightarrow \sum_i [\alpha_{ia}^* + \beta_{ia}^*] \geq X \quad (6.25)$$

$$\exists \mathbf{q} \forall a : \sum_i [\alpha_{ia}(\mathbf{q})] + m_{a+1}(\mathbf{q}) = Y \Rightarrow \sum_i [\alpha_{ia}^*] + m_{a+1}^* \geq Y \quad (6.26)$$

The implication (6.25) is true as a direct result from Lemma 6.4 since if there exists a pose \mathbf{q} that $\alpha_{ia}(\mathbf{q}) + \beta_{ia}(\mathbf{q}) = 1$ then $\alpha_{ia}^* + \beta_{ia}^* = 1$ is also true.

By Property 6.6, Property 6.7 and Lemma 6.5, $\exists \mathbf{q} : \alpha_{ia}(\mathbf{q}) = 1$ implies that $\alpha_{ib}(\mathbf{q}) = \beta_{ib}(\mathbf{q}) = 0$ for links $b > a$ and $\alpha_{ib}^* + \beta_{ib}^* = 1$ for links $a \leq b \leq k_u$, where k_u is the highest link number that cable i is attached to. Hence by the definition of m_{a+1} and m_{a+1}^* , it can be observed that (6.26) is also true for all links. \square

From Theorem 6.3, the *necessary condition* for the WCC from (6.4) can be expressed as

$$\exists \mathbf{q} : \text{WCC}(\mathbf{q}) \Rightarrow m_a^* \geq n_a + 1 \forall a. \quad (6.27)$$

The interpretation of (6.27) is that if there exists some pose in which the WCC is satisfied for an MCDM, then it is necessary that $m_a^* \geq n_a + 1 \forall a$.

The necessary condition from (6.27) has two important characteristics. Firstly, it only provides a necessary condition for the wrench-closure validity of MCDMs expressed with respect to the CRM and hence cable routing. Secondly, it is independent of manipulator pose and attachment locations of the cables. Since (6.27) is a necessary but not sufficient condition, it only provides knowledge on whether a particular cable routing can result

in a design that satisfies wrench-closure validity prior to determining the exact cable attachment locations.

6.4 Analysis of Example Manipulators

To demonstrate the necessary condition on wrench-closure validity that was derived in Section 6.3, analysis is performed on several MCDM examples in this section. In Section 6.4.1, the necessary condition for a single link n DoF CDPM is derived from the CRM, and is shown to be consistent with previous studies that a minimum of $m > n + 1$ cables is required for wrench-closure validity [86]. In Section 6.4.2, the wrench-closure validity is studied for two link MCDMs of various types of joints and degrees of freedom. Furthermore, examples of cable routing that violate the necessary conditions and hence do not satisfy wrench-closure validity are also presented. Section 6.4.3 illustrates the necessary conditions for three link MCDMs.

6.4.1 Single Link Manipulators

As shown in the single CDPM examples in Sections 3.3.1 and 3.3.2, the cables for single link CDPMs route from the base (link 0) to the end-effector (link 1). As a result, the CRM for every cable can be expressed as $C_i = [-1 \ 1] \ \forall i$. By the definition of m_a^* in (6.17), the number of effective cables that have the potential to actuate the manipulator can be expressed as

$$m_1^* = \sum_i \alpha_{i1}^*, \quad (6.28)$$

where

$$\alpha_{i1}^* = \begin{cases} 1 & , \ c_{i12} \neq 0 \\ 0 & , \ \text{otherwise} \end{cases} .$$

For single link CDPMs, $\alpha_{i1}^* = 1 \ \forall i$ since the CRM for all cables are identical and $c_{i12} = 1 \ \forall i$. From (6.28), it can be concluded that $m_1^* = m$, where m is the number of cables for the system. As a result, the necessary condition for n DoF single link MCDMs using (6.27) is $m \geq n + 1$. This necessary condition is consistent with that well established from

previously studies of CDPMs [31, 43, 47, 69, 73, 86, 92, 108, 133].

6.4.2 Two Link Manipulators

In this section, the necessary conditions are demonstrated for two link MCDMs. Denoting $n = n_1 + n_2$ as the number of degrees of freedom for the two link manipulator, n_1 represents the number of degrees of freedom between link 1 and the base, and subsequently n_2 represents the number of degrees of freedom between link 2 and link 1. The number of cables m_1^* and m_2^* that have the potential to actuate link 1 and link 2, respectively, can be determined by (6.17) and expressed as

$$\begin{aligned} m_2^* &= \sum_i \alpha_{i2}^*, \\ m_1^* &= \sum_i \alpha_{i1}^* + \min \left\{ \sum_i \beta_{i1}^*, m_2^* - n_2 \right\}, \end{aligned} \quad (6.29)$$

where

$$\begin{aligned} \alpha_{i1}^* &= \begin{cases} 1 & , \exists j : c_{ij2} \neq 0, c_{ij3} = 0 \forall j \\ 0 & , \text{otherwise} \end{cases} \\ \beta_{i1}^* &= \begin{cases} 1 & , \exists j : c_{ij2} + c_{ij3} \neq 0, \exists j : c_{ij3} \neq 0 \\ 0 & , \text{otherwise} \end{cases} \\ \alpha_{i2}^* &= \begin{cases} 1 & , \exists j : c_{ij3} \neq 0 \\ 0 & , \text{otherwise} \end{cases}. \end{aligned} \quad (6.30)$$

First, consider three types of class 1 cable routings for two link manipulators that were introduced in Figure 4.1 of Section 4.1, as shown in Figure 6.2. As presented in Section 4.3.1, the CRMs for the three types of cable routing can be expressed as

$$C_1 = \begin{bmatrix} -1 & 1 & 0 \\ 0 & 0 & 0 \end{bmatrix}, C_2 = \begin{bmatrix} -1 & 0 & 1 \\ 0 & 0 & 0 \end{bmatrix}, C_3 = \begin{bmatrix} 0 & -1 & 1 \\ 0 & 0 & 0 \end{bmatrix}.$$

Firstly, applying the cable-routing matrix C_1 for Figure 4.1(a) in (6.30) results in $\alpha_{11}^* = 1, \beta_{11}^* = 0, \alpha_{12}^* = 0$. The physical interpretation of these terms is that cable 1 has the poten-

tial to produce motion for link 1 only since $\alpha_{11}^* = 1 \Rightarrow \exists \mathbf{q} : J_{1\mathbf{q}_1}^T(\mathbf{q}) \neq \mathbf{0}, \forall \mathbf{q} J_{1\mathbf{q}_2}^T(\mathbf{q}) = \mathbf{0}$. Furthermore, $\alpha_{12}^* = 0$ implies that cable 1 produces no wrench on the motion of link 2 and hence no forces can propagate from link 2 to link 1 ($\beta_{11}^* = 0$). These observations are consistent with the cable routing as cable 1 is attached from the base to link 1, and is not connected to link 2.

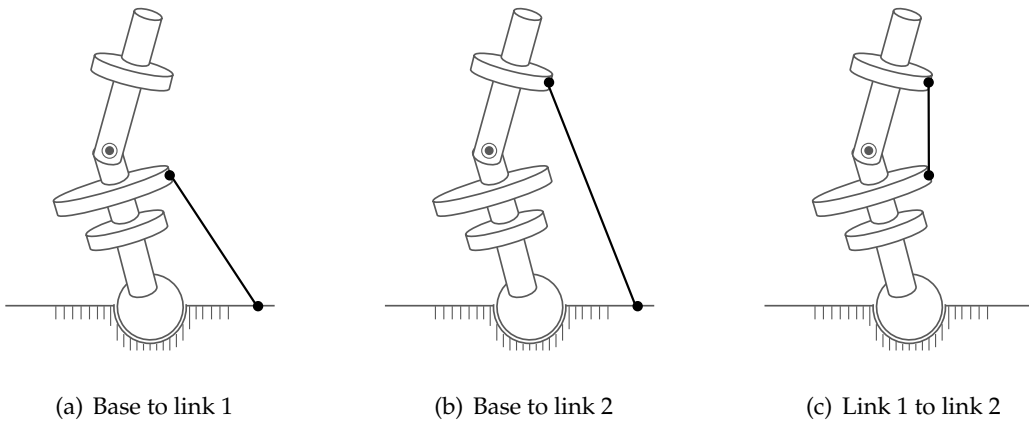


Figure 6.2: The types of class 1 cable routing for the wrench-closure validity analysis of 2 link CDPMs.

In a similar manner, the routing of cable 2 from Figure 4.1(b) results in $\alpha_{21}^* = 0, \beta_{21}^* = 1, \alpha_{22}^* = 1$. This physically corresponds to cable 2 having the potential to actuate both links 1 and 2. Finally, the cable routing from Figure 4.1(c) results in $\alpha_{31}^* = 0, \beta_{31}^* = 0, \alpha_{32}^* = 1$. The physical interpretation of this is that cable 3 has the potential to produce motion on link 2, while the cable produces no resultant wrench on the joint of link 1. From the three examples of single segment cable routings, it is demonstrated that the terms (6.15) and (6.16) indicate whether a type of cable routing has the potential to actuate particular links of the MCDM system.

In a similar manner to the class 1 cable routings, consider the three types of class 2 cable routings that were introduced in Figure 4.2 of Section 4.1, as shown in Figure 6.3. The CRMs of the class 2 cable routings introduced in Section 4.3.1

$$C_4 = \begin{bmatrix} -1 & 1 & 0 \\ 0 & -1 & 1 \end{bmatrix}, \quad C_5 = \begin{bmatrix} -1 & 0 & 1 \\ 0 & 1 & -1 \end{bmatrix}, \quad C_6 = \begin{bmatrix} 1 & -1 & 0 \\ -1 & 0 & 1 \end{bmatrix},$$

Routing type	Class	Description	α_{i1}^*	β_{i1}^*	α_{i2}^*
1	1	base \rightarrow link 1	1	0	0
2	1	base \rightarrow link 2	0	1	1
3	1	link 1 \rightarrow link 2	0	0	1
4	2	base \rightarrow link 1 \rightarrow link 2	0	1	1
5	2	base \rightarrow link 2 \rightarrow link 1	0	1	1
6	2	link 1 \rightarrow base \rightarrow link 2	0	1	1

Table 6.1: The analysis of cable routing for wrench-closure validity for two link MCDMs.

result in $\alpha_{i1}^* = 0, \beta_{i1}^* = 1, \alpha_{i2}^* = 1$ for all class 2 cable routings. The physical interpretation of this is that the cable routings with the CRMs C_4, C_5 and C_6 have the potential to produce a resultant wrench on both link 1 and link 2, and hence can contribute to satisfying the WCC for either link 1 or link 2. Furthermore, cables with more than two segments and that are connected to every link of the MCDM also result in $\alpha_{i1}^* = 0, \beta_{i1}^* = 1, \alpha_{i2}^* = 1$. Table 6.1 summarises the classifications of the 6 types of class 1 and class 2 cable routings for the analysis of wrench-closure validity.

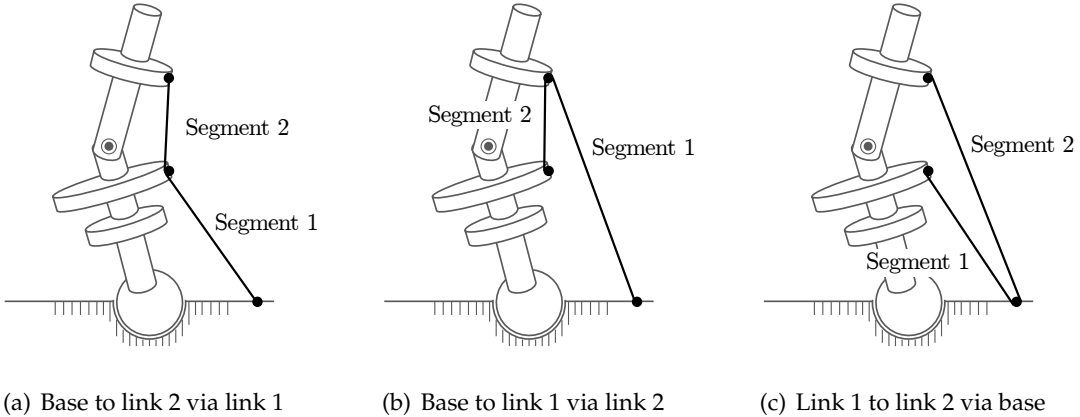


Figure 6.3: The types of class 2 cable routing for the wrench-closure validity analysis of 2 link CDPMs.

The classifications of the cable routing and the values $\alpha_{i1}^*, \beta_{i1}^*$ and α_{i2}^* allow the necessary conditions on the cable routing to satisfy wrench-closure validity to be analysed. For example, consider the 4 DoF 2 link manipulator shown in Figure 5.6 that was studied

in Section 5.6.1. The Spherical-Revolute (SR) manipulator possesses 4 degrees of freedom, where link 1 is constrained to the base by a spherical joint $n_1 = 3$ and link 2 is constrained to link 1 by a revolute joint $n_2 = 1$. Using (6.29), the necessary conditions for the SR manipulator to achieve wrench-closure validity are

$$\begin{aligned} m_2^* &= \sum_i \alpha_{i2}^* \geq 2, \\ m_1^* &= \sum_i \alpha_{i1}^* + \min \left\{ \sum_i \beta_{i1}^*, m_2^* - 1 \right\} \geq 4. \end{aligned} \quad (6.31)$$

If either of the conditions from (6.31) are not satisfied, then the arrangement of cables are unable to satisfy the WCC for all of the manipulator poses. Using Table 6.1, the condition $m_2^* \geq 2$ is satisfied if there are at least two cables that are of type 2, 3, 4, 5 or 6, since $\alpha_{i2}^* = 1$ for routing types 2-6. For example, the SR manipulator shown in Figure 6.4(a) has only one type 2 cable (cable number 5 in the figure) with the remainder cables of type 1. As a result, $m_2^* = 1$ and hence it can be observed that wrench-closure could not be produced on link 2 regardless of the manipulator pose.

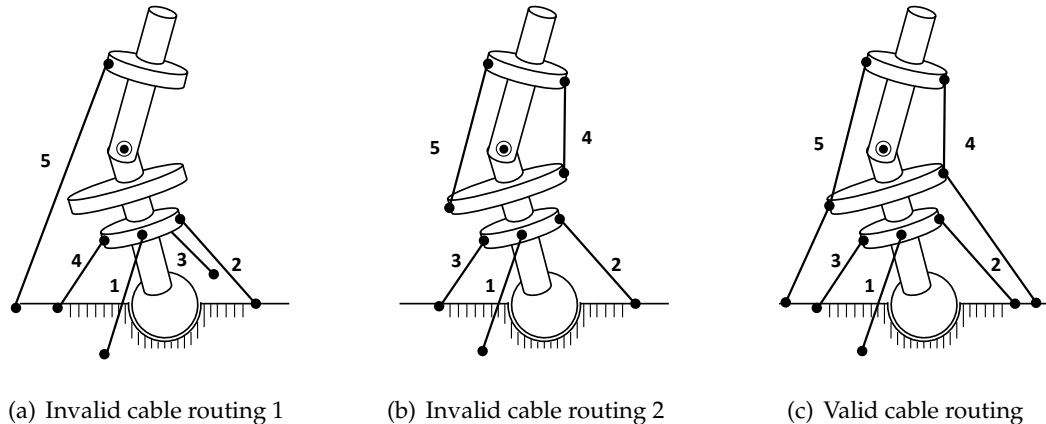


Figure 6.4: Examples of cable arrangement for the two link SR MCDM. (a) and (b) show two examples of cable routing that do not satisfy wrench-closure validity. However, the cable routing in (c) has the potential to satisfy wrench-closure validity depending on the attachment locations of the cables.

Secondly, consider the cable arrangement shown in Figure 6.4(b), where the manipulator is actuated by two cables of type 3 with the remainder three cables of type 1. The

two type 3 cables result in $m_2^* = \sum_i \alpha_{i2}^* = 2$ and hence satisfy the necessary condition for wrench-closure validity for link 2. However, as cables 4 and 5 from Figure 6.4(b) produce no resultant wrench on the spherical joint $\beta_{i1}^* = 0$, $i = 4, 5$, only the three type 1 cables is capable of producing a resultant wrench on the spherical joint. As a result, the wrench-closure validity cannot be achieved for link 1 since $m_1^* = \sum_i \alpha_{i1}^* = 3$. In summary, the cable routing shown in Figure 6.4(b) does not satisfy wrench-closure validity for the SR manipulator for all poses and cable attachment locations.

Finally, the cable arrangement shown in Figure 6.4(c) is an example of cable routing that satisfies the necessary condition for wrench-closure validity. The example consists of two cables of type 4 and three cables of type 1. The wrench-closure validity for link 2 is satisfied since $m_2^* = \sum_i \alpha_{i2}^* = 2$. The number of cables that are attached to link 2 and have the potential to actuate link 1 can be expressed as $\min \{\sum_i \beta_{i1}^*, m_2^* - 1\} = \min \{2, 1\} = 1$. Hence, $m_1^* = 4$ due to the three type 1 cables attached to link 1 and the actuation redundancy inherited from link 2. It can be concluded that the cable routing shown in Figure 6.4(c) satisfies wrench-closure validity. Satisfying the necessary conditions indicates that this cable arrangement has the potential to produce wrench-closure in at least some pose.

It should be noted that since the conditions are only necessary and not sufficient for wrench-closure validity, the cable arrangements that satisfy (6.29) may still result in an empty wrench-closure workspace depending on the exact attachment locations of the cables. Figure 6.5 shows an example where the cable routing satisfies (6.29), but the attachment locations of cables 4 and 5 mean that the WCC could never be satisfied for link 2.

From the performed analysis, it can be observed that the conditions in (6.31) allow the classification of different cable routing arrangements as to whether they have the potential to produce wrench-closure. Table 6.1 can be used in the design of cable routing such that the MCDM has the potential to achieve wrench-closure validity. Arrangements of cables that cannot satisfy wrench-closure validity would result in a limited range of motion for the MCDM. Since the wrench-closure condition is defined as the ability to generate motion in all directions, it should be noted that motion can still be produced in a subset of the directions if wrench-closure is not satisfied.

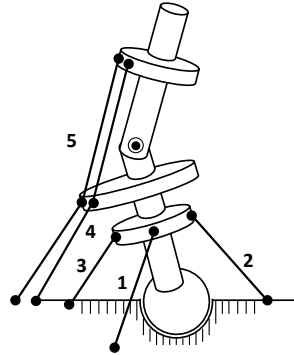


Figure 6.5: Example of cable routing that satisfies the necessary condition on wrench-closure validity but results in a wrench-closure invalid manipulator. The cable routing is identical to that from Figure 6.4(c), but the attachment locations of both cables 4 and 5 are situated on the left-hand side of the revolute joint compared with the example in Figure 6.4(c).

6.4.3 Three Link Manipulators

Performing the analysis in the same manner to that in Section 6.4.2, the conditions on wrench-closure validity can be studied for three link MCDMs. The number of cables m_1^* , m_2^* and m_3^* that have the potential to actuate link 1, link 2 and link 3, respectively, can be determined by (6.17) and expressed as

$$\begin{aligned} m_3^* &= \sum_i \alpha_{i3}^*, \\ m_2^* &= \sum_i \alpha_{i2}^* + \min \left\{ \sum_i \beta_{i2}^*, m_3^* - n_3 \right\}, \\ m_1^* &= \sum_i \alpha_{i1}^* + \min \left\{ \sum_i \beta_{i1}^*, m_2^* - n_2 \right\}, \end{aligned} \quad (6.32)$$

where

$$\begin{aligned} \alpha_{i1}^* &= \begin{cases} 1 & , \exists j : c_{ij2} \neq 0, c_{ij3} = c_{ij4} = 0 \forall j \\ 0 & , \text{otherwise} \end{cases} \\ \beta_{i1}^* &= \begin{cases} 1 & , \exists j : c_{ij2} + c_{ij3} + c_{ij4} \neq 0, \exists j : c_{ij3} + c_{ij4} \neq 0 \\ 0 & , \text{otherwise} \end{cases} \end{aligned}$$

$$\begin{aligned}
 \alpha_{i2}^* &= \begin{cases} 1 & , \exists j : c_{ij3} \neq 0, c_{ij4} = 0 \forall j \\ 0 & , \text{otherwise} \end{cases} \\
 \beta_{i2}^* &= \begin{cases} 1 & , \exists j : c_{ij3} + c_{ij4} \neq 0, \exists j : c_{ij4} \neq 0 \\ 0 & , \text{otherwise} \end{cases} \\
 \alpha_{i3}^* &= \begin{cases} 1 & , \exists j : c_{ij4} \neq 0 \\ 0 & , \text{otherwise} \end{cases} . \tag{6.33}
 \end{aligned}$$

Table 6.2 shows the evaluation of (6.33) for the 30 different types of possible cable routings for three link MCDMs. From the table, the links of the manipulator that can potentially be actuated by the available cables are described for different types of cable routings. For example, for cable routing of type 5, $\alpha_{i1}^* = 0$ and $\beta_{i2}^* = 0$. This indicates that cables with type 5 cable routing are unable to produce resultant motion on the joint of link 1. However, type 5 cable routing cables can potentially actuate links 2 and 3 since $\beta_{i2}^* = 1$ and $\alpha_{i3}^* = 1$. For all of the class 3 cable routing types, it should be noted that $\alpha_{i1}^* = \alpha_{i2}^* = 0$ and $\beta_{i1}^* = \beta_{i2}^* = \alpha_{i3}^* = 1$ as this class of cables are attached to every link of the manipulator.

In the same manner as in Section 6.4.2, all wrench-closure valid three link MCDMs must have cable arrangements that satisfy the necessary conditions from (6.32). For example, consider the 3-revolute (3R) planar manipulator shown in Figure 6.6.

The manipulator possesses 3 degrees of freedom ($n = 3$), where each joint is a single DoF revolute joint and hence $n_1 = n_2 = n_3 = 1$. From the generalised condition (6.27), the necessary conditions for wrench-closure validity for the 3R manipulator are $m_1^* \geq 2$, $m_2^* \geq 2$ and $m_3^* \geq 2$. Using the classifications from Table 6.2 and the definitions in (6.32), it can be observed that $m_3^* \geq 2$ is satisfied if the 3R manipulator possesses at least two cables of type 3, 5, 6, 9-12, or 14-30. Otherwise, the manipulator is unable to satisfy wrench-closure validity. An example of such a cable arrangement is shown in Figure 6.7(a), where the 3R manipulator is actuated by two cables of type 1 (cable numbers 1 and 2 in Figure 6.7(a)), one cable of type 2 (cable number 3) and one cable of type 11 (cable number 4). In such an arrangement, $m_3^* = 1$ and hence the WCC for link 3 can never be achieved.

Routing type	Class	Description	α_{i1}^*	β_{i1}^*	α_{i2}^*	β_{i2}^*	α_{i3}^*
1	1	$0 \rightarrow 1$	1	0	0	0	0
2	1	$0 \rightarrow 2$	0	1	1	0	0
3	1	$0 \rightarrow 3$	0	1	0	1	1
4	1	$1 \rightarrow 2$	0	0	1	0	0
5	1	$1 \rightarrow 3$	0	0	0	1	1
6	1	$2 \rightarrow 3$	0	0	0	0	1
7	2	$0 \rightarrow 1 \rightarrow 2$	0	1	1	0	0
8	2	$0 \rightarrow 2 \rightarrow 1$	0	1	1	0	0
9	2	$0 \rightarrow 1 \rightarrow 3$	0	1	0	1	1
10	2	$0 \rightarrow 3 \rightarrow 1$	0	1	0	1	1
11	2	$0 \rightarrow 2 \rightarrow 3$	0	1	0	1	1
12	2	$0 \rightarrow 3 \rightarrow 2$	0	1	0	1	1
13	2	$1 \rightarrow 0 \rightarrow 2$	0	1	1	0	0
14	2	$1 \rightarrow 2 \rightarrow 3$	0	0	0	1	1
15	2	$1 \rightarrow 3 \rightarrow 2$	0	0	0	1	1
16	2	$1 \rightarrow 0 \rightarrow 3$	0	1	0	1	1
17	2	$2 \rightarrow 0 \rightarrow 3$	0	1	0	1	1
18	2	$2 \rightarrow 1 \rightarrow 3$	0	0	0	1	1
19	3	$0 \rightarrow 1 \rightarrow 2 \rightarrow 3$	0	1	0	1	1
20	3	$0 \rightarrow 1 \rightarrow 3 \rightarrow 2$	0	1	0	1	1
21	3	$0 \rightarrow 2 \rightarrow 1 \rightarrow 3$	0	1	0	1	1
⋮							
30	3	$2 \rightarrow 0 \rightarrow 1 \rightarrow 3$	0	1	0	1	1

Table 6.2: The analysis of cable routing for wrench-closure validity for three link MCDMs.

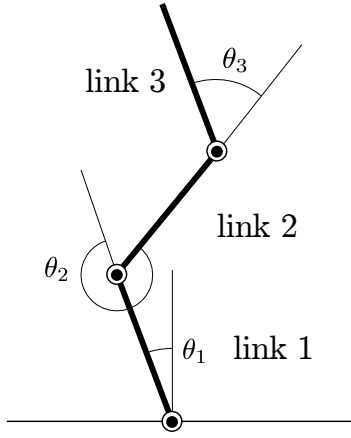


Figure 6.6: 3 link 3-revolute joint (3R) planar MCDM model.

Figure 6.7(b) shows an example of cable arrangement where link 2 does not satisfy wrench-closure validity. The cable arrangement consists of two type 1 cables, one type 11 cable and one type 3 cable. Cable numbers 3 and 4 provide the actuation for link 3 to satisfy wrench-closure since $m_3^* = 2$. From Table 6.2, cables 3 and 4 are also able to produce motion onto link 2 since $\beta_{32}^* = \beta_{42}^* = 1$. However, they are required in producing the wrench-closure on link 3. As a result, the number of effective cables that have the potential to actuate link 2 can be expressed as $m_2^* = \sum_i \alpha_{i2}^* + \min\{2, 1\}$. In this example, there must be at least one more cable that is of type 2, 4, 7, 8 or 13 such that wrench-closure validity can be satisfied for link 2. However, in the example shown in Figure 6.7(b), $\sum_i \alpha_{i2}^* = 0$ and hence $m_2^* = 1$ and wrench-closure validity for the MCDM is not satisfied.

In Figure 6.7(c), link 3 is able to satisfy wrench-closure since $m_3^* = 2$. Furthermore, the addition of two type 4 cables results in $m_2^* = 3$ and hence satisfies the necessary conditions for wrench-closure validity for link 2. However, the number of cables with the potential to provide actuation on link 1 can be expressed as $m_1^* = \min\{1, 2\} = 1$ and hence wrench-closure cannot be achieved for link 1.

Finally, Figure 6.7(d) shows an example of a cable arrangement in which the necessary conditions for wrench-closure validity are satisfied. It can be determined that in this exam-

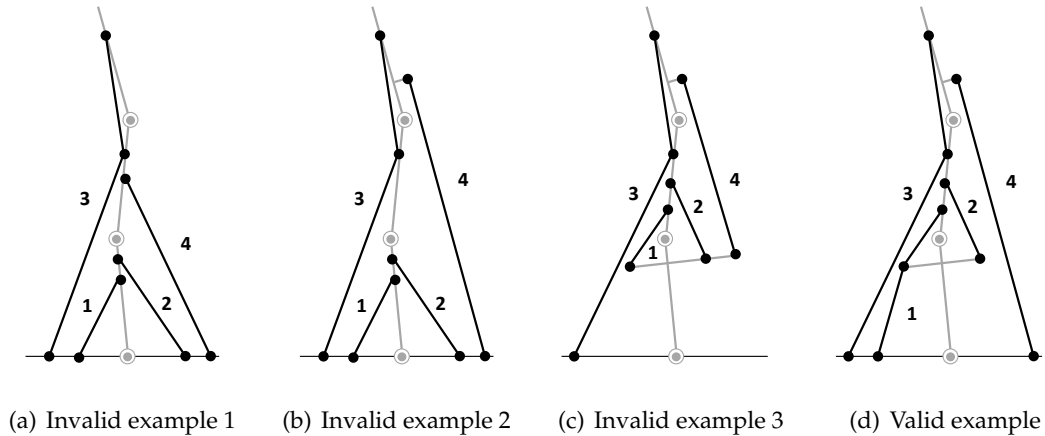


Figure 6.7: Examples of cable arrangement for the three link 3R planar MCDM. (a), (b) and (c) show three examples of cable routing that do not satisfy wrench-closure validity. However, the cable routing in (d) has the potential to satisfy wrench-closure validity depending on the attachment locations of the cables.

ple, link 3 results in $m_3^* = 2$ and link 2 results in $m_2^* = 2 + \min\{2, 1\} = 3$. For link 1, the number of cables with the potential to provide actuation on the link can be determined as $m_1^* = \min\{3, 2\} = 2$. As a result, it can be concluded that this cable arrangement satisfies the necessary condition for wrench-closure validity for a 3R manipulator.

The presented analysis on wrench-closure validity for the 3R manipulator demonstrates that the proposed necessary conditions can be applied on generalised p link MCDMs. For a p link MCDM, (6.27) results in a set of p necessary conditions that the cable routing must satisfy for the manipulator to be considered as wrench-closure valid. As the conditions are formulated with respect to the generalised terms of the CRM, the analysis does not make assumptions on the type of cable routing that is allowed for the system.

6.5 Conclusion

In this chapter, the necessary conditions required for an MCDM to achieve wrench-closure validity were presented. Wrench-closure validity is an important property for CDPMs as manipulators that do not satisfy wrench-closure validity result in a very limited range of motion. Since a manipulator not satisfying wrench-closure validity would have an empty WCW, this implies that motion can only be produced in a limited set of

directions for all poses. From the analysis of the generalised MCDM Jacobian matrix, necessary conditions on wrench-closure validity were expressed with respect to CRM. The primary advantage of these conditions is that MCDMs that cannot satisfy wrench-closure in any pose can be identified using only the cable routing, regardless of the cable attachment locations. Furthermore, in the presented analysis the WCW was not required to be generated. By removing invalid cable routing arrangements from further analysis, the efficiency of the design process in the cable attachment locations of MCDMs is increased. To demonstrate the derived necessary conditions, the analysis was performed on several MCDMs, ranging from single CDPMs to 3 link MCDMs. These examples illustrate how the conditions can be used to validate the cable routing arrangements and to assist in the design of cable routing such that wrench-closure validity may be satisfied. As the analysis was performed on the generalised MCDM model, the derived necessary conditions are applicable to any type of MCDM kinematic structure with arbitrary cable routing.

Chapter 7

Consideration of Muscle Actuation in the Cable Model

In this chapter, the traditional ideal force generator cable model is extended to a more generalised model that considers cables as state dependent force generators. This model allows for a wider range of unilateral actuators to be used in the study of cable-driven parallel manipulators (CDPMs), such as pneumatic artificial muscles and physiological muscles. The state dependent force generator is illustrated through the consideration of the actuation characteristics of physiological muscles in the cable model. Section 7.1 introduces the features of the state dependent actuators relevant to this study. Section 7.2 presents the elements of the Hill-type muscle model. One of the key characteristics of the muscle model is that it can behave as an active or a passive actuator element. Section 7.3 describes the conditions in which a muscle-tendon complex is considered active or passive. The solutions of the forces for a muscle at a given length is presented in Section 7.4. Finally, Section 7.5 concludes the chapter by summarising the contributions.

7.1 Introduction

In previous studies of CDPMs, cables are modelled as *ideal force generators*, which assumes that any magnitude of positive cable force within a given range can be produced. The range of producible cable force is assumed to be a property of the actuator with lower and upper bounds that are constant for all manipulator poses. This assumption is well justified for conventional CDPMs that are actuated by motorised spools, where it is capable of producing a range of motor torque, and hence cable force, from zero to a maximum value.

The ideal force generator model fails when dealing with systems where the ability to produce force is dependent on the state of the system (*state dependent force generator*). The

state of the system refers to the positions and velocities of the manipulator and its cables. State dependent force generators exist in many engineered and biological systems, such as those actuated by pneumatic artificial muscles [53,56] and physiological muscles [145], respectively.

The primary characteristic for the state dependent force generator model is that the force producing ability of the actuator is dependent on the state or the pose and velocity of the system. Firstly, it will be assumed that the actuator can behave as either an active or a passive element at a particular state. Secondly, when the actuator is active, a range of force can be produced, where the range is dependent on the state of the system. Finally, if the actuator is in the passive state, then the actuator produces a fixed force that is also dependent on the system states. Note that in the context for this work, passive does not imply that actuator element can only produce zero force. Mathematically, the force produced by a state dependent force generator can be expressed as $F \in [F_{\min}(\mathbf{q}), F_{\max}(\mathbf{q})]$ when it is active and $F = F_{\text{passive}}(\mathbf{q})$ when it is passive, where \mathbf{q} is the set of generalised coordinates of the manipulator.

7.2 Hill-type Muscle Model

One commonly accepted model of the physiological muscle is the *modified Hill-type model* [145], consisting of tendon and muscle elements connected in series, as shown in Figure 7.1. Tendons are passive elements where the tendon force is a function of the tendon strain, while muscles can behave either as passive or active elements depending on their length. Hence, the force that can be produced by a muscle-tendon complex varies depending on its state. The combined muscle-tendon length l^{mt} can be expressed with respect to the tendon length l^t , muscle length l^m and muscle pennation angle α by

$$l^{mt} = l^t + l^m \cos \alpha . \quad (7.1)$$

The pennation angle represents the angle of the muscle fibres within the muscle-tendon complex.

The force applied along the muscle-tendon complex is transmitted through both the

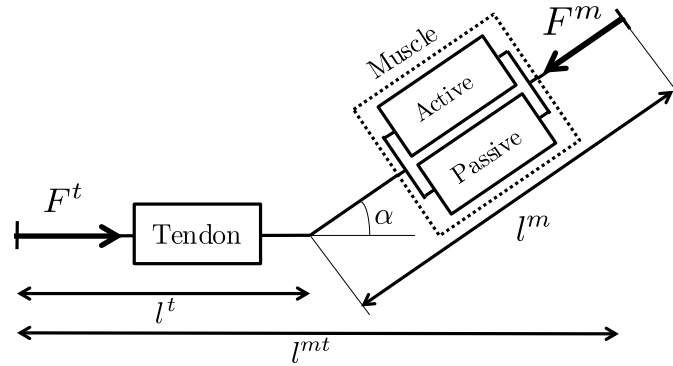


Figure 7.1: The modified Hill-type muscle-tendon model consists of two elements arranged in series: the muscle element and tendon element. The length of the muscle-tendon complex l^{mt} consists of the muscle length l^m and tendon length l^t . The force acting through the muscle and tendon are denoted by F^m and F^t , respectively.

muscle and tendon elements in series. Hence, the muscle-tendon force F^{mt} can be related to the tendon force F^t and the muscle force F^m by the relationship

$$F^{mt} = F^t = F^m \cos \alpha . \quad (7.2)$$

In the Hill-type model, the tendon force F^t and muscle force F^m are modelled by generic force relationships. The generic relationships are described with respect to the five properties that define the muscle-tendon: peak isometric muscle force F_0^m , optimal muscle fibre length l_0^m , optimal muscle fibre pennation angle α_0 , maximum shortening velocity v_{max} , and tendon slack length l_s^t . The force relationships are typically described by splines or analytical expressions that fit experimental data [81, 132]. Sections 7.2.1 and 7.2.2 present the analytical models of the tendon and muscle force relationships, respectively, used in this study.

7.2.1 Tendon Model

The tendon behaves as a passive non-linear elastic element. One model for the generic tendon force-strain relationship [81] consists of linear and non-linear sections that can be

analytically expressed as

$$\hat{F}^t(\varepsilon) = \begin{cases} 0 & \varepsilon < 0 \\ 0.10377(e^{91\varepsilon} - 1) & 0 \leq \varepsilon < 0.01516 \\ 37.526\varepsilon - 0.26029 & 0.01516 \leq \varepsilon < 0.1 \end{cases}, \quad (7.3)$$

where \hat{F}^t and ε are the normalised tendon force and tendon strain, respectively. Tendon strain is defined by $\varepsilon = (l^t - l_s^t)/l_s^t$ and normalised tendon force is $\hat{F}^t = F^t/F_0^m$, where l_s^t is the tendon slack length and F_0^m is the peak isometric muscle force as previously defined.

To illustrate how the generic tendon force relationship from (7.3) describes the tendon element of different muscle-tendon complexes, Figure 7.2 shows the scaled tendon force curves for two example muscle-tendon complexes: the *deltoid anterior* and *supraspinatus* muscles. The tendon force curve for the *deltoid anterior* muscle is shown in Figure 7.2(a), generated from (7.3) using the properties $F_0^m = 1142.6$ N and $l_s^t = 0.093$ m [50]. Similarly, the tendon force curve for the *supraspinatus* muscle is shown in Figure 7.2(b) using the properties $F_0^m = 487.82$ N and $l_s^t = 0.0395$ m. It can be observed that despite the generic force relationship, the resulting tendon force curves of the two muscles are characterised by the different muscle parameters.

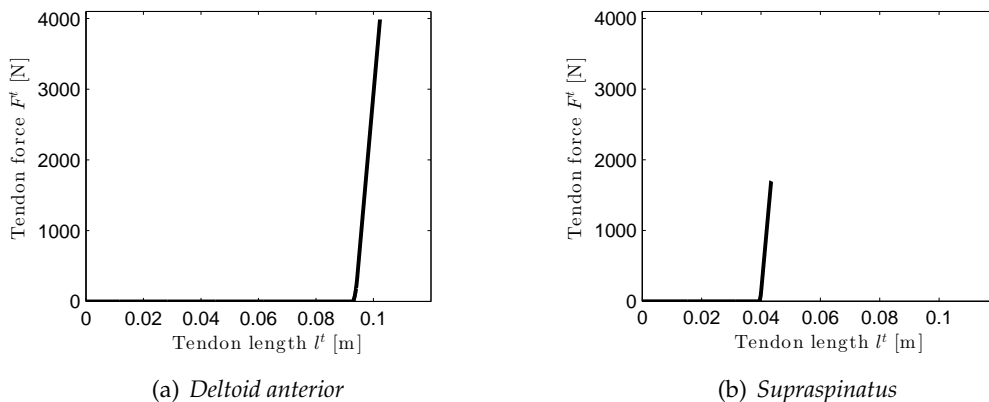


Figure 7.2: The tendon force curves for two example muscle-tendon complexes generated using the generic tendon force relationship equation. The tendon force curve for the *deltoid anterior* muscle is shown in (a) and the tendon force curve for the *supraspinatus* muscle is shown in (b).

7.2.2 Muscle Model

As shown in Figure 7.1, the muscle element consists of two components: an active component capable of producing a normalised force \hat{F}_a^m and a passive component that produces force \hat{F}_p^m . Assuming that the system is in static equilibrium, and hence $\dot{l}^m = 0$ for all muscles, the normalised muscle force $\hat{F}^m = F^m / F_0^m$ can be expressed as

$$\hat{F}^m(\eta) = \hat{F}_a^m(\eta)a(t) + \hat{F}_p^m(\eta), \quad (7.4)$$

where $\eta = l^m / l_0^m$ is the normalised muscle length and $0 \leq a(t) \leq 1$ is the activation level of the muscle at time t .

The force \hat{F}_a^m represents the maximum force that the active component can generate at muscle length l^m . The generic active muscle force curve [81] can be expressed with respect to η as

$$\hat{F}_a^m(\eta) = \begin{cases} 1 - \left(\frac{\eta-1}{0.5}\right)^2 & 0.5 < \eta < 1.5 \\ 0 & \text{otherwise} \end{cases}. \quad (7.5)$$

The passive muscle force curve [132] can be analytically expressed as

$$\hat{F}_p^m(\eta) = \eta^3 e^{8\eta - 12.9}. \quad (7.6)$$

The muscle can be defined as an *active muscle* for $0.5l_0^m < l^m < 1.5l_0^m$, where $\hat{F}_a^m > 0$, such that the muscle can be activated. For $l^m \leq 0.5l_0^m$ or $l^m \geq 1.5l_0^m$, the muscle is considered as a *passive muscle* where $\hat{F}_a^m = 0$ and hence $\hat{F}^m = \hat{F}_p^m$.

The muscle force relationship can then be defined using the active muscle (7.5) and the passive muscle (7.6) expressions within the generic muscle force relationship from (7.4). To illustrate the generic relationship, Figure 7.3 shows the scaled muscle force curves for two example muscle-tendon complexes: the *deltoid anterior* and *supraspinatus* muscles. The muscle force curve for the *deltoid anterior* muscle is shown in Figure 7.3(a), generated from (7.5) and (7.6) using the properties $F_0^m = 1142.6$ N and $l_0^m = 0.0976$ m. Similarly, the muscle curve for the *supraspinatus* muscle is shown in Figure 7.3(b) using the properties $F_0^m = 487.82$ N and $l_0^m = 0.0682$ m.

The muscle force curves for zero muscle activation $a = 0$ and full activation $a = 1$ are shown for both muscles as indicated by the solid and dashed lines, respectively. Similar to the generic tendon force curve presented in Section 7.2.1, the generic muscle force relationship produced different muscle force characteristics depending on the muscle specific parameters.

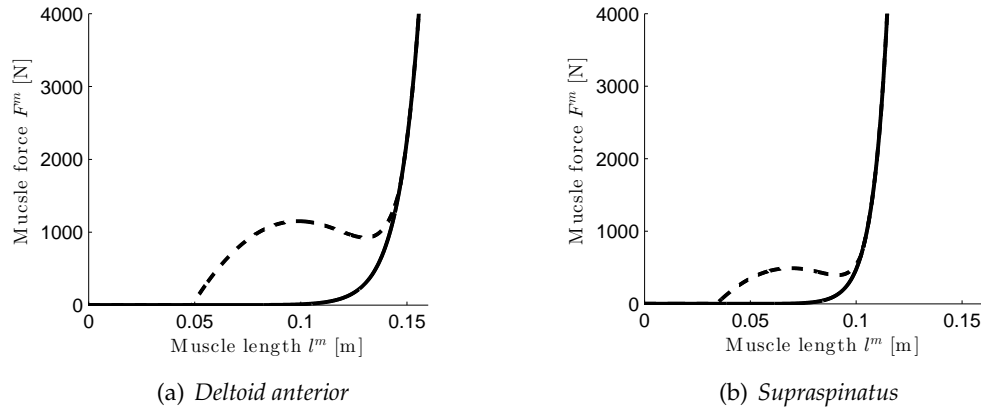


Figure 7.3: The muscle force curves for two example muscle-tendon complexes generated using the generic muscle force relationship equation. The force curve for the *deltoid anterior* muscle is shown in (a) and the force curve for the *supraspinatus* muscle is shown in (b). The muscle forces at no activation $a(t) = 0$ and full activation $a(t) = 1$ are represented by solid and dashed curves, respectively.

7.3 Active and Passive Muscles

From Section 7.2, it can be observed that the actuation force of the muscle is dependent on the muscle length. From the system kinematics, the muscle origin and insertion points only provides the length of the entire muscle-tendon complex l^{mt} . In the study of the musculoskeletal system dynamics, the muscle activation and hence the respective muscle and tendon lengths are determined during inverse dynamic analysis to resolve the muscle forces.

In this section, it will be shown that for static equilibrium ($\dot{a}(t) = 0$), the possible lengths of the muscle and tendon elements can be resolved directly from the muscle-tendon length l^{mt} . The resulting muscle lengths l^m allow the muscle-tendon forces F^{mt}

to be determined. The generic approach allows different equations for the muscle and tendon force relationships to be applied. For the purpose of illustration, the analytical expressions from (7.3), (7.5) and (7.6) presented in Section 7.2 will be used.

Assuming that the muscle belly has a constant thickness and volume [116], the pennation angle α can be expressed as

$$\alpha = \sin^{-1} \left(\frac{l_0^m}{l^m} \sin \alpha_0 \right). \quad (7.7)$$

Substituting (7.7) into (7.4) results in the following relationship between the normalised tendon and the muscle forces

$$\hat{F}^t(\varepsilon) = \left(\hat{F}_a^m(\eta) a(t) + \hat{F}_p^m(\eta) \right) \sqrt{1 - \left(\frac{\sin \alpha_0}{\eta} \right)^2}. \quad (7.8)$$

From (7.1) and (7.7), the tendon strain ε can be expressed with respect to η as

$$\begin{aligned} \varepsilon &= \frac{l^{mt} - l^m \cos \alpha - l_s^t}{l_s^t} \\ &= \frac{l^{mt} - l_0^m \sqrt{\eta^2 - \sin^2 \alpha_0} - l_s^t}{l_s^t}. \end{aligned} \quad (7.9)$$

Expression (7.9) allows the left hand-side of (7.8), that is, $\hat{F}^t(\varepsilon)$, to be expressed with respect to η . Hence for a particular l^{mt} , the solution to (7.8) allows the admissible range of muscle-tendon forces F^{mt} to be determined. Figure 7.4 shows the curves for $F^m \cos \alpha$ and $F^t(\eta)$ for the *deltoid anterior* muscle. The muscle forces $F^m \cos \alpha$ for various activation levels between $a = 0$ and $a = 1$ are shown. The tendon force curve from Figure 7.2(a) is expressed with respect to η by substituting (7.9) into (7.3). The curves F_1^t to F_5^t in Figure 7.4 represent $F^t(\eta)$ for increasing values of l^{mt} .

If the solution for η to (7.8) is within $0.5 < \eta < 1.5$, as shown by example curve $F_3^t(\eta)$ in Figure 7.4, then the muscle is considered *active* and a range of forces can be produced as the activation level varies between $a = 0$ and $a = 1$. In contrast, if the solution η to (7.8) is $\eta \leq 0.5$ or $\eta \geq 1.5$, as shown by example curves $F_1^t(\eta)$ and $F_5^t(\eta)$, respectively, there is only one F^{mt} solution and the muscle is considered *passive*.

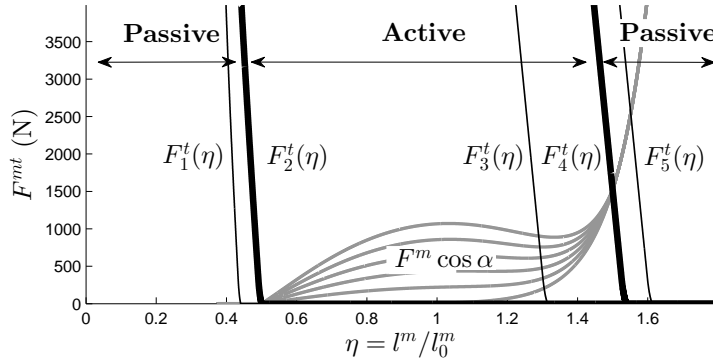


Figure 7.4: Muscle and tendon forces for various muscle-tendon lengths l^{mt} , showing the situations in which the muscle are active and passive. The curves $F^m \cos \alpha$ for various levels of activation between $\alpha = 0$ to $\alpha = 1$ are shown in grey. The curves $F_1^t(\eta)$ and $F_5^t(\eta)$ are two example tendon force curves for when the muscle-tendon is passive. The curve $F_3^t(\eta)$ is an example tendon force curve for when the muscle-tendon is active. The curves $F_2^t(\eta)$ and $F_4^t(\eta)$ are the tendon force curves when $l^{mt} = l_{a,min}^{mt}$ and $l^{mt} = l_{a,max}^{mt}$, respectively.

It can be observed that the increase in l^{mt} translates the curve $F^t(\eta)$ monotonically from left to right. The muscle-tendon lengths corresponding to the tendon force curves $F_2^t(\eta)$ and $F_4^t(\eta)$, as marked as bold lines in Figure 7.4, can be considered as the boundaries between active and passive regions of the muscle. The muscle-tendon length producing $F_2^t(\eta)$ can be regarded as the *minimum* muscle-tendon length $l_{a,min}^{mt}$ for the muscle to be considered as active. Similarly, l^{mt} for $F_4^t(\eta)$ can be regarded as the *maximum* muscle-tendon length $l_{a,max}^{mt}$ for the muscle to be considered as active.

The minimum active muscle-tendon length can be defined as the muscle-tendon length in which $\varepsilon = 0$ and $\eta = 0.5$. Hence from (7.9), $l_{a,min}^{mt}$ can be expressed as

$$l_{a,min}^{mt} = l_0^m \sqrt{(0.5)^2 - \sin^2 \alpha_0} + l_s^t. \quad (7.10)$$

The maximum active muscle-tendon length can be defined as the value of l^{mt} such that (7.8) is satisfied for $\eta = 1.5$

$$\hat{F}^t(\eta = 1.5) = \hat{F}_p^m(\eta = 1.5) \sqrt{1 - \frac{\sin^2 \alpha_0}{1.5^2}}. \quad (7.11)$$

The solution to (7.11) can be determined using the tendon force and passive muscle force relationships from (7.3) and (7.6), respectively. The normalised tendon force at $\eta = 1.5$ can be expressed as

$$\hat{F}_{max}^t = 1.5^2 e^{-0.9} \sqrt{1.5^2 - \sin^2 \alpha_0}. \quad (7.12)$$

It can be observed that for any α_0 , \hat{F}_{max}^t is within the linear region of (7.3). Hence, equating (7.3) and (7.9) results in the following maximum active muscle-tendon length

$$l_{a,max}^{mt} = \frac{(\hat{F}_{max}^t + 37.7863)l_s^t}{37.526} + l_0^m \sqrt{1.5^2 - \sin^2 \alpha_0}. \quad (7.13)$$

From (7.10) and (7.13), it is possible to determine whether a particular muscle is active or passive for a known muscle-tendon length l^{mt} . If $l_{a,min}^{mt} < l^{mt} < l_{a,max}^{mt}$, then the muscle element is considered an active element. Otherwise, if $l^{mt} \leq l_{a,min}^{mt}$ or $l^{mt} \geq l_{a,max}^{mt}$, then the muscle element is considered a passive element.

7.4 Solution of Muscle Forces

In Section 7.3, it was shown that muscles can be classified as active or passive elements depending on their muscle-tendon length. It can be observed in Figure 7.4 that if the muscle-tendon length is in the active muscle region, then there is a range of solutions F^{mt} to (7.8) for activations from $a = 0$ to $a = 1$. Otherwise, if the muscle-tendon length is in the passive muscle region, then there only exists a single solution to (7.8) and the muscle-tendon force F^{mt} is fixed for a given muscle-tendon length. In this section, the muscle forces for both when a muscle is active and passive are presented.

For muscle-tendon lengths $l_{a,min}^{mt} < l^{mt} < l_{a,max}^{mt}$, the muscle-tendon complex can produce a force within the range of $F^{mt} \in [F_{min}^{mt}(\eta), F_{max}^{mt}(\eta)]$ for a given η . From the curves $F_3^t(\eta)$ and $F^m \cos \alpha$ shown in Figure 7.5, it can be observed that F_{min}^{mt} and F_{max}^{mt} can be determined by solving (7.8) for $a(t) = 0$ and $a(t) = 1$, respectively.

As a result, the active muscle force range can be expressed as

$$F_{min}^{mt} = F_0^m \hat{F}^t(\eta = \eta_{min}^*)$$

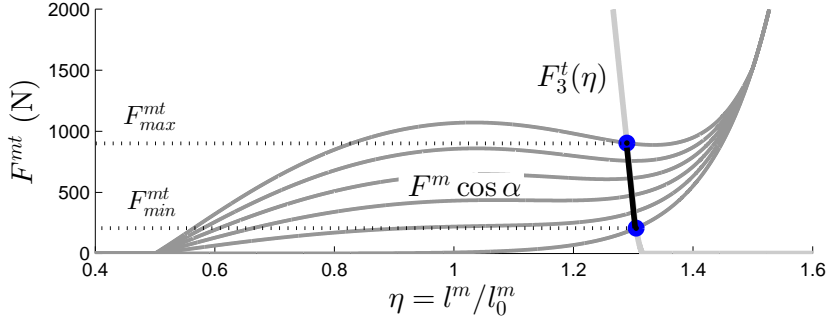


Figure 7.5: The force range solution $F^{mt} \in [F_{min}, F_{max}]$ when the muscle-tendon is active. The minimum and maximum forces are denoted by F_{min} and F_{max} , respectively.

$$F_{max}^{mt} = F_0^m \hat{F}^t(\eta = \eta_{max}^*) , \quad (7.14)$$

where η_{min}^* is the solution to (7.8) for $a = 0$

$$\hat{F}^t(\eta) = \hat{F}_p^m(\eta) \sqrt{1 - \left(\frac{\sin \alpha_0}{\eta} \right)^2} , \quad (7.15)$$

and η_{max}^* is the solution to (7.8) for $a = 1$

$$\hat{F}^t(\eta) = \left(\hat{F}_a^m(\eta) + \hat{F}_p^m(\eta) \right) \sqrt{1 - \left(\frac{\sin \alpha_0}{\eta} \right)^2} . \quad (7.16)$$

Figure 7.6 illustrates the two scenarios when the muscle can be regarded as *passive*. For $l^{mt} \leq l_{a,min}^{mt}$, for example $F_1^t(\eta)$ in Figure 7.6, the solution to (7.8) results in a muscle length less than $0.5l_0^m$ and tendon length less than its slack length l_s^t such that the resulting muscle-tendon force is zero. For $l^{mt} \geq l_{a,max}^{mt}$, for example $F_5^t(\eta)$ in Figure 7.6, the solution to (7.8) results in a muscle length greater than $1.5l_0^m$ for the constraints (7.1) and (7.2) to be satisfied. Hence, the resulting muscle-tendon force when the muscle is passive can be expressed as

$$F^{mt} = \begin{cases} 0 & , l^{mt} \leq l_{a,min}^{mt} \\ F_0^m \hat{F}^t(\eta^*) & , l^{mt} \geq l_{a,max}^{mt} \end{cases} , \quad (7.17)$$

where η^* is the solution to (7.15).

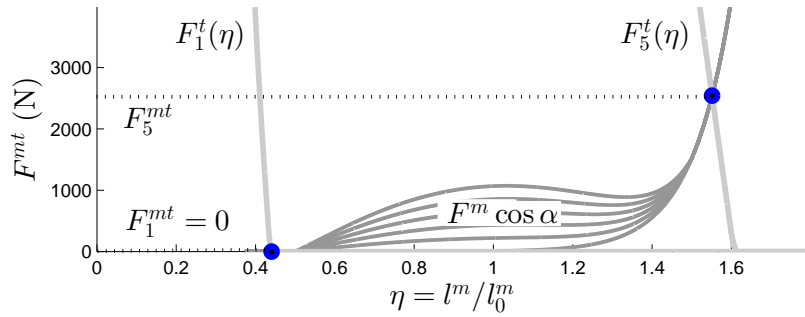


Figure 7.6: The force solutions when the muscle-tendon is passive. The two solutions F_1^{mt} and F_5^{mt} correspond to the cases when $l^{mt} \leq l_{a,min}^{mt}$ and $l^{mt} \geq l_{a,max}^{mt}$, respectively.

Muscle Range of Force Examples

To demonstrate the solution of muscle forces for different poses of a musculoskeletal system, the forces for the *deltoid anterior* and *supraspinatus* shoulder muscles during human shoulder flexion/extension motion are presented. The flexion/extension motion refers to the forward and backward swinging of the arm in the sagittal plane, as shown in Figure 7.7. The angle of flexion and extension can be denoted by the positive and negative values of α , respectively.

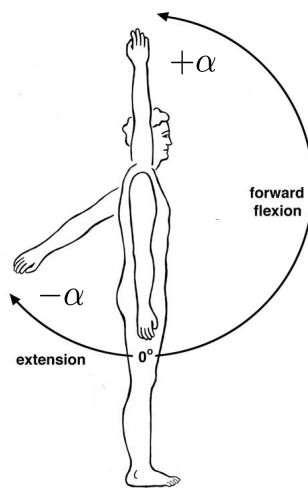


Figure 7.7: The flexion/extension motion is shown for a human shoulder, where the motion is equivalent to the forward and backward swinging of the arm in the sagittal plane. Positive and negative α angles correspond to forward flexion and backward extension motions, respectively.

	F_0^m [N]	l_0^m [m]	l_s^t [N]	α_0 [rad]
Deltoid anterior	1142.60	0.0976	0.0930	0.3840
Supraspinatus	487.82	0.0682	0.0395	0.1222

Table 7.1: The generic muscle-tendon properties for the *deltoid anterior* and *supraspinatus* muscles, where F_0^m , l_0^m , l_s^t and α_0 refer to the peak isometric muscle force, optimal muscle fibre length, tendon slack length and optimal muscle fibre pennation angle, respectively.

The muscle properties [50] for the *deltoid anterior* and *supraspinatus* muscles are summarised in Table 7.1. Flexion/extension motion refers to the poses $-180^\circ \leq \alpha \leq 180^\circ$. As the range of muscle forces varies depending on the muscle-tendon length, the muscle forces must be determined for each muscle-tendon length at angle α . The muscle-tendon lengths were obtained from a well accepted shoulder model [50]. OpenSim is a widely accepted simulation platform in the biomechanics community used in performing analysis on musculoskeletal systems, for example, to study the muscle lengths and forces for a particular trajectory of motion. Using the OpenSim API, the muscle-tendon lengths for a desired shoulder pose can be determined.

Figure 7.8 shows the length of the *supraspinatus* muscle-tendon complex for pure flexion/extension motion. The minimum and maximum muscle-tendon lengths for the *supraspinatus* to be an active muscle were determined from (7.10) and (7.13), respectively. The resulting muscle-tendon lengths $l_{a,min}^{mt} = 0.0726$ m and $l_{a,max}^{mt} = 0.1432$ m are shown as horizontal dashed lines in Figure 7.8. From the muscle-tendon length curve, it is observed that the *supraspinatus* muscle is active for the entire flexion/extension motion $-180^\circ \leq \alpha \leq 180^\circ$.

For each angle α during flexion/extension, the muscle-tendon lengths from Figure 7.8 allow the possible muscle forces to be determined. Since the muscle is active $l_{a,min}^{mt} \leq l^{mt} \leq l_{a,max}^{mt}$ for the entire motion, the minimum and maximum muscle-tendon forces, denoted by F_{min}^{mt} and F_{max}^{mt} , respectively, can be determined from (7.14). Figure 7.9 shows the resulting muscle forces for the *supraspinatus* muscle over the flexion/extension motion.

From Figure 7.9, it can be observed that since the muscle is active, a range of muscle force $F^{mt} \in [F_{min}^{mt}, F_{max}^{mt}]$ can be determined at each pose. Furthermore, for the majority of the flexion/extension motion, the range of force is near to the maximum possible range

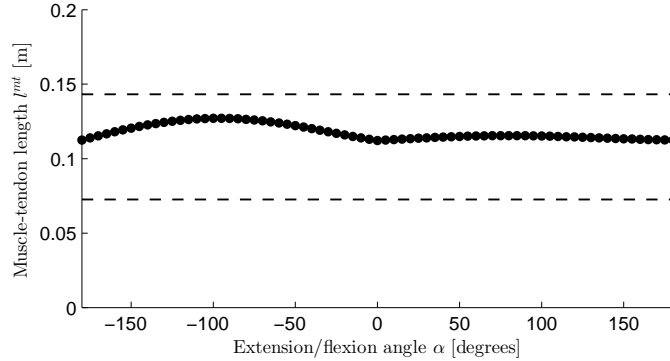


Figure 7.8: Length of the *supraspinatus* muscle during flexion/extension motion, with $l_{a,\min}^{mt} = 0.0726$ m and $l_{a,\max}^{mt} = 0.1432$ m shown as dashed lines.

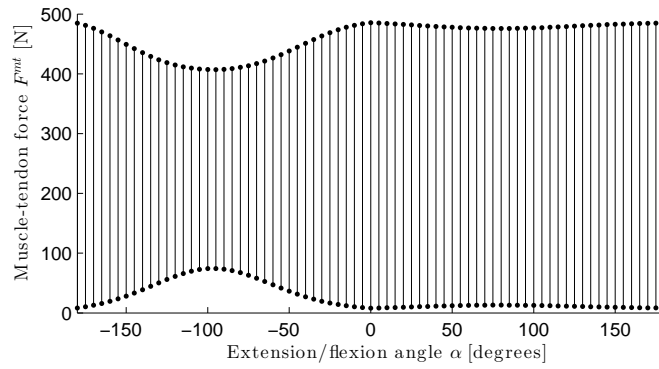


Figure 7.9: Force of *supraspinatus* muscle during flexion/extension motion. The *supraspinatus* muscle is active for the entire flexion/extension motion. The ranges of force are denoted by the vertical lines.

$F^{mt} \in [0, F_0^m]$. This observation can be explained by the fact that the muscle-tendon length is similar to the nominal length of the muscle-tendon $l_0^m + l_s^t = 0.1077$ m for the flexion/extension motion, as shown in Figure 7.8. However, as the muscle-tendon length increases beyond the nominal length $l_0^m + l_s^t = 0.1077$ m, for $-150^\circ \leq \alpha \leq -50^\circ$, the range of force that can be produced by the *supraspinatus* muscle decreases. This observation illustrates the state dependent nature of the muscle's ability to produce force.

Similarly, the lengths of the *deltoid anterior* muscle-tendon complex for pure flexion/extension motion obtained from the OpenSim shoulder model [50] are shown in Figure 7.10. The minimum and maximum muscle-tendon lengths for the *deltoid anterior* to be an active muscle were determined from (7.10) and (7.13), respectively, as $l_{a,\min}^{mt} = 0.1253$

m and $l_{a,max}^{mt} = 0.2387$ m, and are shown as horizontal dashed lines in Figure 7.10. Compared with the *supraspinatus* muscle, the length of the *deltoid anterior* motion varies by a larger range during the motion. Furthermore, it is observed from Figure 7.10 that the *deltoid anterior* muscle becomes passive from $\alpha = -50^\circ$ to $\alpha = -85^\circ$.

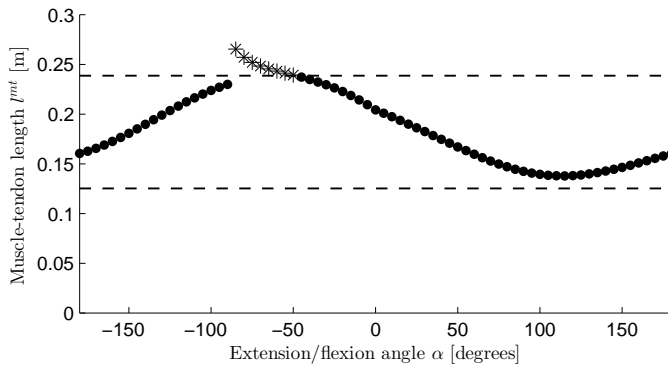


Figure 7.10: Length of the *deltoid anterior* muscle during flexion/extension motion, with $l_{a,min}^{mt} = 0.1253$ m and $l_{a,max}^{mt} = 0.2387$ m shown as dashed lines. The points marked in stars denote that the muscle-tendon complex is passive.

For each flexion/extension angle α , the muscle-tendon length allows the possible muscle forces to be determined. When the muscle is active $l_{a,min}^{mt} \leq l^{mt} \leq l_{a,max}^{mt}$, the minimum and maximum muscle-tendon forces, denoted by F_{min}^{mt} and F_{max}^{mt} , respectively, were determined from (7.14). Otherwise, if the muscle is passive, the passive muscle force was solved from (7.17). From the muscle-tendon lengths, the muscle forces of the *deltoid anterior* during flexion/extension motion is shown in Figure 7.11.

Several features of the *deltoid anterior* muscle forces can be observed from Figure 7.11. Firstly, the muscle produced a varying range of forces at different flexion/extension angles, corresponding with the natural behaviour of the state dependent force generator. Secondly, the *deltoid anterior* muscle produced passive forces between $-85^\circ \leq \alpha \leq -50^\circ$, and was largest in magnitude at $\alpha = -85^\circ$. Finally, the *deltoid anterior* muscle produced the largest range of active force at poses $\alpha = -140^\circ$ and $\alpha = 15^\circ$. However, at flexion/extension angles between $100^\circ \leq \alpha \leq 120^\circ$, $-45^\circ \leq \alpha \leq -30^\circ$ and $-95^\circ \leq \alpha \leq -90^\circ$, the muscle was only able to produce a very limited range of forces.

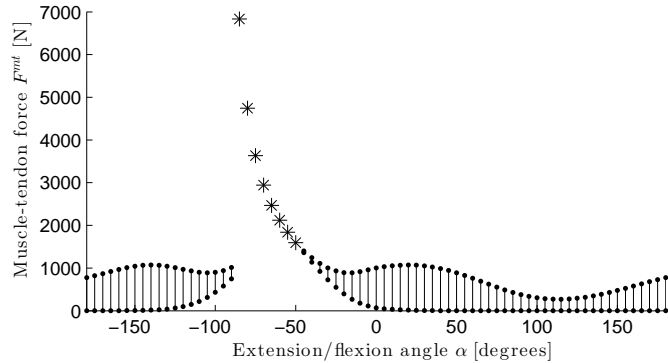


Figure 7.11: Force of the *deltoid anterior* muscle during flexion/extension motion. The ranges of force are denoted by the vertical lines and the points marked in stars denote that the muscle-tendon complex is passive.

7.5 Conclusion

In this chapter, the state dependent force generator was presented. Compared with the traditional ideal force generator model used to model cables, the ability of the state dependent force generator to produce force is dependent on the system states. The physiological Hill-type muscle model was introduced as an example of a state dependent force generator. It was shown that using the muscle-tendon length, the muscle-tendon complex can be classified as active or passive. Furthermore, the force that the muscle can produce for both when the muscle is active and passive was determined. The state dependent nature was demonstrated from the two example muscles within the shoulder during the flexion/extension of the shoulder. By incorporating the state dependent force generator model into the study of CDPMs, a wider range of engineered and biological systems can be studied as CDPMs.

This page is intentionally left (almost) blank.

Chapter 8

Static Workspace Analysis of Musculoskeletal Systems

In this chapter, the static workspace analysis for musculoskeletal systems is formulated and presented. The analysis extends from the traditional workspace analysis for cable-driven parallel manipulators (CDPMs) by allowing cables to act as the state dependent force generators introduced in Chapter 7. Workspace analysis has not previously been conducted for musculoskeletal systems as such analysis of cable robots has always assumed the cables as ideal force generators. To demonstrate the proposed formulation, static workspace analysis is performed on a human shoulder system with the Hill-type physiological muscle model. Section 8.1 presents the motivations for the workspace analysis of musculoskeletal systems by reviewing the existing approaches in the study of human range of motion. The definition of the static workspace for musculoskeletal systems is proposed in Section 8.2. Section 8.3 describes the method to generate the musculoskeletal workspace. The demonstration of the static workspace analysis on the human shoulder system is presented in Section 8.4. Validation of the formulation is performed by comparing the generated shoulder workspace to the range of motion from human benchmarks. The novel formulation provides a new computational approach to perform workspace analysis for a wider range of engineered and biological systems. Finally, Section 8.5 concludes the chapter by summarising the contributions.

8.1 Introduction

CDPMs have been regarded as bio-inspired systems [79, 93, 125] due to their structural and actuation similarities with musculoskeletal systems. Firstly, the muscles and bones are anthropomorphically analogous to the cables and rigid links, respectively. Furthermore, both cables and muscles can only provide unilateral actuation. However, one primarily difference between the two types of systems is that the actuation dynamics in

cables and muscles are significantly different.

In robotics, workspace analysis is a tool that allows the manipulator's operational region to be computationally generated. Different types of workspace for CDPMs have been studied, such as *static workspace* [73, 110], *wrench-closure workspace* [9, 31, 43, 47, 69, 73, 92, 108], *wrench-feasible workspace* [17, 19, 42], and *cable-interference-free workspace* [7, 103, 136]. For example, static workspace refers to the set of poses in which the manipulator can achieve static equilibrium, defined as the ability of the manipulator to sustain its own gravity force under no external wrenches. Workspace analysis provides a complete description of the system's operational region with respect to the manipulator pose. Since previous studies have assumed cables as ideal force generators, the conventional workspace analysis techniques for CDPMs cannot be applied onto musculoskeletal systems as the difference in actuation characteristics would result in inaccurately generated workspace.

In biomechanics studies, human joint limits and muscle function identification have been investigated either experimentally or through the simulation of trajectories. Experimental techniques are performed *in vivo* using sensor systems, such as vision systems [48], motion sensors [13, 55, 83] or electromyography [126], to record the motion of human subjects performing prescribed or random trajectories. There are two major limitations in this experimental approach. Firstly, the recorded motion only represents a subset of the complete operational region, since poses that are not observed do not imply that they are unreachable by the subject. Secondly, this approach does not allow the effects of changes in muscle properties and their attachment locations on the operational region to be studied. Existing computational tools for biomechanics focus on the dynamics of the musculoskeletal system along a prescribed trajectory. While allowing the possibility to simulate the effects of modified muscle properties and attachment locations, existing simulation tools are unable to perform workspace analysis to determine the operational region with respect to the system poses.

The primary motivation of this study is to increase the understanding of human biomechanics through the workspace analysis of musculoskeletal systems. Workspace analysis for such systems addresses some of the issues with the existing techniques in

studying the limits of human joints. Firstly, the complete workspace can be computationally determined with respect to the set of system poses, and is not dependent on a sample set of specific trajectories. Secondly, the computational approach allows the contributions and effects of different muscles to be simulated and observed. Compared to motion-based experimental approach performed in [126], static workspace allows the contribution of muscle function to specific regions of the workspace to be directly investigated.

Musculoskeletal workspace analysis can be beneficial for a range of applications in rehabilitation of motion impairment and biomechatronics. In the treatment of post-stroke rehabilitation, the understanding of muscle contributions to the reachable workspace would eventually allow more targeted rehabilitation treatment of motion impairment. In tendon-transfer surgery, the effects of muscle relocation can be computationally simulated. This surgery is performed to help recover the lost range of motion in a subject, for example due to a shoulder rotator-cuff tear.

8.2 Static Workspace Framework

The static workspace framework for a cable-driven manipulator with a generalised state dependent force generator model is presented in this section. Firstly, the static workspace for traditional CDPMs where cables are assumed to be *ideal force generators* is described. Secondly, the static workspace definition is extended to consider a more general cable model where cables are assumed as *state dependent force generators*. The state dependent force generator model possesses the key characteristic that its ability to actuate is dependent on its displacement.

8.2.1 Ideal Force Generator Model

The static workspace (SW) for CDPMs is defined as the set of poses in which the manipulator can sustain its own weight given the cable actuation forces, under no motion ($\dot{\mathbf{q}} = \ddot{\mathbf{q}} = \mathbf{0}$) and external wrenches ($\mathbf{T}_{ext} = \mathbf{0}$). Hence, from the general form of the equations of motion in (3.2), the static workspace for traditional CDPMs can be defined

as

$$SW = \left\{ \mathbf{q} : \mathbf{G}(\mathbf{q}) = -J^T(\mathbf{q})\mathbf{f}, \exists \mathbf{f} \in [\mathbf{0}, \mathbf{f}_{max}] \right\}, \quad (8.1)$$

where $f_{i,max}$ is the maximum force for cable i and $\mathbf{f}_{max} = [f_{1,max} \ f_{2,max} \ \dots \ f_{m,max}]^T \in \mathbb{R}^m$. The workspace definition from (8.1) assumes that the cables are *ideal force generators*, meaning that each cable has the ability to produce any force up to a maximum value for any manipulator pose.

8.2.2 State Dependent Force Generator Model

The assumption of cables as ideal force generators may not be valid in scenarios where the actuator's ability to produce force is dependent on the system states, for example, in physiological or artificial muscles. To perform workspace analysis on this class of systems, a more generalised cable model was introduced in Chapter 7 possessing two key features. Firstly, cables can be considered as *active* or *passive* elements depending on their length. When a cable is active, it can be actuated within a range of positive cable force, such that $0 \leq f_{i,min} \leq f_i \leq f_{i,max}$ for cable i . Otherwise, the cable is passive and constrained to have a fixed actuation force $f_i = f_p \geq 0$. Note that the definition of passive cable in this context does not imply that no force is produced on the cable. Secondly, the active cable force range and passive cable force are also dependent on its cable length at pose \mathbf{q} .

For a system with m cables, $m = m_a + m_p$, where m_a and m_p represent the number of active and passive cables, respectively. Hence, the set of cable forces is comprised of passive and active cable forces $\mathbf{f} = \{\mathbf{f}_a, \mathbf{f}_p\}$, where $\mathbf{f}_a \in \mathbb{R}^{m_a}$ and $\mathbf{f}_p \in \mathbb{R}^{m_p}$ represent the set of active cable forces and the set of passive cable forces, respectively. As a result, the columns of J^T can be rearranged such that

$$J^T \mathbf{f} = \begin{bmatrix} J_a^T & J_p^T \end{bmatrix} \begin{bmatrix} \mathbf{f}_a \\ \mathbf{f}_p \end{bmatrix}, \quad (8.2)$$

where $J_a^T \in \mathbb{R}^{n \times m_a}$ and $J_p^T \in \mathbb{R}^{n \times m_p}$ are constructed from the columns of J^T that represent the projection of active and passive cable forces onto the manipulator motion, respec-

tively.

The minimum and maximum allowable cable force for active cables can be denoted by vectors $\underline{\mathbf{f}}_a \in \mathbb{R}^{m_a}$ and $\overline{\mathbf{f}}_a \in \mathbb{R}^{m_a}$, respectively, and hence $\mathbf{f}_a \in [\underline{\mathbf{f}}_a, \overline{\mathbf{f}}_a]$. As shown in Chapter 7, the force range for active cables and passive cable force for state dependent force generators are dependent on the cable lengths \mathbf{l} and hence the system pose \mathbf{q} . Substitution of the definition of the active and passive Jacobian matrices from (8.2) into the static workspace definition in (8.1) results in a static workspace definition where cables are state dependent force actuators

$$SW^* = \left\{ \mathbf{q} : G(\mathbf{q}) + J_p^T \mathbf{f}_p(\mathbf{q}) = -J_a^T \mathbf{f}_a, \exists \mathbf{f}_a \in [\underline{\mathbf{f}}_a(\mathbf{q}), \overline{\mathbf{f}}_a(\mathbf{q})] \right\}. \quad (8.3)$$

It should be noted that $J_p^T \mathbf{f}_p \in \mathbb{R}^n$ is a known vector at pose \mathbf{q} .

Several key differences between the definition of the static workspace with ideal force generators in (8.1) and state dependent force generators in (8.3) can be observed. Firstly, the set of active cables is always a subset of the cables in the system, resulting in a reduced number of actuators for a system with state dependent force generators compared to that with ideal force generators. Secondly, the force range $\mathbf{f} \in [\mathbf{0}, \mathbf{f}_{max}]$ from (8.1) implies that cables can produce any force within the constant force range for all manipulator poses. In comparison, $\mathbf{f}_a \in [\underline{\mathbf{f}}_a(\mathbf{q}), \overline{\mathbf{f}}_a(\mathbf{q})]$ from (8.3) allows for a varying range of actuator force that is dependent on the manipulator pose. Thirdly, the passive cable forces produce a resultant wrench $J_p^T \mathbf{f}_p$ that must also be counteracted by the cables of the system to achieve static equilibrium.

8.3 Workspace Generation

To generate the static workspace of musculoskeletal systems, the physiological muscle model presented in Chapter 7 is used as the state dependent force generator within workspace definition formulated in Section 8.2.2. The static workspace is generated using a numerical approach. Firstly, Section 8.3.1 presents the algorithm to determine the static workspace with traditional ideal force generator cables. Section 8.3.2 extends the algorithm to allow the workspace of musculoskeletal systems to be generated.

8.3.1 Ideal Force Generator Static Workspace

In the study of CDPMs, the static workspace (8.1) presented in Section 8.2.1 can be generated through analytical or numerical approaches. In numerical approaches, a discrete search space \mathcal{Q} is defined and for each pose $\mathbf{q} \in \mathcal{Q}$, the condition required to be satisfied for the type of workspace is evaluated. Pose \mathbf{q} is considered as being within the static workspace if the condition from (8.1) is satisfied. Equivalently, pose \mathbf{q} is within the static workspace if there exists a solution to the optimisation problem

$$\begin{aligned}\mathbf{f}^* &= \arg \min_{\mathbf{f}} c(\mathbf{f}) \\ \text{s.t. } G(\mathbf{q}) &= -J^T(\mathbf{q})\mathbf{f} \\ \mathbf{0} \leq \mathbf{f} &\leq \mathbf{f}_{max} ,\end{aligned}\tag{8.4}$$

where $c(\mathbf{f})$ is the objective function to resolve the cable force redundancy. Since workspace analysis is only concerned with the existence of solutions to the workspace condition, any cost function $c(\mathbf{f})$ can be used. Observing that the constraints in (8.4) are linear, the linear cost function $c(\mathbf{f}) = \mathbf{b}^T \mathbf{f}$, where $\mathbf{b} \in \mathbb{R}^m$ is any arbitrary non-zero vector, could be selected and (8.4) results in a linear programming problem. As a result, the existence of solutions to (8.4) can be determined in a more computationally efficient manner than if a non-linear cost function was used. The procedure to generate the static workspace for a CDPM with ideal force generators is described in Algorithm 1.

Algorithm 1 Generation of the static workspace SW

Require: Set of search poses \mathcal{Q}
Ensure: Static workspace SW where $SW \subseteq \mathcal{Q}$

```

for all  $\mathbf{q}$  in  $\mathcal{Q}$  do
    if solution  $\mathbf{f}^*$  exists under (8.4) then
        Add  $\mathbf{q}$  to  $SW$ 
    end if
end for
return  $SW$ 

```

From Algorithm 1, it can be observed that the computational complexity of the numerical approach is $O(p^n)$, where n is number of degrees of freedom for the system $\mathbf{q} \in \mathbb{R}^n$ and p is the number of steps in each dimension of \mathcal{Q} . The fundamental operation of the

algorithm is to check for the existence of a solution to (8.4). The advantage of the computational approach is its algorithmic simplicity, as it only requires a linear programming problem to be solved at each pose within the search space. Compared with analytical approaches, the numerical approach suffers from the effects of discretisation, where the accuracy of workspace depends on the resolution of the search space. Furthermore, the computational cost increases significantly as the resolution is increased for systems with a large number of degrees of freedom.

8.3.2 Musculoskeletal Static Workspace

The static workspace SW^M can be determined by extending the method for ideal force generators presented in Section 8.3.1. The pose \mathbf{q} is considered as being within the musculoskeletal static workspace SW^M if the condition from (8.3) is satisfied, where the physiological muscle model presented in Chapter 7 is the state dependent force generator. Similar to (8.4), the pose \mathbf{q} is within the musculoskeletal static workspace if there exists a solution to the optimisation problem

$$\begin{aligned} \mathbf{f}_a^* &= \arg \min_{\mathbf{f}_a} \mathbf{b}^T \mathbf{f}_a \\ \text{s.t. } & G(\mathbf{q}) + J_p^T \mathbf{f}_p = -J_a^T \mathbf{f}_a \\ & \underline{\mathbf{f}}_a \leq \mathbf{f}_a \leq \bar{\mathbf{f}}_a \end{aligned}, \quad (8.5)$$

where $\mathbf{b} \in \mathbb{R}^{m_a}$ can be any arbitrary non-zero vector.

For the musculoskeletal workspace, the active and passive elements from (8.5) correspond to the active and passive muscles at a particular system pose. The determination of the sets of active and passive muscles, the active muscle force range and the passive muscle force was described in Section 8.2.2, and represents the actuation characteristics for the state dependent force generator. The muscle-tendon lengths are analogous to the lengths of the cables, and can be determined from the system kinematics. Using the muscle properties for a particular muscle, the minimum and maximum active lengths can be determined from (7.10) and (7.13), respectively. A cable is considered active if its length is between $l_{a,min}^{mt} < l^{mt} < l_{a,max}^{mt}$, otherwise it is regarded as a passive element.

The columns in J^T for the active muscles form the columns within the transpose of the active Jacobian matrix J_a^T in (8.2). The minimum and maximum active muscle forces from (7.14) for the set of active muscles form the vectors $\underline{\mathbf{f}}_a$ and $\bar{\mathbf{f}}_a$ within the workspace framework (8.5), respectively. Similarly, the columns in J^T for the passive muscles and the passive muscle force from (7.17) form the columns of J_p^T and elements of \mathbf{f}_p within the framework, respectively. Algorithm 2 summarises the procedure in determining the static workspace for musculoskeletal systems incorporating the physiological muscle model.

Algorithm 2 Generation of the musculoskeletal static workspace SW^M

Require: Search poses \mathcal{Q} and l^{mt}, J^T for each $\mathbf{q} \in \mathcal{Q}$
Ensure: Musculoskeletal static workspace SW^M where $SW^M \subseteq \mathcal{Q}$

```

for all  $\mathbf{q}$  in  $\mathcal{Q}$  do
    for  $i = 1, \dots, m$  do
         $l_{min}^{mt} \leftarrow \min$  active  $l^{mt}$  (7.10) from muscle  $i$  properties
         $l_{max}^{mt} \leftarrow \max$  active  $l^{mt}$  (7.13) from muscle  $i$  properties
        if  $l_{min}^{mt} < l^{mt} < l_{max}^{mt}$  then
            Add column  $i$  of  $J^T$  to  $J_a^T$ 
            Add  $F_{min}^{mt}$  and  $F_{max}^{mt}$  from (7.14) to  $\bar{\mathbf{f}}_a$  and  $\underline{\mathbf{f}}_a$ , respectively
        else
            if  $l^{mt} \leq l_{min}^{mt}$  then
                 $F_p = 0$ 
            else if  $l^{mt} \geq l_{max}^{mt}$  then
                 $F_p = F^{mt}$  from (7.17) with muscle  $i$  properties
            end if
            Add  $F_p$  to  $\mathbf{f}_p$ 
            Add column  $i$  of  $J^T$  to  $J_p^T$ 
        end if
    end for
    if solution  $\mathbf{f}_a$  exists under (8.5) then
        Add  $\mathbf{q}$  to  $SW^M$ 
    end if
end for
return  $SW^M$ 

```

The computational complexity of musculoskeletal static workspace from Algorithm 2 is equivalent to that of the static workspace generation for CDPMs with ideal force generators. In the generation of the static workspace for musculoskeletal systems, numerical approaches are more suitable than analytical approaches due to the active muscle force

ranges and passive muscle forces' dependency on the system pose \mathbf{q} . As such, it may be difficult to produce an analytical solution to the muscle forces and hence the static workspace. On the other hand, the state dependency does not increase the computational complexity in solving for the workspace using numerical approaches as (8.5) is solved for each pose $\mathbf{q} \in \mathcal{Q}$.

8.4 Static Workspace of the Human Shoulder

To demonstrate the musculoskeletal static workspace framework formulated in Section 8.2 and the algorithm to generate the workspace presented in Section 8.3, the musculoskeletal static workspace for a human shoulder is generated and presented in this section.

8.4.1 Shoulder Model

The human shoulder is comprised of three major bones: the *clavicle*, the *scapula* and the *humerus* bones, and one major joint: *glenohumeral* joint. Figure 8.1 shows the OpenSim shoulder model [50] used to obtain the kinematics required to generate the musculoskeletal static workspace for the shoulder.

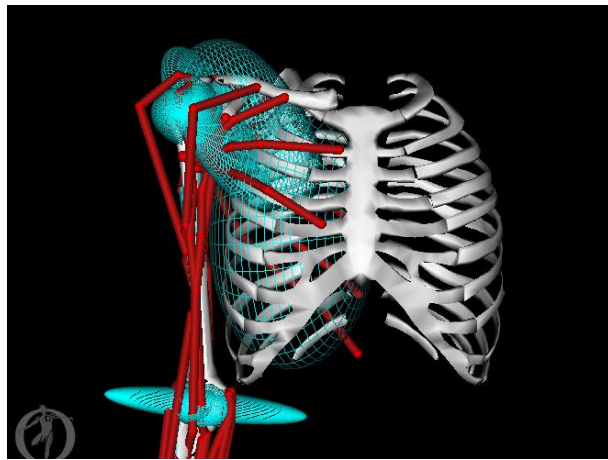


Figure 8.1: The OpenSim model of the human shoulder comprised of the *glenohumeral* joint, *humerus bone* and the major muscles that contribute to shoulder motion.

The developed model [50] for OpenSim [27] is a well accepted model of the human shoulder. The musculoskeletal model was constructed with the aid of clinical and exper-

imental data on human cadavers. The model considers the kinematics of the *clavicle* and *scapula* bone motion, and the wrapping of muscles. These are important in order to obtain accurate muscle kinematics, such as the length, origin and insertion locations. Figure 8.2 shows the kinematics of the human shoulder used in the musculoskeletal workspace analysis. The *humerus* bone can be regarded as the end-effector of the system and is connected to the base through the *glenohumeral* joint.

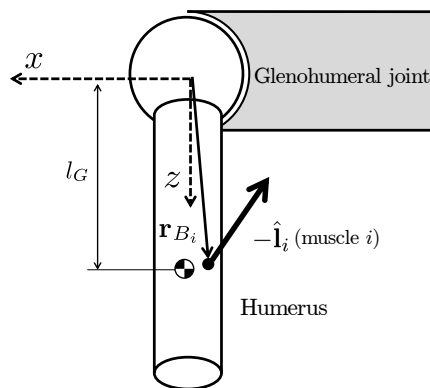


Figure 8.2: Diagram of shoulder model showing the *humerus* bone and the *glenohumeral* joint. The pose of the *humerus* can be described by $\mathbf{q} = [\alpha \ \beta \ \gamma]^T$, where α , β , and γ represent the *xyz*-Euler angles of the *glenohumeral* joint.

The system can be regarded as possessing three degrees-of-freedom and the pose of the system can be represented by $\mathbf{q} = [\alpha \ \beta \ \gamma]^T$, where α , β , and γ represent the *xyz*-Euler angles of the *glenohumeral* joint, respectively. In the study of biomechanics, the rotations in the x , y and z axes correspond to physiologically meaningful rotations. Table 8.1 describes the physical meaning for the positive and negatives rotations in α , β and γ .

Figure 8.3 shows the physical interpretation of the different shoulder motion directions. As shown in Figure 8.3(a), shoulder flexion and extension correspond to the forward and backward swinging of the arm in the sagittal plane, respectively. The outward swinging of the arm in the frontal plane, as shown in Figure 8.3(b), corresponds to the abduction motion of the shoulder complex. Finally, the external and internal rotation corresponds to the outward and inward rotations of the shoulder, respectively, as shown in Figure 8.3(c).

Pure rotation	Physiological meaning
$+\alpha$	flexion
$-\alpha$	extension
$+\beta$	abduction
$-\beta$	adduction
$+\gamma$	external rotation
$-\gamma$	internal rotation

Table 8.1: Rotations of the *glenohumeral* joint and its physiological meaning.

Property	Parameter	Value
Distance to centre of mass	l_G	0.135 m
Mass	m	1.276 kg
Moment of inertia about x	I_{xx}	0.0105 kg·m ²
Moment of inertia about y	I_{yy}	0.0105 kg·m ²
Moment of inertia about z	I_{zz}	0.0013 kg·m ²

Table 8.2: Mass and inertia properties of the shoulder model.

The mass, inertia and length values reported from [144] were used in the modelling of the shoulder for the musculoskeletal workspace analysis, and are shown in Table 8.2. The distance from the *glenohumeral* joint centre to the centre of mass is denoted by l_G .

The model for the shoulder consists of 9 muscle groups that have been identified as the main contributors to shoulder motion [50]: *deltoid (anterior, middle, posterior)*, *supraspinatus*, *infraspinatus*, *subscapularis*, *teres minor*, *teres major*, *pectoralis major (clavicular, sternal, ribs)*, *latissimus dorsi (thoracic, lumbar, iliac)* and *coracobrachialis*. Muscles such as *deltoid*, *pectoralis major* and *latissimus dorsi* are typically divided into separate sub-regions. As a result, the shoulder system can be modelled by a total of $m = 15$ muscle elements. The muscle properties F_0^m , l_0^m , l_s^t and α_0 for each muscle sub-region were obtained from [50] and are shown in Table 8.3.

For the shoulder system, the transpose of the Jacobian matrix can be expressed as

$$J^T = \left[\begin{array}{cccc} \mathbf{r}_{B_1} \times \hat{\mathbf{l}}_1 & \mathbf{r}_{B_2} \times \hat{\mathbf{l}}_2 & \dots & \mathbf{r}_{B_{15}} \times \hat{\mathbf{l}}_{15} \end{array} \right]. \quad (8.6)$$

As shown in Figure 8.2, the vectors \mathbf{r}_{B_i} and $\hat{\mathbf{l}}_i$ represent the insertion location and the di-

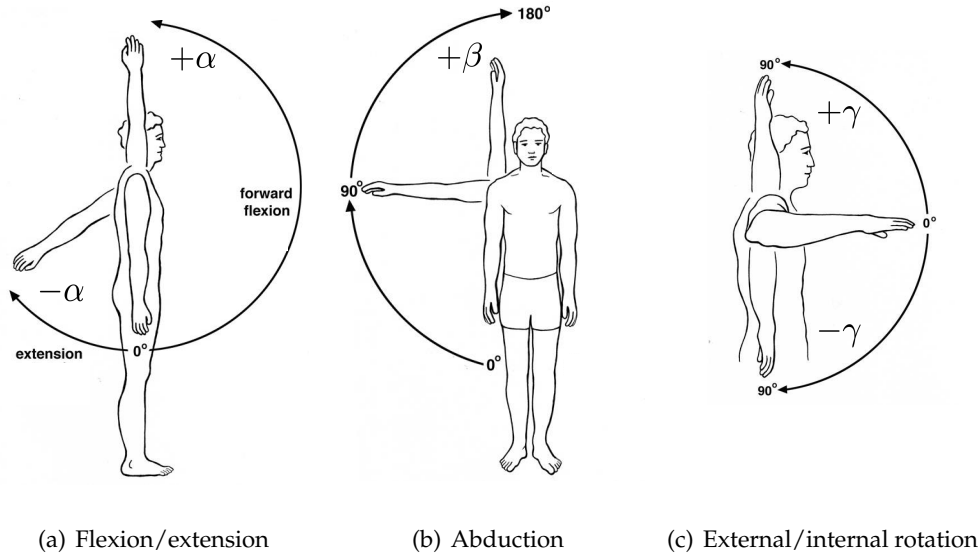


Figure 8.3: The primary directions of motion for the human shoulder [127]. Flexion/extension (a) corresponds to the forward and backward swinging of the arm in the sagittal plane. Abduction (b) corresponds to the outward swinging of the arm in the frontal plane. External/internal rotation (c) corresponds to the outward and inward twisting of the *humerus* bone.

rection vector of the insertion to the *humerus*, respectively, for muscle i . To obtain the accurate muscle-tendon lengths and system Jacobian matrix, the OpenSim shoulder model was used [50]. The muscle-tendon length l_i^{mt} and the vectors \mathbf{r}_{B_i} and $\hat{\mathbf{l}}_i$ were obtained through the OpenSim API library by specifying the pose of the shoulder. As a result, the generated workspace takes into consideration the complexities of the shoulder motion, such as kinematic constraints due to the *glenohumeral* joint, the wrapping of muscles, and the realistic movements of the *scapula* and *clavicle* bones.

To remain consistent with the limitations in the range of motion from the OpenSim shoulder model [50], the search space for the static workspace \mathcal{Q} was defined as $\alpha \in [-180^\circ, 180^\circ]$, $\beta \in [0, 180^\circ]$ and $\gamma \in [-90^\circ, 90^\circ]$. The search region was uniformly discretised into a grid with a grid-size of $\Delta\alpha = \Delta\beta = \Delta\gamma = 1^\circ$. The musculoskeletal static workspace was generated through Algorithm 2, where the muscle-tendon length l_i^{mt} , insertion location \mathbf{r}_{B_i} and muscle insertion direction $\hat{\mathbf{l}}_i$ for every muscle were obtained directly from the OpenSim API. Figure 8.4 shows how the OpenSim API is used in the

		F_0^m [N]	l_0^m [m]	l_s^t [N]	α_0 [rad]
<i>Deltoid</i>	<i>anterior</i>	1142.60	0.0976	0.0930	0.3840
	<i>middle</i>	1142.60	0.1078	0.1095	0.2618
	<i>posterior</i>	259.88	0.1367	0.0380	0.3142
<i>Supraspinatus</i>		487.82	0.0682	0.0395	0.1222
	<i>Infraspinatus</i>	1210.84	0.0755	0.0308	0.3229
	<i>Subscapularis</i>	1377.81	0.0873	0.0330	0.3491
	<i>Teres minor</i>	354.25	0.0741	0.0713	0.4189
	<i>Teres major</i>	425.39	0.1624	0.0200	0.2793
<i>Pectoralis</i>	<i>clavicular</i>	364.41	0.1442	0.0028	0.2967
	<i>sternal</i>	515.41	0.1385	0.0890	0.4363
	<i>ribs</i>	390.55	0.1385	0.1320	0.4363
<i>Latissimi dorsi</i>	<i>thoracic</i>	389.10	0.2540	0.1200	0.4363
	<i>lumbar</i>	389.10	0.2324	0.1765	0.3316
	<i>iliac</i>	281.66	0.2789	0.1403	0.3665
<i>Coracobrachialis</i>		242.46	0.0932	0.0970	0.0000

Table 8.3: The muscle properties for the major muscles responsible for shoulder motion.

proposed method.

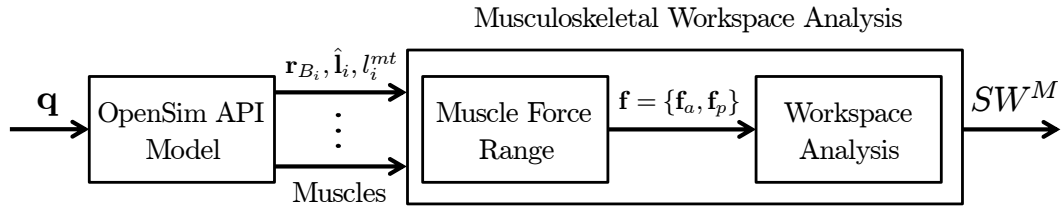


Figure 8.4: Components of the proposed musculoskeletal static workspace analysis.

To illustrate the impact of the physiological muscle on the resulting workspace, the static workspace of an analogous traditional CDPM for the same search space was generated using Algorithm 1. Similarly, the insertion location r_{B_i} and muscle insertion direction \hat{l}_i for the muscles were obtained from the OpenSim model [50]. The maximum force $f_{i,max}$ for cable i was assumed to be the peak isometric force F_0^m for muscle i .

8.4.2 Results

The musculoskeletal static workspace for the human shoulder was generated for the setup described in Section 8.4.1. In the same manner to determine the muscle forces for the *deltoid anterior* and *supraspinatus* muscles shown in Section 7.4, the force ranges for the entire set of shoulder muscles were solved at each pose in \mathcal{Q} . The musculoskeletal workspace was compared with the workspace for an analogous CDPM with ideal force generators. Cross-sections of the workspace for both musculoskeletal and cable-driven shoulder systems are shown in Figure 8.5.

Figure 8.5 shows the α - β cross-sections of the workspace for varying values of gamma $\gamma = -3^\circ, 0^\circ, 3^\circ$. The musculoskeletal static workspace SW^M is shown in Figures 8.5(a), 8.5(c) and 8.5(e), and the static workspace for the cable-driven system SW is shown in Figures 8.5(b), 8.5(d) and 8.5(f).

From the α - β cross-sections, it can be observed that the workspace for the cable-driven system SW with ideal force generators is significantly larger than that of the musculoskeletal system SW^M with the Hill-type muscle model. To quantify this observation, the workspace volumes for the two systems were compared. From the total number of poses that define the discretised search space \mathcal{Q} , the volumes of SW^M and SW were computed to be 82.8% and 98.7% of the total number of poses in \mathcal{Q} , respectively.

Intuitively, it appears that SW^M is a more accurate representation of the human shoulder workspace than SW . The workspace obtained from the ideal force generator model appears to overrepresent the operational region of the shoulder. For example, consider the differences in workspace in the lower left region between SW^M and SW , as shown in Figure 8.5. Figures 8.5(a), 8.5(c) and 8.5(e) suggest that the human shoulder is unable to perform extension motion beyond 29° . On the other hand, the workspace SW from Figures 8.5(b), 8.5(d) and 8.5(f) for the ideal force generator indicates that the system is able to perform an unrealistic amount of extension motion of 114° .

To justify these observations, the musculoskeletal workspace was compared to the range of motion (ROM) benchmarks for the human shoulder from the literature [6, 10, 13, 35, 55]. From the generated workspace of the musculoskeletal and cable-driven systems, the limits for the ROM can be obtained by observing the boundaries between the accepted

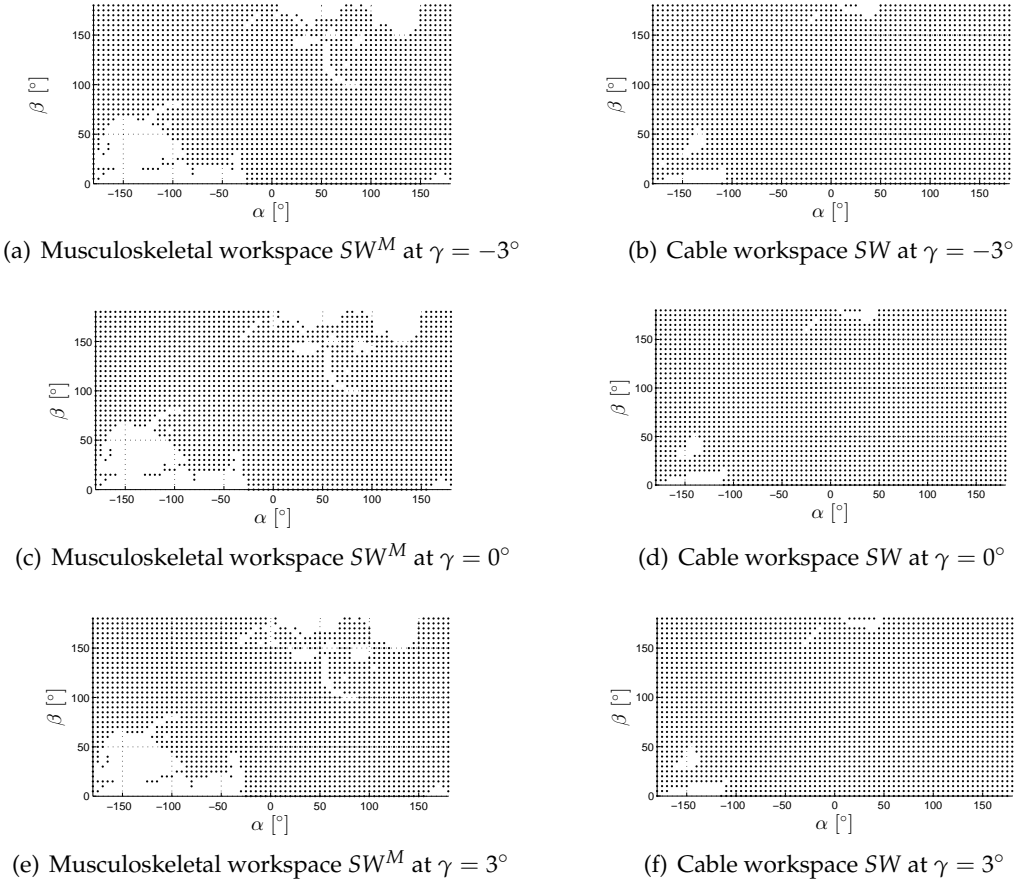


Figure 8.5: α - β cross-sections of the static workspace for the shoulder system from the musculoskeletal workspace analysis and CDPM workspace analysis.

and rejected regions of the workspaces. Table 8.4 shows the comparison in the ROM for flexion, extension, abduction, horizontal flexion, horizontal extension and horizontal abduction. Horizontal flexion and extension refer to the motion in flexion and extension after an initial 90° abduction. Horizontal abduction corresponds to the abduction motion after an initial 90° flexion then 90° abduction of the shoulder.

It should be noted that the ROM for internal and external rotations have been omitted in the comparison since the OpenSim shoulder model [50] only describes the kinematics for the rotation range $\gamma \in [-20^\circ, 90^\circ]$. It could be observed from Table 8.4 that the internal and external rotation ROMs exceed the allowable range in the shoulder model.

The flexion/extension ROM limits can be determined from the minimum and max-

Motion	SW	SW^M	Reported Human Benchmarks
Flexion	180°	158°	$167^\circ \pm 9^\circ$
Extension	114°	29°	$60^\circ \pm 7^\circ$
Abduction	180°	180°	$179^\circ \pm 9^\circ$
Horizontal Flexion	180°	180°	$138^\circ \pm 2^\circ$
Horizontal Extension	180°	90°	45°
Horizontal Abduction	180°	51°	45°
Internal rotation	O/R^*	O/R^*	$56^\circ \pm 14^\circ$
External rotation	O/R^*	O/R^*	$98^\circ \pm 7^\circ$

Table 8.4: The range of motion limit of the human shoulder obtained from the CDPM workspace SW , the musculoskeletal workspace SW^M and reported human benchmark data. *O/R denotes that motion range is outside that allowed by the Holzbaur OpenSim model [50]

imum values of α that define the workspace boundary for zero rotation $\gamma = 0$ and abduction $\beta = 0$. From Figure 8.5(c), it can be observed that the minimum value for α at $\beta = \gamma = 0^\circ$ is $\alpha = -29^\circ$ and the maximum value is $\alpha = 158^\circ$, corresponding to the ROM limits for extension and flexion as 29° and 158° , respectively. Comparing to the benchmark data, it can be observed that the ROM from the musculoskeletal workspace is similar to the ROM of the human shoulder. In comparison, the ROM obtained from the cable-driven system (Figure 8.5(c)) is significantly larger than that from SW^M and the human benchmarks. The overestimation is most apparent in the extension and horizontal abduction directions, where the ROM limits for SW are 114° and 180° , respectively.

In a similar manner, the ROM limits for abduction can be observed from the boundary in the β direction of the musculoskeletal workspace for $\alpha = 0$. However, it is known that small amounts of rotation naturally occurs while measuring the range of motion for abduction in human studies [6]. Hence, small amounts of internal/external rotation $-3^\circ \leq \gamma \leq 3^\circ$ were allowed in obtaining limits in abduction for SW^M and SW . From Figures 8.5(a) and 8.5(b), the abduction ROM obtained for SW^M and SW were both 180° , the maximum possible ranges from kinematic model, and is consistent with the ROM from the benchmark data for the human shoulder.

From the workspace cross-sections in Figure 8.5 and ROM comparison in Table 8.4,

Property	SW^M	SW
Mean error	22.5°	63.2°
Standard deviation of error	19.4°	58.7°
Range of error	$1^\circ - 45^\circ$	$1^\circ - 135^\circ$

Table 8.5: The range of motion (ROM) errors between the generated workspaces (SW^M and SW) with the benchmark data.

the results suggest that the proposed formulation is able to produce a realistic and physically meaningful workspace for the human shoulder. To quantify this observation, the mean and standard deviation in the ROM errors between the generated workspace and benchmark data for both SW^M and SW are compared. From Table 8.4, the mean and standard deviation of the error in the ROM for the generated musculoskeletal static workspace SW^M compared to the benchmark data are computed to be 22.5° and 19.4° , respectively. In comparison, the mean error and standard deviation for the ideal force generator model SW are 63.2° and 58.7° , respectively. Furthermore, the range of error for SW^M is 1° to 45° while for SW is 1° to 135° . Table 8.5 summarises this comparison in the ROM error and Figure 8.6 shows the box plots of the errors for SW^M and SW .

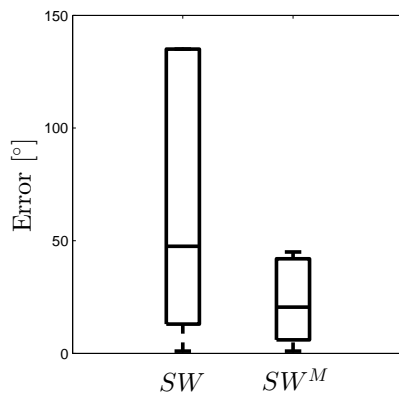


Figure 8.6: Box plot of the ROM errors between the generated workspaces (SW^M and SW) with the benchmark data showing the mean and range of the error.

The low mean, standard deviation and range in the ROM errors compared with benchmark data suggest that the proposed musculoskeletal workspace analysis technique is able to produce a realistic static workspace for the human shoulder. Further-

more, the significance in the inclusion of the physiological muscle as the state dependent for generator is demonstrated in the lower errors compared with that using the traditional ideal force generator cable model.

The inclusion of the physiological muscle model impacts the musculoskeletal static workspace SW^M in several ways, and can aid to explain the observed overestimation of SW compared with SW^M . Firstly, the range of muscle force for an active muscle $[F_{min}^{mt}, F_{max}^{mt}]$ is typically a subset of the range for an ideal force generator cable $[0, F_0^m]$. From Figure 7.5, this can be observed to be true for a majority of the muscle-tendon lengths. As such, the ability of the active muscles to achieve static equilibrium compared with ideal force generators is reduced. Secondly, as described in Section 8.2.2, a physiological muscle may become a passive element depending on its muscle-tendon length. Hence, the set of active muscles may become a subset of the ideal force generators for cable-driven systems. As a result, the available number of force producing actuators to achieve static equilibrium may be reduced.

Despite the apparent overestimation observed, it should be noted that SW^M is not strictly a subset of SW . This can be attributed to the two following factors: firstly, since $[\bar{\mathbf{f}}_a, \bar{\mathbf{f}}_a]$ is not strictly a subset of $[0, \mathbf{f}_{max}]$, particularly for muscle lengths close to $l_{a,max}^{mt}$; secondly, the effects of the passive muscles should also be considered. From Figure 7.6, it can be observed that the passive muscle force can be regarded as a significant component of the muscle-tendon force for muscle lengths $l^{mt} > l_{a,max}^{mt}$. In particular poses, the passive muscle forces result in no muscle forces solution to maintain static equilibrium. But in other poses, the resultant force from the passive muscles may counteract the gravity force and hence assist in achieving static equilibrium.

Workspace analysis of biological systems is an alternative and novel approach in studying the operational region of musculoskeletal systems. Compared with traditional experimental approaches in biomechanics studies, the proposed approach allows the poses in which the system is considered as operational to be computationally generated. Obtaining the complete workspace region may be difficult to obtain experimentally, as it requires the human subject to perform the motion for all possible trajectories.

As a result, the proposed approach may be beneficial in a range of biomechanics, reha-

bilitation and biomechatronic applications. It is possible to gain an increased understanding in the contribution of muscles to shoulder motion from the analysis of workspace. For example, it can be observed from Figure 7.9 that the *deltoid anterior* muscle becomes passive at $\alpha = -50^\circ$. In the range $-45 \leq \alpha \leq -30^\circ$ the muscle is capable of producing only a very limited range of force. Since the *deltoid anterior* muscle is known as a major contributing muscle to extension motion, it can be hypothesised that the SW^M extension limit of 29° is due to the fact that the *deltoid anterior* muscle reaches toward the passive region.

The computational approach allows the impact of changes in the muscles, such as muscle properties and attachment locations, and hence muscle function on the workspace to be predicted. Muscle function refers to the role of muscles in contributing to the motion of a musculoskeletal system. One method to observe muscle function is to consider the muscle forces required to perform a prescribed trajectory. An alternative approach is to consider particular muscles to be passive and observe the range of motion that is lost. By considering a muscle as a passive element, it is assumed that the muscle is still attached within the system but cannot be activated. Through workspace analysis, the contributions of different muscles to the regions of the workspace can be computationally studied.

For example, consider the role of the *deltoid* muscles to the workspace of the shoulder. The function of the *deltoid* muscle group can be examined by setting the *deltoid anterior*, *deltoid middle* and *deltoid posterior* sub-regions to be passive muscles. The comparison between the static workspace of a shoulder with passive *deltoid* muscles and the static workspace with the original set of muscles SW^M is shown in Figure 8.7. The α - β cross-sections of the musculoskeletal static workspace with the *deltoid* muscle group set as passive at $\gamma = -3^\circ$, $\gamma = 0^\circ$ and $\gamma = 3^\circ$ are shown in Figures 8.7(a), 8.7(c) and 8.7(e), respectively. Comparing the α - β workspace cross-sections for the passive *deltoid* muscles with that for the original set of shoulder muscles, shown in Figures 8.7(b), 8.7(d) and 8.7(f), several significant differences in workspace can be observed. Firstly, a large section of the workspace in the abduction (positive β direction) range of motion was lost when the *deltoid* muscles were set as passive. As a result, the range of motion in abduction

decreased from the $[0^\circ, 180^\circ]$ to $[0^\circ, 61^\circ]$. Secondly, a larger region of the backward extension (negative α direction) static workspace was also lost. As a result, the range of motion for pure extension decreased from $[0^\circ, 29^\circ]$ to $[0^\circ, 22^\circ]$. Thirdly, the range of motion for horizontal flexion, horizontal extension and horizontal abduction are also lost if the *deltoid* muscles are passive. These observations are consistent with previous biomechanical studies that the *deltoid* muscle group contributes to the extension and abduction motions of the shoulder complex [114, 118].

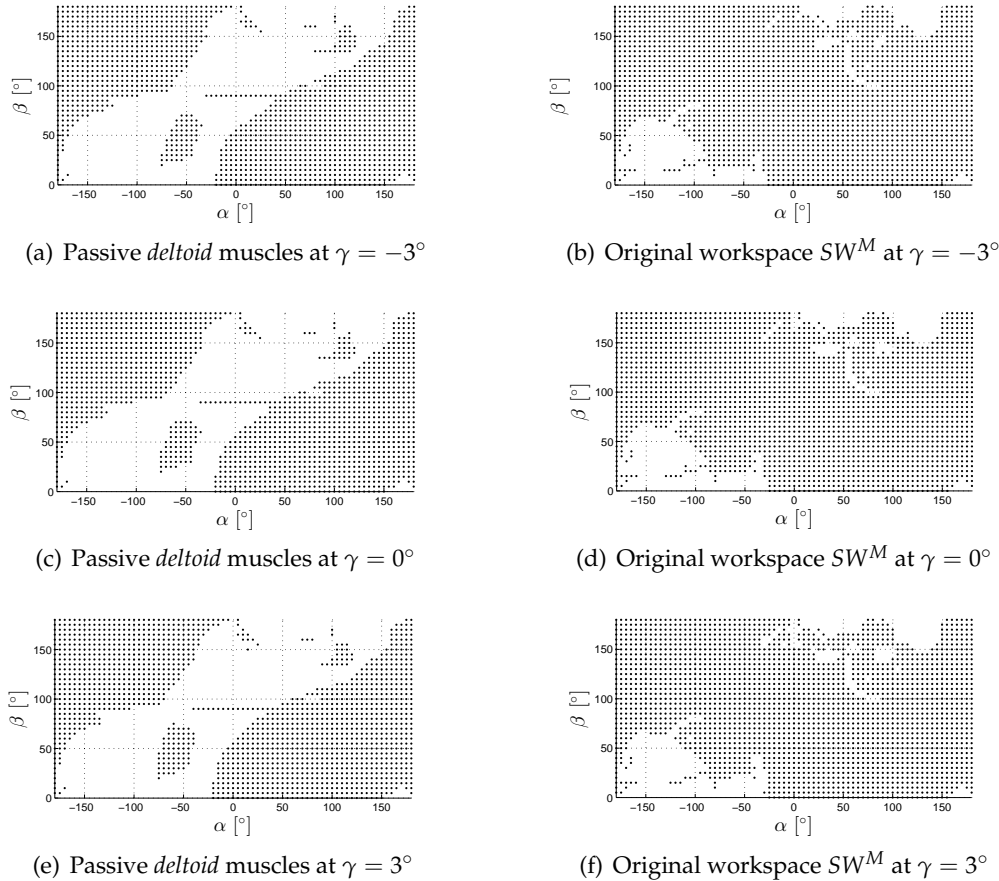


Figure 8.7: α - β cross-sections (a), (c), (e) of the static workspace for the shoulder system with the *deltoid* muscle groups set as passive elements. These are compared with the α - β cross-sections (b), (d), (f) of the static workspace SW^M with no passive muscles.

Similarly, the function of the *pectoral* muscle group can be studied by assuming that the *pectoral clavicular*, *pectoral sternal* and *pectoral ribs* muscles are passive. The comparison between the static workspace of a shoulder with passive *pectoral* muscles and the static

workspace with the original set of muscles SW^M is shown in Figure 8.8. The α - β cross-sections of the musculoskeletal static workspace with the *pectoral* muscle group set as passive at $\gamma = -3^\circ$, $\gamma = 0^\circ$ and $\gamma = 3^\circ$ are shown in Figures 8.8(a), 8.8(c) and 8.8(e), respectively. Compared to the static workspace of the shoulder with the original set of shoulder muscles, shown in Figures 8.8(b), 8.8(d) and 8.8(f), a less significant difference in workspace can be observed compared with that for the original set of muscles.

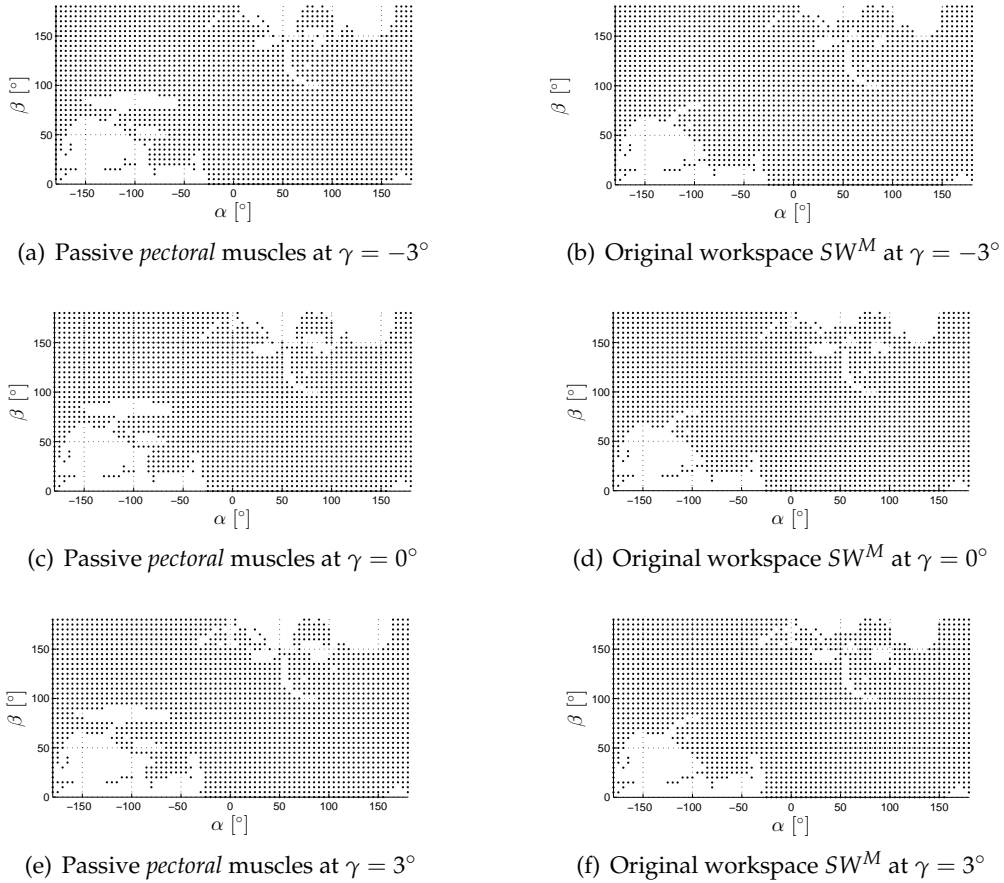


Figure 8.8: α - β cross-sections (a), (c), (e) of the static workspace for the shoulder system with the *pectoral* muscle groups set as passive elements. These are compared with the α - β cross-sections (b), (d), (f) of the static workspace SW^M with no passive muscles.

However, the impact on the ROM can be observed in horizontal flexion and horizontal extension. Table 8.6 compares the differences in the range of motion for passive *deltoid* and passive *pectoral* muscles with that of the musculoskeletal workspace SW^M possessing the original set of muscles. Similarly, the function of the muscles and groups of muscles

Motion	Original muscles	No deltoid	No pectoral
Flexion	[0°, 158°]	[0°, 158°]	[0°, 158°]
Extension	[0°, 29°]	[0°, 22°]	[0°, 29°]
Abduction	[0°, 180°]	[0°, 61°]	[0°, 180°]
Horizontal Flexion	[0°, 180°]	[22°, 154°]	[0°, 95°]
Horizontal Extension	[0°, 90°]	[36°, 67°]	[0°, 72°]
Horizontal Abduction	[0°, 51°]	[0°, 22°]	[0°, 51°]

Table 8.6: The range of motion (*ROM*) of the human shoulder from the musculoskeletal static workspace with passive *deltoid* and *pectoral* muscle groups. Values in bold denote that the ROM has decreased.

for a musculoskeletal system can be studied by observing the static workspace when muscles are set as passive.

In addition to the study of muscle function through setting particular muscle groups to be passive, changes in the workspace due to the relocation of muscle attachments or variation in the muscle properties can also be studied. For example, the effect of an injury, such as rotator cuff tear, can be studied by comparing the resulting workspace with that of a healthy subject. Another example is tendon-transfer surgery, where workspace analysis allows the effectiveness of the proposed muscle attachment relocations to be quantitatively evaluated prior to performing the surgery.

The proposed static workspace formulation is a generic framework that allows for arbitrary joint and actuation models. The formulation does not make any assumptions on the system model defined in (3.2). Furthermore, the generic actuator model allows for any state dependent force generators that can behave as both active and passive elements. The presented muscle and tendon force relationships within the Hill-type muscle model can be redefined depending on the type of actuator. Although the formulation has only been validated for a human shoulder, the generic approach allows the potential to study and validation of other musculoskeletal systems. As a result, the proposed method allows the static workspace for a much wider range of engineered and biological systems to be studied.

8.5 Conclusion

In this chapter, the formulation for the static workspace of musculoskeletal systems was presented. The musculoskeletal static workspace was formulated by extending from traditional CDPM static workspace analysis and incorporating state dependent force generators as the cables within the system. It was shown that the definition of the musculoskeletal static workspace must consider the characteristics of the state dependent force generator. Firstly, the muscle can behave as an active or a passive element, and secondly, the range of actuation force is dependent on the system pose. The impact of the physiological muscle model on the musculoskeletal static workspace was demonstrated by generating the static workspace for the human shoulder. Comparing the ROM of the musculoskeletal static workspace to human benchmark data, it was apparent that the inclusion of the muscle model results in a more realistic human workspace than that from using ideal force generators. As a result, the ability to computationally study musculoskeletal systems as CDPMs, such as static workspace analysis, would be beneficial for a wide range of biomechanics, rehabilitation and biomechatronic applications.

This page is intentionally left (almost) blank.

Chapter 9

Conclusion and Future Direction

In this chapter, the thesis is concluded with a summary of the contributions in Section 9.1 and an outlook on the future directions for this study in Section 9.2.

9.1 Conclusion

In this thesis, the study on the modelling and analysis of anthropomorphic cable-driven robots was presented. The primary goal of this work was to develop a generalised model of anthropomorphic cable-driven parallel manipulators (CDPMs) for both engineering applications and biomechanics studies. This goal was motivated by the structural and actuation similarities between musculoskeletal systems and multilink cable-driven manipulators (MCDMs).

From the review of the state of the arts in CDPMs in Chapter 2, three main research questions were identified.

1. How can MCDMs be modelled such that all of the combinations in cable routing are encapsulated within a single model and representation?
2. How can the analysis of single link CDPMs be extended and applied to generalised MCDMs?
3. How can analysis techniques developed for robotic CDPM systems be extended and applied to musculoskeletal systems to provide a greater understanding in biomechanics?

In Chapter 4, the Cable-Routing Matrix (CRM) was introduced as a generalised representation for cable routing for arbitrarily structured branched MCDMs. The CRM allows arbitrary cable routing to be described within a single representation. As a result, the

CRM resolves a major challenge in modelling arbitrary cable routing for MCDMs possessing a large number of links. It was shown that a generalised definition of the cable segment vector, fundamental to the modelling of MCDMs, can be formulated using the CRM. Using the generalised cable routing, generalised kinematic and dynamic MCDM models were formulated in Chapter 5. The generalised model is a single representation that allows arbitrary cable routing for any open-chain branched rigid body structure. To demonstrate the proposed model, the dynamics for an 8 link 24 degree-of-freedom (*DoF*) human neck inspired MCDM actuated by 76 cables was simulated. The proposed formulation provides the fundamental model for the analysis of arbitrarily complex MCDMs.

To demonstrate the analysis of MCDMs using the generalised model, Chapter 6 derived the necessary conditions required to achieve wrench-closure validity for MCDMs. Wrench-closure validity is important property in the design of CDPMs. Manipulators that cannot not satisfy wrench-closure in any pose would result in a very limited range of motion. Extending from the analysis of single link CDPMs, it was shown that necessary conditions could be derived with respect to the CRM regardless of the exact attachment locations. The derived necessary conditions were demonstrated on single link, two link and three link MCDMs. The examples illustrated how the necessary conditions on the CRM can be used to validate the arrangement of the cables. Furthermore, this study demonstrated the convenience in performing analysis on the CRM based generalised model, as the derived results apply to all types of MCDMs and cable routing.

In all previous studies of CDPMs, cables were assumed to be ideal force generators. However, this assumption is not valid for a range of systems, such as for those actuated by pneumatic artificial muscles and musculoskeletal systems with physiological muscles. As a result, analysis techniques developed for CDPMs would yield unreasonable results on these state dependent force generator systems. In Chapter 7, a more general cable model that allows state dependent force generation was presented. Using the physiological hill-type muscle model, it was shown that it was possible to derive the feasible force range that the muscle could generate for a given manipulator pose. Using the state dependent force generator model, the static workspace analysis for musculoskeletal systems was formulated in Chapter 8. The static workspace analysis is extended beyond

traditional CDPMs by incorporating the more generalised cable actuator model, where cables could be active or passive and produce a range of force depending on their length. The impact of the physiological muscle model on the musculoskeletal static workspace was demonstrated by studying the workspace for a human shoulder. From comparisons in the range of motion (ROM) of the generated workspace to shoulder ROM benchmarks, it was apparent that the inclusion of the state dependent force generator resulted in a more realistic workspace. The ability to realistically apply computational techniques developed for CDPMs to musculoskeletal systems is beneficial for a wide range of robotics and biomechanics applications.

In addressing the main research questions, the fundamental components required in the study of anthropomorphic cable-driven manipulators have been presented. In the thesis, the generalisations of arbitrary cable routing, rigid body structure for MCDMs and the cable actuator model have been addressed. This allows the analysis of a wider range of MCDM systems and is beneficial to both robotics and biomechanics communities. The proposed state dependent force generator model, arbitrary cable routing and the generalised MCDM model demonstrates the potential to study biomechanical systems as MCDMs. For example, the study of static workspace for the human shoulder is an example of a traditional CDPM analysis technique applied to musculoskeletal systems.

9.2 Future Directions

The contributions in this thesis have created opportunities to further study complex anthropomorphic MCDMs both fundamentally and for the study of musculoskeletal systems. Fundamentally, further studies that take advantage of the generalised MCDM model can be performed. For example, as demonstrated in the study of wrench-closure validity, the method in analysing multilink CDPMs may vary from that for single link manipulators. For some problems, such as inverse dynamics or workspace analysis, analysis techniques developed for single link CDPM can be directly applied. However, it was observed that these computational costs increase significantly as the number of links and number of degrees-of-freedom increase. Due to the nature of the system Jacobian matrix,

it is observed that the efficiency of these techniques can potentially be improved by taking advantage of the arrangement of the cable routing. The proposed CRM in this thesis allows approaches that use the cable routing to be developed for the analysis of MCDMs. Furthermore, issues that result from the increased dimensionality of the generalised coordinates space for MCDMs should also be considered. For example, the visualisation of the workspace of manipulators with more than 3 degrees of freedom.

The demonstration of using traditional CDPM analysis techniques to study musculoskeletal systems presented shows great potential in gaining a better understanding in biomechanics. In this thesis, only the static workspace for a human shoulder has been presented. Future work in this area will focus on two directions. Firstly, the study of workspace for a wider range of musculoskeletal systems, such as the human arm, neck or lower limbs. Furthermore, the impact on the workspace due to muscle properties and muscle function will be further explored and quantitatively studied. Secondly, to extend other types of analyses for CDPMs, such as wrench-closure workspace analysis or the evaluation of workspace, to study biomechanical systems.

Bibliography

- [1] Cablecam. [Online]. Available: <http://www.cablecam.com>
- [2] S. K. Agrawal, V. N. Dubey, J. J. Gangloff, Jr., E. Brackbill, Y. Mao, and V. Sangwan, "Design and optimization of a cable driven upper arm exoskeleton," *J. Med. Dev.*, vol. 3, no. 3, pp. 031 004/1–8, 2009.
- [3] S. K. Agrawal, V. N. Dubey, J. J. Gangloff, Jr., E. Brackbill, and V. Sangwan, "Optimization and design of a cable driven upper arm exoskeleton," in *Proc. ASME Int. Des. Eng. Tech. Conf. and Comp. Inf. Eng. Conf.*, 2009, pp. 86 516/1–8.
- [4] J. S. Albus, R. V. Bostelman, and N. Dagalakis, "The NIST robocrane," *J. Robot. Syst.*, vol. 10, no. 5, pp. 709–724, 1993.
- [5] A. B. Alp and S. K. Agrawal, "Cable suspended robots: Design, planning and control," in *Proc. IEEE Int. Conf. Robot. Autom.*, 2002, pp. 4275–4280.
- [6] K. N. An, A. O. Browne, S. Korinek, S. Tanaka, and B. F. Morrey, "3-dimensional kinematics of glenohumeral elevation," *J. Orthop. Res.*, vol. 9, no. 1, pp. 143–149, 1991.
- [7] M. M. Aref and H. D. Taghirad, "Geometrical workspace analysis of a cable-driven redundant parallel manipulator: KNTU CDRPM," in *Proc. IEEE/RSJ Int. Conf. Intell. Robot. Syst.*, 2008, pp. 1958–1963.
- [8] Y. Asano, H. Mizoguchi, T. Kozuki, Y. Motegi, M. Osada, J. Urata, Y. Nakanishi, K. Okada, and M. Inaba, "Lower thigh design of detailed musculoskeletal hu-

- manoid “kenshiro”,” in *Proc. IEEE/RSJ Int. Conf. Intell. Robot. Syst.*, 2012, pp. 4367–4372.
- [9] K. Azizian and P. Cardou, “The dimensional synthesis of planar parallel cable-driven mechanisms through convex relaxations,” *J. Mech. Robot.*, vol. 4, no. 3, pp. 031011/1–13, 2012.
- [10] C. J. Barnes, S. V. Steyn, and R. A. Fischer, “The effects of age, sex and shoulder dominance on range of motion of the shoulder,” *J. Shoulder Elbow Surg.*, vol. 10, no. 3, pp. 242–246, 2001.
- [11] G. Barrette and C. M. Gosselin, “Determination of the dynamic workspace of cable-driven planar parallel mechanisms,” *J. Mech. Des.*, vol. 127, no. 2, pp. 242–248, 2005.
- [12] Y. B. Bedoustanti, H. D. Taghirad, and M. M. Aref, “Dynamics analysis of a redundant parallel manipulator driven by elastic cables,” in *Proc. IEEE Int. Conf. Control Autom. Robot. and Vis.*, 2008, pp. 536–542.
- [13] D. C. Boone and S. P. Azen, “Normal range of motion of joints in male subjects,” *J. Bone Joint Surg.*, vol. 61, no. 5, pp. 756–759, 1979.
- [14] P. H. Borgstrom, N. P. Borgstrom, M. J. Stealey, B. Jordan, G. S. Sukhatme, M. A. Batalin, and W. J. Kaiser, “Design and implementation of NIMS3D, a 3-d cabled robot for actuated sensing applications,” *IEEE Trans. Robot.*, vol. 25, no. 2, pp. 325–339, 2009.
- [15] P. H. Borgstrom, B. L. Jordan, G. S. Sukhatme, M. A. Batalin, and W. J. Kaiser, “Rapid computation of optimally safe tension distributions for parallel cable-driven robots,” *IEEE Trans. Robot.*, vol. 25, no. 6, pp. 1271–1281, 2009.
- [16] P. Bosscher, R. L. Williams II, L. S. Bryson, and D. Castro-Lacouture, “Cable-suspended robotic contour crafting system,” *Autom. Constr.*, vol. 17, no. 1, pp. 45–55, 2007.

- [17] P. Bosscher, A. T. Riechel, and I. Ebert-Uphoff, "Wrench-feasible workspace generation for cable-driven robots," *IEEE Trans. Robot.*, vol. 22, no. 5, pp. 890–902, 2006.
- [18] P. Bosscher, R. L. Williams II, and M. Tummino, "A concept for rapid-deployable cable robot search and rescue systems," in *Proc. ASME Int. Des. Eng. Tech. Conf. and Comp. Inf. Eng. Conf.*, 2005, pp. 84324/1–10.
- [19] S. Bouchard, C. Gosselin, and B. Moore, "On the ability of a cable-driven robot to generate a prescribed set of wrenches," *J. Mech. Robot.*, vol. 2, no. 1, pp. 011010/1–10, 2010.
- [20] R. Bricard, "Mémoire sur la théorie de l'octaèdre articulé," *J. Math. Pures Appl.*, vol. 3, 1897.
- [21] K. L. Cappel, "Motion simulator," U.S. Patent 3 295 224, January 3, 1967.
- [22] A. L. Cauchy, "Deuxième mémoire sur les polygones et les polyèdres," *Journal de l'École Polytechnique*, pp. 87–98, 1813.
- [23] Q. Chen, W. Chen, G. Yang, and R. Liu, "An integrated two-level self-calibration method for a cable-driven humanoid arm," *IEEE Trans. Autom. Sci. Eng.*, vol. 10, no. 2, pp. 380–391, 2013.
- [24] M. Christophy, N. A. Faruk Senan, J. C. Lotz, and O. M. O'Reilly, "A musculo-skeletal model for the lumbar spine," *Biomech. Model. Mechan.*, vol. 11, no. 1-2, pp. 19–34, 2012.
- [25] L. L. Cone, "Skycam: An aerial robotic system," *Byte*, vol. 10, no. 10, p. 122, 1985.
- [26] T. Dallej, M. Gouttefarde, N. Andreff, R. Dahmouche, and P. Martinet, "Vision-based modeling and control of large-dimension cable-driven parallel robots," in *Proc. IEEE/RSJ Int. Conf. Intell. Robot. Syst.*, 2012, pp. 1581–1586.
- [27] S. L. Delp, F. C. Anderson, A. S. Arnold, P. Loan, A. Habib, C. T. John, E. Guendelman, and D. G. Thelen, "OpenSim: Open-source software to create and analyze

- dynamic simulations of movement," *IEEE Trans. Biomed. Eng.*, vol. 54, no. 11, pp. 1940–1950, 2007.
- [28] S. L. Delp and J. P. Loan, "A computational framework for simulating and analyzing human and animal movement," *Compu. Sci. Eng.*, vol. 2, no. 5, pp. 46–55, 2000.
- [29] S. L. Delp, J. P. Loan, M. G. Hoy, F. E. Zajac, E. L. Topp, and J. M. Rosen, "An interactive graphics-based model of the lower extremity to study orthopaedic surgical procedures," *IEEE Trans. Biomed. Eng.*, vol. 37, no. 8, pp. 757–767, 1990.
- [30] A. D. Deshpande, J. Ko, D. Fox, and Y. Matsuoka, "Control strategies for the index finger of a tendon-driven hand," *Int. J. Robot. Res.*, vol. 32, no. 1, pp. 115–128, 2013.
- [31] X. Diao and O. Ma, "A method of verifying force-closure condition for general cable manipulator with seven cables," *Mech. Mach. Theory*, vol. 42, no. 12, pp. 1563–1576, 2007.
- [32] S. Fang, D. Franitza, M. Torlo, F. Bekes, and M. Hiller, "Motion control of a tendon-based parallel manipulator using optimal tension distribution," *IEEE/ASME Trans. Mechatronics*, vol. 9, no. 3, pp. 561–568, 2004.
- [33] F. Ferlay and F. Gosselin, "A new cable-actuated haptic interface design," in *Proc. Int. Conf. on Haptics: Perception, Devices and Scenarios*, 2008, pp. 474–483.
- [34] C. Ferraresi, M. Paoloni, and F. Pescarmona, "A force-feedback six-degrees-of-freedom wire-actuated master for teleoperation: the wiro-6.3," *Industrial Robot-An International Journal*, vol. 34, no. 3, pp. 195–200, 2007.
- [35] R. T. Floyd and C. W. Thompson, *Manual of Structural Kinesiology*. London, United States: McGraw-Hill Education, 2011.
- [36] P. Gallina and G. Rosati, "Manipulability of a planar wire driven haptic device," *Mech. Mach. Theory*, vol. 37, no. 2, pp. 215–228, 2002.
- [37] A. Ghasemi, M. Farid, and M. Eghtesad, "Interference free workspace analysis of redundant 3d cable robots," in *World Autom. Congr.*, 2008, pp. 1–6.

- [38] R. V. Gonzalez, T. S. Buchanan, and S. L. Delp, "How muscle architecture and moment arms affect wrist flexion-extension moments," *J. Biomech.*, vol. 30, no. 7, pp. 705–712, 1997.
- [39] C. Gosselin and J. Angeles, "A global performance index for the kinematic optimization of robotic manipulators," *J. Mech. Des.*, vol. 113, no. 3, pp. 220–226, 1991.
- [40] V. E. Gough, "Contribution to discussion of papers on research in automotive stability, control and tyre performance," in *Proc. Auto Div. Inst. Mech. Eng.*, vol. 171, 1956, pp. 392–395.
- [41] V. E. Gough and S. G. Whitehall, "Universal tyre test machine," in *Proc. 9th Int. Tech. Congress F.I.S.I.T.A*, vol. 117, 1962, pp. 117–135.
- [42] M. Gouttefarde, D. Daney, and J.-P. Merlet, "Interval-analysis-based determination of the wrench-feasible workspace of parallel cable-driven robots," *IEEE Trans. Robot.*, vol. 27, no. 1, pp. 1–13, 2011.
- [43] M. Gouttefarde and C. M. Gosselin, "Analysis of the wrench-closure workspace of planar parallel cable-driven mechanisms," *IEEE Trans. Robot.*, vol. 22, no. 3, pp. 434–445, 2006.
- [44] M. Gouttefarde, J.-P. Merlet, and D. Daney, "Wrench-feasible workspace of parallel cable-driven mechanisms," in *Proc. IEEE Int. Conf. Robot. Autom.*, 2007, pp. 1492–1497.
- [45] J. E. Gwinnett, "Amusement device," U.S. Patent 1 789 680, January 20, 1931.
- [46] M. Hassan and A. Khajepour, "Optimization of actuator forces in cable-based parallel manipulators using convex analysis," *IEEE Trans. Robot.*, vol. 24, no. 3, pp. 736–740, 2008.
- [47] ——, "Analysis of bounded cable tensions in cable-actuated parallel manipulators," *IEEE Trans. Robot.*, vol. 27, no. 5, pp. 891–900, 2011.

- [48] L. Herda, R. Urtasun, P. Fua, and A. Hanson, "Automatic determination of shoulder joint limits using quaternion field boundaries," *Int. J. Robot. Res.*, vol. 22, no. 6, pp. 419–436, 2003.
- [49] T. Higuchi, A. Ming, and J. Jiang-yu, "Application of multi-dimensional wire cranes in construction," in *the 5th Int. Symp. on Robotics in Construction*, 1988, pp. 661–668.
- [50] K. R. S. Holzbaur, W. M. Murray, and S. L. Delp, "A model of the upper extremity for simulating musculoskeletal surgery and analyzing neuromuscular control," *Ann. Biomed. Eng.*, vol. 33, no. 6, pp. 829–840, 2005.
- [51] M. L. Husty, "An algorithm for solving the direct kinematics of general stewart-gough platforms," *Mech. Mach. Theory*, vol. 31, no. 4, pp. 365–380, 1996.
- [52] J. M. Inouye, J. J. Kutch, and F. J. Valero-Cuevas, "A novel synthesis of computational approaches enables optimization of grasp quality of tendon-driven hands," *IEEE Trans. Robot.*, vol. 28, no. 4, pp. 958–966, 2012.
- [53] T. Itto and K. Kogiso, "Hybrid modeling of mckibben pneumatic artificial muscle systems," in *Proc. IEEE Int. Conf. on Industrial Technology*, 2011, pp. 65–70.
- [54] M. Jäntschi, C. Schmaler, S. Wittmeier, K. Dalamagkidis, and A. Knoll, "A scalable joint-space controller for musculoskeletal robots with spherical joints," in *IEEE Int. Conf. Robot. and Biomimetics*, 2011, pp. 2211–2216.
- [55] G. Johnson, N. Fyfe, and M. Heward, "Ranges of movement at the shoulder complex using an electromagnetic movement sensor," *Ann. Rheum. Dis.*, vol. 50, no. 11, pp. 824–827, 1991.
- [56] B.-S. Kang, C. S. Kothera, B. K. S. Woods, and N. M. Wereley, "Dynamic modeling of mckibben pneumatic artificial muscles for antagonistic actuation," in *Proc. IEEE Int. Conf. Robot. Autom.*, 2009, pp. 182–187.

- [57] M. Karkoub, M.-G. Her, C.-C. Peng, C.-C. Huang, and M.-I. Ho, "Design and control of a cable-controlled haptic motion simulator," *Robotica*, vol. 30, no. 5, pp. 709–719, 2012.
- [58] S. Kawamura, W. Choe, S. Tanaka, and S. R. Pandian, "Development of an ultra-high speed robot FALCON using wire drive system," in *Proc. IEEE Int. Conf. Robot. Autom.*, 1995, pp. 215–220.
- [59] S. Kawamura, H. Kino, and C. Won, "High-speed manipulation by using parallel wire-driven robots," *Robotica*, vol. 18, no. 1, pp. 13–21, 2000.
- [60] H. Kobayashi and R. Ozawa, "Adaptive neural network control of tendon-driven mechanisms with elastic tendons," *Automatica*, vol. 39, no. 9, p. 15091519, 2003.
- [61] M. H. Korayem, H. Tourajizadeh, and M. Bamdad, "Dynamic load carrying capacity of flexible cable suspended robot: Robust feedback linearization control approach," *J. Intell. Robot. Syst.*, vol. 60, no. 3-4, pp. 341–363, 2010.
- [62] K. Kozak, Q. Zhou, and J. Wang, "Static analysis of cable-driven manipulators with non-negligible cable mass," *IEEE Trans. Robot.*, vol. 22, no. 3, pp. 425–433, 2006.
- [63] T. Kozuki, H. Mizoguchi, Y. Asano, M. Osada, T. Shirai, J. Urata, Y. Nakanishi, K. Okada, and M. Inaba, "Design methodology for thorax and shoulder of human mimetic musculoskeletal humanoid kenshiro - a thorax with rib like surface -," in *Proc. IEEE/RSJ Int. Conf. Intell. Robot. Syst.*, 2012, pp. 3687–3692.
- [64] J. Lamaury and M. Gouttefarde, "Control of a large redundantly actuated cable-suspended parallel robot," in *Proc. IEEE Int. Conf. Robot. Autom.*, 2013, pp. 4659–4664.
- [65] J. Lamaury, M. Gouttefarde, A. Chemori, and P. Élie Hervé, "Dual-space adaptive control of redundantly actuated cable-driven parallel robots," in *Proc. IEEE/RSJ Int. Conf. Intell. Robot. Syst.*, 2013, pp. 4879–4886.
- [66] S. E. Landsberger and T. B. Sheridan, "A new design for parallel link manipulator," in *Proc. IEEE Int. Conf. Syst. Man. Cybern.*, 1985, pp. 812–814.

- [67] ——, “A minimal, minimal linkage: The tension-compression parallel link manipulator,” in *IMACS/SICE Int. Symp. on Robotics, Mechatronics, and Manufacturing Systems*, 1992, pp. 492–500.
- [68] D. Lau, K. Bhalerao, D. Oetomo, and S. K. Halgamuge, “On the task specific evaluation and optimisation of cable-driven manipulators,” in *Advances in Reconfigurable Mechanisms and Robots I*, J. S. Dai, M. Zoppi, and X. Kong, Eds. Springer London, 2012, ch. 63, pp. 707–716.
- [69] D. Lau, D. Oetomo, and S. K. Halgamuge, “Wrench-closure workspace generation for cable driven parallel manipulators using a hybrid analytical-numerical approach,” *J. Mech. Des.*, vol. 133, no. 7, pp. 071 004/1–7, 2011.
- [70] K.-M. Lee and D. K. Shah, “Kinematic analysis of a three-degrees-of-freedom in-parallel actuated manipulator,” *IEEE Trans. Robot. Autom.*, vol. 4, no. 3, pp. 354–360, 1988.
- [71] C. Li and C. D. Rahn, “Design of continuous backbone, cable-driven robots,” *J. Mech. Des.*, vol. 124, no. 2, pp. 265–271, 2002.
- [72] W. B. Lim, S. H. Yeo, G. Yang, and S. K. Mustafa, “Kinematic analysis and design optimization of a cable-driven universal joint module,” in *Proc. IEEE/ASME Int. Conf. Adv. Int. Mechatronics*, 2009, pp. 1933–1938.
- [73] W. B. Lim, G. Yang, S. H. Yeo, and S. K. Mustafa, “A generic force-closure analysis algorithm for cable-driven parallel manipulators,” *Mech. Mach. Theory*, vol. 46, no. 9, pp. 1265–1275, 2011.
- [74] A. Z. Loloei, M. M. Aref, and H. D. Taghirad, “Wrench feasible workspace analysis of cable-driven parallel manipulators using LMI approach,” in *Proc. IEEE/ASME Int. Conf. Adv. Int. Mechatronics*, 2009, pp. 1034–1039.
- [75] O. Ma and X. Diao, “Dynamics analysis of a cable-driven parallel manipulator for hardware-in-the-loop dynamic simulation,” in *Proc. IEEE/ASME Int. Conf. Adv. Int. Mechatronics*, 2005, pp. 837–842.

- [76] S. Ma, S. Hirose, and H. Yoshinada, "CT ARM-I: coupled tendon-driven manipulator model i-design and basic experiments," in *Proc. IEEE Int. Conf. Robot. Autom.*, 1992, pp. 2094–2100.
- [77] Z. Man, W. Chen, S. Yu, and X. Yu, "Kinematic analysis for a 7-DOF modular hybrid-driven manipulator," in *Proc. IEEE Int. Conf. Indus. Inform.*, 2006, pp. 1363–1368.
- [78] Y. Mao and S. K. Agrawal, "Wearable cable-driven upper arm exoskeleton - motion with transmitted joint force and moment minimization," in *Proc. IEEE Int. Conf. Robot. Autom.*, 2010, pp. 4334–4339.
- [79] ——, "Design of a cable-driven arm exoskeleton (CAREX) for neural rehabilitation," *IEEE Trans. Robot.*, vol. 28, no. 4, pp. 922–931, 2012.
- [80] H. G. Marques, M. Jäntschi, S. Wittmeier, O. Holland, C. Alessandro, A. Diamond, M. Lungarella, and R. Knight, "ECCE1 : The first of a series of anthropomorphic musculoskeletal upper torsos," in *IEEE-RAS Int. Conf. Humanoid Robot.*, 2010, pp. 391–396.
- [81] C. F. Martin and L. Schovanec, "The control and mechanics of human movement systems," *Progress in Systems and Control Theory*, vol. 25, pp. 173–202, 1999.
- [82] D. Mayhew, B. Bachrach, W. Z. Rymer, and R. F. Beer, "Development of the MACARM - a novel cable robot for upper limb neurorehabilitation," in *Proc. IEEE Int. Conf. Rehab. Robot.*, 2005, pp. 299–302.
- [83] P. W. McClure, L. A. Michener, B. J. Sennett, and A. R. Karduna, "Direct 3-dimensional measurement of scapular kinematics during dynamic movements in vivo," *J. Shoulder Elbow Surg.*, vol. 10, no. 3, pp. 269–277, 2001.
- [84] J.-P. Merlet, *Parallel Robots*. Dordrecht: Kluwer, 2000.
- [85] J.-P. Merlet and D. Daney, "A portable, modular parallel wire crane for rescue operations," in *Proc. IEEE Int. Conf. Robot. Autom.*, 2010, pp. 2834–2839.

- [86] A. Ming and T. Higuchi, "Study on multiple degrees-of-freedom positioning mechanism using wires (part 1) - concept, design and control," *Int. J. Japan Social Eng.*, vol. 28, no. 2, pp. 131–138, 1994.
- [87] I. Mizuuchi, Y. Nakanishi, Y. Sodeyama, Y. Namiki, and T. Nishino, "An advanced musculoskeletal humanoid kojiro," in *IEEE-RAS Int. Conf. Humanoid Robot.*, 2007, pp. 294–299.
- [88] I. Mizuuchi, T. Yoshikai, D. Sato, S. Yoshida, M. Inaba, and H. Inoue, "Behavior developing environment for the large-DOF muscle-driven humanoid equipped with numerous sensors," in *Proc. IEEE Int. Conf. Robot. Autom.*, 2003, pp. 1940–1945.
- [89] I. Mizuuchi, T. Yoshikai, Y. Sodeyama, Y. Nakanishi, A. Miyadera, T. Yamamoto, T. Niemelä, M. Hayashi, J. Urata, Y. Namiki, T. Nishino, and M. Inaba, "Development of musculoskeletal humanoid kotaro," in *Proc. IEEE Int. Conf. Robot. Autom.*, 2006, pp. 82–87.
- [90] A. Murai, K. Kurosaki, K. Yamane, and Y. Nakamura, "Musculoskeletal-see-through mirror: Computational modeling and algorithm for whole-body muscle activity visualization in real time," *Prog. Biophys. Mol. Biol.*, vol. 103, no. 2-3, pp. 310–317, 2010.
- [91] S. K. Mustafa and S. K. Agrawal, "Reciprocal screw-based force-closure of an n-DOF open chain: Minimum number of cables required to fully constrain it," in *Proc. IEEE Int. Conf. Robot. Autom.*, 2011, pp. 3029–3034.
- [92] ——, "On the force-closure analysis of n-DOF cable-driven open chains based on reciprocal screw theory," *IEEE Trans. Robot.*, vol. 28, no. 1, pp. 22–31, 2012.
- [93] S. K. Mustafa, G. Yang, S. H. Yeo, W. Lin, and I.-M. Chen, "Self-calibration of a biologically inspired 7 DOF cable-driven robotic arm," *IEEE/ASME Trans. Mechatronics*, vol. 13, no. 1, pp. 66–75, 2008.

- [94] Y. Nakamura, K. Yamane, Y. Fujita, and I. Suzuki, "Somatosensory computation for man-machine interface from motion-capture data and musculoskeletal human model," *IEEE Trans. Robot.*, vol. 21, no. 1, pp. 58–66, 2005.
- [95] Y. Nakanishi, T. Izawa, M. Osada, N. Ito, S. Ohta, J. Urata, and M. Inaba, "Development of musculoskeletal humanoid kenzoh with mechanical compliance changeable tendons by nonlinear spring unit," in *IEEE Int. Conf. Robot. and Biomimetics*, 2011, pp. 2384–2389.
- [96] P. Nanua, K. J. Waldron, and V. Murthy, "Direct kinematic solution of a stewart platform," *IEEE Trans. Robot. Autom.*, vol. 6, no. 4, pp. 438–444, 1990.
- [97] D. Q. Nguyen, M. Gouttefarde, O. Company, and F. Pierrot.
- [98] K. Ning, M. Zhao, and J. Liu, "A new wire-driven three degree-of-freedom parallel manipulator," *J. Manuf. Sci. Eng.*, vol. 128, no. 3, pp. 816–819, 2006.
- [99] S.-R. Oh and S. K. Agrawal, "Cable suspended planar robots with redundant cables: Controllers with positive tensions," *IEEE Trans. Robot.*, vol. 21, no. 3, pp. 457–465, 2005.
- [100] S.-R. Oh, K. Mankala, S. K. Agrawal, and J. S. Albus, "A dual-stage planar cable robot: Dynamic modelling and design of a robust controller with positive inputs," *J. Mech. Des.*, vol. 127, no. 4, pp. 612–620, 2005.
- [101] S.-R. Oh and S. K. Agrawal, "Nonlinear sliding mode control and feasible workspace analysis for a cable suspended robot with input constraints and disturbances," in *American Contr. Conf.*, 2004, pp. 4631–4636.
- [102] S.-R. Oh, J.-C. Ryu, and S. K. Agrawal, "Dynamics and control of a helicopter carrying a payload using a cable-suspended robot," *J. Mech. Des.*, vol. 128, no. 5, pp. 1113–1121, 2005.
- [103] M. J.-D. Otis, S. Perreault, T.-L. Nguyen-Dang, P. Lambert, M. Gouttefarde, D. Laverdeau, and C. Gosselin, "Determination and management of cable interferences

- bewteen two 6-dof foot platforms in a cable-driven locomotion interface," *IEEE Trans. Syst., Man, Cybern. A*, vol. 39, no. 3, pp. 528–544, 2009.
- [104] S. Perreault and C. M. Gosselin, "Cable-driven parallel mechanisms: Application to a locomotion interface," *J. Mech. Des.*, vol. 130, no. 10, pp. 102301/1–8, 2008.
- [105] S. Perreault, P. Cardou, C. M. Gosselin, and M. J.-D. Otis, "Geometric determination of the interference-free constant-orientation workspace of parallel cable-driven mechanisms," *J. Mech. Robot.*, vol. 2, no. 3, pp. 031016/1–9, 2010.
- [106] C. B. Pham, G. Yang, and S. H. Yeo, "Dynamic analysis of cable-driven parallel mechanisms," in *Proc. IEEE/ASME Int. Conf. Adv. Int. Mechatronics*, 2005, pp. 612–617.
- [107] C. B. Pham, S. H. Yeo, G. Yang, and I.-M. Chen, "Workspace analysis of fully restrained cable-driven manipulators," *Robot. Auton. Syst.*, vol. 57, no. 9, pp. 901–912, 2009.
- [108] C. B. Pham, S. H. Yeo, G. Yang, M. S. Kurbanhusen, and I.-M. Chen, "Force-closure workspace analysis of cable-driven parallel mechanisms," *Mech. Mach. Theory*, vol. 41, no. 1, pp. 53–69, 2006.
- [109] W. L. V. Pollard, "Position controlling apparatus," U.S. Patent 2 286 571, June 16, 1942.
- [110] J. Pusey, A. Fattah, S. Agrawal, and E. Messina, "Design and workspace analysis of a 6-6 cable-suspended parallel robot," *Mech. Mach. Theory*, vol. 39, no. 7, pp. 761–778, 2004.
- [111] S. Rezazadeh and S. Behzadipour, "Tensionability conditions of a multi-body system driven by cables," in *Proc. ASME Int. Mech. Eng. Congress and Exposition*, 2007, pp. 1369–1375.
- [112] ——, "Workspace analysis of multibody cable-driven mechanisms," *J. Mech. Robot.*, vol. 3, no. 2, pp. 021005/1–10, 2011.

- [113] N. Riehl, M. Gouttefarde, S. Krut, C. Baradat, and F. Pierrot, "Effects of non-negligible cable mass on the static behaviour of large workspace cable-driven parallel mechanisms," in *Proc. IEEE Int. Conf. Robot. Autom.*, 2009, pp. 2193–2198.
- [114] J. A. Ringelberg, "EMG and force production of some human shoulder muscles during isometric abduction," *J. Biomech.*, vol. 18, no. 12, pp. 939–947, 1985.
- [115] J. K. Salisbury and J. J. Craig, "Articulated hands: Force control and kinematic issues," *Int. J. Robot. Res.*, vol. 1, no. 1, pp. 4–17, 1982.
- [116] S. H. Scott and D. A. Winter, "A comparison of three muscle pennation assumptions and their effects on isometric and isotonic force," *J. Biomech.*, vol. 24, no. 2, pp. 163–167, 1991.
- [117] W.-J. Shiang, D. Cannon, and J. Gorman, "Dynamic analysis of the cable array robotic crane," in *Proc. IEEE Int. Conf. Robot. Autom.*, 1999, pp. 2495–2500.
- [118] G. Sigholm, P. Herberts, C. Almström, and R. Kadefors, "Electromyographic analysis of shoulder muscle load," *J. Orthop. Res.*, vol. 1, no. 4, pp. 379–386, 1983.
- [119] D. Stewart, "A platform with 6 degrees of freedom," *Proc. of Inst. Mech. Eng.*, vol. 180, no. 5, pp. 371–386, 1965.
- [120] E. Stump and V. Kumar, "Workspaces of cable-actuated parallel manipulators," *J. Mech. Des.*, vol. 128, no. 1, pp. 159–167, 2005.
- [121] C. Sui and M. Zhao, "Control of a 3-dof parallel wire driven stiffness-variable manipulator," in *Proc. IEEE Int. Conf. Robot. Autom.*, 2004, pp. 204–209.
- [122] D. Surdilovic, J. Zhang, and R. Bernhardt, "STRING-MAN: Wire-robot technology for safe, flexible and human-friendly gait rehabilitation," in *Proc. IEEE Int. Conf. Rehab. Robot.*, 2007, pp. 446–453.
- [123] S. Tadokoro, Y. Murao, M. Hiller, R. Murata, H. Kohkawa, and T. Matsushima, "A motion base with 6-dof by parallel cable drive architecture," *IEEE/ASME Trans. Mechatronics*, vol. 7, no. 2, pp. 115–123, 2002.

- [124] H. D. Taghirad and Y. B. Bedoustani, "An analytic-iterative redundancy resolution scheme for cable-driven redundant parallel manipulators," *IEEE Trans. Robot.*, vol. 27, no. 6, pp. 1137–1143, 2011.
- [125] T. Takaki and T. Omata, "High-performance anthropomorphic robot hand with grasping-force-magnification mechanism," *IEEE/ASME Trans. Mechatronics*, vol. 16, no. 3, pp. 583–591, 2011.
- [126] J. Ueda, D. Ming, V. Krishnamoorthy, M. Shinohara, and T. Ogasawara, "Individual muscle control using an exoskeleton robot for muscle function testing," *IEEE Trans. Neural Syst. Rehabil. Eng.*, vol. 18, no. 4, pp. 339–350, 2010.
- [127] H. K. Uhthoff, "Shoulder injury and disability," *The Workspace Safety and Insurance Appeals Tribunal*, 2010.
- [128] A. Vafaei, M. M. Aref, and H. D. Taghirad, "Integrated controller for an over-constrained cable driven parallel manipulator: KNTU CDRPM," in *Proc. IEEE Int. Conf. Robot. Autom.*, 2010, pp. 650–655.
- [129] F. Valero, V. Mata, and A. Besa, "Trajectory planning in workspaces with obstacles taking into account the dynamic robot behaviour," *Mech. Mach. Theory*, vol. 41, no. 5, pp. 525–536, 2006.
- [130] A. N. Vasavada, S. Li, and S. L. Delp, "Influence of muscle morphometry and moment arms on the moment-generating capacity of human neck muscles," *Spine*, vol. 23, no. 4, pp. 412–422, 1998.
- [131] A. Vilchis, J. Troccaz, P. Cinquin, K. Masuda, and F. Pellissier, "A new robot architecture for tele-echography," *IEEE Trans. Robot.*, vol. 19, no. 5, pp. 922–926, 2003.
- [132] M. Vilimek, "Musculotendon forces derived by different muscle models," *Acta of Bioeng. and Biomech.*, vol. 9, no. 2, pp. 41–47, 2007.
- [133] P. A. Voglewede and I. Ebert-Uphoff, "Application of the antipodal grasp theorem to cable-driven robots," *IEEE Trans. Robot.*, vol. 21, no. 4, pp. 713–718, 2005.

- [134] R. L. Williams II, J. S. Albus, and R. V. Bostelman, "3D cable-based cartesian metrology system," *J. Robot. Syst.*, vol. 21, no. 5, pp. 237–257, 2004.
- [135] R. L. Williams II, V. Chadaram, and F. Giacometti, "Three-cable haptic interface," in *Proc. ASME Int. Des. Eng. Tech. Conf. and Comp. Inf. Eng. Conf.*, 2006, pp. 99 177 /1–8.
- [136] R. L. Williams II and P. Gallina, "Planar cable-direct-driven robots: Design for wrench exertion," *J. Intell. Robot. Syst.*, vol. 35, no. 2, pp. 203–219, 2002.
- [137] R. L. Williams II, M. Xin, and P. Bosscher, "Contour-crafting-cartesian-cable robot system: Dynamics and controller design," in *DETC 2008: 32nd Annual Mechanisms and Robotics Conference, Vol. 2, Parts A & B*, 2009, pp. 39–45.
- [138] Y. Wischnitzer, N. Shvalb, and M. Shoham, "Wire-driven parallel robot: Permitting collisions between wires," *Int. J. Robot. Res.*, vol. 27, no. 9, pp. 1007–1026, 2008.
- [139] S. Wittmeier, C. Alessandro, N. Bascarevic, K. Dalamagkidis, D. Devereux, A. Diamond, M. Jäntschi, K. Jovanovic, R. Knight, H. G. Marques, P. Milosavljevic, B. Mitra, B. Svetozarevic, V. Potkonjak, R. Pfeifer, A. Knoll, and O. Holland, "Toward anthropomimetic robotics: Development, simulation, and control of a musculo-skeletal torso," *J. Artif. Life*, vol. 19, no. 1, pp. 171–193, 2013.
- [140] S. Wittmeier, M. Jäntschi, K. Dalamagkidis, and A. Knoll, "Physics-based modeling of an anthropomimetic robot," in *Proc. IEEE/RSJ Int. Conf. Intell. Robot. Syst.*, 2011, pp. 4148–4153.
- [141] G. Yang, S. K. Mustafa, C. B. Pham, and S. H. Yeo, "Kinematic design of a 7-DOF cable-driven humanoid arm: a solution-in-nature approach," in *Proc. IEEE/ASME Int. Conf. Adv. Int. Mechatronics*, 2005, pp. 444–449.
- [142] G. Yang, S. K. Mustafa, S. H. Yeo, W. Lin, and W. B. Lim, "Kinematic design of an anthropomimetic 7-dof cable-driven robotic arm," *Front. Mech. Eng.*, vol. 6, no. 1, pp. 45–60, 2011.

- [143] R. Yao, X. Tang, J. Wang, and P. Huang, "Dimensional optimization design of the four-cable-driven parallel manipulator in FAST," *IEEE/ASME Trans. Mechatronics*, vol. 15, no. 6, pp. 932–941, 2010.
- [144] J. Yu, D. C. Ackland, and M. G. Pandy, "Shoulder muscle function depends on elbow joint position: An illustration of dynamic coupling in the upper limb," *J. Biomech.*, vol. 44, no. 10, pp. 1859–1868, 2011.
- [145] F. E. Zajac, "Muscle and tendon: Properties, models, scaling, and application to biomechanics and motor control," *Crit. Rev. in Biomed. Eng.*, vol. 17, no. 4, pp. 359–411, 1989.
- [146] Y.-Q. Zheng, Q. Lin, J.-P. Wu, and P. Mitrouchev, "Analysis of inverse kinematics and dynamics of a novel 6-degree-of-freedom wire-driven parallel gantry crane robot," in *Proc. IEEE/ASME Int. Conf. Adv. Int. Mechatronics*, 2009, pp. 1786–1791.

Appendix A

Wrench-Closure Workspace Generation for Cable-Driven Parallel Manipulators Using a Hybrid Analytical-Numerical Approach

In this paper, a technique to generate the wrench-closure workspace for general case completely restrained cable driven parallel mechanisms is proposed. Existing methods can be classified as either numerically or analytically based approaches. Numerical techniques exhaustively sample the task space, which can be inaccurate due to discretisation and is computationally expensive. In comparison, analytical formulations have higher accuracy, but often provides only qualitative workspace information. The proposed hybrid approach combines the high accuracy of the analytical approach and the algorithmic versatility of the numerical approach. Additionally, this is achieved with significantly lower computational costs compared to numerical methods. It is shown that the wrench-closure workspace can be reduced to a set of univariate polynomial inequalities with respect to a single variable of the end-effector motion. In this form, the workspace can then be efficiently determined and quantitatively evaluated. The proposed technique is described for a 3-DOF and a 6-DOF cable driven parallel manipulator. A detailed example in workspace determination using the proposed approach and comparison against the conventional numerical approach are presented.

A.1 Introduction

Cable driven parallel manipulators are structurally similar to traditional parallel mechanisms, but differ in that rigid links are replaced by cables. The manipulator's movement is regulated through the actuation of the individual cables attached to the end effector on one end and to the actuator located at the base platform on the other. This class of manipulator has been widely studied due to its desirable characteristics over traditional parallel mechanisms: reduced weight and inertia, simplified dynamics modelling, ease of transportation and construction, and ease of reconfigurability.

The use of lightweight cables with negligible inertia simplifies the dynamics, modelling and control of the system. In addition, cable mounting points at the base platform can be relocated to result in a highly reconfigurable and resizable workspace. With these advantages, a range of applications exist for cable driven robots [84], such as manipulation of heavy payloads for manufacturing [4, 58] and cargo handling [100], interaction and sensing with the environment [14, 134], aerial camera, haptics [33] and building construction [16]. Applications in the medical field include rehabilitation [82, 122] and exoskeletons [2, 141].

Knowledge of the end effector's usable workspace is essential for several purposes, such as trajectory planning [129], and the selection and design of manipulator configurations depending on workspace requirements [104]. The configuration of a cable driven manipulator refers to the location of cable attachments at the base platform and the end effector. A unique property of cable driven mechanisms is that cables can only be actuated unilaterally through tension and not compression (*positive cable force*). This limitation creates challenging problems in the control of the manipulator [99] and workspace determination. It also means that techniques to determine the workspace for serial and rigid link parallel manipulators are not directly applicable to cable manipulators. Several types of cable driven parallel manipulator workspace have been investigated, such as the *static workspace* [110], *dynamic workspace* [11], *wrench-feasible workspace* [17, 44, 107], *wrench-closure workspace* [31, 43, 107, 108, 120], and *interference-free workspace* [7, 136]. The *wrench-feasible workspace* (WFW) for the manipulator refers to the set of poses for which the system dynamics can be satisfied with positive cable forces for a specified set of exter-

nal wrenches, velocities, and accelerations, within specified actuation limits of the cables. *The wrench-closure workspace* (WCW) is similar to the WFW, defined as the set of poses in which the manipulator can sustain any arbitrary external wrench when no upper bounds are placed on the cable forces.

Cable manipulators with n degrees-of-freedom (DOF) actuated by m cables can be classified as being incompletely restrained ($m < n + 1$), completely restrained ($m = n + 1$), or redundantly restrained ($m > n + 1$) [86]. Techniques to determine the WCW for redundantly restrained systems have been studied in [43, 108] based on the concept of determining the positive spanning of the task space and on convex analysis, while completely restrained systems were studied in [31]. For redundantly restrained manipulators, workspace can be determined by considering the system as a combinatorial set of completely restrained systems. Approaches for workspace determination can be classified as numerical [31, 108] or analytical [11, 17, 43, 120].

Numerical methods are typically point-wise evaluation techniques, where the task space is exhaustively searched at discrete intervals. This approach provides only a local measure of the workspace at the evaluated points, suffering from the effects of discretisation. The accuracy for this approach is dependent on the interval width (*step-size*), where decreased width results in increased accuracy. The drawback of decreasing interval width is that the computational time will be significantly increased.

Analytical formulations provide a more accurate description of workspace and insights into its geometry. Mathematically, the workspace region can be described as the intersection of a set of inequality equations. Due to the algebraic complexity, previous studies have been concerned with determining only the boundary of the workspace. In [43], the WCW boundary for over-restrained planar cable robots in constant orientation was analytically studied. The boundary was determined to be in the form of a set of second degree conic sections of two variables. In a similar manner, it was shown in [120] that the form for WCW of planar cable manipulators could be expressed as a polynomial of degree 12 in three variables. A similar problem was investigated in [17], where the WFW boundary for a range of systems, planar, spatial and point mass cable robots in constant orientation were analytically determined. The solution was shown to be comprised of

a set of lower and upper boundaries. For the spatial manipulator, the lower boundary is a set of fifth degree polynomial equations in three variables with 56 polynomial coefficients. The upper boundary was observed to be generally not polynomial and hence difficult to solve.

Upon determining the boundaries, the workspace itself can then be located by graphically identifying the regions that satisfy the set of inequalities. During this additional procedure, the manipulator designer can gain an insight into the workspace geometry. Compared to the techniques under numerical approach, the analytical approach typically provides only qualitative information regarding the workspace. The ability to quantitatively describe the generated region is important in determining the cable mounting locations given the desired workspace characteristics. This also allows an automated design process of a mechanism, where quality functions associated with various desired features in the design can be incorporated.

In this paper, an approach to generate the WCW using a hybrid of analytical and numerical methods for completely restrained cable driven manipulators is presented. The analytical solution for the WCW is reduced to a set of univariate polynomial inequalities with respect to a single pose variable by treating the other remaining pose variables as constants. The constant pose variables are then discretely varied over the range of interest, and the analytical form is accurately solved at each iteration. The workspace region can then be determined directly by solving the set of univariate polynomial inequalities. Compared to the conventional point-wise evaluation methods, the proposed technique has the advantages of lower computational complexity and increased accuracy. It is shown that the reduction of the computational speed achieved by the proposed algorithm against the traditional point-wise approach increases with finer evaluation step-size and higher system complexity.

For the test cases presented in this paper, a computational time saving of at least 4 folds for coarse step-sizes and up to orders of magnitude of saving for finer resolutions is achieved. The improvement in computational speed does not guarantee real-time evaluation of a manipulator workspace, as it is dependent of evaluation step-size and system complexity. However, the multiple folds of saving in computational time translates into

tremendous advantage in iterative processes, such as in the design of cable manipulators to achieve optimal workspace [2, 104], resulting in a significant savings in design costs. Another benefit of the proposed approach is the ease and efficiency in which the quality of the workspace in the form of cost functions can be included and evaluated quantitatively.

The remainder of this paper is organised as follows: Section A.2 describes the kinematics and dynamics model for a general spatial cable-driven manipulator. The wrench-closure condition and the corresponding wrench-closure workspace is presented in Section A.3. Section A.4 describes the proposed workspace determination approach for a general 6-DOF spatial manipulator and a 3-DOF ball joint manipulator. The potential of incorporating quality functions to quantitatively evaluate the resulting WCW is also discussed. The simulation setup for the 3-DOF and 6-DOF manipulators will be presented in Section A.5. Section A.6 presents and compares the resulting workspace from the proposed and numerical approaches. Finally, Section A.7 concludes the paper and presents areas of future work.

A.2 Kinematic and Dynamic Model

The model for a general 6-DOF spatial cable driven parallel manipulator is shown in Figure A.1. The cables are attached to the base frame at positions \mathbf{r}_A , and to the end effector at positions \mathbf{r}_B . Vectors \mathbf{r}_A and \mathbf{r}_B are constant in the inertial frame, $\{F_0\}$, and end effector frame, $\{F_E\}$, respectively. The attachment points for cable i can be represented as:

$$\begin{aligned} {}^0\mathbf{r}_{A_i} &= r_{A_{ix}}\mathbf{i}_0 + r_{A_{iy}}\mathbf{j}_0 + r_{A_{iz}}\mathbf{k}_0 \\ {}^E\mathbf{r}_{B_i} &= r_{B_{ix}}\mathbf{i}_e + r_{B_{iy}}\mathbf{j}_e + r_{B_{iz}}\mathbf{k}_e \end{aligned} \quad (\text{A.1})$$

where ${}^0\mathbf{r}$ and ${}^E\mathbf{r}$ represents the vector \mathbf{r} in $\{F_0\}$ and $\{F_E\}$, respectively.

The cable vector can be kinematically defined as:

$$\mathbf{l}_i = \mathbf{r}_{0E} + \mathbf{r}_{B_i} - \mathbf{r}_{A_i} \quad (\text{A.2})$$

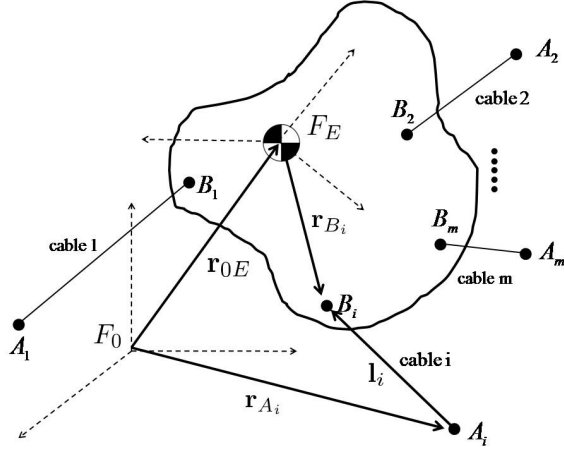


Figure A.1: General Model for Cable Manipulator

Expressing the dynamics of the system in Lagrangian form, the equations of motion for the 6-DOF m -cable system can be defined as:

$$M(\mathbf{x})\ddot{\mathbf{x}} + C(\mathbf{x}, \dot{\mathbf{x}}) + G(\mathbf{x}) + F_{ext}(\mathbf{x}) = -J^T(\mathbf{x})\mathbf{t} \quad (\text{A.3})$$

where \mathbf{x} is the manipulator pose, $M(\mathbf{x})$, $C(\mathbf{x}, \dot{\mathbf{x}})$, $G(\mathbf{x})$, and $F_{ext}(\mathbf{x})$ are the mass inertia matrix, centrifugal and Coriolis force vector, gravitational vector, and external wrench vector, respectively. The resultant of the cable wrenches is denoted by $-J^T\mathbf{t}$, where $-J^T(\mathbf{x})$ represents transformation of the cable forces to the wrench generated due to cable actuation, and $\mathbf{t} = [t_1 \ t_2 \ \dots \ t_m]^T$ is the cable force vector containing the magnitudes of the force for individual cables, where t_i is the cable force in cable i . The positive cable force constraint is denoted by $\mathbf{t} > \mathbf{0}$, that is, all the cable forces, t_i , are required to be positive. The $6 \times m$ transpose of the Jacobian matrix is defined as:

$$J^T = \begin{bmatrix} \hat{\mathbf{l}}_1 & \hat{\mathbf{l}}_2 & \dots & \hat{\mathbf{l}}_m \\ \mathbf{r}_{B_1} \times \hat{\mathbf{l}}_1 & \mathbf{r}_{B_2} \times \hat{\mathbf{l}}_2 & \dots & \mathbf{r}_{B_m} \times \hat{\mathbf{l}}_m \end{bmatrix} \quad (\text{A.4})$$

Expressing J^T terms in the inertial frame in terms of the cable attachment points and manipulator pose:

$${}^0\hat{\mathbf{l}}_i = \frac{{}^0\mathbf{r}_{0E}(\mathbf{x}) + {}^0{}_ER(\mathbf{x})\mathbf{r}_{B_i} - \mathbf{r}_{A_i}}{l_i}$$

$${}^0\mathbf{r}_{B_i} \times {}^0\hat{\mathbf{l}}_i = \frac{({}^0_R(\mathbf{x})\mathbf{r}_{B_i}) \times (\mathbf{r}_{0E}(\mathbf{x}) - \mathbf{r}_{A_i})}{l_i} \quad (\text{A.5})$$

where l_i is the length of the cable i , and 0_R is the rotation matrix from the frame $\{F_0\}$ to $\{F_E\}$, which is dependent on the manipulator pose.

A.3 Wrench-Closure Workspace

The *wrench-closure condition* (WCC) for a particular pose is satisfied if a set of positive cable forces can be determined for any arbitrary external wrench, velocity or acceleration of the manipulator without any upper bound to cable force. Combining the terms representing the dynamics of the system, the equation of motion (A.3) can be expressed as:

$$\mathbf{w} = J^T \mathbf{t} \quad (\text{A.6})$$

where $\mathbf{w} = -[M(\mathbf{x})\ddot{\mathbf{x}} + C(\mathbf{x}, \dot{\mathbf{x}}) + G(\mathbf{x}) + F_{ext}(\mathbf{x})]$. Hence for an n -DOF m -cable system, the WCC can be described as:

$$\forall \mathbf{w} \in \mathbb{R}^n, \exists \mathbf{t} > \mathbf{0} : J^T \mathbf{t} = \mathbf{w} \quad (\text{A.7})$$

The geometrical interpretation of (A.7) is that the WCC is satisfied if the columns of J^T positively span \mathbb{R}^n for full rank J^T . An equivalent definition of the WCC is the existence of some positive cable force vector within the nullspace of J^T [43].

$$\begin{aligned} \text{rank}(J^T) &= n \\ \exists \mathbf{t} \in \text{ker}(J^T) : \mathbf{t} &> \mathbf{0} \end{aligned} \quad (\text{A.8})$$

Another interpretation of (A.7) is that the WCC can be described by performing row reduction on the linear system. Since J^T is of full rank, and considering a completely restrained system, $m = n + 1$, the $n \times (n + 1)$ transpose of the Jacobian matrix can be

expressed in reduced row echelon form:

$$J^T \rightarrow \left[\begin{array}{c|c} I_n & \mathbf{v}(\mathbf{x}) \end{array} \right] \quad (\text{A.9})$$

where $I_n \in \mathbb{R}^{n \times n}$ is an identity matrix and $\mathbf{v} \in \mathbb{R}^n$ is a function of the pose variables. Applying the row reduction as in (A.9) on the WCC in (A.7):

$$\left[\begin{array}{c|c} I_n & \mathbf{v}(\mathbf{x}) \end{array} \right] \mathbf{t} = \mathbf{w}', \mathbf{t} > \mathbf{0} \quad (\text{A.10})$$

where \mathbf{w}' is the wrench vector after row reduction. The interpretation of (A.10) is that if all components of \mathbf{v} are negative, $\mathbf{v} < \mathbf{0}$, then the WCC is satisfied. This can be shown by observing the set of equations from (A.10):

$$t_j + v_j(\mathbf{x})t_m = w'_j, \forall j \in 1, \dots, n \quad (\text{A.11})$$

where j refers to the j^{th} row of (A.10). Given that $t_m \in (0, \infty)$, if $v_j(\mathbf{x}) < 0$, then $v_j t_m \in (-\infty, 0)$ and hence $w'_j \in (-\infty, \infty)$. The result of this is $\mathbf{w} \in \mathbb{R}^n$, satisfying the WCC from (A.7). The WCW for the manipulator is defined as the set of poses in which the WCC is satisfied. This can be defined as:

$$\{\mathbf{x} : \forall \mathbf{w} \in \mathbb{R}^n, \exists \mathbf{t} > \mathbf{0}, J^T(\mathbf{x})\mathbf{t} = \mathbf{w}\} \quad (\text{A.12})$$

An alternative definition of WCC in (A.10) can also be used to define the WCW:

$$\left\{ \mathbf{x} : \mathbf{v}(\mathbf{x}) < \mathbf{0}, J^T \rightarrow \left[\begin{array}{c|c} I_n & \mathbf{v}(\mathbf{x}) \end{array} \right] \right\} \quad (\text{A.13})$$

Hence the resulting workspace can be considered as the intersection of a set of multivariate inequalities. Knowledge of the algebraic form of $\mathbf{v}(\mathbf{x})$, derived in the following section, is required to analytically determine the workspace region. It can also be shown that the WCW boundary is comprised of sections of the curves $\mathbf{v}(\mathbf{x}) = \mathbf{0}$.

A.4 Proposed Workspace Determination Approach

A.4.1 6-DOF Spatial Manipulator

The analytical form for the WCW of a general 6-DOF spatial manipulator based on (A.13) is presented in this section. The pose for the manipulator as shown in Figure A.1 can be defined as $\mathbf{x} = [x \ y \ z \ \alpha \ \beta \ \gamma]^T$, where x, y and z are the translation variables between the origin of the inertial and end-effector coordinate frames, and α, β and γ are the xyz -Euler angles that define the orientation of the manipulator. The relationship between $\{F_0\}$ and $\{F_E\}$ can be described as:

$$\begin{aligned} \mathbf{r}_{0E} &= x\mathbf{i}_0 + y\mathbf{j}_0 + z\mathbf{k}_0 \\ {}^0_E R &= \begin{bmatrix} c_\beta c_\gamma & -c_\beta s_\gamma & s_\beta \\ c_\alpha s_\gamma + s_\alpha s_\beta c_\gamma & c_\alpha c_\gamma - s_\alpha s_\beta s_\gamma & -s_\alpha c_\beta \\ s_\alpha s_\gamma - c_\alpha s_\beta c_\gamma & s_\alpha c_\gamma + c_\alpha s_\beta s_\gamma & c_\alpha c_\beta \end{bmatrix} \end{aligned} \quad (\text{A.14})$$

where c_α, c_β and c_γ , and s_α, s_β and s_γ represent $\cos \alpha, \cos \beta$ and $\cos \gamma$, and $\sin \alpha, \sin \beta$ and $\sin \gamma$, respectively. Without loss of generality, the cable attachment locations from (A.1) can be used. The i^{th} column of J^T matrix (A.4) can be expressed as:

$$\begin{bmatrix} \hat{\mathbf{l}}_i \\ \mathbf{r}_{EB_i} \times \hat{\mathbf{l}}_i \end{bmatrix} = \frac{1}{l_i} \begin{bmatrix} J_{1i} \\ J_{2i} \\ J_{3i} \\ J_{4i} \\ J_{5i} \\ J_{6i} \end{bmatrix} \quad (\text{A.15})$$

where each of the terms can be explicitly derived as:

$$\begin{aligned} J_{1i} &= x + r_{B_{ix}} c_\beta c_\gamma - r_{B_{iy}} c_\beta s_\gamma + r_{B_{iz}} s_\beta - r_{A_{ix}} \\ J_{2i} &= y + r_{B_{ix}} (c_\alpha s_\gamma + s_\alpha s_\beta c_\gamma) + r_{B_{iy}} (c_\alpha c_\gamma - s_\alpha s_\beta s_\gamma) - r_{B_{iz}} s_\alpha c_\beta - r_{A_{iy}} \\ J_{3i} &= z + r_{B_{ix}} (s_\alpha s_\gamma - c_\alpha s_\beta c_\gamma) + r_{B_{iy}} (s_\alpha c_\gamma + c_\alpha s_\beta s_\gamma) + r_{B_{iz}} c_\alpha c_\beta - r_{A_{iz}} \end{aligned}$$

$$\begin{aligned}
J_{4i} &= (r_{B_{ix}}(c_\alpha s_\gamma + s_\alpha s_\beta c_\gamma) + r_{B_{iy}}(c_\alpha c_\gamma - s_\alpha s_\beta s_\gamma) - r_{B_{iz}} s_\alpha c_\beta)(z - r_{A_{iz}}) \\
&\quad - (r_{B_{ix}}(s_\alpha s_\gamma - c_\alpha s_\beta c_\gamma) + r_{B_{iy}}(s_\alpha c_\gamma + c_\alpha s_\beta s_\gamma) + r_{B_{iz}} c_\alpha c_\beta)(y - r_{A_{iy}}) \\
J_{5i} &= -(r_{B_{ix}} c_\beta c_\gamma - r_{B_{iy}} c_\beta s_\gamma + r_{B_{iz}} s_\beta)(z - r_{A_{iz}}) \\
&\quad + (r_{B_{ix}}(s_\alpha s_\gamma - c_\alpha s_\beta c_\gamma) + r_{B_{iy}}(s_\alpha c_\gamma + c_\alpha s_\beta s_\gamma) + r_{B_{iz}} c_\alpha c_\beta)(x - r_{A_{ix}}) \\
J_{6i} &= (r_{B_{ix}} c_\beta c_\gamma - r_{B_{iy}} c_\beta s_\gamma + r_{B_{iz}} s_\beta)(y - r_{A_{iy}}) \\
&\quad - (r_{B_{ix}}(c_\alpha s_\gamma + s_\alpha s_\beta c_\gamma) + r_{B_{iy}}(c_\alpha c_\gamma - s_\alpha s_\beta s_\gamma) - r_{B_{iz}} s_\alpha c_\beta)(x - r_{A_{ix}}) \quad (\text{A.16})
\end{aligned}$$

Previous analytical studies typically assume constant orientation, by treating pose variables, α, β and γ , as constants [31, 107, 108]. This reduces the complexity of the workspace boundary to a set of multivariate polynomial equations. In comparison, the solution for the WCW from (A.13) is a set of multivariate inequalities that are generally not polynomial. The analytical solution can be simplified by expressing the WCW as a function of a single variable, and treating the remaining variables as constant values. As a result, the WCW can be reduced to a set of univariate polynomial inequalities. Any of the six pose variables for the spatial manipulator could be selected to be solved analytically, resulting in different polynomial complexities.

Consider an example where the WCW was to be expressed with respect to the translational pose variable x . It can be observed that the term J_{1i} from (A.16) is a linear function of x expressed in the form:

$$\begin{aligned}
J_{1i} &= ax + b \in O(x) \quad (\text{A.17}) \\
a &= 1 \\
b &= r_{B_{ix}} c_\beta c_\gamma - r_{B_{iy}} c_\beta s_\gamma + r_{B_{iz}} s_\beta - r_{A_{ix}}
\end{aligned}$$

Repeating this analysis on the remaining terms of J^T , the following algebraic complexities are obtained:

$$\begin{aligned}
J_{1i}, J_{5i}, J_{6i} &\in O(x) \\
J_{2i}, J_{3i}, J_{4i} &\in O(1) \quad (\text{A.18})
\end{aligned}$$

where the coefficients of the terms are a function of the constant pose variables y, z, α, β , and γ . Hence, the order of complexity for the terms of J^T can be expressed as:

$$J^T \in \left[\begin{array}{ccccccc} \frac{O(x)}{l_1} & \frac{O(x)}{l_2} & \frac{O(x)}{l_3} & \frac{O(x)}{l_4} & \frac{O(x)}{l_5} & \frac{O(x)}{l_6} & \frac{O(x)}{l_7} \\ \frac{O(1)}{l_1} & \frac{O(1)}{l_2} & \frac{O(1)}{l_3} & \frac{O(1)}{l_4} & \frac{O(1)}{l_5} & \frac{O(1)}{l_6} & \frac{O(1)}{l_7} \\ \frac{O(1)}{l_1} & \frac{O(1)}{l_2} & \frac{O(1)}{l_3} & \frac{O(1)}{l_4} & \frac{O(1)}{l_5} & \frac{O(1)}{l_6} & \frac{O(1)}{l_7} \\ \frac{O(1)}{l_1} & \frac{O(1)}{l_2} & \frac{O(1)}{l_3} & \frac{O(1)}{l_4} & \frac{O(1)}{l_5} & \frac{O(1)}{l_6} & \frac{O(1)}{l_7} \\ \frac{O(x)}{l_1} & \frac{O(x)}{l_2} & \frac{O(x)}{l_3} & \frac{O(x)}{l_4} & \frac{O(x)}{l_5} & \frac{O(x)}{l_6} & \frac{O(x)}{l_7} \\ \frac{O(x)}{l_1} & \frac{O(x)}{l_2} & \frac{O(x)}{l_3} & \frac{O(x)}{l_4} & \frac{O(x)}{l_5} & \frac{O(x)}{l_6} & \frac{O(x)}{l_7} \end{array} \right] \quad (\text{A.19})$$

The complexity of the terms in the vector \mathbf{v} from (A.9) can be determined by applying row reduction on J^T from (A.19). It can be shown that after row reduction, $v_j(x)$ can be expressed in the form of $\frac{l_j p_j(x)}{l_7 d(x)}$, where l_j is the length of cable j , and $p_j, d \in O(x^3)$ are univariate cubic equations. The WCW from (A.13) can be expressed as:

$$\left\{ x : v_j(x) = \frac{l_j p_j(x)}{l_7 d(x)} < 0, \forall v_j(x) \in \mathbf{v}(x) \right\} \quad (\text{A.20})$$

Since all cable lengths are strictly positive, $l_j > 0$, these non-polynomial terms can be ignored. Considering the numerator and denominator polynomial equations separately, the WCW definition from (A.20) can be expressed as a univariate equation:

$$\{x : sgn(p_j(x)) = -sgn(d(x)), p_j(x) \neq 0 \ \forall j \in \{1, \dots, 6\}, d(x) \neq 0\} \quad (\text{A.21})$$

The resulting workspace can be represented as a set of open intervals, $x \in (x_l, x_u)$, where x_l and x_u form the workspace boundaries. Given that p_j and d are cubic equations, its roots and sgn regions can be expressed explicitly in analytical form. Alternatively, (A.21) can be expressed as a set of univariate polynomial inequalities. Algorithm 3 summarises this approach for a general case n -DOF system.

Repeating this analysis, if the WCW was to be expressed as a function of an orientation pose variable, for example, β , then the complexity of the Jacobian terms from (A.16) are:

$$J_{1i}, J_{2i}, J_{3i}, J_{4i}, J_{5i}, J_{6i} \in O(c_\beta + s_\beta) \quad (\text{A.22})$$

Algorithm 3 Determining the values of x for which $\mathbf{v}(x) < \mathbf{0}$ **Require:** $\mathbf{v}(x) \in \mathbb{R}^n$ **Ensure:** $\mathbf{v}(x) < \mathbf{0}$

$d(x) \Leftarrow$ univariate polynomial equation from $\mathbf{v}(x)$ (Eqn. A.20)

for $i = 1$ to n **do**

$p_i(x) \Leftarrow$ univariate polynomial equation from $\mathbf{v}(x)$ (Eqn. A.20)

$W_i = \{x : p_i(x) < 0, d(x) > 0\} \cup \{x : p_i(x) > 0, d(x) < 0\}$ (Eqn. A.21)

end for

return $W_1 \cap W_2 \cap \dots \cap W_n$

Using the Jacobian terms from (A.22), expressing $v_j(\beta)$ as $\frac{l_j}{l_7} \frac{p_j(\beta)}{d(\beta)}$ yields $p_j, d \in O(c_\beta^6 + s_\beta^6)$.

The transcendental terms can be eliminated by introducing the Weierstrass substitution:

$$T = \tan \frac{\beta}{2}, \sin \beta = \frac{2T}{1+T^2}, \cos \beta = \frac{1-T^2}{1+T^2} \quad (\text{A.23})$$

As a result, $p_j(T), d(T) \in O(T^{12})$ become univariate polynomials of degree 12, where the set of constant pose variables are contained within the polynomial coefficients.

Performing this analysis for each of the pose variables, it can be shown that the polynomial complexities for p_j and d will differ. Selection of translational variables x, y or z results in univariate cubic equations, $p_j(T), d(T) \in O(T^3)$, while selecting the orientation variable α yields degree 10 univariate polynomials, $p_j(T), d(T) \in O(T^{10})$ and orientation variable β or γ degree 12 univariate polynomials, $p_j(T), d(T) \in O(T^{12})$. From this analysis, it is apparent that different complexities of polynomial equations arise depending on the degrees of freedom and representation of pose for the manipulator. For workspace determination, the pose variable that results in the simplest form should be chosen where possible. The summary of the algorithm when implemented to determine WCW for an n -DOF completely restrained cable system is given in Algorithm 4.

A.4.2 3-DOF Ball Joint Manipulator

A 3-DOF manipulator constrained at the origin of the inertial frame, $\{F_0\}$, by a ball joint is shown in Figure A.2. The pose of the manipulator can be defined by the xyz -Euler orientation angles $\mathbf{x} = [\alpha \beta \gamma]^T$. Since there are only orientation degrees of freedom, the

Algorithm 4 Determining WCW for an n -DOF $(n+1)$ -cable system

Require: $\{B_1, B_2, \dots, B_n\}$ which are the bounds for variables $\{x_1, x_2, \dots, x_n\}$

Ensure: W is the WCW workspace of manipulator

$\mathbf{x} \Leftarrow \{x_1, x_2, \dots, x_n\} \in \mathbb{R}^n$ (pose variable vector)

$J^T \Leftarrow n \times (n+1)$ transpose of Jacobian matrix (Eqn. A.4)

for all $J_{ij} \in J^T$ **do**

$J_{ij} \Leftarrow$ derive analytical expression (Eqn. A.16)

end for

$\mathbf{v}(\mathbf{x}) \Leftarrow (n+1)^{\text{th}}$ column of row-reduced J^T matrix (Eqn. A.9)

$x_s \Leftarrow$ selected pose variable from \mathbf{x} , e.g. x_n

$\mathbf{x}_c \Leftarrow \{x_1, x_2, \dots, x_{n-1}\} \in \mathbb{R}^{n-1}$ where $x_s \notin \mathbf{x}_c$; \mathbf{x}_c contains the remaining pose variables

for $x_1 \in B_1$ with step-size ΔB_1 **do**

for $x_2 \in B_2$ with step-size ΔB_2 **do**

⋮

for $x_{n-1} \in B_{n-1}$ with step-size ΔB_{n-1} **do**

$\mathbf{v}(x_s) \Leftarrow$ substitute \mathbf{x}_c into $\mathbf{v}(\mathbf{x})$ (Eqn. A.20)

$A \Leftarrow$ region satisfying $\mathbf{v}(x_s) < 0$ (Algorithm 3)

$W \Leftarrow W \cup A$

end for

⋮

end for

end for

return W

transpose of the Jacobian matrix is:

$$J^T = \begin{bmatrix} \mathbf{r}_{B_1} \times \hat{\mathbf{l}}_1 & \mathbf{r}_{B_2} \times \hat{\mathbf{l}}_2 & \mathbf{r}_{B_3} \times \hat{\mathbf{l}}_3 & \mathbf{r}_{B_4} \times \hat{\mathbf{l}}_4 \end{bmatrix} \quad (\text{A.24})$$

The Jacobian matrix terms in (A.24) are equivalent to (A.5) where $\mathbf{r}_{0E} = \mathbf{0}$:

$$\mathbf{r}_{B_i} \times \hat{\mathbf{l}}_i = \frac{\mathbf{r}_{A_i} \times ({}^0_E R(\mathbf{x}) \mathbf{r}_{B_i})}{l_i} \quad (\text{A.25})$$

From (A.15), it can be seen that the Jacobian terms for the particular system can be expressed as:

$$\begin{bmatrix} \mathbf{r}_{EB_i} \times \hat{\mathbf{l}}_i \end{bmatrix} = \frac{1}{l_i} \begin{bmatrix} J_{1i} \\ J_{2i} \\ J_{3i} \end{bmatrix} \quad (\text{A.26})$$

where each term could be explicitly derived from (A.25):

$$\begin{aligned} J_{1i} &= r_{A_{iy}}(r_{B_{ix}}(s_\alpha s_\gamma - c_\alpha s_\beta c_\gamma) + r_{B_{iy}}(s_\alpha c_\gamma + c_\alpha s_\beta s_\gamma) + r_{B_{iz}}c_\alpha c_\beta) \\ &\quad - r_{A_{iz}}(r_{B_{ix}}(c_\alpha s_\gamma + s_\alpha s_\beta c_\gamma) + r_{B_{iy}}(c_\alpha c_\gamma - s_\alpha s_\beta s_\gamma) - r_{B_{iz}}s_\alpha c_\beta) \\ J_{2i} &= -r_{A_{ix}}(r_{B_{ix}}(s_\alpha s_\gamma - c_\alpha s_\beta c_\gamma) + r_{B_{iy}}(s_\alpha c_\gamma + c_\alpha s_\beta s_\gamma) + r_{B_{iz}}c_\alpha c_\beta) \\ &\quad + r_{A_{iz}}(r_{B_{ix}}c_\beta c_\gamma - r_{B_{iy}}c_\beta s_\gamma + r_{B_{iz}}s_\beta) \\ J_{3i} &= r_{A_{ix}}(r_{B_{ix}}(c_\alpha s_\gamma + s_\alpha s_\beta c_\gamma) + r_{B_{iy}}(c_\alpha c_\gamma - s_\alpha s_\beta s_\gamma) - r_{B_{iz}}s_\alpha c_\beta) \\ &\quad - r_{A_{iy}}(r_{B_{ix}}c_\beta c_\gamma - r_{B_{iy}}c_\beta s_\gamma + r_{B_{iz}}s_\beta) \end{aligned} \quad (\text{A.27})$$

The problem can then be reformulated as a univariate polynomial function of one of the pose variables. In this case, the three possible Euler angles will yield the same level of complexity. To illustrate this example, α was selected, and the complexity of the Jacobian terms are:

$$J_{1i}, J_{2i}, J_{3i} \in O(c_\alpha + s_\alpha) \quad (\text{A.28})$$

where the coefficients of the terms are a function of β and γ . After row-reduction on J^T , $v_j(\alpha) = \frac{l_j}{l_4} \frac{p_j(\alpha)}{d(\alpha)}$, where $p_j, d \in O(c_\alpha^3 + s_\alpha^3)$. Introducing the Weierstrass substitution in (A.23), univariate sextics, $p_j, d \in O(T^6)$, are obtained. Hence the WCW definition for this

specific manipulator becomes:

$$W = \left\{ \alpha : T = \tan \frac{\alpha}{2}, \operatorname{sgn}(p_j(T)) = -\operatorname{sgn}(d(T)), p_j(T) \neq 0 \quad \forall j \in \{1, \dots, 3\}, d(x) \neq 0 \right\} \quad (\text{A.29})$$

The resulting workspace can be represented as a set of open intervals, $\alpha \in (\alpha_l, \alpha_u)$, where α_l and α_u form the workspace boundaries.

A.4.3 Workspace Evaluation

The proposed technique inherently accommodates the ability to quantitatively evaluate the WCW in an efficient manner. This is crucial in the optimisation of cable configurations for a particular manipulator design. In the optimisation process, the evaluation of workspace under a desired quantitative measure of quality is required. A trivial example of such a function is the total workspace volume. More sophisticated functions could incorporate levels of desirability in different workspace regions.

Considering the quality of the workspace at a particular pose, \mathbf{x} , as $f(\mathbf{x})$, the total quality of the workspace can be defined as:

$$Q = \int_W f(\mathbf{x}) d\mathbf{x} \quad (\text{A.30})$$

where W represents the WCW of the manipulator. It will be shown that the total workspace quality could be efficiently computed if the integral function of $f(\mathbf{x})$ can be determined analytically with respect to at least one of the pose variables. For example, considering the 3-DOF ball joint manipulator presented in Section A.4.2, the total quality from (A.30) can be expressed as:

$$Q = \int_{\alpha} \int_{\beta} \int_{\gamma} f(\alpha, \beta, \gamma) d\alpha d\beta d\gamma, \quad \forall (\alpha, \beta, \gamma) \in W \quad (\text{A.31})$$

Assuming that the integral of $f(\alpha, \beta, \gamma)$ can be determined with respect to α , $F(\alpha)$, the

quality from (A.31) can be expressed as:

$$\begin{aligned} Q &= \sum_{\gamma} \sum_{\beta} \sum_k \int_{\alpha_{u_l}}^{\alpha_{u_k}} f(\alpha, \beta, \gamma) d\alpha, \forall (\beta, \gamma) \in W \\ &= \sum_{\gamma} \sum_{\beta} \sum_k F(\alpha_{u_k}) - F(\alpha_{u_l}), \forall (\beta, \gamma) \in W \end{aligned} \quad (\text{A.32})$$

where k represents the number of (α_l, α_u) intervals at particular β and γ values. The total quality from (A.32) provides an efficient way to evaluate the workspace by using the lower and upper bounds determined by the analytical WCW form from (A.29). In comparison, the workspace determined by the point-wise approach would require evaluation of $f(\alpha, \beta, \gamma)$ at each (α, β, γ) pose within the WCW. A simple and intuitive quality function is the volume of the workspace, where $f(\alpha, \beta, \gamma) = 1$ and hence $F(\alpha) = \alpha$. The resulting total cost can be expressed as:

$$Q = \sum_{\gamma} \sum_{\beta} \sum_k (\alpha_{u_k} - \alpha_{u_l}), \forall (\beta, \gamma) \in W \quad (\text{A.33})$$

With careful selection of the quality functions, the manipulator's cable configuration can be optimised to possess desirable WCW characteristics in an efficient and autonomous manner.

A.5 Simulation Setup

The WCW for a 3-DOF and 6-DOF completely restrained cable driven parallel manipulator is generated using the proposed approach. The workspace for the 3-DOF manipulator will also be determined using the point-wise approach as a benchmark in terms of accuracy and computational efficiency. The point-wise approach to determine the WCW for a 6-DOF manipulator was not performed due to the inefficiency of the method. The simulation setup and manipulator cable arrangements are presented in this section.

A.5.1 3-DOF Ball Joint Manipulator

The cable attachment points for the proposed 3-DOF manipulator as shown in Figure A.2 are displayed in Table A.1, assuming units in metres. In this configuration, the cables are located symmetrically around the ball joint of the manipulator.

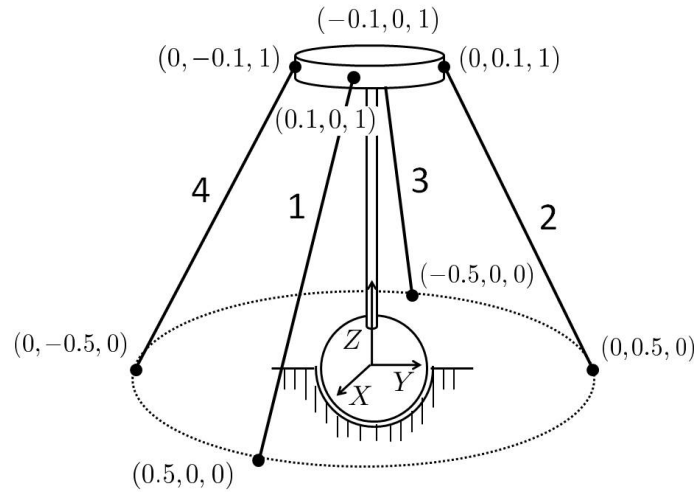


Figure A.2: 3-DOF Ball Joint Manipulator Model

	Base			End Effector		
	${}^0r_{A_{ix}}$	${}^0r_{A_{iy}}$	${}^0r_{A_{iz}}$	${}^Er_{B_{ix}}$	${}^Er_{B_{iy}}$	${}^Er_{B_{iz}}$
Cable 1	0.5	0	0	0.1	0	1
Cable 2	0	0.5	0	0	0.1	1
Cable 3	-0.5	0	0	-0.1	0	1
Cable 4	0	-0.5	0	0	-0.1	1

Table A.1: Cable Configuration for 3-DOF Manipulator

For this manipulator, the bounds for the pose variables in determining the workspace were selected to be $\alpha, \beta \in [-\frac{\pi}{2}, \frac{\pi}{2}]$ rad and $\gamma \in [-\pi, \pi]$ rad. A range of step sizes, $\Delta\alpha$, $\Delta\beta$ and $\Delta\gamma$, were varied to observe the efficiency and accuracy of both techniques. The efficiency of the approach was measured as the computational time required to determine the workspace, and accuracy was compared through graphical representations of the WCW and workspace volumes.

Due to discretisation in the approaches, the workspace volume for the point-wise

approach can be considered as a sum of elementary cubes with volume $\Delta V = \Delta\alpha \cdot \Delta\beta \cdot \Delta\gamma$, and the whole volume of the workspace can be expressed as:

$$V_a = \sum_{\alpha} \sum_{\beta} \sum_{\gamma} \Delta\alpha \cdot \Delta\beta \cdot \Delta\gamma \quad (\text{A.34})$$

For the proposed hybrid approach, the workspace volume can be considered as a sum of thin rectangles with volume $\Delta V = \Delta\beta \cdot \Delta\gamma \cdot (\alpha_u - \alpha_l)$, hence the total volume can be represented as:

$$V_b = \sum_{\beta} \sum_{\gamma} \sum_k \Delta\beta \cdot \Delta\gamma \cdot (\alpha_{u_k} - \alpha_{l_k}) \quad (\text{A.35})$$

where k represents the number of (α_l, α_u) intervals at the β and γ value. Since the point-wise approach is known to underestimate the workspace, the difference in volumes of the two approaches can be expressed by taking a ratio of the volumes from (A.34) and (A.35). If the same step size values, $\Delta\beta$ and $\Delta\gamma$, are used in both approaches, the volume ratio can be expressed as:

$$V_r = \frac{V_a}{V_b} = \frac{\sum_{\beta} \sum_{\gamma} \sum_{\alpha} \Delta\alpha}{\sum_{\beta} \sum_{\gamma} \sum_k (\alpha_{u_k} - \alpha_{l_k})} \quad (\text{A.36})$$

To allow direct comparison of the point-wise approach against the proposed approach, it is assumed that continuous points along α can be considered as a single linear region, relaxing the locality constraint of the point-wise method.

Proposed Hybrid Analytical-Numerical Approach

It was shown in Section A.4.2 that the polynomial coefficients for the WCW in (A.29) will be functions of β and γ . By assuming constant β and γ , polynomial coefficients and subsequently, the solution to the WCW with respect to α , can be determined. In this simulation, β and γ are uniformly varied within the defined bounds as shown in Algorithm 4. At each β and γ iteration, the Weierstrass substitution is applied and the roots of the polynomial equations, $p_1(T), p_2(T), p_3(T)$ and $d(T)$ are determined. This is used to evaluate the sign of the polynomial functions and then to generate the WCW

using (A.29). The proposed approach provides a point-based measure along β and γ , while the WCC is satisfied continuously along $\alpha_l < \alpha < \alpha_u$. The only inaccuracy incurred in this approach is the numerical error involved in solving for the polynomial roots. To determine the computational complexity of the proposed approach, the number of steps for the pose variables α, β and γ can be denoted as a, b and c , respectively. Since only β and γ are varied iteratively, the complexity is $O(bc)$, with the fundamental operation of solving for (A.29) at each iteration.

Point-Wise Evaluation

In the point-wise evaluation approach, pose variables are varied discretely within the defined bounds. At each sample point, if the WCC from (A.13) is satisfied, then the point can be classified as being within the WCW. Workspace obtained through this approach has two main features: identified regions are a collection of points that satisfy WCC locally, and the obtained region underestimate the exact workspace. The first feature implies that the resulting workspace region will be described by a set of points, where the workspace properties between points cannot be concluded. Underestimation of the workspace means that the determined region only approximates the exact solution. As a result, the accuracy is dependent on the step-sizes, $\Delta\alpha$, $\Delta\beta$ and $\Delta\gamma$. In this simulation experiment, the pose variables α, β and γ are varied at uniform intervals, implying that $\Delta\alpha$, $\Delta\beta$ and $\Delta\gamma$ are constant values. Hence, the computational complexity of the uniform interval point-wise approach is $O(abc)$, with the fundamental operation as the verification of the WCC from (A.13).

A.5.2 6-DOF Spatial Manipulator

The general 6-DOF spatial manipulator analysed is of the same type as investigated in [44, 108], consisting of a floating end effector with cables attached to a base frame, as shown in Figure A.3. The cable attachment points for the manipulator are displayed in Table A.2.

To allow visualisation of the resulting workspace, the end effector is assumed to have

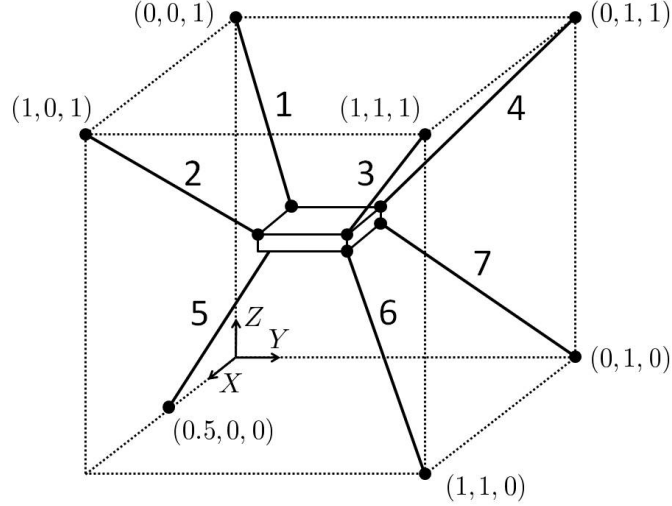


Figure A.3: 6-DOF Ball Joint Manipulator Model

Table A.2: Cable Configuration for 6-DOF Manipulator

	${}^0r_{A_{ix}}$	${}^0r_{A_{iy}}$	${}^0r_{A_{iz}}$	End Effector		
	${}^0r_{B_{ix}}$	${}^0r_{B_{iy}}$	${}^0r_{B_{iz}}$	${}^Er_{B_{ix}}$	${}^Er_{B_{iy}}$	${}^Er_{B_{iz}}$
Cable 1	0	0	1	-0.15	-0.1	0.05
Cable 2	1	0	1	0.15	-0.1	0.05
Cable 3	1	1	1	0.15	0.1	0.05
Cable 4	0	1	1	-0.15	0.1	0.05
Cable 5	0.5	0	0	0	-0.1	-0.05
Cable 6	1	1	0	0.15	0.1	-0.05
Cable 7	0	1	0	-0.15	0.1	-0.05

constant orientation. The WCW of two orientations, $\alpha = \beta = \gamma = 0$, and $\alpha = \beta = 0, \gamma = 5^\circ$, will be presented. The bounds for the translational variables were selected to be $x, y, z \in [0, 1]$ m. The WCW will be determined analytically with respect to pose variable x , for varying values of y and z with step sizes of $\Delta y = \Delta z = 0.01$ m.

Proposed Hybrid Analytical-Numerical Approach

It was shown in Section A.4.1 that the selection of translational generalised variables would result in univariate cubic equations. In this simulation, x is selected and the remaining variables, y, z, α, β and γ are uniformly varied within the defined bounds as

shown in Algorithm 4. The proposed approach provides a point-based measure along y, z, α, β and γ , while the WCC is satisfied continuously along $x_l < x < x_u$. Denoting the number of steps for the pose variables $\alpha, \beta, \gamma, x, y$ and z as a, b, c, d, e and f , respectively, the computational complexity of the proposed approach for non-constant orientation WCW evaluation is $O(abcef)$, with the fundamental operation of solving for (A.21) at each iteration. Performing a similar analysis for the point-wise approach, the computational complexity is expected to be $O(abcdef)$, with the fundamental operation as the verification of the WCC from (A.13).

A.6 Results and Discussion

The $\alpha\text{-}\beta$ cross-sections of the WCW for the 3-DOF manipulator with $\Delta\alpha = \Delta\beta = \Delta\gamma = \frac{\pi}{60}$ rad at $\gamma \approx \frac{\pi}{6}$ rad for the proposed and point-wise approaches are shown in Figures A.4(a) and A.4(b), respectively. Additionally, the admitted workspace satisfying the WCC of each approach is demonstrated through lines and dots, respectively. From the cross-sections, it can be observed that two disconnected workspace volumes exist. Figure A.5 shows the 3D visualisation of one of these volumes determined using each approach. The locality problem for both approaches have been disregarded for the purpose of visualisation.

Comparing the cross-sections and 3D representations of the two techniques, it can be observed that the proposed approach produces a more accurate definition of workspace contour, where as the artifacts of discretisation are more prominent in the point-wise approach. This can be observed when the region size and the step-size are of similar magnitude, where the point-wise evaluation lacks the resolution required to clearly depict the region. The consequence of this is the possibility in misinterpreting the workspace shape. The cross-section at $\gamma \approx \frac{3\pi}{8}$ rad in Figure A.6 shows an example where the workspace shape determined by the point-wise approach is difficult to identify compared to the proposed method. This is further illustrated in the cross-section at $\gamma \approx \frac{7\pi}{16}$ rad in Figure A.7, where the point-wise approach shows two smaller sections that appear to be disconnected. In contrast, the proposed approach clearly shows a single thin segment

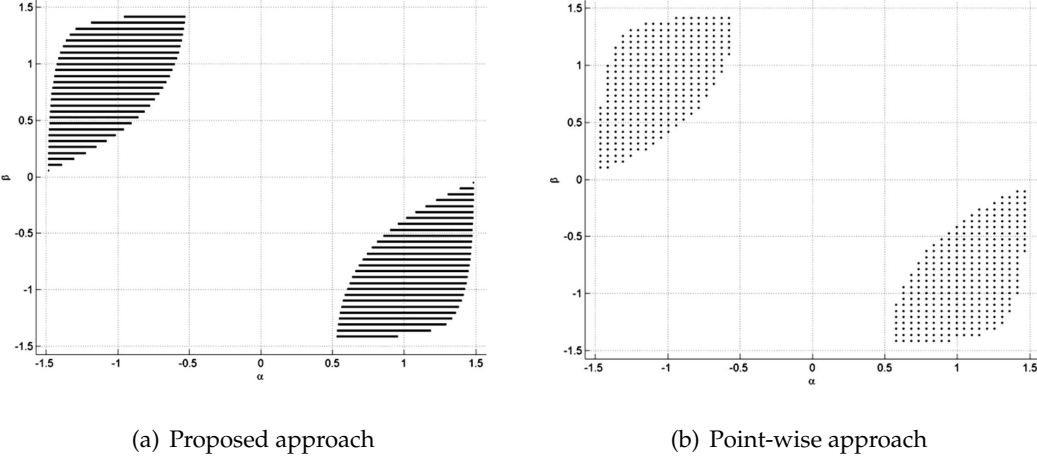


Figure A.4: α - β cross-section of the 3-DOF manipulator's WCW at $\gamma \approx \frac{\pi}{6}$ rad with $\Delta\alpha = \Delta\beta = \Delta\gamma = \frac{\pi}{60}$ rad for $\alpha, \beta \in [-\frac{\pi}{2}, \frac{\pi}{2}]$ rad

of workspace. Although the proposed approach produces solutions local to the β and γ values, the determined workspace boundaries and regions are the exact solutions of the WCW within numerical computational error. This produces a more accurate representation of the workspace geometry without any dependence on $\Delta\alpha$.

The accuracy of the point-wise approach could be increased by using smaller step sizes $\Delta\alpha$, $\Delta\beta$ and $\Delta\gamma$. Figures A.8 and A.9 show the same cross-sections at $\gamma \approx \frac{3\pi}{8}$ rad and $\gamma \approx \frac{7\pi}{16}$ rad with a step-size of $\Delta\alpha = \Delta\beta = \Delta\gamma = \frac{\pi}{200}$ rad. With this step-size, it is apparent that the point-wise approach produces more accurate workspace representations compared to those shown in Figures A.6(b) and A.7(b). Despite the finer step-size, the discretisation around the workspace boundary is still visible. In comparison, the proposed approach provides more information between the gaps for β and γ , as shown in Figures A.8(a) and A.9(a), but has no effect on the accuracy of the solution with respect to α . These observations suggest that the proposed approach can be considered as equivalent to the point-wise approach with $\Delta\alpha = \epsilon$, where ϵ is the numerical error involved in the computation of the polynomial roots. Observing the computational complexity for the point-wise evaluation approach, the increased number of steps in α will have a significant impact on its efficiency.

To compare the approaches, two different scenarios to vary the step-sizes in workspace

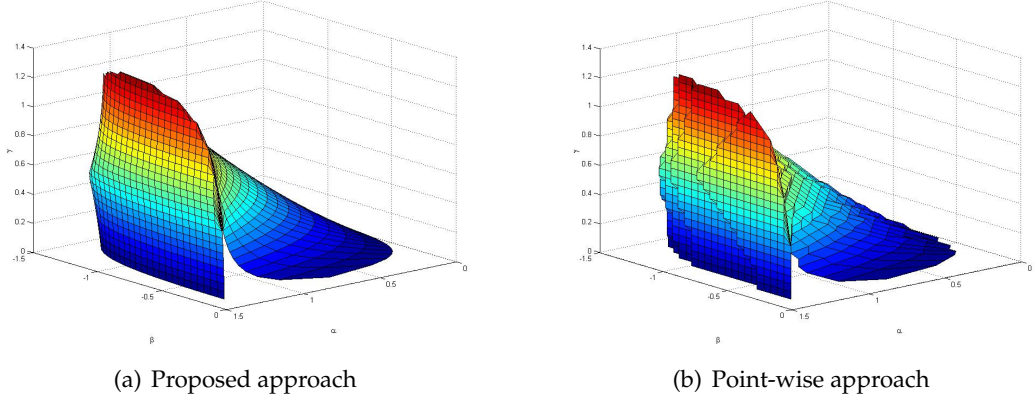


Figure A.5: 3-D Visualisation of the 3-DOF manipulator's workspace for $\alpha, \gamma \in [0, \frac{\pi}{2}]$ rad and $\beta \in [-\frac{\pi}{2}, 0]$ rad

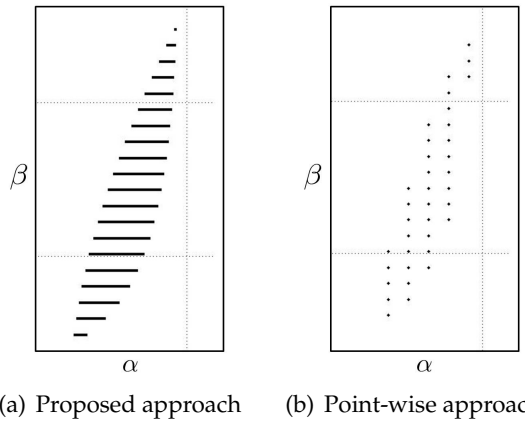


Figure A.6: α - β cross-section of the 3-DOF manipulator's workspace at $\gamma \approx \frac{3\pi}{8}$ rad with $\Delta\alpha = \Delta\beta = \Delta\gamma = \frac{\pi}{60}$ rad

generation have been considered. In both cases, the time efficiency of each approach and the volume ratio from (A.36) have been measured for the setup described in Section A.5.1.

Case 1 : Step-sizes of all pose variables are uniform, $\Delta\alpha = \Delta\beta = \Delta\gamma = \Delta x$, and varied between $\frac{\pi}{20}$ and $\frac{\pi}{200}$ rad. This is expected to be the more commonly used scenario when performing analysis on the workspace geometry and features.

Case 2 : Step-sizes of pose variables β and γ , $\Delta\beta$ and $\Delta\gamma$ are chosen as a constant value of $\Delta\beta = \Delta\gamma = \frac{\pi}{20}$ rad, while $\Delta\alpha$ is varied between $\frac{\pi}{20}$ and $\frac{\pi}{3200}$ rad. This allows a more direct comparison on the accuracy between the approaches for varying $\Delta\alpha$.

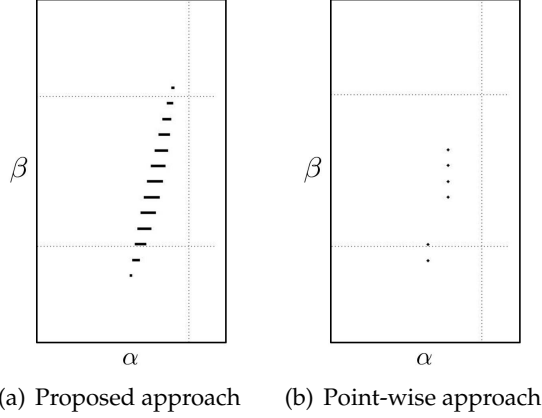


Figure A.7: α - β cross-section of the 3-DOF manipulator's workspace at $\gamma \approx \frac{7\pi}{16}$ rad with $\Delta\alpha = \Delta\beta = \Delta\gamma = \frac{\pi}{60}$ rad

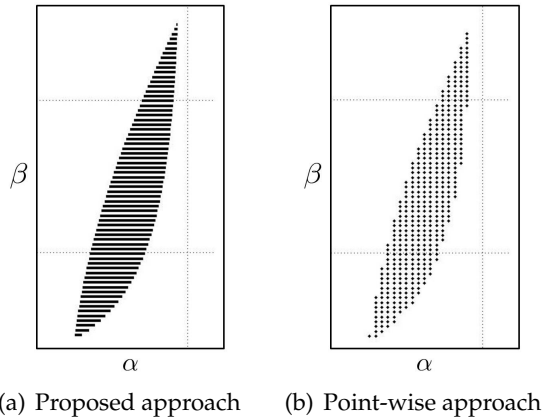


Figure A.8: α - β cross-section of the 3-DOF manipulator's workspace at $\gamma \approx \frac{3\pi}{8}$ rad with $\Delta\alpha = \Delta\beta = \Delta\gamma = \frac{\pi}{200}$ rad

The results for case 1 are shown in Table A.3, where it can be observed that the proposed approach has much lower computational times than the point-wise approach. Furthermore, this becomes increasingly significant for smaller step-sizes, conforming to the computational complexities determined previously. Denoting the number of steps in γ as c , derived from step-size $\Delta\gamma$ and bounds on γ , the commonly used point-wise approach has an algorithmic complexity of $O(c^3)$, while for the proposed approach it is $O(c^2)$. Despite having different fundamental operations in the complexity analysis, it appears that the numerical polynomial root solving is more efficient in comparison to

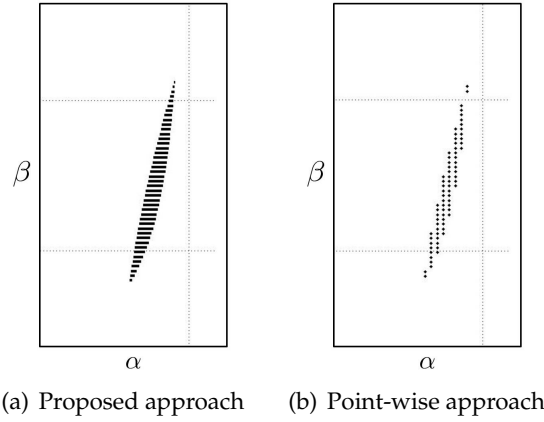


Figure A.9: α - β cross-section of the 3-DOF manipulator's workspace at $\gamma \approx \frac{7\pi}{16}$ rad with $\Delta\alpha = \Delta\beta = \Delta\gamma = \frac{\pi}{200}$ rad

multiple point-wise evaluations. In addition to the advantage in efficiency, the volume ratio shows that the proposed approach has a higher accuracy in workspace determination. With decreasing step-size, it can be observed that the volume ratio approaches unity, suggesting that the workspace region from the point-wise approach is converging to the proposed approach. It is important to note that the volume ratio is not an absolute measure of accuracy and is highly dependent on the workspace geometry for the particular cable configuration. Since the error in the point-wise approach occurs due to the discretisation of the workspace boundary by Δx , the magnitude of this error is dependent on the workspace's surface to volume ratio. Hence the volume ratio can only be used as an indication of accuracy for this cable configuration.

Δx (rad)	Computational Time (sec)		V_r
	Proposed Approach	Point-wise Evaluation	
$\pi/20$	1.0608	4.6176	0.7217
$\pi/40$	3.2292	33.9146	0.8458
$\pi/60$	6.8328	109.7311	0.9067
$\pi/80$	11.9185	258.0569	0.9280
$\pi/100$	18.5797	507.9081	0.9430
$\pi/200$	73.4453	3973	0.9720

Table A.3: Computational time and volume ratio for varying $\Delta\alpha = \Delta\beta = \Delta\gamma = \Delta x$

Table A.4 shows the computational time and volume ratio for case 2, where $\Delta\alpha$ is

varied for constant β and γ . The computational complexity of the proposed and point-wise approaches are constant, $O(1)$, and linear, $O(a)$, respectively, where a represents the number of steps in the iteration of α as defined in Section A.5.1. The constant computational complexity for the proposed approach is expected as there is no dependency on $\Delta\alpha$. Similar to the case with uniformly varying step-size, a decrease in step-size shows a convergence of the volume ratio towards unity. The results suggest that the proposed approach has the accuracy of the point-wise approach with $\Delta\alpha = \epsilon \ll \frac{\pi}{3200}$.

$\Delta\alpha$ (rad)	Computational Time (sec)		V_r
	Proposed Approach	Point-wise Evaluation	
$\pi/20$	1.0608	4.6176	0.7217
$\pi/50$	1.1076	11.2633	0.8860
$\pi/100$	1.0920	21.8401	0.9405
$\pi/200$	1.0452	42.9939	0.9704
$\pi/400$	1.1232	85.5821	0.9850
$\pi/800$	1.0843	171.3359	0.9920
$\pi/1600$	1.2012	336.2602	0.9960
$\pi/3200$	1.1700	673.2379	0.9980

Table A.4: Computational time and volume ratio for varying $\Delta\alpha$ with $\Delta\beta = \Delta\gamma = \frac{\pi}{20}$ rad

Although comparable accuracy can be achieved using the point-wise approach with an extremely small step-size, it is apparent that the efficiency is significantly impacted. In addition, the interval-based satisfaction of the WCC of the proposed approach is desirable over the point-based locality of the point-wise approach, since the condition is satisfied for all continuous values along α within the lower and upper bounds (α_l, α_u). It should be noted that in achieving these advantages, the proposed approach requires explicit determination of the polynomials p_j and d in (A.29) from J^T , which are different depending on the manipulator topology. In comparison, the WCC condition in (A.13) can be utilised for the point-wise approach once J^T has been determined, regardless of manipulator topology.

Similarly, for the 6-DOF manipulator, the proposed algorithm was implemented to generate the x - y cross sections of the WCW for two constant orientations, $\alpha = \beta = \gamma = 0$, and $\alpha = \beta = 0, \gamma = 5^\circ$ for varying z values, as shown in Figures A.10 and A.11,

respectively. Advantages of the proposed algorithm are similarly observed in this 6-DOF case, such as: the accurate determination of the WCW without any discretisation in the x dimension and the reduction of one exponential order in the expected computational time compared to the point-wise approach. The resulting workspace can be compared to the results of [108], and was observed to display similar symmetry and asymmetry in the admitted workspace, as shown in Figures A.10 and A.11, respectively. The asymmetry is introduced by the non-zero γ constant orientation.

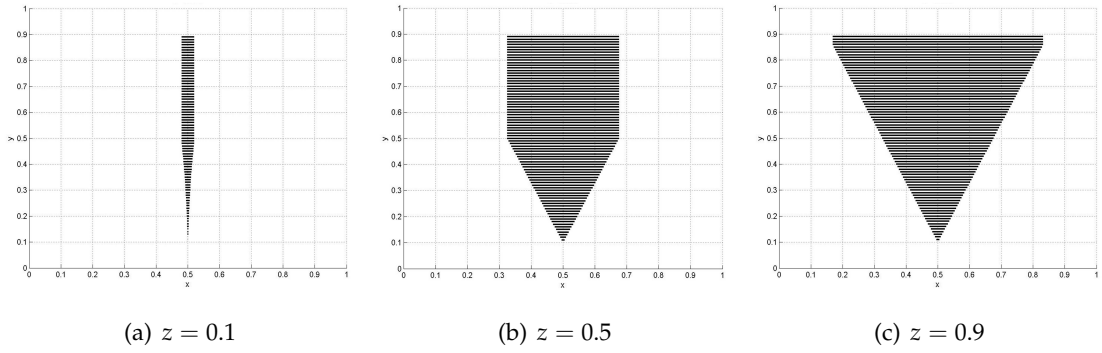


Figure A.10: x - y cross-section of 6-DOF manipulator's WCW at $\alpha = \beta = \gamma = 0^\circ$ with $\Delta y = 0.01$ m for $x, y \in [0, 1]$ m

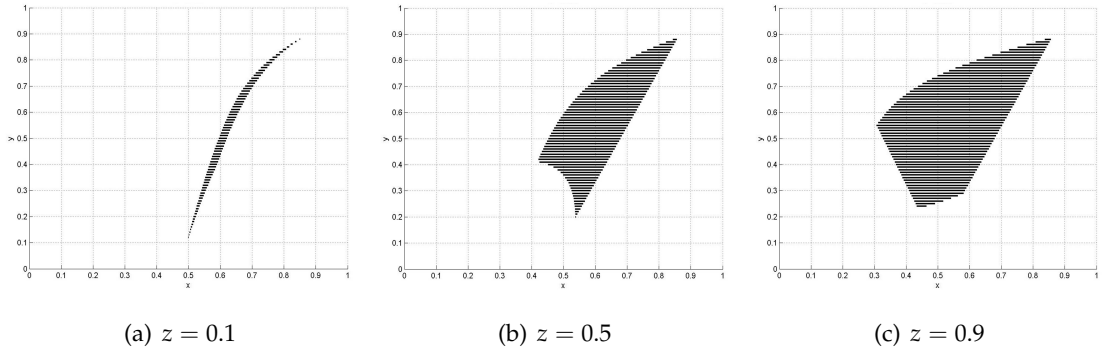


Figure A.11: x - y cross-section of 6-DOF manipulator's WCW at $\alpha = \beta = 0^\circ, \gamma = 5^\circ$ with $\Delta y = 0.01$ m for $x, y \in [0, 1]$ m

The proposed approach can be regarded as a hybrid of numerical and analytical techniques, where the analytical form of the workspace region is solved with respect to a single variable, and the remaining pose variables are iteratively varied in the evaluation

of the WCW within the region of interest, as discussed in Section A.4. As a result, the level of accuracy known from the purely analytical techniques is maintained while significantly reducing its algebraic complexity.

A.7 Conclusions

A hybrid approach utilising analytical formulations within conventional numerical methods for a completely restrained cable driven manipulator was presented. It was shown that despite the complexity, the algebraic inequalities defining the WCW can be simplified to a set of univariate polynomial inequalities by considering a single variable for analysis. The complexities of the polynomial inequalities were determined for a general spatial manipulator and a 3-DOF manipulator. It was shown that this approach is significantly more efficient compared to exhaustive numerical search techniques that evaluate in a point-wise manner. Efficient generation and evaluation of workspace provided by the proposed WCW determination approach allows the potential of comparing and optimising cable arrangements in an automated manner. Future work will focus on utilising the proposed technique in determining other types of cable driven parallel manipulator workspace, and to apply these in the optimisation of cable configurations given the desired workspace characteristics.

Appendix B

On the Task Specific Evaluation and Optimisation of Cable-Driven Parallel Manipulators

Cable-driven manipulators are traditionally designed for general performance objectives, such as maximisation of workspace. To take advantage of the reconfigurability of cable-driven mechanisms, the optimisation of cable-configurations for specific tasks is presented. Specifically, two types of task specific objectives are explored, the minimisation of cable forces over a desired trajectory and the maximisation of workspace about a desired pose. The formulation and incorporation to the optimisation problem for both task specific objectives are presented. Illustrated using a 3-DoF manipulator example, the results clearly demonstrated the advantages of optimising cable configurations for specific tasks. The potential ease of relocation in cable attachments makes task dependent reconfiguration feasible.

B.1 Introduction

Cable-driven parallel manipulators refer to mechanisms where the end-effector is controlled through cables. Cables are attached to the end effector on one end and to the actuator located at the base platform on the other. Desirable characteristics over traditional parallel mechanisms include: reduced weight and inertia, simplified dynamics modelling and the ease of transportation. The unique property of cable driven mechanisms is that its cables can only be actuated unilaterally through tension and not com-

pression (*positive cable force*).

Due to the potential ease in relocating the cable attachment locations (*cable configuration*) on the end effector and base platform, cable-driven manipulators can be regarded as a reconfigurable mechanism. A wide range of applications exist for cable-driven mechanisms, such as such as manufacturing [4], rehabilitation [122] and exoskeletons [141]. For a given application, cable configuration can be either determined by the designer or through an optimisation process [2, 72, 104].

Naturally, the selection of an appropriate objective function is crucial in the determination of a desired cable configuration. In [2], the workspace volume was maximised for a two-link upper arm exoskeleton. Maximisation of tension-closure workspace volume and Global Conditioning Index (*GCI*) was performed on a cable-driven universal joint module [72]. In [104], the configuration for a locomotion interface actuated by 16 cables was determined. The objectives involved the maximisation of mechanism workspace volume while minimising cable interference.

Objective functions such as workspace volume and *GCI* are similar to those employed in the design of rigid link mechanisms [39]. The goal is to achieve desirable general performance, as opposed to the efficiency of specific tasks. To take advantage of the potential reconfigurability of cable-driven manipulators, optimisation for specific tasks should be considered. For example, manipulators designed with a large workspace may not be energy efficient for a prescribed trajectory. This saving is particularly significant for highly repetitive tasks, such as pick-and-place in manufacturing or rehabilitation treatment for stroke patients.

In this paper, objective functions to evaluate the desirability of cable-driven manipulator configurations for specific tasks are investigated. Two classes of objective functions are presented, one based on the minimisation of cable forces for a desired trajectory, and the second is based on desired regions of the manipulator workspace. It is shown how workspace properties can be efficiently evaluated by extending the workspace analysis technique proposed in [69]. The impact of the proposed objective functions is illustrated through the optimisation of a 3-DoF manipulator, using a standard Particle Swarm Optimisation (*PSO*) algorithm. The results highlight the potential of task specific cable ar-

angement over a manipulator that is optimised for general or global performance.

The remainder of this paper is organised as follows: Section B.2 presents the manipulator model, inverse dynamics problem and workspace analysis. The task specific objective functions and optimisation problem are formulated in Section B.3. The results for the optimisation of an example 3-DOF manipulator are presented and discussed in Section B.4. Finally, Section B.5 concludes the paper and presents areas of future work.

B.2 Manipulator Model and Background

Consider the model shown in Figure B.1, where \mathbf{r}_{A_i} and \mathbf{r}_{B_i} represents the cable attachments at the base and the end effector for cable i , respectively. The vector \mathbf{r}_{0E} represents the translation from the origin of the inertial frame $\{F_0\}$ to the origin of the end effector frame $\{F_E\}$.

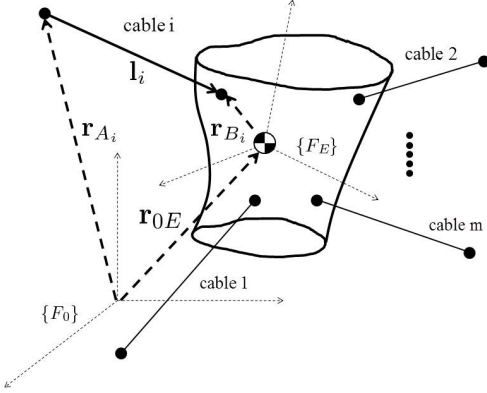


Figure B.1: General Model for Cable Manipulator

The equations of motion a general n -DOF manipulator actuated by m -cables can be expressed in the form

$$M(\mathbf{q})\ddot{\mathbf{q}} + \mathbf{C}(\mathbf{q}, \dot{\mathbf{q}}) + \mathbf{G}(\mathbf{q}) = -J^T(\mathbf{q})\mathbf{f}, \quad (\text{B.1})$$

where $\mathbf{q} = [q_1 \ q_2 \ \dots \ q_n]^T \in \mathbb{R}^n$ represents the manipulator pose, M , \mathbf{C} , and \mathbf{G} are the mass inertia matrix, centrifugal and Coriolis force vector, and gravitational vector,

respectively. The resultant of the cable wrenches is denoted by $-J^T \mathbf{f}$, where $J^T(\mathbf{q}) \in \mathbb{R}^{n \times m}$ is the transpose of the Jacobian matrix. For a 6-DOF spatial manipulator

$$J^T = \begin{bmatrix} \hat{\mathbf{l}}_1 & \hat{\mathbf{l}}_2 & \dots & \hat{\mathbf{l}}_m \\ \mathbf{r}_{B_1} \times \hat{\mathbf{l}}_1 & \mathbf{r}_{B_2} \times \hat{\mathbf{l}}_2 & \dots & \mathbf{r}_{B_m} \times \hat{\mathbf{l}}_m \end{bmatrix}. \quad (\text{B.2})$$

where \mathbf{l}_i is the cable vector of cable i , defined as $\mathbf{l}_i = \mathbf{r}_{0E} + \mathbf{r}_{B_i} - \mathbf{r}_{A_i}$. The cable force vector is denoted by $\mathbf{f} = [f_1 \ f_2 \ \dots \ f_m]^T \in \mathbb{R}^m$, where f_i is the cable force in cable i . The allowable cable force range in cable i can be defined as

$$0 < f_{i,min} \leq f_i \leq f_{i,max}, \quad (\text{B.3})$$

where $f_{i,min}$ ensures positive cable force and prevents cable slackness, while $f_{i,max}$ provides an upper limit on allowable actuation through the cable.

B.2.1 Inverse Dynamics Problem

For a desired manipulator trajectory $\mathbf{q}_r(t)$, $\dot{\mathbf{q}}_r(t)$ and $\ddot{\mathbf{q}}_r(t)$, the system dynamics from (B.1) at time t can be expressed as a linear equation

$$-J^T \mathbf{f} = \mathbf{w}, \quad (\text{B.4})$$

where $\mathbf{w} = M(\mathbf{q})\ddot{\mathbf{q}} + C(\mathbf{q}, \dot{\mathbf{q}}) + G(\mathbf{q})$. The inverse dynamics problem refers to the determination of cable forces, $\mathbf{f}(t)$, subject to the constraints from (B.3) to satisfy the system dynamics in (B.4). For completely and redundantly restrained cable systems ($m \geq n + 1$) an infinite number of solutions exist [86]. One approach to resolve the cable force redundancy is to introduce an objective function for cable forces [15, 46, 99]. The minimisation of the sum of the squared cable forces results in a Quadratic Programming problem

$$\begin{aligned} \mathbf{f}^* &= \arg \min_{\mathbf{f}} \mathbf{f}^T H \mathbf{f} \\ \text{s.t.} \quad &-J^T \mathbf{f} = \mathbf{w} \\ &\mathbf{f}_{min} \leq \mathbf{f} \leq \mathbf{f}_{max}, \end{aligned} \quad (\text{B.5})$$

where H is a positive definite weighting matrix and \mathbf{f}^* is the cable force solution. The cable force constraint refers to the allowable cable forces described in (B.3).

B.2.2 Wrench-Closure Workspace

The Wrench-Closure Workspace (WCW) is defined as the poses in which the manipulator can sustain any arbitrary wrench without any upper cable force bounds

$$W = \{\mathbf{q} : \forall \mathbf{q} \in \mathbb{R}^n, \exists \mathbf{f} > \mathbf{0}, -J(\mathbf{q})^T \mathbf{f} = \mathbf{w}\}, \quad (\text{B.6})$$

where $\mathbf{f} > \mathbf{0}$ denotes the positive cable force constraint. Point-based evaluation techniques to determine the WCW have been studied in [31, 43]. In [69], a hybrid numerical-analytical approach was proposed to generate the WCW with increased accuracy and efficiency compared to point-wise methods. In this approach, the WCW from (B.6) is reduced to a set of univariate polynomial inequalities and analytically solved. From this approach, the workspace is represented by a set of linear regions defined by $\mathbf{q}_r \in \mathbb{R}^{n-1}$, the constant pose for $n - 1$ variables, and the continuous region (q_l, q_u) , where q_l and q_u are the lower and upper bounds for variable q , respectively. This approach is extended to evaluate the workspace in Section B.3.2.

B.3 Optimisation Problem and Evaluation Methods

The cable configuration optimisation problem can be expressed as

$$\begin{aligned} \mathbf{x}^* = \{\mathbf{r}_A^*, \mathbf{r}_B^*\} &= \arg \min_{\mathbf{r}_A, \mathbf{r}_B} C(\mathbf{r}_A, \mathbf{r}_B) \\ \text{s.t.} &\quad \mathbf{r}_A \in \mathcal{A}, \mathbf{r}_B \in \mathcal{B}, \end{aligned} \quad (\text{B.7})$$

where \mathbf{r}_A^* and \mathbf{r}_B^* denote the optimal cable attachment locations at the base and end effector, respectively. The sets \mathcal{A} and \mathcal{B} represent the possible attachment locations at the base and end effector, respectively, and form the constraints on the optimisation variables. The objective function, $C(\mathbf{r}_A, \mathbf{r}_B)$, represents desired properties of the manipulator and is dependent on cable configuration. Two classes of task specific objectives appropriate to

cable-driven manipulators are presented in this section.

B.3.1 Cable Force Characteristics

The evaluation of cable force is a direct and meaningful measure on the configuration's performance in executing a desired trajectory, $\mathbf{q}_r(t)$, $\dot{\mathbf{q}}_r(t)$ and $\ddot{\mathbf{q}}_r(t)$, for a time period of $0 \leq t \leq t_{max}$. Denoting a penalty function for cable forces at time t as $h(\mathbf{f}^*, t)$, the objective function to minimise the penalty over the entire trajectory can be expressed as

$$C(\mathbf{r}_A, \mathbf{r}_B) = \int_0^{t_{max}} h(\mathbf{f}^*, t) dt , \quad (\text{B.8})$$

where \mathbf{f}^* represents the cable forces from the inverse dynamics problem in (B.5). One possible cable force penalty function at time t is

$$h(\mathbf{f}^*, t) = \begin{cases} Q(\mathbf{f}^*) & , \mathbf{f}_{min} \leq \mathbf{f}^* \leq \mathbf{f}_{max} \\ Q(\mathbf{f}_b) & , \text{otherwise} \end{cases} , \quad (\text{B.9})$$

where Q is the function from (B.5), and $\mathbf{f}_b > \mathbf{f}_{max}$ represents penalty cable forces when there are no solutions for (B.5), penalising configurations in which the trajectory cannot be executed.

B.3.2 Workspace Evaluation

Upon determination of the workspace, for example, WCW, existence of desired regions can be evaluated. This is particularly to ensure that the designed manipulator is able to operate within a specifically prescribed region for a desired task. By prescribing a desirability of manipulator pose \mathbf{q} within the workspace W as $v(\mathbf{q})$, the objective function to achieve maximum workspace desirability can be expressed as

$$C(\mathbf{r}_A, \mathbf{r}_B) = - \int_W v(\mathbf{q}) dW . \quad (\text{B.10})$$

One of the simplest measures of workspace is its volume, where the entire workspace is equally weighted $v_1(\mathbf{q}) = 1$. The disadvantage in such a general performance measure

is that the maximisation of volume does not imply that the manipulator can operate in a desired region. To accommodate for this, $v(\mathbf{q})$ can be constructed to favour desired regions. For example, if the desired workspace region is the region about a manipulator pose $\mathbf{q}_s = \{q_{s_1}, q_{s_2}, \dots, q_{s_n}\}$, where q_{s_i} corresponds to the pose variable q_i , respectively, one weighting function can be

$$v_2(\mathbf{q}) = \frac{1}{1 + a_1(q_1 - q_{s_1})^2 + \dots + a_{n-1}(q_{n-1} - q_{s_{n-1}})^2 + a_n(q_n - q_{s_n})^2}. \quad (\text{B.11})$$

The properties of (B.11) are $v_2(\mathbf{q}_s) = 1$, $v_2(\mathbf{q}) \leq 1$, and $v_2(\mathbf{q}) \rightarrow 0$, $\|\mathbf{q} - \mathbf{q}_s\| \rightarrow \infty$. The constant a_i corresponds weighting in dimension i .

Taking advantage of the workspace generation approach proposed in [69], the workspace desirability from (B.10) can be expressed as

$$C = - \sum_{q_{r_1}} \sum_{q_{r_2}} \dots \sum_{q_{r_{n-1}}} \int_{q_l}^{q_u} v(\mathbf{q}_r, q) dq \cdot \Delta q_{r_{n-1}} \dots \Delta q_{r_2} \cdot \Delta q_{r_1}, \quad (\text{B.12})$$

where $\mathbf{q}_r = \{q_{r_1}, q_{r_2}, \dots, q_{r_{n-1}}\}$ represents the constant variables and q is the analytical variable. It is important to note that if the definite integral of $v(\mathbf{q}_r, q)$ with respect to q can be determined analytically, then (B.12) becomes

$$C = - \sum_{q_{r_1}} \sum_{q_{r_2}} \dots \sum_{q_{r_{n-1}}} (V(q_u) - V(q_l)) \cdot \Delta q_{r_{n-1}} \dots \Delta q_{r_2} \cdot \Delta q_{r_1}, \quad (\text{B.13})$$

where V is the definite integral of $v(\mathbf{q}_r, q)$ with respect to q . It is worth noting that for both the volume and proposed task specific workspace region function from (B.11), $V(q) = \int v(\mathbf{q}) dq$ can be determined. Evaluation of workspace in such a manner preserves the advantages of the workspace generation from [69], increased efficiency and accuracy.

B.4 Simulation and Results

To illustrate and compare the different task specific objective functions, the optimisation of a completely restrained 3-DoF manipulator driven by 4-cables is presented. As shown in Figure B.2, the manipulator is constrained at the base through a ball joint, and the pose

Function	Type	Description
C_1	$WCWregion$	Function from (B.14) with weight values of $a_\alpha = a_\beta = a_\gamma = 100$ about pose $\alpha_s = -1, \beta_s = 0.5, \gamma_s = \frac{2\pi}{5}$
C_2	$Trajectory$	$\mathbf{q}_s = \left[\begin{array}{ccc} -\frac{\pi}{10} & \frac{\pi}{10} & 0 \end{array} \right]^T, \mathbf{q}_e = \left[\begin{array}{ccc} \frac{\pi}{10} & -\frac{\pi}{10} & 0 \end{array} \right]^T$ and $t_{max} = 1$
C_3	$Trajectory$	$\mathbf{q}_s = \left[\begin{array}{ccc} \frac{3\pi}{10} & \frac{2\pi}{5} & -\frac{\pi}{6} \end{array} \right]^T, \mathbf{q}_e = \left[\begin{array}{ccc} \frac{\pi}{3} & \frac{\pi}{5} & -\frac{\pi}{3} \end{array} \right]^T$ and $t_{max} = 1$
C_4	WCW	WCW volume (general performance measure as a baseline)

Table B.1: Evaluation Function Descriptions

of the manipulator can be defined as $\mathbf{q} = [\alpha \beta \gamma]^T$, where α, β , and γ are the *xyz*-Euler angles of rotation, respectively.

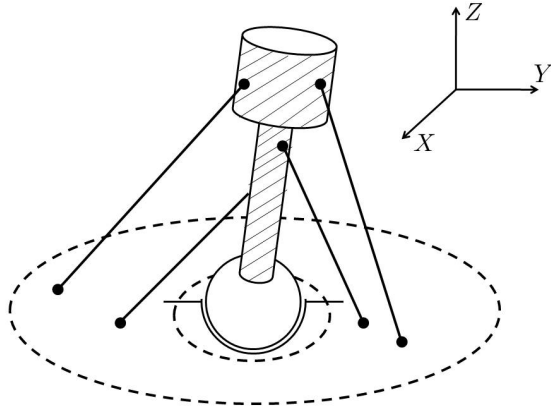


Figure B.2: 3-DOF Ball Joint Manipulator

For the presented manipulator, three task specific objective functions C_1 to C_3 and one general measure C_4 have been selected for optimisation. These objective functions are described in Table B.1. Trajectories are defined by a starting pose \mathbf{q}_s and ending pose \mathbf{q}_e , assuming zero starting and ending velocities and accelerations $\dot{\mathbf{q}}_s = \dot{\mathbf{q}}_e = \ddot{\mathbf{q}}_s = \ddot{\mathbf{q}}_e = \mathbf{0}$. The trajectory $\mathbf{q}(t)$ is then generated from $t = 0$ to $t = t_{max}$ by quaternion interpolation. The evaluation function for a desired workspace region from (B.11) for the 3-DoF manipulator is

$$v_2(\mathbf{q}) = \frac{1}{1 + a_\alpha(\alpha - \alpha_s)^2 + a_\beta(\beta - \beta_s)^2 + a_\gamma(\gamma - \gamma_s)^2}. \quad (B.14)$$

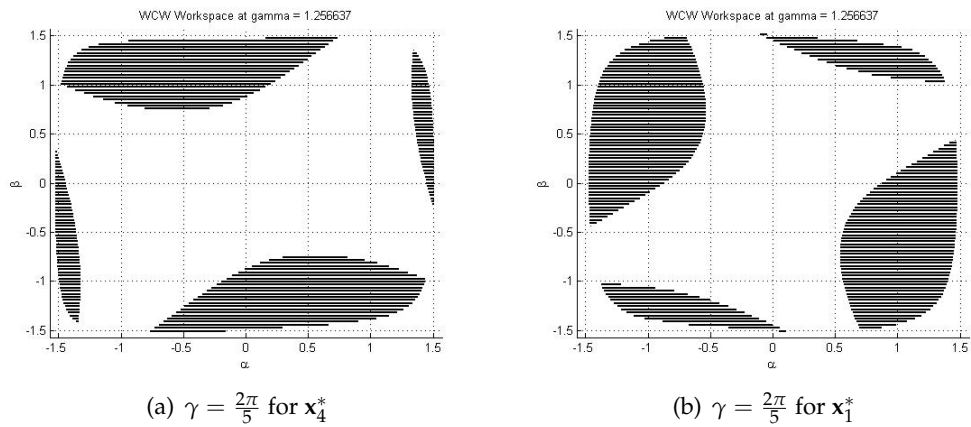
For evaluation function C_i , the optimal cable configuration \mathbf{x}_i^* was determined through

	x_1^*	x_2^*	x_3^*	x_4^*
C_1	-282.3	-161	-11.05	-216.7
C_2	116.7	3.8	8080006.5	13.9
C_3	2333536.2	1864.8	282.6	6973
C_4	-35543	-29966	-2884	-36321

Table B.2: Comparison of Evaluation Functions

a standard Particle Swarm Optimisation (*PSO*) algorithm. To allow comparison between task specific evaluation functions, each optimal configuration was also evaluated for C_1 to C_4 . The results for these evaluations are shown in Table B.2, where the minimum value representing the optimal cost is highlighted.

The optimal cable configuration for the WCW volume x_4^* is a robust configuration that allows the manipulator to satisfy a wide range of tasks. The disadvantage of such a configuration is that efficiency for specific tasks are not considered. For example, the α - β cross section of the WCW at $\gamma_s = \frac{2\pi}{5}$ is shown in Figure B.3(a). It can be observed that workspace does not exist about pose $\alpha = -1$ and $\beta = 0.5$. In comparison, the workspace from configuration x_1^* , optimised for the workspace region about $(\alpha, \beta, \gamma) = (-1, 0.5, \frac{2\pi}{5})$, is shown in Figure B.3(b), where the workspace about the desired location is satisfied. This is particularly useful to ensure that a manipulator is more robust to operate at a desired workspace region.

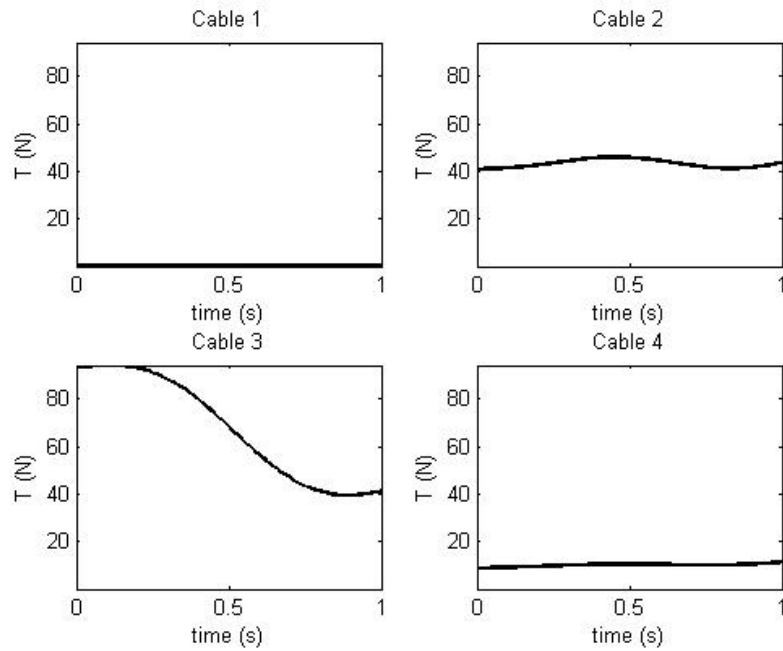
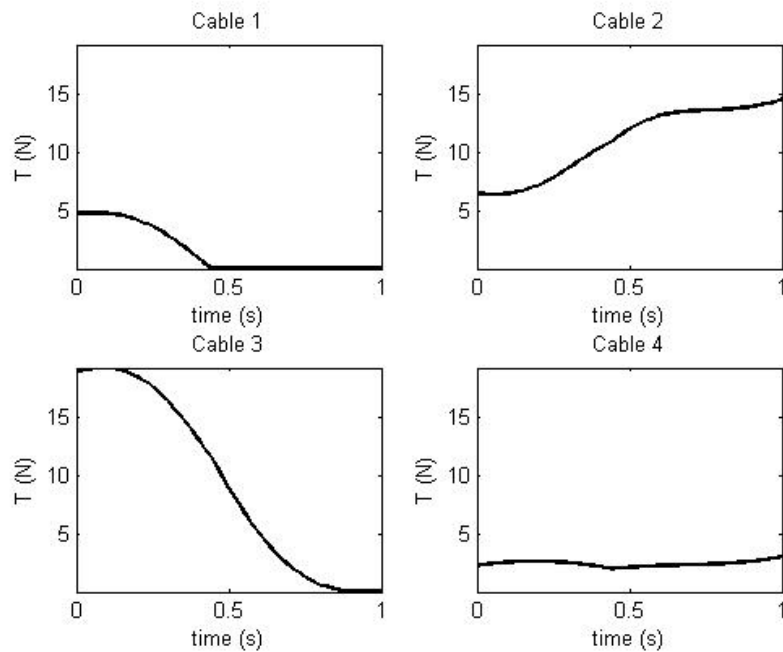
Figure B.3: WCW for optimal configurations x_4^* and x_1^*

The benefits of task specific evaluations can be further observed for the minimisation of trajectory cable forces. It can be observed that x_4^* can perform the trajectories C_2 and C_3 , but much less efficiently than the optimal configurations x_2^* and x_3^* , respectively. The comparison in cable forces required to generate trajectory C_3 between configurations x_4^* and x_3^* is shown in Figure B.4. It is clear that x_3^* from Figure B.4(b) performs the trajectory much more efficiently, with a maximum force of approximately 20N, compared to the maximum force of 100N from x_4^* .

From the comparison, the benefits in task specific evaluation to determine optimal cable configurations can be observed. This study suggests that it is difficult to obtain a robust cable configuration to satisfy a wide range of tasks, while performing them efficiently. In addition, the optimal configuration for one task specific objective typically performs poorly for another. Due to the potential reconfigurability of cable-driven systems, the adaptation of task specific objectives become feasible.

B.5 Conclusion

A study to compare the effectiveness of different task specific evaluation functions for optimising cable-driven manipulators was presented. Two classes of tasks were considered, minimisation of cable force to perform a trajectory, and maximisation of a workspace region. In addition, an efficient method to evaluate the quality of WCW was demonstrated extending from [69]. Performing optimisation on a 3-DoF cable-driven manipulator, the results indicated the improvement and savings of task specific objectives, as compared to a robust performance measure such as workspace volume. Future work should consider other task specific measures, such as cable interference, and to extend this to the optimisation of multilink manipulators.

(a) Cable Forces for x_4^* (b) Cable Forces for x_3^* Figure B.4: Cable Forces for Trajectory C_3 for optimal configurations x_4^* and x_3^*

University Library



MINERVA
ACCESS

A gateway to Melbourne's research publications

Minerva Access is the Institutional Repository of The University of Melbourne

Author/s:

Lau, Darwin Tat Ming

Title:

Modelling and analysis of anthropomorphic cable-driven robots

Date:

2014

Persistent Link:

<http://hdl.handle.net/11343/39607>

File Description:

Modelling and analysis of anthropomorphic cable-driven robots